UNIVERSITÀ DEGLI STUDI DI BRESCIA

Dottorato di Ricerca in
Metodi e Modelli Matematici per l'Ingegneria

Settore Scientifico Disciplinare: ICAR/08 Scienza delle Costruzioni

XXVII Ciclo

Multiscale and Multiphysics Modeling of Li-Ion Battery Cells

Relatore:

Prof. Alberto Salvadori

Tesi di Dottorato di:

Davide Grazioli

Correlatore:

Prof. Allan F. Bower

Coordinatore del Dottorato:

Prof. Paolo Secchi

Abstract

Lithium-ion batteries application to high power and high capacity demanding systems still encounters limitations. This technology is based on the classical intercalation reaction, during which Li is inserted into or extracted from electrodes. During this process the hosting material experiences large volume changes, leading to mechanical degradation, loss of integrity and of electric contact with current collectors. Nano-structured and composite material electrodes may reduce such damaging phenomena.

An electrochemical cell must include two electrodes, a separator, and an electrolytic solution. Depending on the phase, different mobile species carry the electric charges: electrons in the electrode and ions in the electrolyte. Ions must be transported through the electrolyte from one electrode to the other to bring reactants to the interfaces. Mass transfer in an electrolytic solution requires a description of the motion of mobile ionic species which is governed by diffusion, driven by gradients of concentration, and by migration, driven by an electric field for any charged particles.

Computational modeling and simulations may be helpful in designing new combinations of materials and geometries. To simulate a whole battery cell at the scale at which Lithium intercalate would be computationally unfeasible. A multi-scale approach is desirable and the computational homogenization technique is here adopted. This allows to track micro structural events that initiate damage and lead to macroscopic failure from macroscopic boundary conditions, while limiting the computational cost.

The adopted approach originates from the fundamental balance laws of mass, force and charge. Electroneutrality assumption has been taken into account. Maxwell's equations are considered in a quasi-static sense in a rigorous setting. The weak formulation derived preserves an energetical meaning, as required by the multiscale framework tailored on compuatational homogenization.
Microscopic processes within a composite electrode are investigated. All the materials forming the multi-component porous electrode are clearly identified. Migration, diffusion, and intercalation of Lithium in the active particles are modeled. Constitutive assumptions, that emanate from a rigorous thermodynamic setting, complete the formulation.
After spatial discretization, time-advancing algorithms have been implemented using a Wolfram Mathematica package script and by means of an Abaqus User Element (UEL) script. Different finite elements have been designed to deal with the electrolyte, the electrodes and the reaction layer between them. Several case studies have been simulated to validate the implemented formulation.

Sommario

L'applicazione delle batterie agli ioni di Litio in impianti e infrastrutture che richiedono elevate potenze e capacità trova ancora oggi limitazioni. L'intercalazione e lo stoccaggio del Litio, ripetutamente inserito ed estratto dagli elettrodi, sta alla base di tale tacnologia. Durante questo processo il materiale ospitante è soggetto a sensibili variazioni di volume, con conseguente danneggiamento meccanico, perdita di integrità e di contatto con il collettore di corrente elettrica. Materiali compositi e nano-strutturati possono contribuire alla riduzione di questi effetti deleteri.
Una cella elettrochimica necessita la presenza di due elettrodi, un separatore e una soluzione elettrolitica. A ciascuno di essi corrisponde un diverso vettore per le cariche elettriche: elettroni negli elettrodi e ioni nell'elettrolita. Gli ioni si muovono da un elettrodo all'altro attraverso l'elettolita, consentendo ai reagenti di giungere alle interfacce. Il moto della massa entro una soluzione elettrolitica richiede la descrizione del moto di speci ioniche, governato da diffusione, associata a gradienti di concentraione, e migrazione, associato alla presenza di un campo elettrico a cui le speci cariche sono sensibili.
Modelli computazionali e simulazioni numeriche possono offrire un notevole supporto alla progettazione e realizzazione di combinazioni di materiali e geometrie innovativi. Tuttavia, la simulazione numerica dell'intera batteria, alla scala spaziale a cui gli il Litio intercala, è computazionalmente proibitiva. Un approccio multiscala è da ritenersi più opportuno, da cui, la scelta di adottare la tecnica denominata *omogenizzazione computazionale* nel presente lavoro di tesi. Tale soluzione permette di tenere traccia dei fenomeni microstrutturali da cui il collasso macroscopico ha inizio, a partire da condizioni al contorno proprie della macroscala, limtando il costo computazionale nel contempo.
L'approccio perseguito si basa sulle leggi di conservazione della massa, delle forze e della carica. L'ipotesi di eletroneutralità è stata propriamente adottata. Le equazioni di Maxwell sono state rigorosamente consideate secondo la formulazione detta *quasi-statica*. La forma debole ottenuta preserva un significato energetico, imprescindibile in un'ottica multiscala basata sull'omogenizzazione computazionale.
I processi microscopici cui sono soggetti gli elettrodi compositi sono stati accuratamente investigati in seguito all'indentificazione delle diverse fasi costituenti. La migrazione, diffusione e intercalazione di Litio nei materiali attivi sono state direttamente modellate. I legami costitutivi adotatti a completamento della formulazione soddisfano le restrizioni termodinamiche.
A seguito della discretizzazione spaziale delle equazioni governanti, gli algoritmi di avanzamento nel tempo sono stati implementati utilizzando i codici commerciali Wolfram Mathematica e Abaqus (User element). Diversi tipi di elementi finiti sono stati implementati per la simulazione del comportamento degli elettrodi, dell'elettrolita e dell'interfaccia che li separa. Molteplici casi studio sono stati considerati ai fini della validazione.

Contents

Nomenclature

Notation

Vectors $\vec{a}$ will be denoted by an over-right-arrow, second order tensors $\boldsymbol{A}$ by bold face, exception made for symbol $\mathbb{1}$ denoting the identity matrix. This notation does not apply to operators.

Operators

- the symbol $\mathrm{tr}\,[-]$ denotes the trace operator
- the symbol $\mathrm{dev}\,[-]$ denotes the deviator operator
- the symbol $\mathrm{div}\,[-]$ denotes the divergence operator
- the symbol $\nabla\,[-]$ denotes the gradient operator
- the symbol $\mathrm{curl}\,[-]$ denotes the curl operator
- the symbol $\Delta\,[-]$ denotes the Laplace operator
- the symbol $\cdot$ denotes the single contraction of two vectors or two tensors
- the symbol : denotes the double contraction of two tensors
- the symbol $||x||^2$ denotes the squared norm of vector $\vec{x}$ or tensor $\boldsymbol{x}$
- the symbol ^{T} denotes the transpose of a tensor

Subscripts and superscripts

- the subscript $_{\mathrm{Li^+}}$ identifies quantities for Lithium cations, at both scales
- the subscript $_{\mathrm{X^-}}$ identifies quantities for anions, at both scales
- the subscript $_{\mathrm{Li}}$ identifies quantities referring to neutral Lithium, at both scales
- the subscript $_{\mathrm{H}}$ identifies quantities referring to Hydrogen
- the subscript $_L$ identifies quantities referring to Hydrogen within the lattice
- the subscript $_T$ identifies quantities referring to trapped Hydrogen
- the subscript $_a$ identifies active particles
- the subscript $_c$ identifies conductive particles
- the subscript $_s$ identifies solid phase
- the subscript $_e$ identifies electrolyte
- the subscript ^{m} identifies the microscopic variables
- the subscript ^{M} identifies the macroscopic macroscale
- the subscript $_{BV}$ identifies the Butler-Volmer equation
- the subscript $_{\mathrm{e^-}}$ identifies the electrons
- the superscript ^{m} identifies the microscopic variables
- the superscript ^{M} identifies the macroscopic variables
- the superscript ^{max} identifies the saturation limit of a chemical species

Variables and parameters

Electromagnetic variables and fields

- $\vec{B}$ denotes magnetic field
- $\vec{D}$ denotes electric displacement field
- $\vec{E}$ denotes electric field
- $\vec{H}$ denotes magnetizing field
- $\vec{i}$ denotes the electric current density
- ϕ denotes the electric potential
- ζ denotes the charge density
- $\mathbb{\zeta}$ denotes the state of charge
- $\mathbb{\epsilon}$ denotes the permittivity
- κ denotes the electric conductivity

Mechanical variables and fields

- $\boldsymbol{\sigma}$ denotes the stress tensor
- $\boldsymbol{\varepsilon}$ denotes the small strain tensor
- $\vec{b}$ denotes the body forces
- $\vec{p}$ denotes the contact forces
- $\vec{u}$ denotes the displacement field
- $\vec{v}$ denotes the velocity field
- E denotes the Young's modulus
- K denotes the bulk modulus
- G denotes the shear modulus
- ν denotes the Poisson's ratio
- σ_Y Yield stress
- $\bar{\varepsilon}^p$ equivalent plastic strain
- K^p hardening modulus

Mass transport variables and fields

- c denotes the concentration measure called molarity
- $\vec{h}_\alpha$ denotes the mass flux of species α - z_α denotes the valency of ion α
- μ denotes the chemical potential, also known as partial molar free energy
- $\overline{\mu}$ denotes the electrochemical potential
- $\mathbb{\mu}$ denotes the permeability
- $\mathbb{\chi}$ denotes the exchange factor
- K^{eq} equilibrium constant
- ΔE_τ additive inverse of the trap binding energy

Chemical (interface kinetics) variables and fields

- i_0, denotes the exchange current density in the Butler-Volmer interface conditions
- β denotes the symmetry factor in the Butler-Volmer interface conditions
- γ denotes the thermodynamic imbalance at electrode-electrolyte interface
- ξ denotes the discontinuity for the electrostatic potential
- χ denotes denotes the surface over-potential

Geometrical variables and fields

- $\vec{n}$ denotes the outward normal direction on a surface
- V denotes a domain at the microscale
- ∂V denotes a boundary or an interface between domains at the micro scale
- Ω denotes a domain at the macro scale
- $\partial\Omega$ denotes a boundary or an interface between domains at the macro scale
- Γ denotes a boundary or an interface between domains

Other variables and fields

- t denotes time
- v denotes the porosity
- T denotes the absolute temperature
- $\vec{q}$ denotes the heat flux vector
- q denotes the heat supply
- s denotes mass supply

Constants and parameters

- N_A is Avogadro's number, $N_A = 6.02214129(27) \times 10^{23}\ \mathrm{mol}^{-1}$
- e is elementary charge, $e = 1.602176565(35) \times 10^{-19}\ \mathrm{C}$
- $F = N_A\, e$ is Faraday's constant, $F = 96485.3383\ \mathrm{C\,mol}^{-1}$
- R is the universal gas constant $8.3144621\ \mathrm{JK}^{-1}\mathrm{mol}^{-1}$
- ϵ_0 is the vacuum permittivity, $8.85418782 \times 10^{-12}\ \mathrm{F\,m}^{-1}$
- μ_0 is the vacuum permeability $= 4\pi \times 10^{-7}\mathrm{N\,A}^{-2}$

Chapter 1
Introduction

Developing the next generation of batteries for higher capacity and longer life of cycling is one of the strategic challenges facing the energy storage planning of mankind. Lithium ion (Li-ion henceforth) batteries currently have the highest energy storage density of any rechargeable battery technology [1]. The present commercial realities, however, are not yet at such a technological level to meet the requirements of two main applications that show great potential for Li-ion batteries: Electric Vehicles and Smart Grids.

Major advances may be obtained only by moving towards new materials, as also pointed out in the European Strategic Energy Technology (SET) Plan, 2007, in the following SET Plan Materials Road Map, 2011 as well as in the recent (2013) recommendations on their implementation. In contrast to attempting to tailor a single electrode material, nano-structured materials, composites, and architectures can provide an optimum way of crafting desired characteristics. Appealing classes of materials are Li metal alloys, e.g. Silicon (Li-Si), and Tin (Li-Sn), due to their specific capacity which largely exceeds that of conventional anode based on graphite. The potentialities of these materials have been known for some time, but their exploitation has been until recently prevented by serious mechanical issues [2]. Similar concerns apply to the technology of graphene in battery electrodes, of very recent investigation [3, 4].

Theoretical and computational modeling provide the ability to predict, tailor, and shape new material properties. Material modeling of the multiscale and multiphysics processes that take place during charge/discharge can play a valuable role in battery design and lifetime prediction. This is the focus of the present thesis[1].

1.1 Thesis outline

Basic ideas of Li-ion batteries composition and core functioning are summarized in *chapter* 1 together with some insights about computational homogenization technique. A short review of the literature is also provided.

Part I provides an overview of the multiscale model tailored on Lithium ion batteries.

In *chapter 2* the fundamental balance laws of mass, force, charge and Maxwell's laws are recalled. Proper assumptions are introduced (and discussed) to reshape the equations and make them suitable for the description of the problem at hand.

If a system involving n different ionic species is considered, the n mass balance equations contain $n+1$ unknowns, i.e. n mass concentrations plus the electric potential. An additional relation is sufficient to solve the set of equations and the most common selection in battery

[1] The present chapter extends the contents available in [5]

modeling (see among others [6], page 286) is the *electroneutrality* condition. In several studies, the electroneutrality condition is thus used *instead of Gauss's law* for the electric field.

It is paramount to point out however that electroneutrality is *not* a fundamental law, but rather *an approximation* towards the solution [7]. In the approach proposed here (according to [8, 9]), rather then imposing the electroneutrality condition as an equation to be fulfilled, the impact that it has on the fundamental balance laws is investigated. For some of them, typically the force balance, the impact is major because the effects of the Lorentz interactions on bulk forces are minuscule (although they do not vanish) with respect to the mechanical effects due to the constrained swelling. On the contrary, electroneutrality has no influence on Maxwell's law because the bulk terms cannot be disregarded, at least according to the current numerical and experimental evidences. As previously observed, taking electroneutrality as a fundamental equation leads to the paradox of an electric field that is incompatible with Maxwell's laws [7, 10].

In the batteries modeling literature [6, 11, 12], it is generally assumed that the electromagnetic fields and their interactions are *static*. This assumption implies vanishing interference effects between the electric and magnetic phenomena. As a consequence, the set of Maxwell's equations are replaced by their electrostatic counterparts, as for the steady current case [13].

In the approach proposed here, the electro-magnetics is explicitly taken in to account via the *electro-quasi-static* formulation [14]. Capacitive but inductive effects are included, making the electro-quasi-statics different from the static approach, since Maxwell's correction is preserved within Ampère's law, i.e. the effect of the magnetizing field is still taken into account.

As insightfully noticed in [14], electrostatics is a particular case of the general Maxwell's equations but electro-quasi-statics is not, it is *an approximation*. The conditions at which the quasi-static solution to Maxwell's equations becomes exact are discussed in [14] and have been verified for battery cells in section 2.2.

In *chapter 3* a computational homogenization technique is tailored to Li-ion batteries using a multiscale scheme with a complex multi-particle representative volume element (RVE). Scales separation in term of characteristic length and time evolution are discussed.
The model is formulated assuming small displacements and strains. The battery cell is supposed to have a *single* binary electrolyte which is a solution of a binary salt, say LiX, plus solvent, say a polymer, in which the concentrations of ionic species vary with location in the cell. Active particles in the composite electrodes are idealized as network solids following *Larché and Cahn* [15], with the lattice material assumed as insoluble in the electrolyte. The concentration of ions in the solid phases is neglected.

A rigorous analysis of general principles of non-equilibrium thermodynamics is performed in *Part II* following the approach of [16, 17] both for the electrolyte and active material. Constitutive relations, meeting the thermodynamic restrictions derived, complete the set of governing equations. Validation of the numerical algorithms descending from them have been carried out.

In *chapter* 4 the electrochemical potential is defined moving from the rate at which power is expended on a material region, in terms of mechanical contribution as well as of the power due to mass transport and to electromagnetic interactions. All processes are taken to be

isothermal. The entropy imbalance and the Coleman-Noll procedure provide thermodynamic restrictions, satisfied by the usual Fickian description of diffusion and migration in terms of electrochemical potential, defined as in [18, 19]. Ideal, infinitely dilute solutions as well as dilute solutions taking into accounting the saturation limit have been contemplated.

A weak form has been derived for balance and for governing equations in terms of the selected thermodynamic fields, namely concentrations, displacements, and the electric potential. After spatial discretization, a Backward Euler time-advancing algorithm has been implemented into a *Wolfram Mathematica* package script.
A one-dimensional ionic transport process in Li-ion batteries electrolyte has been simulated, inspired by [10].

Modification to the liquid electrolyte model have been introduced to catch peculiarities of solid-electrolyte arising during batteries operation. Li^+ ions are generated or consumed by ionization reaction. The latter acts as a rate controller: at all points where Li^+ accumulates during battery operations more immobile oxygen-binded Lithium is created, and vice versa, resulting in a mass supply within the mass balance equation for ionic species.

The same methodology has been pursued in *chapter* 5 to model the active materials.
Linear Fickian-diffusion law accounting for saturation limit is drew up for the Lithium diffusion in the electrodes. At high C-rates, which are indeed expected in real batteries or super capacitors, peaks of Lithium concentration can be observed in the electrodes, making regular solution [19, 20] a more suitable model.
Differently from the electrolyte, diffusion and stress evolution are thermodynamically coupled in terms of constitutive prescriptions. A standard J_2 flow theory with isotropic hardening is used to account for plastic material response. Analogies with hydrogen embrittlement modeling have been emphasized.

A Backward Euler time-advancing algorithm has been implemented into an *Abaqus User Element (UEL)* script. A numerical benchmark accounting for stress-diffusion coupling in a tube-like axisymmetric cross section has been used for validation.

In *chapter* 6 the set of governing equations described in chapters 4 and 5 has been applied to an all-solid-state battery, reproducing the analysis proposed in [21], to validate the overall model.
The outcomes of the numerical analyses show that the multiphase model developed for porous electrodes, chapter 3, well reproduces the behavior of each component of a Li-ion batteries and their interactions. The processes affecting the cell during a single discharge process are well cached by the simulations, denoting the robustness of the approach.

Part III is devoted to future developments.

The solution of nested boundary value problems can be only approximated numerically through a fully coupled analysis, not attained within this work exclusively because of the lack of time. Nevertheless, a two-scale Newton-Raphson algorithm is provided in *chapter* 7.

Preliminary attempts towards multiscale numerical analyses are reported. The framework described in chapter 4 has been applied to a two-dimensional problem. The micro structural behavior of a multi phases separator has been investigated. Boundary conditions descend from a multi scale theoretical formulation for batteries discussed in chapter 2. A strong influence of the geometry is observed from the outcomes, in particular at the interface between fluid electrolyte and the separator membrane. This numerical evidence strengthens the conceptual framework of the multi scale approach that permeates this work, namely that

electrochemical and mechanical performance of Li batteries strongly depends on the interaction between micro and nano-scale phenomena, in particular within the electrodes.

1.2 Li-ion batteries in brief

Composition

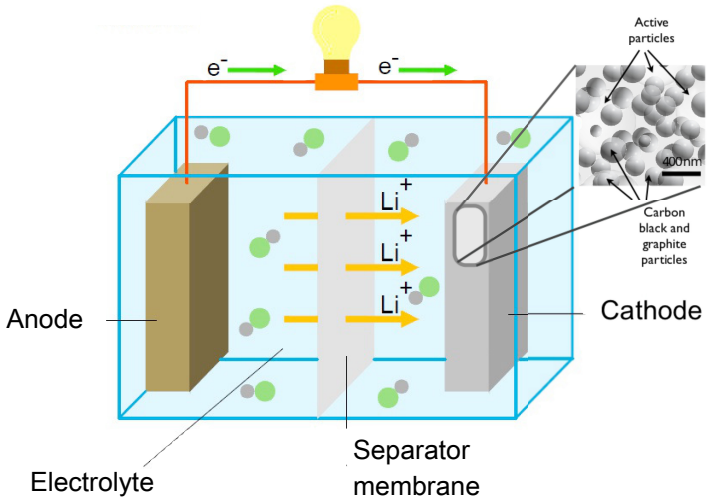

Figure 1.1: *Li-ion battery scheme and detail showing the composite microstruture of cathode electrode (Courtesy of M. Magri).*

Electrochemical cells necessarily consists of several phases [6] (see Figure 1.1) which must include current collectors, two electrodes, a separator, and an electrolytic solution.

Metallic *current collectors* are required to connect the battery to external circuit. They drive the electron flux from the external circuit to the electrodes.

Charge is transported through the *electrode* by the movement of electrons. Typical electrode materials include solid metals (e.g., Pt, Au), liquid metals (Hg, amalgams), carbon (graphite), and semiconductors (indium-tin oxide, Si) [11].
Nevertheless, composite porous electrodes are nowadays widespread. A solid matrix made by particles of *active material* is bounded by a polymer *binder* to a network of *conductive particles*. Active particles are prone to Lithium insertion, while conductive particles improve/accelerate the flux of electrons between active particles and the current collector.
Beneficial effects follow from composite porous structure: at first, the diffusion path for ions and electrons is shortened due to the possibility of the electrolyte to fill the pores; furthermore, the effective area available for chemical reactions increases due to the micrometric dimensions of the active particles (being the surface-area-to-volume ratio proportional to the inverse of the characteristic length) [22].

The *electrolyte* is a conducting medium laying between the electrodes in which electric current flows due to the transport of ions.
The most frequently used electrolytes are liquid solutions containing ionic species (cations, carrying positive charge and anions, carrying negative charge) in either water or a non-aqueous solvent. Ionic species result from the dissociation of a salt. *Binary ionic compound*

refers to a salt that dissociates into two ions only.
To physically separate electrodes a porous polymeric membrane is usually inserted. The latter is placed between the electrodes to prevent short circuit. The pores of the membrane are filled by the electrolyte, allowing ions to transfer charges from one electrode to the other. The term *separator* indicates the system formed by electrolyte/membrane.
Less conventional electrolytes include fused salts (e.g., molten NaCl-KCl eutectic) and ionically conductive polymers (e.g., Nation, polyethylene oxide-$LiClO_4$). Solid electrolytes also exist, in which ions move under the influence of an electric field even in the absence of solvent [11]. In Lithium based solid electrolyte (e.g. Li_3PO_4) Lithium atoms may either be mobile or not in the hosting matrix. Depending on battery operation the transition from one state to the other results in a local Li-ion source or consumption.
The issues related to solid electrolyte modeling will be addressed in section 4.11.

Core functioning

Li-ion batteries are based on the classical intercalation reaction during which neutral Li is inserted into or extracted from electrodes. The essential processes that take place in a Li-ion battery cell can be sketched as follows. During discharge, charges flow (electrons externally, ions across the separator) from the anode towards the cathode.
When the battery cell is first assembled, ions in the electrolyte/separator are provided by the dissociation of the (binary) salt into the organic electrolyte, which is supposed to be complete, and are free to flow into the latter. In the absence of *convection*, as usually assumed and henceforth, movement of ionic species is governed by *diffusion*, driven by gradients of concentration, and by *migration* driven by an electric field. X^- anions can not enter electrodes, and Li^+ cannot intercalate into conductive particles.
An oxidation/reduction reaction occurs at the active particle/electrolyte interface, within an atomistic size layer. During oxidation Li^+ ions are generated while during reduction those ions meet the electrons to produce neutral Lithium. The latter intercalates into the active particles causing large volume changes, inelastic effects [23, 24], phase-segregation [25, 26], micro-cracks and particle fracture [27], decrepitation or pulverization and loss of integrity; these damaging phenomena that may lead to electrodes failure in few cycles.

In order to address the problem of the mechanical failure of particles in the electrode, optimization of their morphology is required. Nanostructured configurations, capable of buffering large volume changes, are expected to ensure longer cycle life and higher specific capacity [1].
Since the seminal work of *Doyle et al.* [28], there have been a number of fundamental studies of Li-ion battery operation based on porous electrode theory. This theory accounts for distinct phases within the battery using superposition and does not require detailed knowledge of the surface morphology of electrodes and separator. The microstructure is accounted for only with a pore volume fraction and the field variables are computed in a volume-averaged sense [29].

1.3 Multiscale modeling

The behavior of the battery cell is intrinsically *multiscale*, because the multiphysics phenomena involving diffusion, migration, intercalation, and the accompanying mechanical effects take place at the characteristic length scale of the electrode compound, which is three order of magnitudes smaller than the battery cell size. Directly resolving all scales and modeling all

particles in the electrodes is computationally unfeasible. A more efficient way to deal with multiscale modeling is represented by homogenization methods, by which the nano-scale effects are incorporated into a microscale problem.

The complex microstructural behaviour made the computational homogenization (CH) technique attractive, since it provides valuable information on the local microstructural fields as well as the effective material properties. Assuming separation of scales [30], these method allows to compute effective properties of composites by averaging the micro-level behavior which incorporates the nano-scale effects. Those effective quantities are then directly used at the macroscopic scale which is usually considered as a classical continuum.

Computational homogenization technique and its application within the context of mechanics of material is first introduced to set up notation and terminology. An introduction about computational homogenization for batteries will follow, while a more extensive discussion is postponed to chapter 3.

1.3.1 Computational homogenization in mechanics

Since a few years, substantial progress has been made in the two-scale computational homogenization of complex multi-phase solids. This technique is essentially based on the solution of nested boundary value problems, one for each scale. Focusing on the nonlinear characteristics of the material behaviour, this technique proves to be a valuable tool in retrieving the constitutive response. First-order (i.e. including first-order gradients of the macroscopic displacement field only) computational homogenization schemes fit entirely in a standard continuum mechanics framework and are now readily available in literature [31–35]. Main features of this numerical method are:

- The constitutive response at the macro scale is a priori undetermined. No explicit assumptions are required at that level, since the macroscopic constitutive behaviour ensues from the solution of the micro scale boundary value problem.
- The method is suitable for large displacements (large strains and rotations) provided that the microstructural constituents are modelled adequately.
- The different phases in the microstructure can be modelled with arbitrary nonlinear and time-dependent constitutive models.
- The influence of the evolution of the microstructure (as described on the micro-scale) can be assessed directly on the macro-scale.
- The micro scale problem is a classical boundary value problem, for which any appropriate solution strategy can be used. Finite Element Method is often succesfully adopted [31, 34, 35].
- Macroscopic constitutive tangent operators can be obtained from the microscopic overall stiffness tensor through static condensation. Consistency is preserved through this scale transition.

In spite of the huge computational cost of a nested two-scale solution problem, efficiency can be achieved by solving the problem through parallel computations [34, 36]. Another option is selective usage, where non-critical regions are modelled by continuum closed-form homogenized constitutive relations or by the constitutive tangents obtained from the microstructural analysis but kept constant in the elastic domain, while in the critical regions the multi-scale

analysis of the microstructure is fully performed. Despite the large computational requirements, the computational homogenization technique has proven to be a valuable tool to establish non-linear micro-macro structure-property relations, especially in the cases where the complexity of the mechanical and geometrical microstructural properties prohibit the use of other homogenization methods. The first-order technique is by now well-established and widely used in the scientific and engineering community (the reader should refer to [30] for a review).

Principles and assumptions

At the macro-scale, the material is considered as a homogeneous continuum, whereas at the micro level it is not (the morphology consists of distinguishable components or phases), as schematically illustrated in Figure 1.2. The microscopic length scale is much larger than the molecular dimensions $l_{discrete}$, so that a continuum approach is justified for every constituent[2]. At the same time, in the context of the principle of separation of scales, the microscopic length scale l_{micro} is assumed to be much smaller than the characteristic length l_{macro} over which the size of the macroscopic loading varies in space, i.e.

$$l_{discrete} \ll l_{micro} \ll l_{macro} \tag{1.1}$$

This is named after *principle of scale separation.*

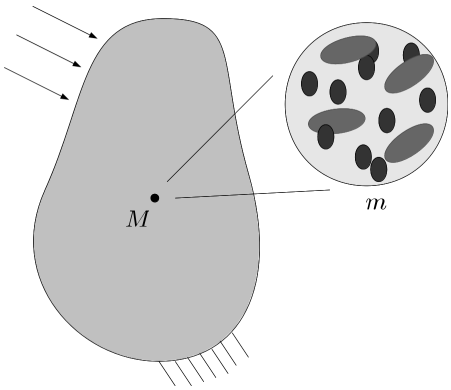

Figure 1.2: *Continuum representation of the macroscale (M) and correspondent underlying microstructure (m)*

Most of the homogenization approaches rely on the assumption of *global periodicity* of the microstructure, implying that the whole macroscopic domain consists of spatially repeated unit cells. In a computational homogenization approach, a more realistic assumption is made, which is commonly denoted by *local periodicity.* According to that, different microstructures may correspond to different macroscopic points.

The basic principles of computational homogenization have gradually evolved from the concepts employed in other homogenization methods and well fit into the four-steps homogenization scheme established by *Suquet* [32]:

1. definition of a microstructural representative volume element (RVE), in which the constitutive behaviour of individual constituents is assumed to be known;

[2]Chemical processes will be modeled, within a computational homogenization framework for Li-ion batteries (see chapter 3), from a continuum level perspective.

2. formulation of the microscopic boundary conditions from the macroscopic input variables and their application on the RVE (macro-to-micro transition);

3. evaluation of the macroscopic output variables from the analysis of the deformed microstructural RVE (micro-to-macro transition);

4. obtaining the (numerical) relation between the macroscopic input and output variables.

The main ideas of the first-order computational homogenization have been established in [32, 37, 38] and further developed and improved in more recent works [31, 33, 34].

Computational homogenization scheme

A computational homogenization scheme generally departs from the computation of a macroscopic deformation tensor, $\nabla \left[\vec{u}^M \right]$, calculated for every material point of the macrostructure (here and in the following denoted with the subscript M).
The deformation tensor $\nabla \left[\vec{u}^M \right]$ is next used to formulate the boundary conditions to be imposed on the microscopic RVE related to this point. Upon the solution of the microscale boundary value problem, the macroscopic stress tensor $\boldsymbol{\sigma}^M$ is obtained by averaging the stress field over the volume of the RVE. Consequently, the (numerical) stress-deformation relationship at the macroscopic point is available. Additionally, the local macroscopic consistent tangent is extracted from the microstructural stiffness. The entire framework is schematically illustrated in Figure 1.3.
The computational homogenization technique defined in this sense may be categorized as a *first-order deformation driven* approach, being the macroscopic material point response dependent on the first gradient of the displacement field only.

A *stress driven* procedure (given a local macroscopic stress, obtain the deformation) is also possible. However, it does not directly fit into a standard displacement-based finite element framework, usually employed to solve the macroscopic boundary value problem. Moreover, in case of large deformations the macroscopic rotational effects have to be added to the stress tensor in order to uniquely determine the deformation gradient tensor, thus complicating the implementation. Therefore, the "stress driven" approach, is generally not adopted in coupled multi-scale computational homogenization strategies of the type described here.

In order to limit repetitions, scale transition conditions will be discussed in section 3.4 within the context of CH particularized to Lithium batteries. Mechanical aspects will be emphasized therein.

1.3.2 Computational homogenization for batteries

The computational homogenization technique is tailored here to model the multiphysics events that coexist during batteries charging and discharging cycles [8, 9]. Two nested boundary value problems have to be solved, one for each scale. At the macroscale, diffusion–advection equations model the coupling between electrochemistry and mechanics in the whole cell. The multi-component porous electrode, migration, diffusion, and intercalation of Lithium in the active particles, the swelling of the latter are modeled at the micro-scale.
A complete set of equations and boundary conditions governing displacements, electric, chemical, and electrochemical potentials will be derived in chapters 3-5 for the whole battery cell at both scales following non-equilibrium thermodynamics of porous electrodes [6, 39].

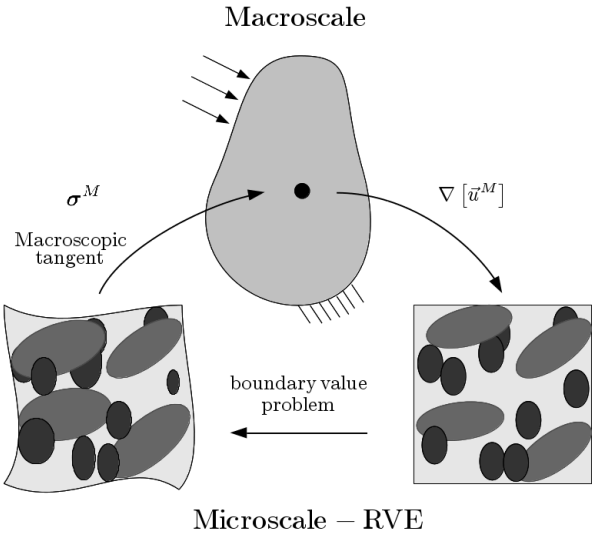

Figure 1.3: *Computational homogenization scheme*

1.4 Literature review

An up-to-date literature review on battery modeling is reported. The target is to underline the efforts of the scientific community in modeling and simulating Li-ion batteries, by no means presuming to be exhaustive of the widespread literature available on the topic.

Batteries are by far the most common form of storing energy [12]. Among the various existing technologies, Li-based batteries currently outperform other systems, accounting for 63% of worldwide sales values in portable batteries [40]. In 2013, consumers bought five billions of Li-ions cells to supply laptops, cameras, mobile phones and electric cars [41].
Being Lithium the most electropositive as well as the lightest metal in nature, it allows Li-ion batteries to posses the highest energy densities (capability to store energy per unit weight or volume) among all rechargeable batteries, see Figure 1.4 [40]. This is the main reason of the wide diffusion of this technology. Other advantages related with Li-ion batteries are a relatively low self-discharge rate, about 5% per month compared with more than 20-30% per month for Ni-metal hydride and Ni-Cd batteries respectively, and wide temperature range, $-25 \div 50°\text{C}$ [2].
Li-ion batteries are more environmentally friendly with respect to most others [2, 22]: Lithium can be found in unlimited quantities in sea water or be concentrated from brines, which is anyway a much greener process than conventional mining.
The demand for lithium could also be eased by recycling [42], which has already proved its value with lead-acid batteries [22]. Long-term considerations, involving all the phases of the life cycle, are extremely relevant for the choice of the materials for future generations of batteries.

Research activities carried out worldwide in the last few years call attention to the connection between Li-ion batteries performance and the materials used for electrodes and electrolyte. An accurate description of prominent phenomena occurring during common operations as well as of the material response to solicitations and of ageing mechanism [43] are crucial for the development of the next generation of batteries.

An example of an interconnected computational framework together with a 3D validation

study is presented in *Allu et al.* [44]

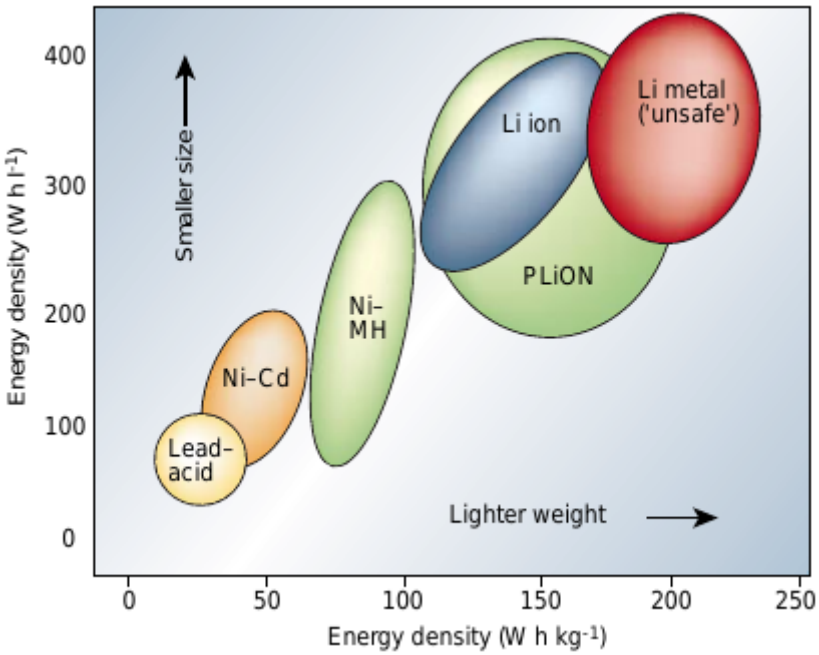

Figure 1.4: Battery technology comparison [40]

Electrolyte

Mass must be transported through the electrolyte from one electrode to the other to bring reactants to the interfaces. Mass transfer in an electrolytic solution requires a description of the motion of mobile ionic species which is due to three contributions: diffusion, caused by concentration gradients; migration, caused by the applied electric field; convection, due to movement of bulk electrolyte solution [6]. Even if the latter contribution might be relevant for some electrochemical systems [45, 46], it is natural to neglect this term in Li-ion battery models, see among others [10, 47–51].

In many cases, ionic transport is described assuming the electrolyte as an ideal infinitely dilute solution. Under this hypothesis the energetic interactions between different species are neglected; hence, the flux of a species is proportional to the gradient of the electrochemical potential of the species itself [10].

Electroneutrality[3] [6, 10] is another widely used hypothesis in the electrochemical literature. Since a huge electric field would be required to separate positive from negative charges, it is admissible to assume that charges cannot separate within the electrolyte bulk. Such an assumption is valid for material points far enough from the electrode/electrolyte interfaces.

However, electroneutrality is not a fundamental law, but rather an approximation towards the solution, which can lead to paradoxes if not consciously adopted. To this end, *Dickinson et al.* [7] show that electroneutrality does not constrain in any way the electric field to satisfy Maxwell's equations. *Danilov and Notten* [10], discussing results obtained from numerical simulations moving from electroneutrality assumption for an electrolyte model, show that

[3] that is: over macroscopic distances the difference among concentrations of the ionic species is small compared to the total concentration [52]

despite numerical advantages and good estimation of ionic concentration distribution, this approximation yet leads to an unjustified electric field.

Although one dimensional mathematical description is generally accepted for the separator, owing to the geometry of the battery cell, such a geometrical description reflects reality only in an average sense. The porous separator of an electrolytic cell is in fact a multi-phase structure that includes a network of interconnected and irregular pores and channels [53].

Multiscale approaches have already been adopted to evaluate stresses induced on the separator microstructure [54] during charge/discharge cycles.

Intercalation in active materials

Lithium intercalates inside active material in neutral form. Active particles are often treated as a binary Larché-Cahn system: the hosting material filled with Lithium and the free interstitial lattice material [15, 55]. As the internal concentration of Li increases, the hosting material swells, and experiences stresses which may be sufficient to cause inelastic effects as plastic flow, as shown by *Sethuraman et al.* [56], eventually leading to failure.

Fragmentation, disintegration and fracturing, and concomitant loss in contact of the electrode material with the current collector result in severe capacity fade with electrochemical cycling, which ultimately renders the electrode material unsuitable for further cycling. Hence, stress development in electrode materials is one of the primary causes for capacity fade and eventual failure of Li-ion batteries [2].

Mechanical effects in battery microstructures have been experimentally observed and modeled in several recent publications. Most of them concern single particle analysis [57–61], nano-wires [62–65], or thin films [23, 66–68].

While the evaluation of stresses in composite electrodes is still an open challenge, some researchers [23, 56, 69] have recently employed optical stress sensors to track stress generation during electrochemical cycling of thin film electrode materials.

To avoid the complexity of the non-uniform intercalation current density within each porous electrode, it is quite customary in literature [29, 55, 59, 60, 70], to restrict the analysis to a single active particle without modeling the surrounding material and phenomena; neither the electrolyte nor the interface reaction are directly considered, but the electrochemical interactions are replaced by “a priori” given incoming flux. Diffusion equation (neutral species moving in an electrically conductive medium [29, 49]) has to be adopted [49, 59, 60, 70].

Since atomic diffusion in solids is much slower than deformation, mechanical equilibrium is assumed to be immediately established at all instants, hence a mechanically equilibrated problem is formulated in time. An exhaustive literature review about stress-diffusion coupling can be found in *Yang* [71].

Elastic material response

The simplest way to model mass diffusion-induced stress is in analogy to thermoelasticity. In *Cheng and Verbrugge* [59, 60] any influence of the mechanics on concentration distribution is disregarded, diffusion equation is solved independently and stress distribution estimated thereafter according to small strain linear elastic theory. A more complete model has been proposed by *Zhang et al.* [70], where stress and concentration distribution are fully coupled through constitutive laws, extending the formulation presented by *Li* [72].

Elastic stresses arising due to interactions between particles undergoing swelling have been included in the models proposed by *Purkayastha and McMeeking* [48] and *Aifantis and Dempsey* [73].

Non-linear material response

Experimental observations show that active materials experience phase transition and large deformations while lithiated [56, 63, 68, 74]. As a consequence, plastic deformations and fractures arise, making an elastic characterization of the material not realistic.

More refined models accounting for non-linear response have been developed [55, 58, 67, 73, 75–77]. Many of the latter report numerical analysis results relative to 1D problems, restricting the attention to spherical particles or thin films.

Both crystalline and amorphous Silicon undergo phase transformation [25, 57, 62]. Crystalline Silicon electrodes react with Lithium at room temperature forming an amorphous phase of lithiated Silicon with atomically sharp (about 1nm thickness [78]) reaction front. Since lithiated Silicon is an electron conductor, Lithium ions and electrons recombine into Lithium atoms upon reaching the Silicon electrode. Lithium atoms then diffuse through the lithiated Silicon, and react with the crystalline Silicon, at the reaction front, to form fresh lithiated Silicon. The reaction causes the lithiated Silicon to grow at the expense of the crystalline Silicon and metallic Lithium.

Evidence shown [62, 79] that, in nanostructured electrodes, the velocity of the reaction front is not limited by the diffusion of Lithium through the occupied phase, but by the reaction of Lithium at the interface front. Under a constant voltage the displacement of the reaction front is linear in time [62] indicating that the rate of lithiation is limited by short-range processes, such as breaking and forming atomic bonds.

Migration of Lithium ions in the electrolyte is relatively fast, so that the diffusion of Lithium through the lithiated Silicon and the reaction between Lithium and Silicon at the front may limit the velocity of the reaction front [79].

Huang et al. [61] and *Zhao et al.* [79] investigated the distribution of stresses, accounting for plastic strains, in a spherical particle, fixing a priori the law which the two phases separation front obeys while moving from the outer boundary of the particle toward the center.

A different methodology has been chosen by *Drozdov* [80, 81]. Lithiation process is considered after splitting guest atoms into mobile and immobilized, following the approach previously suggested by [20, 82, 83] to study hydrogen diffusion in metals. The major advantage of this approach is that, for trapping rate strongly exceeding the rate of diffusion, a sharp interphase naturally appears, without any a priori assumption.

In recent works of *Anand* [20] a continuum-level thermodynamically consistent theory is formulated to couple species diffusion with large elastic-plastic deformations of a body. A classical Cahn-Hilliard theory was developed to account for phase segregation caused by the diffusing species. The phase-interface is modeled as a diffuse-interface: the concentration field takes distinct values in each of the phases with a smooth change between the values around the interface, permitting a regularization of the problem.

For a complete review about models and experimental measurement of stresses in Li-ion battery electrodes, the reader may refer to *Mukhopadhyay and Sheldon* [2].

Analysis of stress affecting Li-ion batteries have been carried out also at higher scales. Examples can be found in *Zhang et al.* [84], where diffusion-induced stress in layered structure (multilayer electrode plate including active plates as well as current collector) has been

investigated and [85–87] where *Wierzbicki* and his co-workers investigate structural response of battery cells subjected to externally applied mechanical stresses.

Interface reaction

The electrode/electrolyte interface controls the overall behavior of the battery cell. Such an interface is the location where the mechanism of charge transfer changes: in the electrolyte, charges are carried by ions and driven by concentration and electric potential gradients (when convective contribution to ion motion is neglected); in the electrodes, charges are carried by electrons and driven by the electric potential gradient only.

Assuming $LiCoO_2$ to be the positive electrode material for instance, the following electrochemical charge transfer reaction holds

$$LiCoO_2 \rightleftarrows Li_{1-x}CoO_2 + x\,Li^+ + x\,e^- \qquad 0 \leq x \leq \frac{1}{2} \tag{1.2a}$$

If graphite is taken to serve as anode material, intercalation and extraction are described by

$$C_6 + z\,Li^+ + z\,e^- \rightleftarrows Li_zC_6 \qquad 0 \leq z \leq 1 \tag{1.2b}$$

Mass is transported through the electrolyte from one electrode to the other, to bring reactants to the interfaces for the electrochemical charge transfer reactions (1.2) to take place. The latter relates charge and mass transfer through the interface. When the Lithium ions are reduced to neutral state variation in electric potential does not affect their transport any more.

Since the cell is first assembled, the charges are localized around the interface between electrode and electrolyte, causing an intense electric field to develop in a region (known as the Stern Layer) with atomic-scale dimensions adjacent to the interface, together with a more diffuse region of charge (known as the Gouy-Chapman layer) in the electrolyte [88]. These regions together (in the order of 10 to 20nm according to the literature [6]) define a so-called *electric double layer*.

An exhaustive dissertation about the electric double layer can be found in *Newman and Thomas-Alyea* [6] as well as in *Bard and Faulkner* [11]. *Biesheuvel et al.* [89] report a recent review of the relevant literature and a mathematical model of the steady state behavior of a galvanic cell that includes the double layer description.

In Li-ion battery modeling literature, specific description of the double layer is generally disregarded with a few exceptions (e.g. *Bazant et al.* [52], *Marcicki et al.* [29]), local electroneutrality is assumed throughout the electrolyte and a discontinuity in the electrostatic potential across the electrode/electrolyte boundary is allowed for (see among others [10, 45, 46, 48, 90]). The electric double layer is thus assumed as infinitesimally narrow, allowing for a distribution of a charge layer in the electrolytic solution equal and opposite to the charge layer on the surface of the electrode.

A semiempirical equation, named after Butler and Volmer, is used to relate the local intercalation current to the potential difference between the working electrode and the point in solution immediately beyond the ideally narrow double layer [48, 49, 67, 75, 91]. *Streeter and Compton* [92] critically discuss the *electroneutrality* and *negligibly small double layer* approximations, showing they are appropriate only if the (active) particles of the electrode are much larger than the electric double layer.

SEI layer

Electrode/electrolyte interface is affected by the formation of a so-called *solid electrolyte interphase* layer (SEI). The SEI layer is a passivating film that appears since the first time the electrode contracts the electrolyte solvent and is made by electrolyte decomposition products [93]. Its composition, formation, and functioning are still under investigation because the SEI effects can be either beneficial (it prevents uncontrolled Li-intercalation in the electrode) and negative (excessive SEI formation may lead to undesirable Li-ions consumption and active electrode area reducing). Attempts to include SEI growth in Li-ion battery models can be found in literature, see for example *Xie et al.* [94] and *Pinson and Bazant* [95].

Complete battery cell models

A simplified model of galvanostatic charge/discharge process of a complete battery cell has been proposed by *Doyle et al.* [28], considering one-dimensional transport from a lithium anode to a composite cathode through the separator. In this model no mechanical contribution has been taken into account.

A whole battery cell with two porous electrodes has been considered in [29, 90, 91]. Porous electrode theory models the overall battery, but particles that make up the intercalation electrodes are assumed to be spherical, thus allowing for a 1D description.

2D models of half battery cell are presented in *Purkayastha and McMeeking* [48] and *Garcia et al.* [49] in which all the phases are fully described. It was envisaged in [49] that the level of stresses experienced by the active particles during electric cycles may depend on their location with respect to the separator.

Multiscale battery cell models

Multiscale approaches have been pursued in Li-ion batteries: *Golmon et al.* [50, 51] considered the Mori-Tanaka approach at a meso-scale; Hashin-Strickman as well as Wiener bounds have been considered by *Ferguson and Bazant* [39].

Computational homogenization schemes, also called FE^2, are based on the solution of two nested boundary value problems (*Suquet* [96]; *Miehe et al.* [33]; *Feyel and Chaboche* [34]; *Geers et al.* [30]). Upscaling of the effective behavior is usually achieved according to the Hill-Mandel principle of macro-homogeneity which ensures energy consistency between the two scales, *Hill* [97].

CH mechanical schemes are well-established, the reader may refer to *Geers et al.* [30] for a detailed review. In recent publications this technique has been extended to problems in which multiphysics comes into play. *Özdemir et al.* [98, 99] have recently extended this approach to the thermo-mechanical coupling; *Wu et al.* [100, 101] have set a thermo-chemo-mechanical coupled multiscale model to deal with concrete failure due to chemical reaction; *Zäh and Miehe* [102] developed a CH framework for dissipative electro-mechanically coupled materials.

In two-scale formulations for heat conduction [98, 99], a steady-state mass transport hypothesis was adopted at the microscale. Steady-state mass and charge transport is justified at the micro level in the presence of fast diffusive response or negligibly small RVEs. Steady-state would imply instantaneous changes for concentration and potentials at the micro scale, dictated through the boundary conditions that originate from the macro scale problem, which is time-dependent. From a simple estimate it turns out that the steady-state mass and charge transport hypothesis at the microscale is not satisfied for the battery problem

[9]. Accordingly, a concurrent time modeling between the macro and micro scales will be carried out in the present work.

CH scheme with non-steady state microstructures is not a novelty. *Larsson et al.* [103], in the context of transient thermal problems, adopted a scheme to predict the thermal response of composites with non-steady state microstructures. *Pham et al.* [104] applied CH technique to metamaterials subject to dynamic excitation.

Part I

Balance equations and multiscale formulation

Chapter 2
Overview

Despite many progresses have been made in the last decades, modeling the complex structure of batteries still represents an open challenge. The different nature of the phenomena involved - mechanical, electrical, electrochemical and thermal (the latter not discussed in this work) - lead to a mathematical framework that entails a high number of unknowns (displacements, electric potential, concentration, temperature...). Additional complexities are provided by both multiphysics (coupling among variables often arise through non-linear relations) and multiscale (different observation scales are involved).

Basic ingredients underling the developed model are described in the chapter.
The set of equations involved in the multiphysics description is then introduced. The limits of electro-quasi-static formulation, used in place of the complete set of Maxwell's law, and of electroneutrality assumption are rigorously discussed[1].

2.1 Balance laws

2.1.1 Mass balance

The mass balance equation may be written as

$$\frac{\partial c_\alpha}{\partial t} + \operatorname{div}\left[\,\vec{h}_\alpha\,\right] = s_\alpha \tag{2.1}$$

where: c_α is the *molarity* (i.e. the number of moles per unit volume) of a generic species α; $\vec{h}_\alpha$ is the mass flux in terms of moles, i.e. the number of moles of species α measured per unit area per unit time; s_α is the mass supply rate in terms of moles, i.e. the number of moles of species α measured per unit volume per unit time. It applies to ions Li^+, X^-, electrons e^-, as well as neutral Li. Concentrations are defined in space $\vec{x} \in V$ and time $0 \leq t \leq t_f$, i.e. $c_\alpha = c_\alpha(\vec{x}, t)$. Functional dependence however is specified when necessary only, to enhance readability.

2.1.2 Faraday's law

Charges in the solution are transported by dissociated ions. Therefore, the charge density ζ is related to their concentrations.

$$\zeta = F \sum_\alpha z_\alpha \, c_\alpha \tag{2.2}$$

where $F = 96485.3383\ \mathrm{C\,mol^{-1}}$ is Faraday's constant and z_α is the valency[2] of ion α. The flux of mass in balance (2.1) of each species contributes to a current density $\vec{i}$ and a charge

[1] This chapter extends contents of [8, 9]

[2] i.e. the number of electrons transferred per ion, typically $+1$ for Li^+ cations and -1 for X^- anions.

supply rate s^{c} in view of Faraday's law of electrolysis

$$\vec{i} = F \sum_{\alpha} z_\alpha \, \vec{h}_\alpha \; , \qquad s^{\mathsf{c}} = F \sum_{\alpha} z_\alpha \, s_\alpha \tag{2.3}$$

2.1.3 Maxwell's equations in matter

Maxwell's equations describe electric and magnetic fields and their reciprocal interactions[3]. Gauss's law relates the electric (in Volts per meter) and magnetic fields emanating from a distribution of free electric charge ζ_f (in Coulomb per unit volume).

$$\operatorname{div}\left[\vec{D}\right] = \zeta_f \tag{2.4}$$

$$\operatorname{div}\left[\vec{B}\right] = 0 \tag{2.5}$$

$\vec{D}$ is termed *electric displacement field* and $\vec{B}$ is known as the *magnetic field*. Maxwell-Faraday's law of induction describes how the variation in time of the magnetic field induces an electric field.

$$\operatorname{curl}\left[\vec{E}\right] = -\frac{\partial \vec{B}}{\partial t} \tag{2.6}$$

$\vec{E}$ denotes the *electric field*. Finally, the Ampère's law (with Maxwell correction) relates the electrical current and the time variation of the electric displacement field to the magnetic field.

$$\operatorname{curl}\left[\vec{H}\right] = \vec{i}_f + \frac{\partial \vec{D}}{\partial \, t} \tag{2.7}$$

$\vec{H}$ is termed the *magnetizing field* and $\vec{i}_f$ is the free current density.

Equations (2.4 - 2.7) depend only on free charges and currents, whereas the contribution of bound quantities is included in the two additional electric $\vec{D}$ and magnetic $\vec{H}$ fields. Phenomenological splitting related those quantities to $\vec{E}$ and $\vec{B}$. The splitting is a definition, it does not entail any constitutive nature.

$$\vec{D} = \text{ɬ}_0 \, \vec{E} + \vec{P}$$

$$\vec{H} = \frac{1}{\text{ɭ}_0} \, \vec{B} - \vec{M}$$

The factor ɬ_0 is termed vacuum permittivity or electric constant. Its value is $8.85418782 \times 10^{-12} \mathrm{C\,V^{-1}\,m^{-1}}$. The factor ɭ_0 is termed vacuum permeability or magnetic constant. Its value is $4\pi \times 10^{-7} \mathrm{N\,A^{-2}}$.

Vector $\vec{P}$ is termed polarization field and represents the dipole moment of bound charges ζ_b per unit volume. Magnetization vector $\vec{M}$ takes into account the bound currents $\vec{i}_b$. They hold:

$$\operatorname{div}\left[\vec{P}\right] + \zeta_b = 0$$

[3]The equations have two variants. The so called "microscopic" set of equations involve total charge and current, which means that atomic charges and current must be included to model bound quantities. Maxwell's equations in matter model the latter by means of two auxiliary fields, the polarization $\vec{P}$ and the magnetization $\vec{M}$

$$\frac{\partial \vec{P}}{\partial t} + \mathrm{curl}\left[\vec{M}\right] = \vec{i}_b$$

with total charge and current defined by the sums $\zeta = \zeta_f + \zeta_b$, $\vec{i} = \vec{i}_f + \vec{i}_b$.

In order to lighten the modelization burden, it will be assumed that bound charges play a secondary effect, i.e. materials are without polarization and magnetization. Such an hypothesis *is constitutive* in nature and as a result all currents and charges are free and will be denoted henceforth as ζ and $\vec{i}$. Equations (2.4 - 2.7) thus trivially modify as follows:

$$\mathrm{div}\left[\vec{D}\right] = \zeta \tag{2.8}$$

$$\mathrm{curl}\left[\vec{H}\right] = \vec{i} + \frac{\partial \vec{D}}{\partial t} \tag{2.9}$$

Their combination lead to the continuity law (mathematical expression of conservation of charge) in terms of charge density ζ, electric current density $\vec{i}$ (in Ampères per unit area) and charge supply s^{c} (in Coulombs per unit volume per unit time). It reads

$$\frac{\partial \zeta}{\partial t} + \mathrm{div}\left[\vec{i}\right] = s^{\mathsf{c}} \tag{2.10}$$

with s^{c} deriving from a charge supply s^{ζ}, implicitly included in equation (2.8) as a part of charge ζ.

2.1.4 Balance of momentum

Following [20], the fundamental assumption will be made that the power expended by each "rate-like" kinematical descriptor can be expressed in terms of an associated force consistent with its own balance. Assuming small displacements and strains, the conjugated pairs within the internal expenditure of virtual power $\mathcal{W}_{\mathrm{int}}$ are the Cauchy stress $\boldsymbol{\sigma}$ and the infinitesimal strain tensor $\boldsymbol{\varepsilon}$, whose hatted amount $\hat{\boldsymbol{\varepsilon}}$ is taken here as a *virtual* velocity gradient. The principle of virtual power (with the two requirements: Power balance $\mathcal{W}_{\mathrm{ext}} = \mathcal{W}_{\mathrm{int}}$ in any sub volume, frame indifference for $\mathcal{W}_{\mathrm{int}}$ in any sub volume for any virtual velocity) leads to the usual balance of forces:

$$\mathrm{div}\left[\,\boldsymbol{\sigma}\,\right] + \vec{b} = \vec{0} \tag{2.11}$$

and to the symmetry of tensor $\boldsymbol{\sigma}$. Among bulk forces $\vec{b}$ the Lorentz forces of interaction of a moving charge density ζ with velocity $\vec{v}$ in an electric field $\vec{E}$ and magnetic field $\vec{B}$ will be denoted by $\vec{b}_{\zeta} = \zeta\,(\vec{E} + \vec{v} \times \vec{B})$. Balance equation (2.11) states that electric and stress fields are unavoidably related in the presence of charge densities. Such a relationship has a fundamental nature.

Note that the mass balance equations *relate to charged or neutral species* and Maxwell's equations *pertain to charged species, i.e. to ions and electrons* that flow into a lattice. The force balance *applies to a continuum, i.e. to the macroscopic, averaged, description of the lattice itself* which ions, electrons, and/or neutral particles flow through. The electrostatic forces are the only interactions between flowing particles and the lattice. If charge density vanishes - as for neutral Lithium intercalation into active particles or in view of the electroneutrality assumption, for instance - there is no coupling between flows and forces at all.

A coupling is indeed still expected in view of the influence of the stress state of the lattice on the predisposition of the lattice itself to convey mass flux. In other terms, of the swelling effect induced by the species concentration deforming the lattice. Such a coupling has a different, *constitutive* origin.

2.2 Electro-quasi-static Maxwell's law assumption

It is usual in the batteries literature not to consider the contribution of the magnetic field [6, 11, 12]. To formalize this simplification, the electro-quasi-static (EQS) model [14] is here adopted in place of the full Maxwell's equations set. Interference between the electric and magnetic phenomena are restricted to capacitive effects only (i.e. non inductive). By these assumptions, the time-dependent hyperbolic Maxwell's equations are replaced by parabolic equations that can be solved in a more simple way (see for instance [105], chapter 10).

In the light of EQS model, the time derivative of the magnetic field is negligible within Maxwell-Faraday's law of induction, which thus reads

$$\operatorname{curl}\left[\,\vec{E}\,\right] = \vec{0} \tag{2.12}$$

Accordingly, the electric field is irrotational and derives from an *electrostatic potential* ϕ:

$$\vec{E} = -\nabla\left[\,\phi\,\right] \tag{2.13}$$

The impingement of the magnetizing field field $\vec{H}$ in Ampère's law cannot be disregarded in the simplified framework of electro-quasi-statics[4]. Since $\operatorname{div}\left[\operatorname{curl}\left[\,\vec{H}\,\right]\right] = 0$, a differential form can be straightforwardly obtained from Ampère's law (2.9), after application of the divergence operator:

$$\operatorname{div}\left[\frac{\partial \vec{D}}{\partial\, t} + \vec{i}\right] = 0 \tag{2.14}$$

This form will be used in the sequel of the work, together with (2.13).

2.2.1 A simple justification

The origin of the electromagnetic waves is the coupling between the laws of Faraday and Ampère through the magnetic induction and the displacement current. By disregarding the induction contribution $\frac{\partial \vec{B}}{\partial t} \sim 0$ in Maxwell-Faraday's law (2.12), the electromagnetic waves are neglected as well. In support of the electro-quasi-static approximation, the following arguments can be forwarded, consistent with [106].

For the electro-quasi-static approximation to hold, the error introduced on $\vec{E}$ by ignoring the induction contribution $\frac{\partial \vec{B}}{\partial t}$ must be small compared to the quasi-static field $\vec{E}$ itself. According to [106], chapter 3, the electro-quasi-static approximation implies "sufficiently" slow time variations τ and small dimensions L so that

$$L\,\sqrt{\sharp\,\mathbb{\mu}} \ll \tau \tag{2.15}$$

[4] It will be shown in section 3.2.3 that Ampère's law plays a basic role in the interface conditions at the micro scale. The magnetizing field is customarily *linearly* related to the magnetic field by the constitutive relation $\vec{H} = \frac{1}{\mathbb{\mu}}\vec{B}$, $\mathbb{\mu}$ being the magnetic permeability of an isotropic material.

with $(\epsilon\mu)^{(-1/2)}$ the velocity of traveling electromagnetic waves in the material, provided that ϵ and μ are respectively the permittivity and the permeability of the same. $\epsilon = \epsilon_r \epsilon_0$ quantifies a material's ability to transmit (or "permit") an electric field. The permittivity of a homogeneous material is usually given relative to that of vacuum ϵ_0, as a relative permittivity ϵ_r. In the same way, $\mu = \mu_r \mu_0$ quantifies a material's ability to support the formation of a magnetic field and is usually given relative to that of vacuum μ_0, as a relative permeability μ_r.
The left hand side in formula (2.15) is the time required for an electromagnetic wave to propagate at velocity $(\epsilon\mu)^{(-1/2)}$ over a length L characterizing the system, e.g. the length of the edge of the RVE. τ is the characteristic time scale, i.e. a fraction (typically the time increment Δt in a time stepping procedure) of the time required by an ionic charge to cross the RVE. A simple estimate for Δt is the ratio

$$\frac{L}{v_{\mathrm{Li}^+}}$$

with v_{Li^+} the average velocity of the Lithium ions. The order of magnitude of such a velocity is evaluated by

$$\vec{h}_{\mathrm{Li}^+} = c_{\mathrm{Li}^+}\, \vec{v}_{\mathrm{Li}^+} = -D\, \nabla\, [\, c_{\mathrm{Li}^+}\,]$$

For a one-dimensional flow (with no tortuosity) it comes out

$$|v_{\mathrm{Li}^+}| = D\, \frac{|\nabla\, [\, c_{\mathrm{Li}^+}\,]\,|}{c_{\mathrm{Li}^+}} \sim 2\frac{D}{L}$$

thus ending up with the following condition

$$2D\, \sqrt{\epsilon\mu} \ll L \tag{2.16}$$

for the electro-quasi-static approximation to hold. Typical values of diffusivities for electrolytes are in the order of $10^{-11} m^2 s^{-1}$ whereas $\sqrt{\epsilon\mu}$ is in the order of $10^{-8} m^{-1} s$. For a characteristic RVEs size of $10^{-5} m$ this condition is largely satisfied.

2.3 The electroneutrality approximation

The mechanism of charge transport is radically different in solid particles and in the fluid electrolyte.

In *active particles*, charges are essentially transported by pure electrical conduction; the large mobility of electrons grants charge neutrality. The charge of Li^+ cation after intercalation into the active particles is instantaneously wiped out by the transport of electrons over the current collectors towards the Stern and the Gouy-Chapman layers. As a consequence, the intercalation of Lithium in active particles is considered to be neutral.

Charge transport in the *electrolyte* on the other side is exclusively due to ionic transport. In fact the transfer of electrons into the electrolyte would result in the reduction of Lithium ions in the electrolyte to metallic Lithium. Such a process is considered to be an interesting potential degradation mechanism in Li-ion batteries but it is not taken into account in the present model.

Charges localize in the electrolyte near the interface with active particles, causing an intense electric field to develop in two regions (the Stern and the Gouy-Chapman layers)

where the oxidation-reduction reactions effectively take place. According to the literature [6], the size of such a diffuse double layer structure is in the order of 10 to $20nm$. The RVE that will be analyzed (see Section 3.1.1) has a characteristic length three orders of magnitudes larger than the double layer size. Concentrated electrolytes are neutral on this scale due to the strong Coulomb interactions between the ions leading to an extremely small Debye screening length.

Intermezzo *- An excellent discussion on the origin of the electroneutrality assumption was disclosed in [7]. By combining Gauss's Law (2.8) in terms of the electrostatic potential (2.13) with charge density (2.2), the well-known Poisson equation results*

$$\Delta\,[\,\phi\,] + \frac{F}{\mathfrak{f}} \sum_{\alpha} z_\alpha\, c_\alpha = 0 \tag{2.17}$$

To write a dimensionless form of the Poisson equation in terms of concentration and electric potential one makes use of the "thermal voltage" $\phi^* = RT/F$ and the bulk concentration of the electrolyte c_{bulk} to write:

$$\frac{RT\,\mathfrak{f}}{F^2 c_{bulk}}\,\Delta\left[\,\frac{\phi}{\phi^*}\,\right] + \sum_{\alpha} z_\alpha\,\frac{c_\alpha}{c_{bulk}} = 0 \tag{2.18}$$

The ratio

$$r_D = \sqrt{\frac{1}{2}\,\frac{\mathfrak{f}}{c_{bulk}}\,\frac{RT}{F^2}} \tag{2.19}$$

is termed Debye length[5]*. It assesses a charge electrostatic effect in solution, and measures how far those effects persist. The Debye length is the characteristic length scale in equation (2.18) and sets the scale for variations in the potential and in the concentrations of charged species. As it is typically in the order of a few nanometers in battery cells electrolyte, for bounded potential second derivatives it holds*

$$\left|\sum_{\alpha} z_\alpha\, c_\alpha\right| \ll 1 \tag{2.20}$$

Enforcing that the sum $\sum_\alpha z_\alpha\, c_\alpha$ is identically zero leads to a new equation, which is often used instead of the Gauss law. In the present paper this approach is not pursued, rather the influence of equation (2.20) is investigated in the balance equations of Section 2.1. □

The distribution of electric charge ζ in the electrolyte solution is due to an unbalance of concentration between anions and cations, in light of Faraday's law. Electroneutrality, justified as in (2.20), implies that charge separation is almost impossible, i.e. that neutrality is maintained in the solution. Equation (2.20) reflects physical properties of the processes in an average sense, and has to be considered as an approximation, as correctly pointed out in recent literature [7].

Notwithstanding its nature, electroneutrality in the form

$$\sum_{\alpha} z_\alpha\, c_\alpha = 0 \tag{2.21}$$

[5] c_{bulk} [$\mathrm{mol\,m^{-3}}$] stands for the bulk concentration of salt LiX, T [K] for the absolute temperature, R [$\mathrm{J\,K^{-1}\,mol^{-1}}$] for the universal gas constant, F [$\mathrm{A\,s\,mol^{-1}}$] for Faraday's constant. The Debye length r_D is therefore measured in m.

has been largely used instead of Gauss's law (2.8) in batteries modeling (see among others [6], page 286). As the latter is a fundamental balance equation, using electroneutrality in its place leads to the paradox that the electric field is not constrained to satisfy Maxwell's equations (see for instance [10], fig. 3 and comments therein).

Numerical analyses reveal that the deviation from electroneutrality is small, ten orders of magnitude with respect to the equilibrium electrolyte concentration (see [6], page 286 and [10]). According to the data commonly available in the literature [10], the order of magnitude of the Lorentz forces $\vec{b}_\zeta$ is a few Newtons per cubic meter, completely insignificant with respect to those due to purely mechanical effects. The evidence is obvious for electrostatic forces in deformable dielectric materials [107] and was observed by Toupin in the fifties [108]. Electroneutrality assumption therefore allows to uncouple the mechanical and electric fields in the force balance equation (2.11), which in the absence of mechanical body forces becomes homogeneous.

The electric charge ζ is related by eq. (2.2) to the unbalance of concentration by Faraday's constant. Since the ratio of Faraday's constant and the permittivity amounts at $\frac{F}{\mathfrak{f}} \sim 1.1 \cdot 10^{17} \mathfrak{f}_r \, \frac{\mathrm{Vm}}{\mathrm{mol}}$, the observed deviation from electroneutrality may provide electric field contributions comparable to those in the battery cell (see again [10]). Accordingly, usage of electroneutrality *inside Gauss's law does not seem to be appropriate.*

Chapter 3
Multiscale formulation

3.1 Computational homogenization in batteries

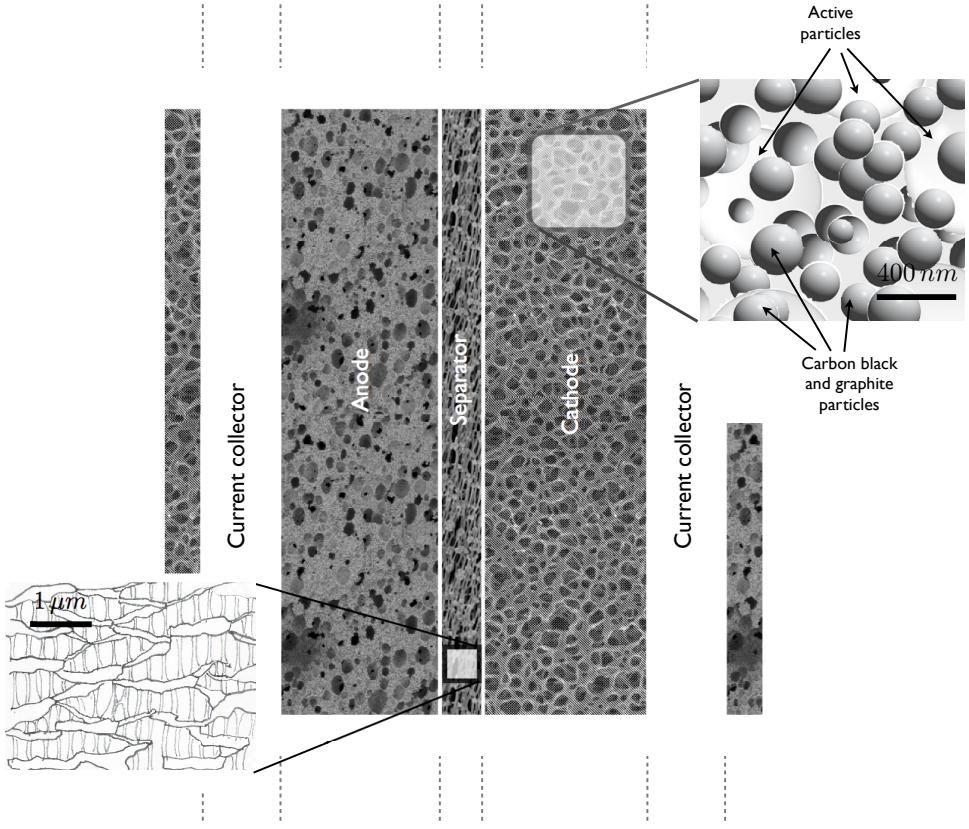

Figure 3.1: *Sketch of a Li-ion battery cell with porous electrodes. Additives are used to create conductive networks in both electrodes, to increase the electronic conductivity. Additives include large (graphite) and small (carbon black) conductive particles, that are bound to the active particles that host Lithium by a polymer binder (PVDF for instance). Separator scanning electrode microscope images can be found for instance in [53].*

Two scales will be considered in modeling *composite electrodes and porous separators* Ω_s whereas a single macroscopic scale is adequate to model the *metallic electrodes*, the *current collectors*, as well as all other parts that are homogeneous - see Figure 3.1.

The macroscopic scale modeling hinges on the theory for porous materials, taking into account the pore-filling electrolyte[1] (from now on with subscript e) and the porous solid material (subscript s). At the microscopic level, the electrolyte is also denoted with subscript e and the electrode (subscript s) is separated into its particles compound (active particles (subscript a) and conducting particles (subscript c)). The RVE contains all solid phases and the pore-filling electrolyte. Superscript M still refers to the macro scale and distinguishes it from the microscale, denoted with a lower case superscript m.

At the macroscopic scale, the intercalation of Lithium into the particles is described by a volume supply s_{Li}. The amount of the intercalated Lithium s_{Li} and the constitutive behavior for all phenomena involved (diffusion, migration, intercalation, and the mechanical coupling) are to be determined. Those quantities are upscaled from the underlying microstructure.

At the micro-scale all fundamental mechanisms are modeled in detail. Scale transitions are invoked to:

- define the micro scale boundary value problem (*macro to micro* scale transition, section 3.4.1) by linking it to the controlling macroscopic variables;
- provide tangent operators and updated values of the (dual) macroscopic fields (*micro to macro* scale transition, section 3.4.2), i.e. the average stress field, ionic mass fluxes, electron current density, concentration of ions in the electrolyte and of Lithium in the electrode, intercalation supply of neutral Lithium in the electrode. In order to upscale all these quantities, a suitably extended Hill-Mandel condition and the mass conservation across the scales will be imposed.

3.1.1 RVE dimensions

The choice of the RVE is a fundamental issue in the theory of composite materials. According to *Drugan and Willis* [110], an RVE may be defined in two different ways. It can be considered as the smallest microstructural volume for which the averages of properties as stresses, strains, constitutive moduli represent with "sufficient accuracy" the mean macroscopic response (see e.g. [97]). Accordingly, RVE's size is influenced by the material behaviour of the microstructural components. A second definition requires the RVE to be statistically representative of the microstructure, that is to essentially include a sampling of all possible microstructural configurations occurring in the composite. This definition leads to significantly larger RVEs than in the former case, as the microstructural element must incorporate several kinds of material heterogeneities. Based on this definition, statistical methods have been presented to determine the size of the RVE and the number of inclusions to consider, see among the others [111–113].

In order to clearly describe the physical range of the RVE dimensions, the electrode compound materials should be specified. Representative models of the battery microstructure based on experimentally obtained statistical information have been addressed in the literature. In [114], the three dimensional microstructure of a *graphite* porous electrode has been analyzed via tomographic techniques. The minimum RVE size is estimated as $43 \times 60 \times 60 \mu m$ according to tailored statistical analyses. An estimate of the characteristic dimensions of the RVE is derived in [115] for $LiCoO_2$ electrode material (RVE edge $\approx 30 \mu m$). The microscale arrangement of active particles, carbon, binder and pores is recovered from statistical analyses of 2D cross sections of the electrode achieved through scanning electron microscope with

[1] The electrolyte in the current technology of Li-ion batteries [12] might be a solid, a liquid or a gel. An up to date discussion on the subject can be found in [109].

focused ion beam. A similar approach is employed for electrodes utilizing $LiFePO_4$ as active material where the RVE size is measured as $5 \times 5 \times 15 \mu m$ [116].

3.1.2 Concurrent time modeling

Time modeling at the microscale

In two-scale formulations for heat conduction [98, 99], a *steady-state mass transport* hypothesis was adopted at the microscale. Steady-state mass and charge transport is justified at the micro level in the presence of fast diffusive response[2] or negligibly small RVEs. Steady-state would imply instantaneous changes for concentration and potentials at the micro scale, dictated through the boundary conditions that originate from the macro scale problem, which is time-dependent.

In order to verify if steady-state mass and charge transport can be applied to battery modeling, dimensional analysis arguments are invoked. By choosing a trivial, yet compatible, constitutive law of the kind

$$\vec{h}_\alpha = -D \, \nabla [\, c_\alpha \,]$$

and no bulk terms for all α, the mass balance equations lead to the homogeneous diffusion equation

$$\frac{\partial c_\alpha}{\partial t} - D \, \Delta [\, c_\alpha \,] = 0 \tag{3.1}$$

Assuming a one-dimensional flow and defining a non-dimensional time $t^* = t/\bar{t}$, length $s = x/L$ and concentration $\xi = c/c_{bulk}$ the following non-dimensional form of the homogeneous diffusion equation results

$$\frac{L^2}{D\bar{t}} \frac{\partial \xi_\alpha}{\partial t^*} = \Delta [\, \xi_\alpha \,] \tag{3.2}$$

If the dimensionless number $\frac{L^2}{D\bar{t}}$ would be zero, then $\Delta [\, \xi_\alpha \,] = 0$, which is precisely the steady-state mass and charge transport hypothesis at the microscale. Such an hypothesis can be thus justified for "sufficiently small" values of $\frac{L^2}{D\bar{t}}$, at least for smooth variations in time of the concentration. Typical values of diffusivities for electrolytes are in the order of $10^{-11} m^2 s^{-1}$, whereas characteristic RVEs size described in literature and reviewed in Section 3.1.1 is in the order of $10^{-5} m$. Literature analysis show [10] that the time-frame required for the development of a steady concentration profile in the electrolyte is in the order of $10^2 \div 10^3 s$, with a typical time step in the order of $1s$ in numerical schemes. From this rough estimate it turns out that $\frac{L^2}{D\bar{t}} \sim 10$, which implies that the steady-state mass and charge transport hypothesis at the microscale is *not* satisfied for the battery problem.

Time scale separation

Assume that a liquid electrolyte fills voids in porous electrodes and separators. The time scales during lithiation/extraction are dictated by two mobilities, the one of the ions in the electrolyte and the one of the neutral Lithium in the active particles during intercalation/deintercalation. The two mobilities differ several order of magnitudes: the diffusivity for ions is in the order of $10^{-11} m^2 s^{-1}$, whereas the one for neutral Lithium takes a value in the order of $10^{-15} m^2 s^{-1}$. According to the literature, the average size for the active particles is in the order of $1 \mu m$ or even less for Silicon particles [57], whereas the electrode length is

[2] Diffusive processes scale with $1/L^2$, L being the length scale [117]. The time for a particle to reach the steady state when concentration is changed scales with $1/L^2$.

in the order of $100\mu m$ - see [48] and references therein. As shown in equation (3.2) diffusive processes scale with L^2, i.e. the time scale for the species (either an ion in the solution or neutral Lithium in the active particle) to travel a distance L is given on the average by L^2/D. By comparing the macroscopic and microscopic ratios L^2/D, it turns out that time scales do not separate, i.e. all active particles in the *electrode* are lithiated concurrently. Accordingly, a concurrent time modeling between the macro and micro scales will be carried out.

3.2 Microscale

The evolution of electrochemical and mechanical fields at the finest scale is defined in an RVE of volume V and boundary ∂V. It is provided with the essential physical and geometrical information on the microstructural components, i.e. the active particles, the conductive particles, and the pore filling electrolyte[3].

Two kinds of particles are modeled within the RVE: the active particles (collectively occupying domain V_a) and the conductive particles that define domain V_c. Accordingly, the *solid* phase will occupy volume $V_s = V_a \cup V_c$. The electrolyte will fill all the remaining part V_e of the RVE; V_e is such that $V = V_s \cup V_e$.

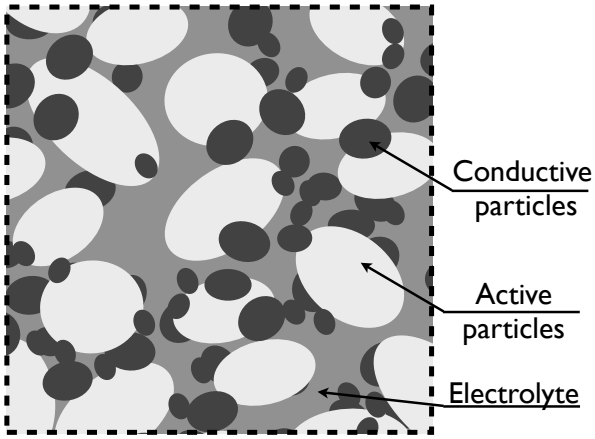

Figure 3.2: *Sketch of an RVE*

3.2.1 Balance equations

The microscopic *mass balance* equations characterize the species transport in two phases, namely the transport of neutral Lithium in the active particles and the transport of Li^+ and X^- ions in the electrolyte.

$$\frac{\partial c^m_{\mathrm{Li}}}{\partial t} + \mathrm{div}\left[\vec{h}^m_{\mathrm{Li}}\right] = 0 \qquad \vec{x} \in V_a \tag{3.3a}$$

$$\frac{\partial c^m_{\mathrm{Li^+}}}{\partial t} + \mathrm{div}\left[\vec{h}^m_{\mathrm{Li^+}}\right] = 0 \qquad \vec{x} \in V_e \tag{3.3b}$$

$$\frac{\partial c^m_{\mathrm{X^-}}}{\partial t} + \mathrm{div}\left[\vec{h}^m_{\mathrm{X^-}}\right] = 0 \qquad \vec{x} \in V_e \tag{3.3c}$$

[3]This chapter extends contents of [8, 9]

The concentration of neutral Lithium is identically zero in the conductive particles. There is no supply of species at the micro scale, as: i) intercalation phenomena are analytically described as mass fluxes across interfaces; ii) the degree of dissociation of the binary salt in the solution is assumed to be complete. The latter condition is generally not satisfied in reality, as it is known from literature that the degree of dissociation of Li-salts dissolved in an organic solvent is incomplete. Modeling the dissociation rate would require a bulk term in the mass balance equation of the ionic species accompanied with a further mass balance equation for the undissociated salt [10].

Current density in active and conductive particles is due to electron transport, and the local form of mass and charge conservation read:

$$\frac{\partial c^m_{\mathrm{e}^-}}{\partial t} + \operatorname{div}\left[\,\vec{h}^m_{\mathrm{e}^-}\,\right] = \frac{\partial c^m_{\mathrm{e}^-}}{\partial t} - \frac{1}{F}\operatorname{div}\left[\,\vec{i}^m_{\mathrm{e}^-}\,\right] = 0 \qquad \vec{x} \in \{V_a \cup V_c\} \tag{3.4}$$

Charge and mass equations for electrons are equivalent in the assumption that the positively charged cores are steady.

Either by applying the divergence operator to Ampère's law (2.9) or by the time derivative of Gauss's law (2.8), taking into account Faraday's law (2.3), the electric displacement field (in the electrolyte denoted with $\vec{D}^m_e$, in the electrode with $\vec{D}^m_s$) is governed by the following rate equations

$$\operatorname{div}\left[\,\frac{\partial \vec{D}^m_e}{\partial t} + F\,(\vec{h}^m_{\mathrm{Li}^+} - \vec{h}^m_{\mathrm{X}^-})\,\right] = 0 \qquad \vec{x} \in V_e \tag{3.5a}$$

$$\operatorname{div}\left[\,\frac{\partial \vec{D}^m_s}{\partial t} + \vec{i}^m_{\mathrm{e}^-}\,\right] = 0 \qquad \vec{x} \in \{V_a \cup V_c\} \tag{3.5b}$$

Inertia effects as well as non electrostatic bulk forces are neglected. In light of the electroneutrality assumption, electrostatic forces are of secondary order. The *balance of momentum* (2.11) specializes as:

$$\operatorname{div}[\,\boldsymbol{\sigma}^m\,] = \vec{0} \qquad \vec{x} \in V \tag{3.6a}$$

$$\operatorname{skw}[\,\boldsymbol{\sigma}^m\,] = \mathbf{0} \qquad \vec{x} \in V \tag{3.6b}$$

3.2.2 An "averaged" description of electrode kinetics

Consider the Lithium deposition or dissolution reaction

$$\mathrm{Li} \rightleftarrows \mathrm{Li}^+ + \mathrm{e}^- \tag{3.7}$$

that takes place at the active particle/electrolyte interface, which is assumed to be equipped with all thermodynamic requirements as in [118].

If the chemical potential μ_{Li} exceeds the sum of the electrochemical potential of the Lithium ions in the solution $\overline{\mu}_{\mathrm{Li}^+}$ and of the electrons in the metal $\overline{\mu}_{\mathrm{e}^-}$ then Li dissolution takes place. The imbalance of electrochemical potentials in the reaction (3.7) is the driving force for the electrode reaction. It is measured by the amount

$$\overline{\gamma} = \mu_{\mathrm{Li}} - \overline{\mu}_{\mathrm{e}^-} - \overline{\mu}_{\mathrm{Li}^+} \tag{3.8}$$

which is usually termed thermodynamic excess. Thermodynamic equilibrium is reached if and only if $\overline{\gamma} = 0$.

Reaction (3.7) cannot be treated as a simple chemical reaction in a single phase since the process must generate or consume electrical charge, and this will always be accompanied by the formation of an electric field and an electrostatic potential difference between the two phases. A large gradient in the electric field takes place in a nano metric size double layer, that is here[4] identified with a discontinuity locus at the interface between solid particles and electrolyte.

By identifying the double layer as a zero-thickness interface, a discontinuity $\xi = [\![\phi]\!]$ in electrical potential arises between an electrode and its surrounding solution.

It will be assumed henceforth that the rate of chemical reaction (3.7) is very rapid compared to the mass flux governed by mass balance equations. Such an assumption usually connotes a *nerstian reaction*. Under this condition (see [11], chapter 1.4), surface concentration of species are related to the electrode potential by the well known Nernst equation. By denoting the reaction Gibbs energy with

$$\gamma = \mu_{\mathrm{Li}} - \mu_{\mathrm{e}^-} - \mu_{\mathrm{Li}^+} \tag{3.9}$$

Nernst equation reads

$$\xi + \frac{\gamma}{F} = 0 \tag{3.10}$$

It describes the conversion of the Gibbs reaction energy into electric energy and holds if the kinetics of electron transfer is rapid, so that the concentration of Li and Li^+ at the electrode surface can be assumed *locally* at equilibrium $\overline{\gamma} = 0$ with the electrode potential[5].

When a battery cell is assembled at open circuit, electrochemical reactions take place and a potential discontinuity ξ rises to inhibit further dissolution, leading the *whole system* to equilibrium with a vanishing net current across the interface. The value of ξ at such a global thermodynamic equilibrium for reaction (3.7) is termed ξ^{Nernst} and the potential difference

$$\chi = \xi - \xi^{Nernst} \tag{3.11}$$

is called *surface over-potential*. A net current passing between electrode and solution is related to χ.

The current density in the outward normal direction $\vec{i} \cdot \vec{n}$ at the surface of an electrode will be denoted by i_{BV}. The relationship between averaged current density and surface over-potential is usually described by means of the *Butler-Volmer equation* [6, 11, 88, 118]:

$$i_{BV} = \mathrm{i}_0 \left\{ \exp\left[\frac{(1-\beta)}{RT} F \chi\right] - \exp\left[-\frac{\beta}{RT} F \chi\right] \right\} \tag{3.12}$$

There are two kinetic parameters in equation (3.12), namely i_0 and β. Experimental data are required to estimate these parameters. Factor i_0, termed *exchange current density*, depends

[4] The modeling of the double layer is mainly based on the work of Stern, Gouy and Chapman, see [88] for details.

[5] This assumption reminds to Oriani's law for H_2 diffusion in metals, according to which different populations of H are in thermodynamic equilibrium during the whole diffusion process [119].

on the composition of the solution adjacent to the electrode - see [11], formula (3.4.4). It is often assumed to be constant at a metallic anode. Parameter β is a *symmetry factor* and represents the fraction of the surface over-potential that promotes cathodic reaction. It is widely assumed to be $\beta = 1/2$. The reader may refer to specialized literature [6, 11, 120] for further details.

The mass flux in the outward normal direction $\vec{h} \cdot \vec{n}$ at the surface of an electrode will be denoted by h_{BV}. It is related by stoichiometry (3.7) and by Faraday's law to the current density in the same direction at the same location

$$i_{BV} = F\, h_{BV} \tag{3.13}$$

Nernst equation (3.10) induces a constraint along the active particles/electrolyte interface to the otherwise independent chemical and electric potential fields.

At low surface over-potentials, Butler-Volmer equation can be linearized as

$$i_{BV} = \frac{\mathrm{i}_0}{RT}\, F\, \chi \tag{3.14}$$

providing a significant computational simplification.

As observed in [121], by using the Butler-Volmer equation, stress can only influence the reaction through the electrochemical potentials, i.e. by altering the concentrations of the reacting species, because mechanical fields do not enter equation (3.12) directly. A more refined model of the interaction of mechanics and electrochemical reactions involve the mechanical characterization of the Stern and Gouy-Chapman layers, the former of which has atomistic size. Such an attempt is not carried out here, the reader may refer to [88, 121].

3.2.3 Weak form and interface conditions

Weak form - This section aims at building up the weak form of the balance equations to be used for the micro to macro scale transition and, upon further development at a later stage, to enable a numerical approximation of the partial differential equations problem at the micro-scale. Formally speaking, the weak formulation is obtained after multiplication of the strong form of the balance equations (3.3-3.6) by a suitable set of test functions and performing an integration upon the domain, exploiting Green's formula with the aim of reducing the order of differentiation. Such a weak form is given here in terms of the scalar potentials and displacements, collected in column y^m, in a time interval $[0, t_f]$ as:

$$\text{Find } y^m \in \mathcal{V}^{[0,t_f]} \text{ such that } \quad \frac{\mathrm{d}}{\mathrm{d}t} b^m\left(\hat{y}^m, z^m(t)\right) + a^m(\hat{y}^m, y^m(t)) = f(\hat{y}^m) \quad \forall \hat{y}^m \in \mathcal{V}$$

where b^m, z^m, a^m, and f will be detailed in what follows.

Let's construct the weak form of the generic mass balance equation (3.3)

$$\begin{aligned}
&\int_{V_\alpha} \hat{\mu}_\alpha^m \left\{ \frac{\partial c_\alpha^m}{\partial t} + \operatorname{div}\left[\, \vec{h}_\alpha^m \,\right] \right\} \mathrm{d}V = \\
&= \int_{V_\alpha} \hat{\mu}_\alpha^m \, \frac{\partial c_\alpha^m}{\partial t} \, \mathrm{d}V + \int_{V_\alpha} \hat{\mu}_\alpha^m \operatorname{div}\left[\, \vec{h}_\alpha^m \,\right] \mathrm{d}V = \\
&= \int_{V_\alpha} \hat{\mu}_\alpha^m \, \frac{\partial c_\alpha^m}{\partial t} \, \mathrm{d}V + \int_{V_\alpha} \operatorname{div}\left[\, \hat{\mu}_\alpha^m \, \vec{h}_\alpha^m \,\right] - \nabla\left[\, \hat{\mu}_\alpha^m \,\right] \cdot \vec{h}_\alpha^m \, \mathrm{d}V = \\
&= \int_{V_\alpha} \hat{\mu}_\alpha^m \, \frac{\partial c_\alpha^m}{\partial t} \, \mathrm{d}V - \int_{V_\alpha} \nabla\left[\, \hat{\mu}_\alpha^m \,\right] \cdot \vec{h}_\alpha^m \, \mathrm{d}V + \int_{\partial V_\alpha} \hat{\mu}_\alpha^m \, \vec{h}_\alpha^m \cdot \vec{n} \, \mathrm{d}\Gamma = 0
\end{aligned} \tag{3.15}$$

Within (3.15) one recognizes: i) a "time derivative" contribution $\int_{V_\alpha} \hat{\mu}_\alpha^m \, \frac{\partial c_\alpha^m}{\partial t} \, \mathrm{d}V$ to be included within the bilinear form $b^m(\hat{y}^m, z^m)$; ii) a bulk term $\int_{V_\alpha} \nabla[\,\hat{\mu}_\alpha^m\,] \cdot \vec{h}_\alpha^m \, \mathrm{d}V$ that fits into $a^m(\hat{y}^m, y^m(t))$; iii) a contribution defined at the interface between particles and electrolyte as well as at the RVE boundary.

Likewise, the weak form of Ampère's law (3.5) is given as

$$\begin{aligned} &\int_{V_\alpha} \hat{\phi}_\alpha^m \, \mathrm{div} \left[\frac{\partial \vec{D}_\alpha^m}{\partial t} + \vec{i}_\alpha^m \right] \mathrm{d}V = \\ &\quad - \int_{V_\alpha} \nabla \left[\hat{\phi}_\alpha^m \right] \cdot \frac{\partial \vec{D}_\alpha^m}{\partial t} \, \mathrm{d}V - \int_{V_\alpha} \nabla \left[\hat{\phi}_\alpha^m \right] \cdot \vec{i}_\alpha^m \, \mathrm{d}V + \\ &\quad + \int_{\partial V_\alpha} \hat{\phi}_\alpha^m \left\{ \frac{\partial \vec{D}_\alpha^m}{\partial t} + \vec{i}_\alpha^m \right\} \cdot \vec{n} \, \mathrm{d}\Gamma = 0 \end{aligned} \tag{3.16}$$

and will be written for the electrolyte and the electrode, without separating active and conductive particles.

Similarly for the equilibrium equations (3.6) in rate[6] form

$$\begin{aligned} &\int_V \hat{\vec{u}}^m \cdot \, \mathrm{div} \left[\frac{\partial \boldsymbol{\sigma}^m}{\partial t} \right] \mathrm{d}V = \\ &\quad - \int_V \hat{\boldsymbol{\varepsilon}}^m : \frac{\partial \boldsymbol{\sigma}^m}{\partial t} \, \mathrm{d}V + \int_{\partial V} \hat{\vec{u}}^m \cdot \, \frac{\partial \boldsymbol{\sigma}^m}{\partial t} \cdot \vec{n} \, \mathrm{d}\Gamma = 0 \end{aligned} \tag{3.17}$$

on the whole RVE.

Faraday's law (3.13) is weakly imposed along the boundary of the electrolyte, i.e. at the location where the oxidation/reduction reaction takes place, through the multiplication for a Lagrange multiplier λ which takes the meaning of the *projection of the curl of the magnetizing field along the normal* $\vec{n}_e$

$$\int_{\partial V_s \cap \partial V_e} \hat{\lambda}^m \, \left[\lambda^m - F \, h_{BV}\left(\chi^m\right) \right] \, \mathrm{d}\Gamma = 0 \tag{3.18}$$

Interface conditions - In the present multiscale framework, continuity of displacements and surface tractions equilibrium are imposed along all interfaces. Referring to Figure 3.3 for notation, the aforementioned conditions along an interface $\partial V_a \cap \partial V_c$ between active particles and conductive particles read

$$\lim_{V_a \ni \vec{y} \to \vec{x}} \vec{u}\,(\vec{y}) = \lim_{V_c \ni \vec{z} \to \vec{x}} \vec{u}\,(\vec{z}) \tag{3.19a}$$

$$\lim_{V_a \ni \vec{y} \to \vec{x}} \boldsymbol{\sigma}^m(\vec{y}) \cdot \vec{n}_a\,(\vec{x}) + \lim_{V_c \ni \vec{z} \to \vec{x}} \boldsymbol{\sigma}^m(\vec{z}) \cdot \vec{n}_c\,(\vec{x}) = \vec{0} \tag{3.19b}$$

Similar conditions can be stated for active-active particles interfaces and conductive-conductive particles interfaces. This coupling is strong and implies essentially that the binder is modeled as a perfect adhesive with zero thickness. A cohesive interface model may be more adequate in terms of capability of transferring mass and charge against a critical detachment of particles but is still useless at this point since interface parameters cannot be measured yet. This relates to the failure mode of the electrodes, a topic that goes beyond the scope of the present paper and which constitutes subject of forthcoming work.

[6]The rate form choice has been made to give the meaning and the dimension of power to all contributions of the weak form. It's a purely formal choice, which however is required also in order to derive the dimensionless numbers that govern the numerical stability of the problem. In the implementation, other choices can of course be made.

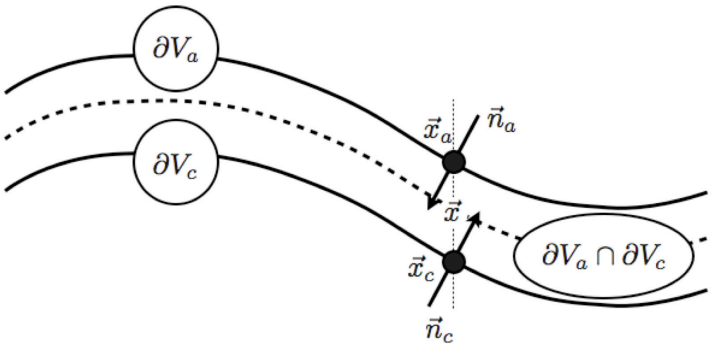

Figure 3.3: *Sketch of an interface $\partial V_a \cap \partial V_c$ between active particles and conductive particles and of the mechanical interaction that takes place. The interface $\partial V_a \cap \partial V_c$ is defined as the set of points $\vec{x}$ in which active V_a and conductive V_c particles are in contact. Therefore all point $\vec{x}$ that concurrently belong to the boundaries ∂V_a and ∂V_c constitute the interface. Outward normals $\vec{n}_a$ and $\vec{n}_c$ along ∂V_a and ∂V_c are defined as usual. In this figure, boundaries ∂V_a and ∂V_c are vertically translated with respect to the actual interface $\partial V_a \cap \partial V_c$ for the sake of clarity.*

Interface between active particles and conductive particles $\partial V_c \cap \partial V_a$ - Electrons are free to flow without causing discontinuities in the electric field and in potentials ϕ, μ_{e^-}. Neutral Lithium does not intercalate into conductive particles.

$$\vec{h}^m_{\mathrm{Li}} \cdot \vec{n}_a = 0 \qquad \vec{x} \in \partial V_c \cap \partial V_a \tag{3.20}$$

Interface between electrolyte and conductive particles $\partial V_e \cap \partial V_c$ - There is no intercalation neither of Li-ions nor of counterions. Electrons do not flow through the interface. The mass fluxes interface conditions are thus homogeneous:

$$\vec{h}^m_{\mathrm{Li}^+} \cdot \vec{n}_e = 0 \qquad \vec{x} \in \partial V_c \cap \partial V_e \tag{3.21a}$$
$$\vec{h}^m_{\mathrm{X}^-} \cdot \vec{n}_e = 0 \qquad \vec{x} \in \partial V_c \cap \partial V_e \tag{3.21b}$$
$$\vec{h}^m_{\mathrm{e}^-} \cdot \vec{n}_e = 0 \qquad \vec{x} \in \partial V_c \cap \partial V_e \tag{3.21c}$$

and there is no current transport along these interfaces.

In order to devise the interface conditions for the electric potential - see equation (3.16), Ampère's law (2.9) is invoked

$$\left(\frac{\partial \vec{D}^m}{\partial t} + \vec{i}^m \right) \cdot \vec{n} = \mathrm{curl} \left[\vec{H}^m \right] \cdot \vec{n} \tag{3.22}$$

It turns out therefore that the evaluation of the magnetizing field $\vec{H}^m$ is required. In order to evaluate it across interfaces, the differential problem (2.5) for $\vec{B}$ must be solved. In fact, interface conditions are the mere link between the magnetic and electric fields in the electro-quasi-static assumption. It will be assumed henceforth that the curl of the magnetizing field is continuous across all interfaces when projected in the normal direction

$$\left(\frac{\partial \vec{D}^m_s}{\partial t} + \vec{i}^m_{\mathrm{e}^-} \right) \cdot \vec{n}_c + \left(\frac{\partial \vec{D}^m_e}{\partial t} + \vec{i}^m_e \right) \cdot \vec{n}_e = 0 \qquad \vec{x} \in \partial V_c \cap \partial V_e$$

Under this assumption the evaluation of the magnetizing field $\vec{H}^m$ is not necessary and a Lagrange multipliers formulation, that will be described at a later stage (chapter 6), suffices.

Interface between electrolyte and active particles $\partial V_e \cap \partial V_a$ - There is no intercalation of X-anions, whereas a Faradaic reaction converts the oxidized Lithium to its neutral state before its diffusion into the active particles lattice. Electrode kinetics is here modeled via the Butler-Volmer equation (3.12), in terms of surface over potential χ, defined in equations (3.11). Interface conditions read:

$$\vec{h}^m_{\mathrm{Li}^+} \cdot \vec{n}_e = -h_{BV} \qquad \vec{x} \in \partial V_a \cap \partial V_e \tag{3.23a}$$

$$\vec{h}^m_{\mathrm{Li}} \cdot \vec{n}_a = h_{BV} \qquad \vec{x} \in \partial V_a \cap \partial V_e \tag{3.23b}$$

$$\vec{h}^m_{\mathrm{e}^-} \cdot \vec{n}_a = -h_{BV} \qquad \vec{x} \in \partial V_a \cap \partial V_e \tag{3.23c}$$

$$\vec{h}^m_{\mathrm{X}^-} \cdot \vec{n}_e = 0 \qquad \vec{x} \in \partial V_a \cap \partial V_e \tag{3.23d}$$

$$\left(\frac{\partial \vec{D}^m_s}{\partial t} + \vec{i}^m_{\mathrm{e}^-}\right) \cdot \vec{n}_a + \left(\frac{\partial \vec{D}^m_e}{\partial t} + \vec{i}^m_e\right) \cdot \vec{n}_e = 0 \qquad \vec{x} \in \partial V_a \cap \partial V_e \tag{3.23e}$$

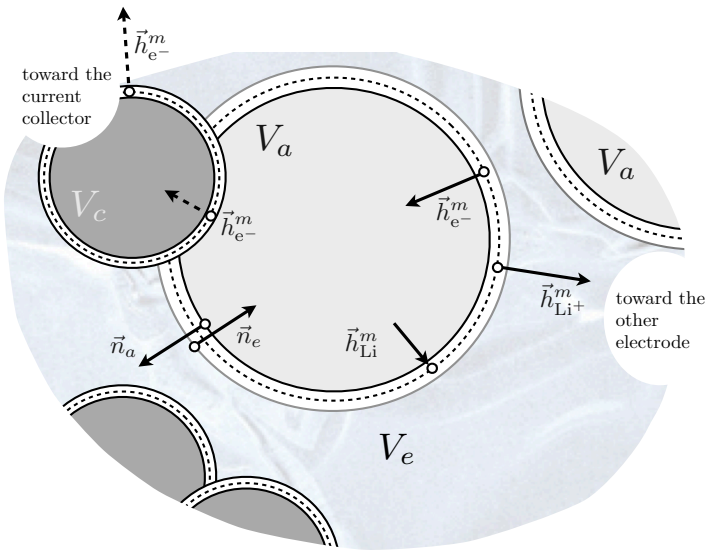

Figure 3.4: *Sketch of a process of* Li *oxidation in porous electrodes and its modeling by interface conditions (3.23)a-d. The Stern and Gouy-Chapman layers are here idealized as a zero-thickness interface $\partial V_a \cap \partial V_e$ between active particles and electrolyte, here depicted with a dashed line. The chemical reaction is thermodynamically described as a nernstian process [11]. Accordingly, the interface entails a discontinuity locus for the electric and the chemical potentials, (respectively the electric and the reaction Gibbs energies [118]). The chemical reaction kinetics is described by a Butler-Volmer equation, expressing the current density as a non linear function of the surface over-potential. Owing to Faraday's law, mass fluxes are related to the current density, as stated in conditions (3.23)a-d.*

In conclusion, a weak form can be given in terms of the potentials and displacements in a time interval $[0, t_f]$ as:

$$\text{Find } y^m \in \mathcal{V}^{[0,t_f]} \text{ such that} \qquad \frac{\mathrm{d}}{\mathrm{d}t} b^m\left(\hat{y}^m, z^m(t)\right) + a^m(\hat{y}^m, y^m(t)) = f(\hat{y}^m) \quad \forall \hat{y}^m \in \mathcal{V}$$

where

$$
\begin{aligned}
b^m\left(\hat{y}^m, z^m\right) = \\
&- \int_{V_a} \hat{\mu}^m_{\mathrm{Li}}\, c^m_{\mathrm{Li}}\, \mathrm{d}V - \int_{V_a \cup V_c} \hat{\mu}^m_{\mathrm{e}^-}\, c^m_{\mathrm{e}^-}\, \mathrm{d}V - \int_{V_e} \hat{\mu}^m_{\mathrm{Li}^+}\, c^m_{\mathrm{Li}^+} + \hat{\mu}^m_{\mathrm{X}^-}\, c^m_{\mathrm{X}^-}\, \mathrm{d}V + \\
&- \int_{V_a \cup V_c} \nabla\left[\,\hat{\phi}^m_s\,\right] \cdot \vec{D}^m_s\, \mathrm{d}V - \int_{V_e} \nabla\left[\,\hat{\phi}^m_e\,\right] \cdot \vec{D}^m_e\, \mathrm{d}V + \int_V \hat{\boldsymbol{\varepsilon}}^m : \boldsymbol{\sigma}^m\, \mathrm{d}V
\end{aligned}
$$

$$
\begin{aligned}
a^m\left(\hat{y}^m, y^m\right) = \\
&+ \int_{V_a} \nabla\left[\,\hat{\mu}^m_{\mathrm{Li}}\,\right] \cdot \vec{h}^m_{\mathrm{Li}}\, \mathrm{d}V + \int_{V_a \cup V_c} \nabla\left[\,\hat{\mu}^m_{\mathrm{e}^-}\,\right] \cdot \vec{h}^m_{\mathrm{e}^-}\, \mathrm{d}V + \\
&+ \int_{V_e} \nabla\left[\,\hat{\mu}^m_{\mathrm{Li}^+}\,\right] \cdot \vec{h}^m_{\mathrm{Li}^+} + \nabla\left[\,\hat{\mu}^m_{\mathrm{X}^-}\,\right] \cdot \vec{h}^m_{\mathrm{X}^-}\, \mathrm{d}V + \\
&- \int_{V_a \cup V_c} \nabla\left[\,\hat{\phi}^m_s\,\right] \cdot \left(-F\, \vec{h}^m_{\mathrm{e}^-}\right) \mathrm{d}V - \int_{V_e} \nabla\left[\,\hat{\phi}^m_e\,\right] \cdot \left(F\, \left(\vec{h}^m_{\mathrm{Li}^+} - \vec{h}^m_{\mathrm{X}^-}\right)\right)\, \mathrm{d}V + \\
&- \int_{\partial V_s \cap \partial V_e} \hat{\xi}^m\, \lambda^m + \hat{\gamma}^m\, h_{BV}(\chi^m) + \hat{\lambda}^m\, \left[\lambda^m - F\, h_{BV}\left(\chi^m\right)\right]\, \mathrm{d}\Gamma
\end{aligned}
\tag{3.24}
$$

with $z^m = \{c^m_{\mathrm{Li}},\, c^m_{\mathrm{e}^-},\, c^m_{\mathrm{Li}^+},\, c^m_{\mathrm{X}^-}\}$, $y^m = \{\mu^m_{\mathrm{Li}}, \mu^m_{\mathrm{e}^-}, \mu^m_{\mathrm{Li}^+}, \mu^m_{\mathrm{X}^-}, \phi^m_s, \phi^m_e, \vec{u}^m, \lambda^m\}$. The unknown field λ^m along the interface acts as a Lagrange multiplier[7]. The Gibbs reaction energy is defined according to equations (3.9) as

$$
\hat{\gamma}^m = \hat{\mu}^m_{\mathrm{Li}} - \hat{\mu}^m_{\mathrm{e}^-} - \hat{\mu}^m_{\mathrm{Li}^+} \tag{3.25}
$$

the potential jump as

$$
\hat{\xi}^m = \hat{\phi}^m_s - \hat{\phi}^m_e
$$

Mass flux across the interface obeys to Butler-Volmer equation

$$
h_{BV}(\chi^m) = \frac{\mathrm{i}_0}{F}\, \left\{ \exp\left[\frac{(1-\beta)}{R\,T}\, F\, \chi^m\right] - \exp\left[-\frac{\beta}{R\,T}\, F\, \chi^m\right] \right\} \tag{3.26}
$$

with the surface over potential χ^m defined by equation (3.11) and imposing $h_{BV} = 0$ along interface $\partial V_c \cap \partial V_e$. The right hand side $f(\hat{y}^m)$ is a functional on $\mathcal{V}^{[0,t_f]}$ that accounts for possible non-homogeneous Neumann boundary conditions, as bulk terms vanish in the strong form of the balance equations. A discussion on these boundary conditions is deferred to section 3.4.1, where it will be clarified that $f(\hat{y}^m)$ vanishes. A formal proof is given in appendix 3.5.

Note that in the weak form (3.24) Faraday's law has been imposed strongly, by implicitly defining

$$
\vec{i}^m_{\mathrm{e}^-} = -F\, \vec{h}^m_{\mathrm{e}^-}\,, \qquad \vec{i}^m_e = F\, \left(\vec{h}^m_{\mathrm{Li}^+} - \vec{h}^m_{\mathrm{X}^-}\right) \tag{3.27}
$$

The identification of the functional spaces $\mathcal{V}^{[0,t_f]}, \mathcal{V}$ falls beyond the scope of the present paper. Columns z^m and y^m collect the time-dependent unknown fields. Column $\hat{y}^m$ collects the steady-state test functions that correspond to the unknown fields in y^m.

[7]The weak form proof, deferred in appendix 3.5, manifests that λ^m has the meaning of the projection of the curl of the magnetizing field along the normal across an interface

The weak form here proposed is remarkably different from other forms in the literature [48, 50, 51] since it is written in terms of potentials rather than concentrations. Through this choice, the weak form maintains the usual physical meaning of power expenditure, which is mandatory to establish the correct scale transitions. A similar path of reasoning has been recently followed for the problem of hydrogen embrittlement [83], that indeed shows several similarities with the one at hand.

To computationally solve the (either weak or strong) problem, constitutive equations must be specified. Column z^m is dependent on y^m through the constitutive equations. Ellipticity of operators, functional and numerical properties of the solution and of its approximation depend on the constitutive assumptions and on the choice of the correct functional spaces $\mathcal{V}^{[0,t_f]}, \mathcal{V}$.

It has been observed that the surface over-potential depends on the reaction (3.7) rate. The modeling here proposed captures this behavior relating the surface over-potential to the macroscopic boundary conditions at the largest scale, i.e. χ will depend on the charge/discharge rates.

3.3 Macroscale

At each point $\vec{x}$ of porous composite electrodes Ω_s - see Figure 3.1 - two continuous phases superpose as usual for models of porous materials [122].

The porosity v_e is the fraction of void space in the porous material. It is defined by the ratio:

$$v_e = \frac{V_e}{V}$$

where V_e is the volume of void-space - filled by the electrolyte - and V is the total volume of material, including the solid and void components. The complementary ratio is denoted by $v_s = 1 - v_e$.

In more detail, the volume ratios of each microscopic phase with respect to the overall volume V *in the electrodes* is defined as:

$$v_a = \frac{V_a}{V}\,, \qquad v_c = \frac{V_c}{V} \tag{3.28}$$

It turns out $v_s = v_a + v_c = V_s/V$, where $V_s = V_a + V_c$ is the volume of the electrode compound. Porosity can actually be considered a macroscopic property, being uniquely defined at each point of the macroscopic domain on the basis of the underlying microstructure. For the sake of readability the superscript M will be omitted for v.

3.3.1 Balance equations

The macroscopic *mass balance* equations characterize the species transport in the phases of composite compounds, namely: i) the transport of neutral Lithium in the active particles, *when present*, macroscopically undistinguished from the other particles in the porous electrode; ii) the transport of Li^+ cations and X^- anions in the electrolyte.

$$\frac{\partial c^M_{\mathrm{Li}}}{\partial t} + \operatorname{div}\left[\vec{h}^M_{\mathrm{Li}}\right] = s_{\mathrm{Li}} \qquad \vec{x} \in \Omega_s \times [0, t_f] \tag{3.29a}$$

$$\frac{\partial c^M_{\mathrm{Li}^+}}{\partial t} + \mathrm{div}\left[\,\vec{h}^M_{\mathrm{Li}^+}\,\right] = s_{\mathrm{Li}^+} \qquad \vec{x}\in\Omega_s\times[0,t_f] \tag{3.29b}$$

$$\frac{\partial c^M_{\mathrm{X}^-}}{\partial t} + \mathrm{div}\left[\,\vec{h}^M_{\mathrm{X}^-}\,\right] = 0 \qquad \vec{x}\in\Omega_s\times[0,t_f] \tag{3.29c}$$

The source term s_{Li} averages the amount of neutral Lithium that intercalates in the active particles at the micro scale, leaving the electrolyte because of chemical reactions at the particle/electrolyte interface[8] as modeled in equations (3.12, 3.23).

Macroscopic stoichiometry of the oxidation/reduction reaction of Lithium requires[9]

$$v_e\; s_{\mathrm{Li}^+} = -v_a\; s_{\mathrm{Li}}$$

The flux of charge in the electrode is caused by the transport of electrons $\vec{h}^M_{\mathrm{e}^-}$ in the solid particles. For each ion that leaves the electrolyte an electron corresponds that leaves the flux $s_{\mathrm{e}^-} = s_{\mathrm{Li}}$. The balance of mass for electrons thus read

$$\frac{\partial c^M_{\mathrm{e}^-}}{\partial t} + \mathrm{div}\left[\,\vec{h}^M_{\mathrm{e}^-}\,\right] = s_{\mathrm{e}^-} \qquad \vec{x}\in\Omega_s\times[0,t_f] \tag{3.29d}$$

Ampère's law (2.14) must be rephrased for the macro scale in terms of the macroscopic electric displacement field and of the macroscopic current. Two separated electric displacements fields are considered at each point, one pertaining to the electrolyte $\vec{D}^M_e$ and one to the electrode $\vec{D}^M_s$. They are specified as follows:

$$\mathrm{div}\left[\,\frac{\partial \vec{D}^M_e}{\partial t} + F\,\left(\vec{h}^M_{\mathrm{Li}^+} - \vec{h}^M_{\mathrm{X}^-}\right)\right] = r_{\mathrm{Li}^+} \qquad \vec{x}\in\Omega_e\times[0,t_f] \tag{3.30a}$$

$$\mathrm{div}\left[\,\frac{\partial \vec{D}^M_s}{\partial t} - F\,\vec{h}^M_{\mathrm{e}^-}\right] = -\,r_{\mathrm{e}^-} \qquad \vec{x}\in\Omega_s\times[0,t_f] \tag{3.30b}$$

with r_{Li^+} and r_{e^-} bulk terms that macroscopically average the projection of the curl of the magnetizing field along the normal across the interface between electrolyte and electrode[10].

Equilibrium holds as in (2.11). Bulk forces are here neglected in view of the electroneutrality assumption

$$\mathrm{div}\left[\,\boldsymbol{\sigma}^M\,\right] = \vec{0} \qquad \vec{x}\in\Omega_s\times[0,t_f] \tag{3.33}$$

$$\mathrm{skw}[\,\boldsymbol{\sigma}^M\,] = \mathbf{0} \qquad \vec{x}\in\Omega_s\times[0,t_f] \tag{3.34}$$

[8] Intercalation is accounted for at the micro scale by boundary fluxes driven by chemical reactions, which within the multi scale modeling are macroscopically accounted for via volumetric source terms: s_{Li} will be estimated by a scale transition in the homogenization framework - see section 3.4 and in particular formula (3.58f). The concentrations and the mass fluxes $\vec{h}^M_\alpha$ will be upscaled within the homogenization procedure as well.

[9] It could be argued if such a constraint can be imposed *a priori*. In fact bulk contributions are upscaled and question raises if the stoichiometric constraint should be part of the scale transitions. As will be pointed out in section 3.4, the scale transitions only involve one parameter (say s_{Li}) that averages the Butler-Volmer intercalation amount along the interfaces, thus allowing the stoichiometry equations to be imposed macroscopically. Note that the mass of an electron 9.109×10^{-28}g is neglected with respect to the atomic mass of Lithium 1.153×10^{-23}g.

[10] To substantiate formulae (3.30), one may move from Gauss's law imposed in both phases and exploit Faraday's law (2.2). By means of the *mass balance* equations (3.29b-d), easy algebra leads to

$$\mathrm{div}\left[\,\frac{\partial \vec{D}^M_e}{\partial t} + F\,\left(\vec{h}^M_{\mathrm{Li}^+} - \vec{h}^M_{\mathrm{X}^-}\right)\right] = F\,s_{\mathrm{Li}^+} \qquad \vec{x}\in\Omega_s\times[0,t_f] \tag{3.31a}$$

3.3.2 Boundary and initial conditions

Whereas *balance* equations have a fundamental nature and describe in a general way all classes of Li-ion batteries problems, boundary and initial conditions are particular for each problem to be solved. There is a broad literature on the topic.

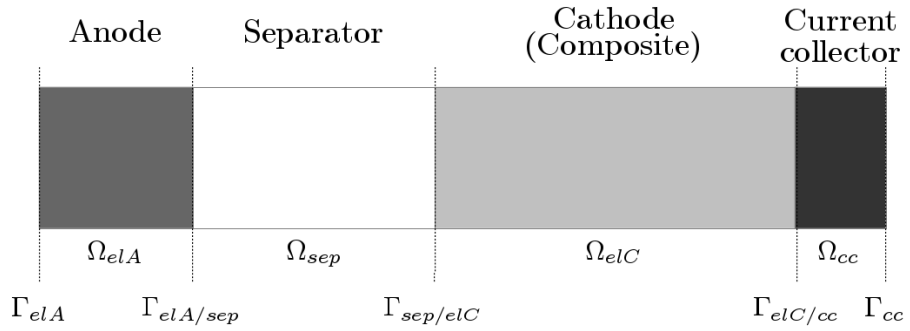

Figure 3.5: *A schematic of a lithium ion battery half cell and of the notation used for domains and interfaces at the macro-scale. A metallic anode is here depicted. Aluminum foils are generally used for cathodes current collectors.*

An example is reported here assuming a Li-metal anode according to [8] (see Figure 3.5). Extension to porous anode is straightforward: it will be sufficient to apply at the anode the path of reasoning that will be here applied to the porous cathode.

Initial conditions are suitably taken, depending on the process that is simulated: galvanostatic/potentiostatic, charge/discharge. The battery cell is initially modeled as undeformed in any case.

At the *anode current collector interface* Γ_{elA} the electric potential is set to zero, according with the selection of the Li-anode as the reference electrode. As in [121], the electric field outside of system is assumed to vanish, thus $\vec{E} = \vec{0}$ at the exterior surfaces of the electrodes. Mechanical boundary conditions consider no displacements at both ends or an external pressure applied at the boundaries Γ_{elA} and Γ_{cc}. During a galvanostatic discharge process with steady current density I, the boundary condition $F\vec{h}^M_{e^-} \cdot \vec{n}_{elA} = I$ holds at a generic point $\Omega_{elA} \ni \vec{x} \to \Gamma_{elA}$, assuming homogeneous distribution of electric current. $\vec{n}_{elA}$ refers to the outward normal direction along the boundary of Ω_{elA}.

At interface $\Gamma_{elA/sep}$ three conditions are enforced. Anions cannot leave the separator,

$$\operatorname{div}\left[\frac{\partial \vec{D}^M_s}{\partial t} - F\,\vec{h}^M_{\mathrm{e}^-}\right] = -F\,s_{\mathrm{e}^-} \qquad \vec{x} \in \Omega_s \times [0, t_f] \tag{3.31b}$$

which are a specification of (3.30). Both (3.30) and (3.31) are evidently incompatible with Ampère's law in form (2.9) unless the mass supply rates vanish. Compatibility can be recovered if mass supply rates can be written as the divergence of two otherwise arbitrary vectors. In such a case however, Faraday's law for the current and mass fluxes (2.3) no longer applies. Indeed Faraday's law at the macro scale looses its original interpretation of electrolysis production, which is valid only microscopically where electrolysis is described explicitly. It is here considered that macroscopically Faraday's law has to take into account the average Lithium ions that leave the solution due to chemical reactions and similarly for the electron flow in the electrode. It is thus assumed that macroscopically Faraday's law can be written as

$$\vec{i}^M = \sum_\alpha z_\alpha\, F\, \vec{h}^M_\alpha \; + \vec{r}_\alpha \tag{3.32}$$

with $\vec{r}_\alpha$ providing bulk terms r_{Li^+} and r_{e^-} by means of the divergence operator into Ampère's law in form (2.14).

therefore $\vec{h}^M_{\mathrm{X}^-} \cdot \vec{n}_{sep} = \vec{0}$ at a generic point $\Omega_{sep} \ni \vec{x} \to \Gamma_{elA/sep}$. Moreover, for every electron that leaves the anode, a Li^+ ion enters the electrolyte: thus $F\, v_e\, \vec{h}^M_{\mathrm{Li}^+} \cdot \vec{n}_{sep} = -I$ at point $\Omega_{sep} \ni \vec{x} \to \Gamma_{elA/sep}$. Here the normal is outward with respect to the separator, coherently with the choice of $\vec{x} \in \Omega_{sep}$. Finally, a boundary condition of an influx of Li^+ ions is stated in terms of the surface over potential[11] χ^M and of the thermodynamic excess γ^M by the Butler-Volmer equation (3.12)

$$v_e\, \vec{h}^M_{\mathrm{Li}^+} \cdot \vec{n}_S \;=\; \frac{\mathrm{i}_0}{F} \left\{ \exp\left[\frac{1-\beta}{R\,\vartheta}\gamma^M\right] - \exp\left[-\frac{\beta}{R\,\vartheta}\gamma^M\right] \right\} \qquad \vec{x} \in \Gamma_{elA/sep}$$

The open circuit potential ξ^{Nernst} in equation (3.11) can be taken as zero if the anode is used as reference electrode. A further boundary condition is derived from Ampère's law (2.9)

$$\left(\frac{\partial \vec{D}^M_s}{\partial t} + \vec{i}^M_{\mathrm{e}^-}\right) \cdot \vec{n}_{An} + v_e \left(\frac{\partial \vec{D}^M_e}{\partial t} + \vec{i}^M_e\right) \cdot \vec{n}_S \;=\; 0 \qquad \vec{x} \in \Gamma_{elA/sep}$$

At interface $\Gamma_{sep/elC}$ continuity conditions for potentials and fluxes are imposed because anions and cations are free to pass from the separator to the electrolyte in the porous cathode in a thermodynamic equilibrium condition. Electrons and neutral Lithium cannot exit the cathode, therefore $\vec{i}^M_{\mathrm{e}^-} \cdot \vec{n}_{elC} = \vec{0}$ as well as $\vec{h}^M_{\mathrm{Li}} \cdot \vec{n}_{elC} = 0$ at $\Omega_{elC} \ni \vec{x} \to \Gamma_{sep/elC}$.

At the cathode-current collector interface $\Gamma_{elC/cc}$, neither Lithium ions, nor counterions, nor neutral Lithium can leave the battery $\vec{h}^M_{\mathrm{Li}^+} \cdot \vec{n}_{elC} = \vec{h}^M_{X^-} \cdot \vec{n}_{elC} = \vec{h}_{\mathrm{Li}} \cdot \vec{n}_{elC} = \vec{0}$ at $\Omega_{elC} \ni \mathbf{x} \to \Gamma_{elC/cc}$. The electrode carries all the current $v_s\, \vec{i}^M_{\mathrm{e}^-} \cdot \vec{n}_{elC} = I$. Such a current is constant in the current collector. In case of potentiostatic process, the electric potential at the current collector boundary Γ_{cc} is given.

3.3.3 Weak forms

The weak form for the macroscale balance equations and boundary conditions[12] can be given, either for a complete cell or for a part of it, following the same path of reasoning for the micro scale. In modeling a complete cell, the boundary conditions are indeed the ones that drive the problem, whereas the specifications at interfaces between electrodes, separator, and collectors follow from continuity equations. On the other hand, to write the weak form for each single part is more readable. For this sake, the weak form for the macroscale balance equations and boundary conditions on electrodes (*el*), the separator (*sep*), current collectors (*cc*) are here separately considered, in terms of the potentials and displacements in a time interval $[0, t_f]$. By denoting, as for the micro scale, $z^M = \{c^M_{\mathrm{Li}},\, c^M_{\mathrm{e}^-},\, c^M_{\mathrm{Li}^+},\, c^M_{\mathrm{X}^-}\}$ and $y^M = \{\mu^M_{\mathrm{Li}}, \mu^M_{\mathrm{e}^-}, \mu^M_{\mathrm{Li}^+}, \mu^M_{\mathrm{X}^-}, \phi^M_s, \phi^M_e, \vec{u}^M\}$, the weak forms read

Any $y^M \in \mathcal{V}^{[0,t_f]}$ such that

$$\frac{\mathrm{d}}{\mathrm{d}t} b_{el}\left(\hat{y}^M, z^M(t)\right) + a_{el}(\hat{y}^M, y^M(t)) = f_{el}(\hat{y}^M) + j_{el}(\hat{y}^M) \quad \forall \hat{y}^M \in \mathcal{V} \tag{3.35a}$$

Any $y^M \in \mathcal{V}^{[0,t_f]}$ such that

[11] Such a condition is expected at the micro scale only. This is correct for porous materials. However, as the anode foil is here described as homogeneous, the Butler-Volmer interface condition is expressed macroscopically, too.

[12] As no constitutive laws are assumed at the macro-scale the notion of governing equations is vacuous at such a scale.

$$\frac{\mathrm{d}}{\mathrm{d}t} b_{sep}\left(\hat{y}^M, z^M(t)\right) + a_{sep}(\hat{y}^M, y^M(t)) = f_{sep}(\hat{y}^M) + j_{sep}(\hat{y}^M) \quad \forall \hat{y}^M \in \mathcal{V} \tag{3.35b}$$

Any $y^M \in \mathcal{V}^{[0,t_f]}$ such that

$$\frac{\mathrm{d}}{\mathrm{d}t} b_{cc}\left(\hat{y}^M, z^M(t)\right) + a_{cc}(\hat{y}^M, y^M(t)) = f_{cc}(\hat{y}^M) + j_{cc}(\hat{y}^M) \quad \forall \hat{y}^M \in \mathcal{V} \tag{3.35c}$$

The identification of the functional spaces $\mathcal{V}^{[0,t_f]}, \mathcal{V}$ falls beyond the scope of the present contribution. The former space includes time dependent functions, whereas space $\mathcal{V}$ does not (see [123], chapter 12). Vector $\hat{y}^M$ collects the steady-state test functions that correspond to the unknown fields in y^M. Vector z^M is dependent on y^M by constitutive equations, that are imposed only incrementally with tangent moduli upscaled from the micro scale as usual in computational homogenization. The bilinear forms a and b for *porous electrode materials* in eqns. (3.35) read[13]

$$b_{el}\left(\hat{y}^M, z^M\right) = \int_\Omega b^M\left(\hat{y}^M, z^M\right) \mathrm{d}\Omega \tag{3.36a}$$

$$a_{el}\left(\hat{y}^M, z^M\right) = \int_\Omega a^M\left(\hat{y}^M, z^M\right) \mathrm{d}\Omega \tag{3.36b}$$

$$f_{el}\left(\hat{y}^M\right) = \int_\Omega f^M\left(\hat{y}^M\right) \mathrm{d}\Omega \tag{3.36c}$$

with integrands defined by

$$\begin{aligned} b^M\left(\hat{y}^M, z^M\right) = \\ -\left\{ v_a\, \hat{\mu}^M_{\mathrm{Li}}\, c^M_{\mathrm{Li}} + v_s\, \hat{\mu}^M_{\mathrm{e}^-}\, c^M_{\mathrm{e}^-} + v_e\, \left(\hat{\mu}^M_{\mathrm{Li}^+}\, c^M_{\mathrm{Li}^+} + \hat{\mu}^M_{\mathrm{X}^-}\, c^M_{\mathrm{X}^-}\right)\right\} + \\ -\left\{ v_s \nabla\left[\,\hat{\phi}^M_s\,\right] \cdot \vec{D}^M_s + v_e \nabla\left[\,\hat{\phi}^M_e\,\right] \cdot \vec{D}^M_e \right\} + \hat{\boldsymbol{\varepsilon}}^M : \boldsymbol{\sigma}^M \end{aligned}$$

$$\begin{aligned} a^M\left(\hat{y}^M, y^M\right) = \\ v_a \nabla\left[\,\hat{\mu}^M_{\mathrm{Li}}\,\right] \cdot \vec{h}^M_{\mathrm{Li}} + v_s \nabla\left[\,\hat{\mu}^M_{\mathrm{e}^-}\,\right] \cdot \vec{h}^M_{\mathrm{e}^-} + v_e \left(\nabla\left[\,\hat{\mu}^M_{\mathrm{Li}^+}\,\right] \cdot \vec{h}^M_{\mathrm{Li}^+} + \nabla\left[\,\hat{\mu}^M_{\mathrm{X}^-}\,\right] \cdot \vec{h}^M_{\mathrm{X}^-}\right) \\ -\left\{ v_s \nabla\left[\,\hat{\phi}^M_s\,\right] \cdot (-F\, \vec{h}^M_{\mathrm{e}^-}) + v_e \nabla\left[\,\hat{\phi}^M_e\,\right] \cdot F\, \left(\vec{h}^M_{\mathrm{Li}^+} - \vec{h}^M_{\mathrm{X}^-}\right)\right\} \end{aligned}$$

$$f^M\left(\hat{y}^M\right) = -\left\{ s\, \hat{\gamma}^M - r\, \hat{\xi}^M \right\}$$

under the stoichiometric constraints for the macroscopic supply rates:

$$s = v_a\, s_{\mathrm{Li}} = -v_s\, s_{\mathrm{e}^-} = -v_e\, s_{\mathrm{Li}^+}\,, \qquad r = -v_e\, r_{\mathrm{Li}^+} = -v_s\, r_{\mathrm{e}^-}$$

The *pointwise* thermodynamic excess and potential difference are defined as

$$\hat{\gamma}^M = \hat{\mu}^M_{\mathrm{Li}} - \hat{\mu}^M_{\mathrm{e}^-} - \hat{\mu}^M_{\mathrm{Li}^+}\,, \qquad \hat{\xi}^M = \hat{\phi}^M_s - \hat{\phi}^M_e$$

Contributions at interfaces between electrodes, separator, and collectors are included in $j_{el}\left(\hat{y}^M\right)$, detailed in appendix 3.6 together with proofs.

[13] The weak form contributions in the separator and anode can be derived in a similar manner and are not provided explicitly here.

3.4 Scales transitions

3.4.1 Macro to micro scales transitions

Despite its recent application to a wide range of problems, as emphasized in section 1.4, computational homogenization has been first adopted to characterize mechanical response of material with non-homogeneous microstructure (see [30] for a review). Within this field, the computational homogenization generally departs from the computation of a macroscopic deformation tensor $\nabla \left[\vec{u}^M \right]$, which is evaluated at every material point of the macrostructure (e.g. the integration points within a macroscopic finite element domain). This tensor is next used to formulate the boundary conditions to be imposed on the microstructural RVE through proper macro-micro scale transition.
In classical approaches this is achieved either by assuming that all the microstructural constituents undergo a uniform deformation identical to the macroscopic one (the Taylor or Voigt assumption) or imposing a uniform stress (and additionally identical rotation) to all the components (the Sachs or Reuss assumption) or by intermediate procedures. However, these simplified methods provide only rough estimates of the effective material properties, leading to overestimation (Taylor) or underestimation (Sachs) of the overall stiffness, suggesting that different macro-micro scale transition condition have to be selected.

A first-order computational homogenization scheme stems on the classical linearization of the microscopic displacement field

$$\vec{u}^m(\vec{x}) = \vec{u}^m(\vec{x}^{\,\mathsf{ref}}) + \nabla \left[\vec{u}^M \right] \cdot (\vec{x} - \vec{x}^{\,\mathsf{ref}}) + \tilde{\vec{u}}(\vec{x}) \,, \qquad \vec{x} \in V \tag{3.37}$$

where $\vec{x}^{\,\mathsf{ref}}$ represents a reference point over the RVE domain V, necessary to eliminate rigid body displacements, and $\tilde{\vec{u}}$ is the microfluctuation field, unknown at the microscale.

Assuming that $\nabla \left[\vec{u}^M \right]$ is known, use is made of a scale transition relation that enforces the macroscopic deformation gradient to be equal to the volume average of its microscopic counterparts

$$\nabla \left[\vec{u}^{\,M} \right] = \frac{1}{V} \int_V \nabla \left[\vec{u}^{\,m} \right] \mathrm{d}V \tag{3.38}$$

By making use of linear decomposition (3.37)

$$\int_V \nabla \left[\vec{u}^{\,m} \right] \mathrm{d}V = \nabla \left[\vec{u}^{\,M} \right] + \int_V \nabla \left[\tilde{\vec{u}}^{\,m} \right] \mathrm{d}V \tag{3.39}$$

and enforcing (3.38) a boundary integral constraint arise for the microfluctuation (through application of the divergence theorem)

$$\int_V \nabla \left[\tilde{\vec{u}}^{\,m} \right] \mathrm{d}V = \int_{\partial V} \tilde{\vec{u}}^{\,m} \otimes \vec{n} \, \mathrm{d}\Gamma = \mathbf{0} \tag{3.40}$$

where $\vec{n}$ is the outward unit normal on the boundary of the RVE ∂V.

For the first-order CH, the solution, in terms of deformed shape of the RVE and stress state extracted from it, does not depend on the choice of the reference point used to eliminate rigid body displacements.

Different kinds of microscopic boundary conditions may arise from constraint (3.40). Taylor conditions trivially satisfies (3.40) being the microfluctuation field zero on the entire volume V. The position of all points at the boundary are determined through the macroscopic deformation, leading to a linear mapping of the RVE boundary. Notwithstanding

their simplicity, these set of conditions is often too stiff.
The weakest way to impose requirement (3.40) is by applying traction-like boundary conditions as discussed in [124, 125]. However they are a priori not appropriate in a deformation driven procedure, as the one described here, generally yielding unsatisfactory results.

Periodic boundary conditions will be applied instead on the microfluctuation displacement field $\tilde{\vec{u}}$. They represent the best compromise between the limiting cases just mentioned, providing a better estimation of the overall properties (see for example [35, 126]).

Denoting with l the length of the side of the square RVE, and with $\partial^L V$ and $\partial^B V$ its left and bottom sides, the periodic boundary conditions read:

$$\tilde{\vec{u}}(\vec{x}) = \tilde{\vec{u}}(\vec{x} + l\vec{e}_1) \,, \qquad \vec{x} \in \partial^L V \tag{3.41a}$$

$$\tilde{\vec{u}}(\vec{x}) = \tilde{\vec{u}}(\vec{x} + l\vec{e}_2) \,, \qquad \vec{x} \in \partial^B V \tag{3.41b}$$

or, equivalently, in terms of the displacement field $\vec{u}^m$

$$\vec{u}^m(\vec{x} + l\vec{e}_1) - \vec{u}^m(\vec{x}) = l\, \boldsymbol{\varepsilon}^M \vec{e}_1 \,, \qquad \vec{x} \in \partial^L V \tag{3.42a}$$

$$\vec{u}^m(\vec{x} + l\vec{e}_2) - \vec{u}^m(\vec{x}) = l\, \boldsymbol{\varepsilon}^M \vec{e}_2 \,, \qquad \vec{x} \in \partial^B V \tag{3.42b}$$

Due to microstructural equilibrium, tractions will be anti periodic on the opposite sides of the RVE

$$\vec{\overline{p}}^m(\vec{x}) = -\vec{\overline{p}}^m(\vec{x} + l\vec{e}_1) \,, \qquad \vec{x} \in \partial^L V \tag{3.43a}$$

$$\vec{\overline{p}}^m(\vec{x}) = -\vec{\overline{p}}^m(\vec{x} + l\vec{e}_2) \,, \qquad \vec{x} \in \partial^B V \tag{3.43b}$$

resulting into a vanishing power expenditure along the boundary of the RVE for periodic boundary conditions. Accordingly, displacement boundary conditions do not provide any contribution to the right hand side $f(\hat{y}^m)$ of the weak form (3.24). Conditions (3.42) and (3.43) ensure that condition (3.40) is satisfied and that solution in terms of $\nabla[\,\vec{u}^m\,]$ and $\boldsymbol{\sigma}^m$ is unique, as demonstrated by *Suquet* [96].
The extension to a three dimensional RVE is trivial.

The path of reasoning just illustrated is not limited to mechanical problems. Generalization to multiphysic problems is straightforward with minor modifications.
As for the weak form (3.24), the problem will be formulated in terms of an independent variable set y that includes displacements $\vec{u}$, chemical μ_{Li}, μ_{Li^+}, μ_{X^-}, μ_{e^-}, and electric ϕ_s, ϕ_e potentials. Scalar fields in y will be collectively bundled under the symbol π, and denoted with π^m at the micro-scale. The geometrical support of field π will be denoted with V_π.

All micro-scale fields can be decomposed without loss of generality in a macroscopic contribution linearized over the microscale domain and in a microfluctuation field, denoted with the symbol $\tilde{\ }$

$$\pi^m(\vec{x}) = \pi^m(\vec{x}_\pi^{\,\mathsf{ref}}) + \nabla\left[\,\pi^M\,\right] \cdot (\vec{x} - \vec{x}_\pi^{\,\mathsf{ref}}) + \tilde{\pi}(\vec{x}) \,, \qquad \vec{x} \in V_\pi \tag{3.44a}$$

$$\vec{u}^m(\vec{x}) = \vec{u}^m(\vec{x}_u^{\,\mathsf{ref}}) + \nabla\left[\,\vec{u}^M\,\right] \cdot (\vec{x} - \vec{x}_u^{\,\mathsf{ref}}) + \tilde{\vec{u}}(\vec{x}) \,, \qquad \vec{x} \in V \tag{3.44b}$$

subscripts π and u identify quantities related to fields π^m and $\vec{u}^m$ respectively. At the microscale each phase occupies only a portion of the RVE, hence the variables are defined on different domains for which it is possible to choose the proper reference point.

Order one scale transition conditions on the average values of the gradients of the independent variable fields are enforced

$$\nabla \left[\pi^M \right] = \frac{1}{V_\pi} \int_{V_\pi} \nabla \left[\pi^m \right] \mathrm{d}V \tag{3.45a}$$

$$\nabla \left[\vec{u}^{\,M} \right] = \frac{1}{V} \int_{V} \nabla \left[\vec{u}^{\,m} \right] \mathrm{d}V \tag{3.45b}$$

leading to a set of integral constraints on the microfluctuation fields:

$$\int_{V_\pi} \nabla \left[\tilde{\pi}^m \right] \mathrm{d}V = \int_{\partial V_\pi} \tilde{\pi}^m \, \vec{n} \, \mathrm{d}\Gamma = \vec{0} \tag{3.46}$$

which will be satisfied through the definition of proper boundary conditions for fields π^m along ∂V_π and $\vec{u}^{\,m}$ along ∂V.

As already discussed, if the choice falls on periodic boundary conditions for $\vec{u}^m$ restrictions (3.42) are derived. In view of the assumption made (refer to equations (3.19)) displacements are continuous over the whole RVE, justifying $V_u = V$.

The boundary conditions for the electrochemical and electric potentials have to be formulated in a different way, because the boundary of each phase does not coincide with the boundary of the RVE. Constraint (3.46-a) is imposed along the interfaces $\partial V_j \cap \partial V_i$, $i, j = a, e, s$ as well as along the sides of the RVE, $\partial V_j \cap \partial V$, $j = a, e, s$. The easiest way to satisfy (3.46) is to set vanishing fluctuations along the interfaces and the RVE boundary

$$\tilde{\mu}_{\mathrm{Li^+}}|_{\partial V_e} = \tilde{\mu}_{\mathrm{X^-}}|_{\partial V_e} = \tilde{\mu}_{\mathrm{Li}}|_{\partial V_a} = \tilde{\mu}_{\mathrm{e^-}}|_{\partial V_s} = \tilde{\phi}_s\Big|_{\partial V_s} = \tilde{\phi}_e\Big|_{\partial V_e} = 0 \tag{3.47}$$

In terms of microscopic fields

$$\mu^m_{\mathrm{Li^+}}(\vec{x}) = \nabla \left[\mu^M_{\mathrm{Li^+}} \right] \cdot (\vec{x} - \vec{x}_{G(V)}) + \mu^M_{\mathrm{Li^+}} \,, \qquad \vec{x} \in \partial V_e \tag{3.48a}$$

$$\mu^m_{\mathrm{X^-}}(\vec{x}) = \nabla \left[\mu^M_{\mathrm{X^-}} \right] \cdot (\vec{x} - \vec{x}_{G(V)}) + \mu^M_{\mathrm{X^-}} \,, \qquad \vec{x} \in \partial V_e \tag{3.48b}$$

$$\mu^m_{\mathrm{Li}}(\vec{x}) = \nabla \left[\mu^M_{\mathrm{Li}} \right] \cdot (\vec{x} - \vec{x}_{G(V)}) + \mu^M_{\mathrm{Li}} \,, \qquad \vec{x} \in \partial V_a \tag{3.48c}$$

$$\mu^m_{\mathrm{e^-}}(\vec{x}) = \nabla \left[\mu^M_{\mathrm{e^-}} \right] \cdot (\vec{x} - \vec{x}_{G(V)}) + \mu^M_{\mathrm{e^-}} \,, \qquad \vec{x} \in \partial V_s \tag{3.48d}$$

$$\phi^m_s(\vec{x}) = \nabla \left[\phi^M_s \right] \cdot (\vec{x} - \vec{x}_{G(V)}) + \phi^M_s \,, \qquad \vec{x} \in \partial V_s \tag{3.48e}$$

$$\phi^m_e(\vec{x}) = \nabla \left[\phi^M_e \right] \cdot (\vec{x} - \vec{x}_{G(V)}) + \phi^M_e \,, \qquad \vec{x} \in \partial V_e \tag{3.48f}$$

As these scalar fields do not vanish along the boundary of the RVE, non-homogeneous boundary terms arise. However they are of Dirichlet type and, in a formal setting, they enter the definition of the functional space $\mathcal{V}^{[0,t_f]}$ and have no impact on the right hand side $f(\hat{y}^m)$ in weak form (3.24). It is therefore concluded that $f(\hat{y}^m) = 0$.

In a finite element numerical approximation of the problem however, it is classical to look for solutions in homogeneous functional spaces, by extending the Dirichlet boundary given conditions into the whole domain. This approach, detailed for instance in [123], is not discussed here yet deferred to a companion publication focused on the numerical approximation of the problem.

A scale transition of *order zero* is required by the interface condition (3.12), through which the values assumed by variables along the electrode/electrolyte interface directly affect the amount of charge and lithium that cross the boundary. This is a peculiarity of the model

reported here. In classical computational homogenization problems only the gradient of the unknowns (typically $\nabla[\,\vec{u}\,]$) is relevant for scale transition conditions.

Order zero scale transition is enforced to variables π in two ways. The Hill-Mandel extended equation in Section 3.4.2 requires the microscopic field at the reference point to equate the corresponding macroscopic field:

$$\pi^m(\vec{x}_\pi^{\,\mathsf{ref}}) = \pi^M \tag{3.49}$$

Furthermore, the macroscopic and microscopic fields are enforced to satisfy the volume average condition

$$\pi^M = \frac{1}{V_\pi}\int_{V_\pi} \pi^m \mathrm{d}V \tag{3.50}$$

which implies the integral constraint

$$\frac{1}{V_\pi}\int_{V_\pi} \nabla\left[\,\pi^M\,\right]\cdot(\vec{x}-\vec{x}_\pi^{\,\mathsf{ref}}) + \tilde{\pi}(\vec{x})\mathrm{d}V = 0$$

in view of linearization (3.44-a). A simple way to satisfy the constraint above is to impose that: i) the reference point $\vec{x}_\pi^{\,\mathsf{ref}}$ coincides with the centroid $\vec{x}_{G(V_\pi)}$ of V_π; ii) the average of the micro fluctuation over the domain is vanishing:

$$\frac{1}{V_\pi}\int_{V_\pi} \tilde{\pi}(\vec{x})\mathrm{d}V = 0$$

Statistically, the centroid of active and conductive particles is close to the centroid of any "sufficiently large" domain in the light of randomness of the particle distribution. Accordingly, for the RVE to be "representative" it is expected that the reference points for all subdomains V_π collapse in a single point located in the centroid $\vec{x}_{G(V)} = \vec{x}_{G(V_\pi)}$ of the RVE. Under this further assumption, the constraints on the microscopic fields read

$$\int_{V_\pi} \pi^m(\vec{x}) - \pi^M - \nabla\left[\,\pi^M\,\right]\cdot(\vec{x}-\vec{x}_{G(V)})\mathrm{d}V = 0 \tag{3.51}$$

An additional scale transition is enforced, based on the conservation of mass through the scales:

$$\begin{aligned} c^M_{\mathrm{Li}} &= \frac{1}{V_a}\int_{V_a} c^m_{\mathrm{Li}}\,\mathrm{d}V\,, \quad c^M_{\mathrm{Li^+}} = \frac{1}{V_e}\int_{V_e} c^m_{\mathrm{Li^+}}\,\mathrm{d}V\,, \\ c^M_{\mathrm{X^-}} &= \frac{1}{V_e}\int_{V_e} c^m_{\mathrm{X^-}}\,\mathrm{d}V\,, \quad c^M_{\mathrm{e^-}} = \frac{1}{V_s}\int_{V_E} c^m_{\mathrm{e^-}}\,\mathrm{d}V \end{aligned} \tag{3.52}$$

The displacement field at reference point $\vec{x}_u^{\,\mathsf{ref}}$ is set to zero in order to eliminate rigid body translations; the rigid body rotation will be suppressed through the microscopic boundary conditions.

3.4.2 Micro to macro scales transitions

The homogenized macroscopic quantities are extracted from the solution of the microscale problem and upscaled. To do so, it is generally assumed that the internal expenditure of virtual power $\mathcal{W}_{\text{int}}$ is preserved in the scale transition:

$$\mathcal{W}_{\text{int}}^{M} = \mathcal{W}_{\text{int}}^{m} \tag{3.53}$$

with superscripts M and m denoting macro and micro scale, as usual. Such a condition in the mechanical context is named after Hill-Mandel [127].

As in the previous section, attention is first limited to the mechanics. Hill-Mandel condition in the most classical feature reads:

$$\boldsymbol{\sigma}^{M} \,:\boldsymbol{\varepsilon}^{M} = \frac{1}{V}\int_{V} \boldsymbol{\sigma}^{m} \,:\boldsymbol{\varepsilon}^{m}\mathrm{d}V \tag{3.54}$$

Postulating (3.54) for an RVE with kinematic boundary conditions, as the case of (3.42), the volume average $\frac{1}{V}\int_V \boldsymbol{\sigma}^m \mathrm{d}V$ equals the macroscopic stress tensor $\boldsymbol{\sigma}^M$. Making use of (3.6) and (3.37) and of divergence theorem the averaged microstructural work $\mathcal{W}_{\text{mech}}^{m}$, appearing in right hand side of (3.54), may be expressed as follows

$$\begin{aligned}
\mathcal{W}_{\text{mech}}^{m} &= \int_V \boldsymbol{\sigma}^m : \boldsymbol{\varepsilon}^m \,\mathrm{d}V = \int_V \boldsymbol{\sigma}^m : (\,\boldsymbol{\varepsilon}^M + \nabla\left[\,\vec{\tilde{u}}\,\right])\,\mathrm{d}V = \\
&= \int_V \boldsymbol{\sigma}^m \,\mathrm{d}V : \boldsymbol{\varepsilon}^M + \int_V \left(\mathrm{div}\left[\,\boldsymbol{\sigma}^m \cdot \vec{\tilde{u}}\,\right] - \mathrm{div}\left[\,\boldsymbol{\sigma}^m\,\right]\cdot\vec{\tilde{u}}\right)\mathrm{d}V = \\
&= \int_V \boldsymbol{\sigma}^m \,\mathrm{d}V : \boldsymbol{\varepsilon}^M + \int_{\partial V} (\boldsymbol{\sigma}^m\cdot\vec{n})\cdot\vec{\tilde{u}}\,\mathrm{d}\Gamma = \int_V \boldsymbol{\sigma}^m \,\mathrm{d}V : \boldsymbol{\varepsilon}^M
\end{aligned} \tag{3.55}$$

Anti-periodicity of tractions (3.43) over the boundary of the RVE has been considered, leading to equality

$$\boldsymbol{\sigma}^{M} = \int_V \boldsymbol{\sigma}^m \,\mathrm{d}V \tag{3.56}$$

In the present work, assumption (3.53) is extended, so that the internal expenditure of virtual power of mechanical forces, of charge and mass fluxes is preserved in the scale transition.
As motivated in section 3.1.2, a concurrent time modeling between macro and micro scales seems appropriate. In this regard, the expenditure of virtual power between the scales will be preserved *at all times* t, for being t the same instant at both scales.

In view of the choice made to adopt as independent variable fields the potentials rather than the concentrations, the power expenditure can be easily extracted from the weak forms (3.24, 3.35). Taking an electrode as an example for equation (3.36), the extended Hill-Mandel condition reads

$$\begin{aligned}
\frac{1}{V}\,&\left[\frac{\mathrm{d}}{\mathrm{d}t}\,b^m\left(z^m(t),\hat{y}^m\right) + a^m(y^m(t),\hat{y}^m)\right] = \\
&\frac{\mathrm{d}}{\mathrm{d}t}\,b^M\left(z^M(t),\hat{y}^M\right) + a^M(y^M(t),\hat{y}^M) - f^M\left(\hat{y}^M\right)
\end{aligned} \tag{3.57}$$

written extensively in appendix 3.7. In view of the arbitrariness of each variation $\hat{y}^m, \hat{y}^M$ in the virtual power, the mechanical, migration, and diffusion contributions can be separately dealt with. The micro to macro scale transitions can be summarized as follows:

$$\boldsymbol{\sigma}^{M} = \frac{1}{V}\int_V \boldsymbol{\sigma}^m \,\mathrm{d}V \tag{3.58a}$$

$$v_a \vec{h}^M_{\mathrm{Li}} = \frac{1}{V}\left[\int_{V_a} \vec{h}^m_{\mathrm{Li}}\,\mathrm{d}V - \int_{V_a} \dot{c}^m_{\mathrm{Li}}\,(\vec{x}-\vec{x}^{\,\mathsf{ref}})\,\mathrm{d}V - \int_{\partial V_a\cap\partial V_e} h_{BV}\,(\vec{x}-\vec{x}^{\,\mathsf{ref}})\,\mathrm{d}\Gamma\right] \tag{3.58b}$$

$$v_s \vec{h}^M_{\mathrm{e^-}} = \frac{1}{V}\left[\int_{V_s} \vec{h}^m_{\mathrm{e^-}}\,\mathrm{d}V - \int_{V_s} \dot{c}^m_{\mathrm{e^-}}\,(\vec{x}-\vec{x}^{\,\mathsf{ref}})\,\mathrm{d}V + \int_{\partial V_a\cap\partial V_e} h_{BV}\,(\vec{x}-\vec{x}^{\,\mathsf{ref}})\,\mathrm{d}\Gamma\right] \tag{3.58c}$$

$$v_e \vec{h}^M_{\mathrm{Li^+}} = \frac{1}{V}\left[\int_{V_e} \vec{h}^m_{\mathrm{Li^+}}\,\mathrm{d}V - \int_{V_e} \dot{c}^m_{\mathrm{Li^+}}\,(\vec{x}-\vec{x}^{\,\mathsf{ref}})\,\mathrm{d}V + \int_{\partial V_a\cap\partial V_e} h_{BV}\,(\vec{x}-\vec{x}^{\,\mathsf{ref}})\,\mathrm{d}\Gamma\right] \tag{3.58d}$$

$$v_e \vec{h}^M_{\mathrm{X^-}} = \frac{1}{V}\left[\int_{V_e} \vec{h}^m_{\mathrm{X^-}}\,\mathrm{d}V - \int_{V_e} \dot{c}^m_{\mathrm{X^-}}\,(\vec{x}-\vec{x}^{\,\mathsf{ref}})\,\mathrm{d}V\right] \tag{3.58e}$$

$$s = -\frac{1}{V}\int_{\partial V_a\cap\partial V_e} h_{BV}\,\mathrm{d}\Gamma \tag{3.58f}$$

$$v_a \dot{c}^M_{\mathrm{Li}} = \frac{1}{V}\int_{V_a} \dot{c}^m_{\mathrm{Li}}\,\mathrm{d}V \tag{3.58g}$$

$$v_e \dot{c}^M_{\mathrm{X^-}} = \frac{1}{V}\int_{V_e} \dot{c}^m_{\mathrm{X^-}}\,\mathrm{d}V \tag{3.58h}$$

$$v_e \dot{c}^M_{\mathrm{Li^+}} = \frac{1}{V}\int_{V_e} \dot{c}^m_{\mathrm{Li^+}}\,\mathrm{d}V \tag{3.58i}$$

$$v_s \dot{c}^M_{\mathrm{e^-}} = \frac{1}{V}\int_{V_s} \dot{c}^m_{\mathrm{e^-}}\,\mathrm{d}V \tag{3.58j}$$

$$r = \frac{1}{V}\int_{\partial V_s\cap\partial V_e} \lambda^m\,\mathrm{d}\Gamma \tag{3.58k}$$

$$v_e \frac{\partial \vec{D}^M_e}{\partial t} = \frac{1}{V}\left[\int_{V_e} \frac{\partial \vec{D}^m_e}{\partial t}\,\mathrm{d}\Omega + F\int_{V_e} (\dot{c}^m_{\mathrm{Li^+}} - \dot{c}^m_{\mathrm{X^-}})\,(\vec{x}-\vec{x}^{\,\mathsf{ref}})\,\mathrm{d}\Omega + \right.$$
$$\left. -F\int_{\partial V_a\cap\partial V_e} h_{BV}\,(\vec{x}-\vec{x}^{\,\mathsf{ref}})\mathrm{d}\Gamma - \int_{\partial V_s\cap\partial V_e} \lambda^m\,(\vec{x}-\vec{x}^{\,\mathsf{ref}})\mathrm{d}\Gamma\right] \tag{3.58l}$$

$$v_s \frac{\partial \vec{D}^M_s}{\partial t} = \frac{1}{V}\left[\int_{V_a\cup V_c} \frac{\partial \vec{D}^m_s}{\partial t}\,\mathrm{d}V - F\int_{V_a\cup V_c} \dot{c}^m_{\mathrm{e^-}}\,(\vec{x}-\vec{x}^{\,\mathsf{ref}})\,\mathrm{d}V + \right.$$
$$\left. +F\int_{\partial V_a\cap\partial V_e} h_{BV}\,(\vec{x}-\vec{x}^{\,\mathsf{ref}})\mathrm{d}\Gamma + \int_{\partial V_s\cap\partial V_e} \lambda^m\,(\vec{x}-\vec{x}^{\,\mathsf{ref}})\mathrm{d}\Gamma\right] \tag{3.58m}$$

with all details collected in appendix 3.7.

3.5 Appendix: Weak form at the micro scale

The weak form for the microscale problem can be given in terms of the potentials and displacements in a time interval $[0, t_f]$ as

$$\begin{aligned} &\text{Find } y^m \in \mathcal{V}^{[0,t_f]} \text{ such that} \\ &\qquad \frac{\mathrm{d}}{\mathrm{d}t} b^m\left(\hat{y}^m, z^m(t)\right) + a^m(\hat{y}^m, y^m(t)) = 0 \quad \forall \hat{y}^m \in \mathcal{V} \end{aligned}$$

where

$$\begin{aligned} b^m\left(\hat{y}^m, z^m\right) = & \\ & - \int_{V_a} \hat{\mu}^m_{\mathrm{Li}}\, c^m_{\mathrm{Li}}\, \mathrm{d}V - \int_{V_a \cup V_c} \hat{\mu}^m_{\mathrm{e}^-}\, c^m_{\mathrm{e}^-}\, \mathrm{d}V - \int_{V_e} \hat{\mu}^m_{\mathrm{Li}^+}\, c^m_{\mathrm{Li}^+} + \hat{\mu}^m_{\mathrm{X}^-}\, c^m_{\mathrm{X}^-}\, \mathrm{d}V + \\ & - \int_{V_a \cup V_c} \nabla\left[\,\hat{\phi}^m_s\,\right] \cdot \vec{D}^m_s\, \mathrm{d}V - \int_{V_e} \nabla\left[\,\hat{\phi}^m_e\,\right] \cdot \vec{D}^m_e\, \mathrm{d}V + \int_V \hat{\boldsymbol{\varepsilon}}^m : \boldsymbol{\sigma}^m\, \mathrm{d}V \end{aligned}$$

$$\begin{aligned} a^m\left(\hat{y}^m, y^m\right) = & \\ & + \int_{V_a} \nabla\left[\,\hat{\mu}^m_{\mathrm{Li}}\,\right] \cdot \vec{h}^m_{\mathrm{Li}}\, \mathrm{d}V + \int_{V_a \cup V_c} \nabla\left[\,\hat{\mu}^m_{\mathrm{e}^-}\,\right] \cdot \vec{h}^m_{\mathrm{e}^-}\, \mathrm{d}V + \\ & + \int_{V_e} \nabla\left[\,\hat{\mu}^m_{\mathrm{Li}^+}\,\right] \cdot \vec{h}^m_{\mathrm{Li}^+} + \nabla\left[\,\hat{\mu}^m_{\mathrm{X}^-}\,\right] \cdot \vec{h}^m_{\mathrm{X}^-}\, \mathrm{d}V + \\ & - \int_{V_a \cup V_c} \nabla\left[\,\hat{\phi}^m_s\,\right] \cdot \vec{i}^m_{\mathrm{e}^-}\, \mathrm{d}V - \int_{V_e} \nabla\left[\,\hat{\phi}^m_e\,\right] \cdot \vec{i}^m_e\, \mathrm{d}V + \\ & - \int_{\partial V_s \cap \partial V_e} \hat{\gamma}^m\, h_{BV}\, + \hat{\xi}^m\, \lambda^m\, + \hat{\lambda}^m \left(\frac{\gamma^m}{F} + \xi^m\right) \mathrm{d}\Gamma \end{aligned} \tag{3.59}$$

with $y^m = \{\mu^m_{\mathrm{Li}}, \mu^m_{\mathrm{e}^-}, \mu^m_{\mathrm{Li}^+}, \mu^m_{\mathrm{X}^-}, \phi^m_s, \phi^m_e, \vec{u}^m, \lambda^m\}$. The "hatted counterpart" of Gibbs reaction energy is defined according to equations (3.9) as

$$\hat{\gamma}^m = \hat{\mu}^m_{\mathrm{Li}} - \hat{\mu}^m_{\mathrm{e}^-} - \hat{\mu}^m_{\mathrm{Li}^+} \tag{3.60}$$

the potential jump as $\hat{\xi}^m = \hat{\phi}^m_s - \hat{\phi}^m_e$. Mass flux across the interface obeys to Butler-Volmer equation

$$h_{BV} = \frac{\mathrm{i}_0}{F} \left\{ \exp\left[\frac{(1-\beta)}{RT} F\, \chi^m\right] - \exp\left[-\frac{\beta}{RT} F\, \chi^m\right] \right\} \tag{3.61}$$

with the surface over potential χ^m defined by equation (3.11) and imposing h_{BV} to be zero along interface $\partial V_c \cap \partial V_e$

$$h_{BV} = 0 \qquad\qquad \vec{x} \in \partial V_c \cap \partial V_e \tag{3.62}$$

Finally, Faraday's law imposed *a priori* by defining

$$\vec{i}^m_{\mathrm{e}^-} = -F\, \vec{h}^m_{\mathrm{e}^-}\,, \qquad \vec{i}^m_e = F\left(\vec{h}^m_{\mathrm{Li}^+} - \vec{h}^m_{\mathrm{X}^-}\right) \tag{3.63}$$

Proof - By applying the divergence theorem to mass contributions in $a\left(\hat{y}^m, y^m\right)$ it comes out:

$$\begin{aligned}
&\int_{V_a} \nabla\left[\,\hat{\mu}^m_{\mathrm{Li}}\,\right]\cdot\vec{h}^m_{\mathrm{Li}}\,\mathrm{d}V + \int_{V_a\cup V_c} \nabla\left[\,\hat{\mu}^m_{\mathrm{e}^-}\,\right]\cdot\vec{h}^m_{\mathrm{e}^-}\,\mathrm{d}V + \\
&+\int_{V_e} \nabla\left[\,\hat{\mu}^m_{\mathrm{Li}^+}\,\right]\cdot\vec{h}^m_{\mathrm{Li}^+} + \nabla\left[\,\hat{\mu}^m_{\mathrm{X}^-}\,\right]\cdot\vec{h}^m_{\mathrm{X}^-}\,\mathrm{d}V = \\
&-\int_{V_a} \hat{\mu}^m_{\mathrm{Li}}\,\mathrm{div}\left[\,\vec{h}^m_{\mathrm{Li}}\,\right]\mathrm{d}V - \int_{V_a\cup V_c} \hat{\mu}^m_{\mathrm{e}^-}\,\mathrm{div}\left[\,\vec{h}^m_{\mathrm{e}^-}\,\right]\mathrm{d}V + \\
&-\int_{V_e} \hat{\mu}^m_{\mathrm{Li}^+}\,\mathrm{div}\left[\,\vec{h}^m_{\mathrm{Li}^+}\,\right] + \hat{\mu}_{\mathrm{X}^-}\,\mathrm{div}\left[\,\vec{h}^m_{\mathrm{X}^-}\,\right]\mathrm{d}V + \\
&+\int_{\partial V_a} \hat{\mu}^m_{\mathrm{Li}}\,\vec{h}^m_{\mathrm{Li}}\cdot\vec{n}_a\,\mathrm{d}\Gamma + \int_{\partial V_s} \hat{\mu}^m_{\mathrm{e}^-}\,\vec{h}^m_{\mathrm{e}^-}\cdot\vec{n}_s\,\mathrm{d}\Gamma + \\
&+\int_{\partial V_e} \hat{\mu}^m_{\mathrm{Li}^+}\,\vec{h}^m_{\mathrm{Li}^+}\cdot\vec{n}_e + \hat{\mu}^m_{\mathrm{X}^-}\,\vec{h}^m_{\mathrm{X}^-}\cdot\vec{n}_e\,\mathrm{d}\Gamma
\end{aligned}$$

By virtue of the $b\left(z^m(t), \hat{y}^m\right)$ contribution to the weak form, the homogenous equations of mass balances (3.3 - 3.4) are recovered. Let the boundary contribution be split into the sum of the terms along interface $\partial V_a \cap \partial V_e$ and the remaining parts $\partial V_c \cap \partial V_e$ and $\partial V_c \cap \partial V_a$. It turns out along $\partial V_a \cap \partial V_e$:

$$\begin{aligned}
&\int_{\partial V_a\cap\partial V_e} \hat{\mu}^m_{\mathrm{Li}}\,\vec{h}^m_{\mathrm{Li}}\cdot\vec{n}_a\,\mathrm{d}\Gamma + \int_{\partial V_a\cap\partial V_e} \hat{\mu}^m_{\mathrm{e}^-}\,\vec{h}^m_{\mathrm{e}^-}\cdot\vec{n}_a\,\mathrm{d}\Gamma + \\
&+\int_{\partial V_a\cap\partial V_e} \hat{\mu}^m_{\mathrm{Li}^+}\,\vec{h}^m_{\mathrm{Li}^+}\cdot\vec{n}_e + \hat{\mu}^m_{\mathrm{X}^-}\,\vec{h}^m_{\mathrm{X}^-}\cdot\vec{n}_e\,\mathrm{d}\Gamma + \\
&-\int_{\partial V_a\cap\partial V_e} h_{BV}\,(\hat{\mu}^m_{\mathrm{Li}} - \hat{\mu}^m_{\mathrm{e}^-} - \hat{\mu}^m_{\mathrm{Li}^+})\mathrm{d}\Gamma = 0
\end{aligned}$$

whence the interface conditions (3.23a-d) come out. On interface $\partial V_c \cap \partial V_e$ the following equality holds:

$$\begin{aligned}
&\int_{\partial V_c\cap\partial V_e} \hat{\mu}^m_{\mathrm{e}^-}\,\vec{h}^m_{\mathrm{e}^-}\cdot\vec{n}_c\,\mathrm{d}\Gamma + \int_{\partial V_c\cap\partial V_e} \hat{\mu}^m_{\mathrm{Li}^+}\,\vec{h}^m_{\mathrm{Li}^+}\cdot\vec{n}_e + \hat{\mu}^m_{\mathrm{X}^-}\,\vec{h}^m_{\mathrm{X}^-}\cdot\vec{n}_e\,\mathrm{d}\Gamma + \\
&-\int_{\partial V_c\cap\partial V_e} h_{BV}\,(\hat{\mu}^m_{\mathrm{Li}} - \hat{\mu}^m_{\mathrm{e}^-} - \hat{\mu}^m_{\mathrm{Li}^+})\mathrm{d}\Gamma = 0
\end{aligned}$$

In view of the arbitrariness of $\hat{\mu}^m_{\mathrm{Li}}$ the identity above is satisfied if and only if $h_{BV} = 0$ along $\partial V_c \cap \partial V_e$ as stated by condition (3.62). Accordingly, conditions (3.21) comes out. Finally, along interface $\partial V_c \cap \partial V_a$ it holds

$$\int_{\partial V_a\cap\partial V_e} \hat{\mu}^m_{\mathrm{Li}}\,\vec{h}^m_{\mathrm{Li}}\cdot\vec{n}_a\,\mathrm{d}\Gamma = 0$$

whence condition (3.20) immediately descends.

By applying the divergence theorem to electric field contributions it comes out:

$$
\begin{aligned}
&-\int_{V_a\cup V_c} \nabla\left[\,\hat{\phi}_s^m\,\right]\cdot\left(\frac{\partial\vec{D}_s^m}{\partial t}+\vec{i}_{\mathrm{e}^-}^m\right)\,\mathrm{d}V-\int_{V_e}\nabla\left[\,\hat{\phi}_e^m\,\right]\cdot\left(\frac{\partial\vec{D}_e^m}{\partial t}+\vec{i}_e^m\right)\,\mathrm{d}V\\
&\quad-\int_{\partial V_s\cap\partial V_e}\hat{\xi}^m\,\lambda^m\,\mathrm{d}\Gamma=\\
&\qquad\int_{V_a\cup V_c}\hat{\phi}_s^m\,\mathrm{div}\left[\frac{\partial\vec{D}_s^m}{\partial t}+\vec{i}_{\mathrm{e}^-}^m\right]\,\mathrm{d}V+\int_{V_e}\hat{\phi}_e^m\,\mathrm{div}\left[\frac{\partial\vec{D}_e^m}{\partial t}+\vec{i}_e^m\right]\,\mathrm{d}V+\\
&\qquad\quad-\int_{\partial V_s}\hat{\phi}_s^m\left(\frac{\partial\vec{D}_s^m}{\partial t}+\vec{i}_{\mathrm{e}^-}^m\right)\cdot\vec{n}_s\,\mathrm{d}\Gamma-\int_{\partial V_e}\hat{\phi}_e^m\left(\frac{\partial\vec{D}_e^m}{\partial t}+\vec{i}_e^m\right)\cdot\vec{n}_e\,\mathrm{d}\Gamma+\\
&\qquad\quad-\int_{\partial V_s\cap\partial V_e}\hat{\xi}^m\,\lambda^m\,\mathrm{d}\Gamma
\end{aligned}
$$

Equations (3.5) are recovered in view of Faraday's law constraints (3.63). Furthermore, one has along $\partial V_s\cap\partial V_e$:

$$
-\int_{\partial V_s\cap\partial V_e}\hat{\phi}_s^m\left[\left(\frac{\partial\vec{D}_s^m}{\partial t}+\vec{i}_{\mathrm{e}^-}^m\right)\cdot\vec{n}_s+\lambda^m\right]\,\mathrm{d}\Gamma-\int_{\partial V_s\cap\partial V_e}\hat{\phi}_e^m\left[\left(\frac{\partial\vec{D}_e^m}{\partial t}+\vec{i}_e^m\right)\cdot\vec{n}_e-\lambda^m\right]\,\mathrm{d}\Gamma \tag{3.64}
$$

whence interface condition (3.23e) is recovered. Nernst equation (3.10) is also recovered from

$$
\int_{\partial V_s\cap\partial V_e}\hat{\lambda}^m\left(\xi^m+\frac{\gamma^m}{F}\right)\,\mathrm{d}\Gamma
$$

in a weak form. By comparing equation (3.22) with (3.64), the meaning of the Lagrange multiplier λ^m is apparent.

Faraday's law (3.13) is also recovered from

$$
\int_{\partial V_s\cap\partial V_e}\hat{\lambda}^m\,\left[\lambda^m-F\,h_{BV}\left(\chi^m\right)\right]\,\mathrm{d}\Gamma \tag{3.65}
$$

in a weak form. By comparing equation (3.22) with (3.64), the meaning of the Lagrange multiplier λ^m is apparent.

By applying the divergence theorem to the mechanical contributions it comes out:

$$
\int_V\hat{\boldsymbol{\varepsilon}}^m:\dot{\boldsymbol{\sigma}}^m\,\mathrm{d}V=-\int_V\hat{\vec{u}}^m\cdot\mathrm{div}\left[\,\dot{\boldsymbol{\sigma}}^m\,\right]\,\mathrm{d}V+\int_{\partial V}\hat{\vec{u}}^m\cdot\left(\dot{\boldsymbol{\sigma}}^m\cdot\vec{n}\right)\,\mathrm{d}\Gamma
$$

Force balance equation (3.6) and interface conditions come out. Finally, the boundary conditions on the RVE must satisfy the constraints

$$
\begin{aligned}
&\int_{\partial RVE}\hat{\vec{u}}^m\cdot\left(\dot{\boldsymbol{\sigma}}^m\cdot\vec{n}\right)\,\mathrm{d}\Gamma-\int_{\partial V_s\cap\partial RVE}\hat{\phi}_s^m\left(\frac{\partial\vec{D}_s^m}{\partial t}+\vec{i}_{\mathrm{e}^-}^m\right)\cdot\vec{n}_s\,\mathrm{d}\Gamma+\\
&\quad-\int_{\partial V_e\cap\partial RVE}\hat{\phi}_e^m\left(\frac{\partial\vec{D}_e^m}{\partial t}+\vec{i}_e^m\right)\cdot\vec{n}_e\,\mathrm{d}\Gamma+\int_{\partial V_a\cap\partial RVE}\hat{\mu}_{\mathrm{Li}}^m\,\vec{h}_{\mathrm{Li}}^m\cdot\vec{n}_a\,\mathrm{d}\Gamma+\\
&\quad+\int_{\partial V_s\cap\partial RVE}\hat{\mu}_{\mathrm{e}^-}^m\,\vec{h}_{\mathrm{e}^-}^m\cdot\vec{n}_s\,\mathrm{d}\Gamma+\int_{\partial V_e\cap\partial RVE}\hat{\mu}_{\mathrm{Li}^+}^m\,\vec{h}_{\mathrm{Li}^+}^m\cdot\vec{n}_e+\hat{\mu}_{\mathrm{X}^-}^m\,\vec{h}_{\mathrm{X}^-}^m\cdot\vec{n}_e\,\mathrm{d}\Gamma=0
\end{aligned}
$$

The first term in the sum

$$
\int_{\partial RVE}\hat{\vec{u}}^m\cdot\left(\dot{\boldsymbol{\sigma}}^m\cdot\vec{n}\right)\,\mathrm{d}\Gamma
$$

vanishes in view of the periodic boundary conditions for displacements. All other terms vanish because in view of (3.48) the boundary ∂RVE is of Dirichlet type and the functional space $\mathcal{V}$ is taken homogeneous as usual. Boundary conditions (3.48) formally enter the definition of the functional space $\mathcal{V}^{[0,t_f]}$.

3.6 Appendix: Weak form at the macro scale

The weak form for the macroscale balance equations and boundary conditions on an electrode - in terms of the potentials and displacements in a time interval $[0, t_f]$ - is here considered. By denoting, as for the micro scale, $y^M = \{\mu^M_{\rm Li}, \mu^M_{\rm e^-}, \mu^M_{\rm Li^+}, \mu^M_{\rm X^-}, \phi^M_s, \phi^M_e, \vec{u}^M\}$, the weak form reads

$$\text{Any } y^M \in \mathcal{V}^{[0,t_f]} \text{ such that}$$
$$\frac{\rm d}{{\rm d}t}\, b_{el}\left(\hat{y}^M, z^M(t)\right) + a_{el}(\hat{y}^M, y^M(t)) = f_{el}(\hat{y}^M) + j_{el}(\hat{y}^M) \quad \forall \hat{y}^M \in \mathcal{V}$$

where

$$b_{el}\left(\hat{y}^M, z^M\right) = - \int_\Omega v_a\, \hat{\mu}^M_{\rm Li}\, c^M_{\rm Li} + v_s\, \hat{\mu}^M_{\rm e^-}\, c^M_{\rm e^-} + v_e\, \left(\hat{\mu}^M_{\rm Li^+}\, c^M_{\rm Li^+} + \hat{\mu}^M_{\rm X^-}\, c^M_{\rm X^-}\right) {\rm d}\Omega - \int_\Omega v_s\, \nabla\left[\,\hat{\phi}^M_s\,\right]\cdot \vec{D}^M_s + v_e\, \nabla\left[\,\hat{\phi}^M_e\,\right]\cdot \vec{D}^M_e - \hat{\boldsymbol{\varepsilon}}^M : \boldsymbol{\sigma}^M {\rm d}\Omega$$

$$a_{el}\left(\hat{y}^M, \mathbf{y}^M\right) = \int_\Omega v_a\, \nabla\left[\,\hat{\mu}^M_{\rm Li}\,\right]\cdot \vec{h}^M_{\rm Li} + v_s\, \nabla\left[\,\hat{\mu}^M_{\rm e^-}\,\right]\cdot \vec{h}^M_{\rm e^-} + v_e\, \left(\nabla\left[\,\hat{\mu}^M_{\rm Li^+}\,\right]\cdot \vec{h}^M_{\rm Li^+} + \nabla\left[\,\hat{\mu}^M_{\rm X^-}\,\right]\cdot \vec{h}^M_{\rm X^-}\right) {\rm d}\Omega - \int_\Omega v_s\, \nabla\left[\,\hat{\phi}^M_s\,\right]\cdot \vec{i}^M_{\rm e^-} + v_e\, \nabla\left[\,\hat{\phi}^M_e\,\right]\cdot F\, \left(\vec{h}^M_{\rm Li^+} - \vec{h}^M_{\rm X^-}\right) {\rm d}\Omega$$

$$f_{el}\left(\hat{y}^M\right) = - \int_\Omega s\, \hat{\gamma}^M - r\, \hat{\xi}^M {\rm d}\Omega$$

under the stoichiometric constraints $s = v_a\, s_{\rm Li} = -v_s\, s_{\rm e^-} = -v_e\, s_{\rm Li^+}$, $r = -v_e\, r_{\rm Li^+} = -v_s\, r_{\rm e^-}$. The *pointwise* thermodynamic excess and potential difference are defined as $\hat{\gamma}^M = \hat{\mu}^M_{\rm Li} - \hat{\mu}^M_{\rm e^-} - \hat{\mu}^M_{\rm Li^+}$ and $\hat{\xi}^M = \hat{\phi}^M_s - \hat{\phi}^M_e$. Specification along interfaces between electrodes, separator, and collectors are included in

$$j_{el}\left(\hat{y}^M\right) = \int_{\partial^{cc}\Omega} \hat{\mu}^M_{\rm e^-}\, \overline{h}^M_{\rm e^-}\, {\rm d}\Gamma + \int_{\partial^{sep}\Omega} \hat{\mu}^M_{\rm Li^+}\, \overline{h}^M_{\rm Li^+} + \hat{\mu}^M_{\rm X^-}\, \overline{h}^M_{\rm X^-}\, {\rm d}\Gamma + + \int_{\partial\Omega} \vec{\overline{t}}\cdot \vec{\hat{u}}^M - \hat{\phi}^M_E\, \overline{i}^M_E - \hat{\phi}^M_e\, \overline{i}^M_e\, {\rm d}\Gamma$$

Proof - By applying the divergence theorem to mass contributions in $a_{el}\left(\hat{y}^M, y^M\right)$ it comes out:

$$\int_\Omega v_a\, \nabla\left[\,\hat{\mu}^M_{\rm Li}\,\right]\cdot \vec{h}^M_{\rm Li} + v_s\, \nabla\left[\,\hat{\mu}^M_{\rm e^-}\,\right]\cdot \vec{h}^M_{\rm e^-} + v_e\, \left(\nabla\left[\,\hat{\mu}^M_{\rm Li^+}\,\right]\cdot \vec{h}^M_{\rm Li^+} + \nabla\left[\,\hat{\mu}^M_{\rm X^-}\,\right]\cdot \vec{h}^M_{\rm X^-}\right) {\rm d}\Omega = - \int_\Omega v_a\, \hat{\mu}^M_{\rm Li}\, {\rm div}\left[\,\vec{h}^M_{\rm Li}\,\right] + v_s\, \hat{\mu}^M_{\rm e^-}\, {\rm div}\left[\,\vec{h}^M_{\rm e^-}\,\right] + v_e\, \left(\,\hat{\mu}^M_{\rm Li^+}\, {\rm div}\left[\,\vec{h}^M_{\rm Li^+}\,\right] + \hat{\mu}^M_{\rm X^-}\, {\rm div}\left[\,\vec{h}^M_{\rm X^-}\,\right]\right) {\rm d}\Omega + + \int_{\partial\Omega} v_a\, \hat{\mu}^M_{\rm Li}\, \vec{h}^M_{\rm Li}\cdot\vec{n} + v_s\, \hat{\mu}^M_{\rm e^-}\, \vec{h}^M_{\rm e^-}\cdot\vec{n} + v_e\, \left(\,\hat{\mu}^M_{\rm Li^+}\, \vec{h}^M_{\rm Li^+}\cdot\vec{n} + \hat{\mu}^M_{\rm X^-}\, \vec{h}^M_{\rm X^-}\cdot\vec{n}\right) {\rm d}\Gamma$$

By virtue of the $b_{el}\left(\hat{y}^M, z^M(t)\right)$ contribution to the weak form and of the given terms $f_{el}\left(\hat{y}^M\right)$, the equations of mass balances are recovered in the following form:

$$\frac{\partial c^M_{\rm Li}}{\partial t} + {\rm div}\left[\,\vec{h}^M_{\rm Li}\,\right] = \frac{s}{v_a}\,, \qquad \vec{x}\in\Omega \tag{3.66a}$$

$$\frac{\partial c^M_{\mathrm{Li^+}}}{\partial t} + \operatorname{div}\left[\,\vec{h}^M_{\mathrm{Li^+}}\,\right] = -\frac{s}{v_e}\,, \qquad \vec{x}\in\Omega \tag{3.66b}$$

$$\frac{\partial c^M_{\mathrm{X^-}}}{\partial t} + \operatorname{div}\left[\,\vec{h}^M_{\mathrm{X^-}}\,\right] = 0\,, \qquad \vec{x}\in\Omega \tag{3.66c}$$

$$\frac{\partial c^M_{\mathrm{e^-}}}{\partial t} + \operatorname{div}\left[\,\vec{h}^M_{\mathrm{e^-}}\,\right] = -\frac{s}{v_s}\,, \qquad \vec{x}\in\Omega \tag{3.66d}$$

They coincide with (3.29) in view of the stoichiometric constraints. Along the boundary $\partial\Omega$ the following boundary conditions are derived, owing to $j_{el}\left(\hat{y}^M\right)$:

$$\vec{h}^M_{\mathrm{Li}}\cdot\vec{n} = 0\,, \qquad \vec{x}\in\partial\Omega \tag{3.67a}$$

$$\vec{h}^M_{\mathrm{e^-}}\cdot\vec{n} = 0\,, \qquad \vec{x}\in\partial^{sep}\Omega\,; \qquad \vec{h}^M_{\mathrm{e^-}}\cdot\vec{n} = \frac{\overline{h}^M_{\mathrm{e^-}}}{v_s}\,, \qquad \vec{x}\in\partial^{cc}\Omega \tag{3.67b}$$

$$\vec{h}^M_{\mathrm{Li^+}}\cdot\vec{n} = 0\,, \qquad \vec{x}\in\partial^{cc}\Omega\,; \qquad \vec{h}^M_{\mathrm{Li^+}}\cdot\vec{n} = \frac{\overline{h}^M_{\mathrm{Li^+}}}{v_e}\,, \qquad \vec{x}\in\partial^{sep}\Omega \tag{3.67c}$$

$$\vec{h}^M_{\mathrm{X^-}}\cdot\vec{n} = 0\,, \qquad \vec{x}\in\partial^{cc}\Omega\,; \qquad \vec{h}^M_{\mathrm{X^-}}\cdot\vec{n} = \frac{\overline{h}^M_{\mathrm{X^-}}}{v_e}\,, \qquad \vec{x}\in\partial^{sep}\Omega \tag{3.67d}$$

By applying the divergence theorem to electric field contributions it comes out:

$$\begin{aligned}
&\int_\Omega v_s\,\nabla\left[\,\hat{\phi}^M_s\,\right]\cdot\left(\frac{\partial\vec{D}^M_s}{\partial t}+\vec{i}^M_{\mathrm{e^-}}\right)+v_e\,\nabla\left[\,\hat{\phi}^M_e\,\right]\cdot\left(\frac{\partial\vec{D}^M_e}{\partial t}+F\,\left(\vec{h}^M_{\mathrm{Li^+}}-\vec{h}^M_{\mathrm{X^-}}\right)\right)\mathrm{d}\Omega = \\
&-\int_\Omega v_s\,\hat{\phi}^M_s\,\operatorname{div}\left[\,\frac{\partial\vec{D}^M_s}{\partial t}+\vec{i}^M_{\mathrm{e^-}}\,\right]+v_e\,\hat{\phi}^M_e\,\operatorname{div}\left[\,\frac{\partial\vec{D}^M_e}{\partial t}+F\,\left(\vec{h}^M_{\mathrm{Li^+}}-\vec{h}^M_{\mathrm{X^-}}\right)\right]\mathrm{d}\Omega+ \\
&+\int_{\partial\Omega} v_s\,\hat{\phi}^M_s\left(\frac{\partial\vec{D}^M_s}{\partial t}+\vec{i}^M_{\mathrm{e^-}}\right)\cdot\vec{n}+v_e\,\hat{\phi}^M_e\left(\frac{\partial\vec{D}^M_e}{\partial t}+F\,\left(\vec{h}^M_{\mathrm{Li^+}}-\vec{h}^M_{\mathrm{X^-}}\right)\right)\cdot\vec{n}\,\mathrm{d}\Gamma
\end{aligned}$$

Incremental Gauss's laws are recovered in the following form:

$$\operatorname{div}\left[\,\frac{\partial\vec{D}^M_s}{\partial t}+\vec{i}^M_{\mathrm{e^-}}\,\right] = \frac{r}{v_s}\,, \qquad \vec{x}\in\Omega \tag{3.68a}$$

$$\operatorname{div}\left[\,\frac{\partial\vec{D}^M_e}{\partial t}+F\,\left(\vec{h}^M_{\mathrm{Li^+}}-\vec{h}^M_{\mathrm{X^-}}\right)\right] = -\frac{r}{v_e}\,, \qquad \vec{x}\in\Omega \tag{3.68b}$$

They coincide with (3.30) in view of the stoichiometric constraints. Along the boundary $\partial\Omega$ the following boundary conditions are derived, owing to $j_{el}\left(\hat{y}^M\right)$:

$$\left(\frac{\partial\vec{D}^M_s}{\partial t}+\vec{i}^M_{\mathrm{e^-}}\right)\cdot\vec{n} = \frac{\overline{i}^M_E}{v_s}\,, \qquad \vec{x}\in\partial\Omega \tag{3.69a}$$

$$\left(\frac{\partial\vec{D}^M_e}{\partial t}+F\,\left(\vec{h}^M_{\mathrm{Li^+}}-\vec{h}^M_{\mathrm{X^-}}\right)\right)\cdot\vec{n} = \frac{\overline{i}^M_e}{v_e}\,, \qquad \vec{x}\in\partial\Omega \tag{3.69b}$$

By applying the divergence theorem to the mechanical contributions in $a\left(\hat{y}^M, y^M\right)$ it comes out:

$$\int_\Omega \hat{\boldsymbol{\varepsilon}}^M : \dot{\boldsymbol{\sigma}}^M\,\mathrm{d}\Omega = -\int_\Omega \vec{\hat{u}}^M\cdot\operatorname{div}\left[\,\dot{\boldsymbol{\sigma}}^M\,\right]\,\mathrm{d}\Omega+\int_{\partial\Omega}\vec{\hat{u}}^M\cdot\left(\dot{\boldsymbol{\sigma}}^M\cdot\vec{n}\right)\,\mathrm{d}\Gamma$$

Force balance equation (3.33) comes out, together with the incremental traction boundary conditions along the Neumann part of the boundary.

3.7 Appendix: Hill Mandel extended equation

Taking an electrode as an example for equation (3.36), the extended Hill-Mandel condition (3.57) reads at full length:

$$
\begin{aligned}
&\frac{1}{V}\Bigg[-\int_{V_a}\hat{\mu}^m_{\mathrm{Li}}\;\frac{\partial}{\partial t}\,c^m_{\mathrm{Li}}\,\mathrm{d}V-\int_{V_a\cup V_c}\hat{\mu}^m_{\mathrm{e^-}}\;\frac{\partial}{\partial t}\,c^m_{\mathrm{e^-}}\,\mathrm{d}V+\\
&\quad-\int_{V_e}\hat{\mu}^m_{\mathrm{Li^+}}\;\frac{\partial}{\partial t}\,c^m_{\mathrm{Li^+}}+\hat{\mu}^m_{\mathrm{X^-}}\;\frac{\partial}{\partial t}\,c^m_{\mathrm{X^-}}\,\mathrm{d}V-\int_{V_a\cup V_c}\nabla\left[\,\hat{\phi}^m_s\,\right]\cdot\;\frac{\partial}{\partial t}\,\vec{D}^m_s\,\mathrm{d}V+\\
&\quad\quad-\int_{V_e}\nabla\left[\,\hat{\phi}^m_e\,\right]\cdot\;\frac{\partial}{\partial t}\,\vec{D}^m_e\,\mathrm{d}V+\int_V\hat{\boldsymbol{\varepsilon}}^m:\;\frac{\partial}{\partial t}\,\boldsymbol{\sigma}^m\,\mathrm{d}V+\\
&\quad\quad+\int_{V_a}\nabla\left[\,\hat{\mu}^m_{\mathrm{Li}}\,\right]\cdot\vec{h}^m_{\mathrm{Li}}\,\mathrm{d}V+\int_{V_a\cup V_c}\nabla\left[\,\hat{\mu}^m_{\mathrm{e^-}}\,\right]\cdot\vec{h}^m_{\mathrm{e^-}}\,\mathrm{d}V+\\
&\quad\quad\quad+\int_{V_e}\nabla\left[\,\hat{\mu}^m_{\mathrm{Li^+}}\,\right]\cdot\vec{h}^m_{\mathrm{Li^+}}+\nabla\left[\,\hat{\mu}^m_{\mathrm{X^-}}\,\right]\cdot\vec{h}^m_{\mathrm{X^-}}\,\mathrm{d}V+\\
&\quad\quad\quad\quad+\int_{V_a\cup V_c}\nabla\left[\,\hat{\phi}^m_s\,\right]\cdot F\,\vec{h}^m_{\mathrm{e^-}}\,\mathrm{d}V-\int_{V_e}\nabla\left[\,\hat{\phi}^m_e\,\right]\cdot F\,\left(\vec{h}^m_{\mathrm{Li^+}}-\vec{h}^m_{\mathrm{X^-}}\right)\mathrm{d}V+\\
&\quad\quad\quad\quad\quad-\int_{\partial V_s\cap\partial V_e}h_{BV}\,\hat{\gamma}^m+\hat{\xi}^m\,\lambda^m\;\mathrm{d}\Gamma\Bigg]=\\
&=-\left\{\,v_a\,\hat{\mu}^M_{\mathrm{Li}}\;\frac{\partial}{\partial t}\,c^M_{\mathrm{Li}}+v_s\,\hat{\mu}^M_{\mathrm{e^-}}\;\frac{\partial}{\partial t}\,c^M_{\mathrm{e^-}}+v_e\left(\hat{\mu}^M_{\mathrm{Li^+}}\;\frac{\partial}{\partial t}\,c^M_{\mathrm{Li^+}}+\hat{\mu}^M_{\mathrm{X^-}}\;\frac{\partial}{\partial t}\,c^M_{\mathrm{X^-}}\right)\right\}+\\
&\quad-\left\{\,v_s\,\nabla\left[\,\hat{\phi}^M_s\,\right]\cdot\;\frac{\partial}{\partial t}\,\vec{D}^M_s+v_e\,\nabla\left[\,\hat{\phi}^M_e\,\right]\cdot\;\frac{\partial}{\partial t}\,\vec{D}^M_e\right\}+\\
&\quad\quad+\hat{\boldsymbol{\varepsilon}}^M:\;\frac{\partial}{\partial t}\,\boldsymbol{\sigma}^M+\;v_a\,\nabla\left[\,\hat{\mu}^M_{\mathrm{Li}}\,\right]\cdot\vec{h}^M_{\mathrm{Li}}+\;v_s\,\nabla\left[\,\hat{\mu}^M_{\mathrm{e^-}}\,\right]\cdot\vec{h}^M_{\mathrm{e^-}}+\\
&\quad\quad+v_e\left(\nabla\left[\,\hat{\mu}^M_{\mathrm{Li^+}}\,\right]\cdot\vec{h}^M_{\mathrm{Li^+}}+\nabla\left[\,\hat{\mu}^M_{\mathrm{X^-}}\,\right]\cdot\vec{h}^M_{\mathrm{X^-}}\right)+\\
&\quad\quad\quad+\left\{\,v_s\,\nabla\left[\,\hat{\phi}^M_s\,\right]\cdot F\,\vec{h}^M_{\mathrm{e^-}}-v_e\,\nabla\left[\,\hat{\phi}^M_e\,\right]\cdot F\,\left(\vec{h}^M_{\mathrm{Li^+}}-\vec{h}^M_{\mathrm{X^-}}\right)\right\}+\\
&\quad\quad\quad\quad+\left\{\,s\,\hat{\gamma}^M-\,r\,\hat{\xi}^M\right\}
\end{aligned}
\tag{3.70}
$$

Term by term the different contributions will be analyzed. *Mechanical contribution* - The micro to macro scale transition (3.70) implies:

$$\frac{1}{V}\int_V\hat{\boldsymbol{\varepsilon}}^m:\dot{\boldsymbol{\sigma}}^m\,\mathrm{d}V=\hat{\boldsymbol{\varepsilon}}^M:\dot{\boldsymbol{\sigma}}^M$$

By means of linearization (3.44-a), applying the divergence theorem it comes out:

$$
\begin{aligned}
&\int_V\dot{\boldsymbol{\sigma}}^m:\hat{\varepsilon}^m\,\mathrm{d}V=\int_V\dot{\boldsymbol{\sigma}}^m:(\,\hat{\boldsymbol{\varepsilon}}^M+\nabla\left[\,\vec{\vec{u}}\,\right])\,\mathrm{d}V=\\
&\quad\int_V\dot{\boldsymbol{\sigma}}^m\,\mathrm{d}V:\,\hat{\boldsymbol{\varepsilon}}^M+\int_V\left(\mathrm{div}\left[\,\dot{\boldsymbol{\sigma}}^m\cdot\vec{\vec{u}}\,\right]-\mathrm{div}\left[\,\dot{\boldsymbol{\sigma}}^m\,\right]\cdot\vec{u}\right)\mathrm{d}V=\\
&\quad\quad\int_V\dot{\boldsymbol{\sigma}}^m\,\mathrm{d}V:\,\hat{\boldsymbol{\varepsilon}}^M+\int_{\partial V}(\dot{\boldsymbol{\sigma}}^m\cdot\vec{n})\cdot\vec{u}\,\mathrm{d}\Gamma=\int_V\dot{\boldsymbol{\sigma}}^m\,\mathrm{d}V:\,\hat{\boldsymbol{\varepsilon}}^M
\end{aligned}
\tag{3.71}
$$

due to the anti-periodicity of the tractions $\vec{\vec{p}}^m=\boldsymbol{\sigma}^m\cdot\vec{n}$ over the boundary of the RVE and to the assumption of vanishing body forces, that takes into account of electroneutrality. It

finally holds:

$$\dot{\boldsymbol{\sigma}}^M \;=\; \frac{1}{V}\int_V \dot{\boldsymbol{\sigma}}^m \tag{3.72}$$

Diffusion contribution - For the *neutral Lithium* intercalation/extraction the micro to macro scale transition (3.70) implies:

$$\begin{aligned}\frac{1}{V}\;\Big[\int_{V_a}\nabla\,[\,\hat{\mu}^m_{\rm Li}\,]\cdot\vec{h}^m_{\rm Li}\,{\rm d}\Omega-\int_{V_a}\hat{\mu}^m_{\rm Li}\,\dot{c}^m_{\rm Li}\,{\rm d}\Omega-\int_{\partial V_a\cap\partial V_e}h_{BV}\;\hat{\mu}^m_{\rm Li}\,{\rm d}\Gamma\Big]=\\ v_a\,\Big(\nabla\,[\,\hat{\mu}^M_{\rm Li}\,]\cdot\vec{h}^M_{\rm Li}-\hat{\mu}^M_{\rm Li}\,\dot{c}^M_{\rm Li}\Big)+\;s\;\hat{\mu}^M_{\rm Li}\end{aligned} \tag{3.73}$$

while linearization (3.44-a) specifies as:

$$\hat{\mu}^m_{\rm Li}(\vec{x}) \;=\; \hat{\mu}^m_{\rm Li}(\vec{x}^{\,\rm ref})+\nabla\,[\,\hat{\mu}^M_{\rm Li}\,]\cdot(\vec{x}-\vec{x}^{\,\rm ref})+\hat{\tilde{\mu}}^m_{\rm Li}(\vec{x})\,,\qquad \vec{x}\in V_a \tag{3.74}$$

Owing to the following identity

$$\begin{aligned}&\int_{V_a}\nabla\Big[\,\hat{\tilde{\mu}}^m_{\rm Li}\,\Big]\cdot\vec{h}^m_{\rm Li}\;-\;\hat{\tilde{\mu}}^m_{\rm Li}(\vec{x})\,\dot{c}^m_{\rm Li}\,{\rm d}\Omega=\\ &\int_{V_a}-\hat{\tilde{\mu}}^m_{\rm Li}\underbrace{\Big(\,{\rm div}\Big[\,\vec{h}^m_{\rm Li}\,\Big]+\;\dot{c}^m_{\rm Li}\,\Big)}_{=\,0\text{ in view of (3.3)}}{\rm d}\Omega+\underbrace{\int_{\partial V_a}\hat{\tilde{\mu}}^m_{\rm Li}\;\vec{h}^m_{\rm Li}\cdot\vec{n}\,{\rm d}\Gamma}_{=\,0\text{ in view of (3.47)}}=0\end{aligned} \tag{3.75}$$

the left hand side of eq. (3.73) can be rephrased as:

$$\begin{aligned}&\int_{V_a}\Big(\nabla\,[\,\hat{\mu}^M_{\rm Li}\,]+\;\nabla\Big[\,\hat{\tilde{\mu}}^m_{\rm Li}\,\Big]\Big)\cdot\vec{h}^m_{\rm Li}\,{\rm d}\Omega+\\ &-\int_{V_a}\Big(\hat{\mu}^m_{\rm Li}(\vec{x}^{\,\rm ref})+\nabla\,[\,\hat{\mu}^M_{\rm Li}\,]\cdot(\vec{x}-\vec{x}^{\,\rm ref})+\hat{\tilde{\mu}}^m_{\rm Li}(\vec{x})\Big)\;\dot{c}^m_{\rm Li}\,{\rm d}\Omega+\\ &-\int_{\partial V_a\cap\partial V_e}h_{BV}\;\Big(\hat{\mu}^m_{\rm Li}(\vec{x}^{\,\rm ref})+\nabla\,[\,\hat{\mu}^M_{\rm Li}\,]\cdot(\vec{x}-\vec{x}^{\,\rm ref})+\hat{\tilde{\mu}}^m_{\rm Li}(\vec{x})\Big)\;{\rm d}\Gamma=\\ &=\nabla\,[\,\hat{\mu}^M_{\rm Li}\,]\cdot\Big[\int_{V_a}\vec{h}^m_{\rm Li}\,{\rm d}\Omega-\int_{V_a}\dot{c}^m_{\rm Li}\,(\vec{x}-\vec{x}^{\,\rm ref})\,{\rm d}\Omega+\\ &\quad-\int_{\partial V_a\cap\partial V_e}h_{BV}\;(\vec{x}-\vec{x}^{\,\rm ref})\,{\rm d}\Gamma\Big]+\\ &\quad+\hat{\mu}^m_{\rm Li}(\vec{x}^{\,\rm ref})\Big[-\int_{\partial V_a\cap\partial V_e}h_{BV}\;{\rm d}\Gamma-\int_{V_a}\dot{c}^m_{\rm Li}\,{\rm d}\Omega\Big]+\\ &\quad+\underbrace{\int_{V_a}\nabla\Big[\,\hat{\tilde{\mu}}^m_{\rm Li}\,\Big]\cdot\vec{h}^m_{\rm Li}-\;\hat{\tilde{\mu}}^m_{\rm Li}(\vec{x})\,\dot{c}^m_{\rm Li}\,{\rm d}\Omega}_{=\,0\text{ in view of (3.75)}}-\underbrace{\int_{\partial V_a\cap\partial V_e}h_{BV}\;\hat{\tilde{\mu}}^m_{\rm Li}(\vec{x})\;{\rm d}\Gamma}_{=\,0\text{ in view of (3.47)}}\end{aligned}$$

In view of constraints

$$\begin{aligned}\hat{\mu}^m_{\rm Li}(\vec{x}^{\,\rm ref})&=\hat{\mu}^M_{\rm Li}\\ c^M_{\rm Li}&=\frac{1}{V_a}\int_{V_a}c^m_{\rm Li}\end{aligned}$$

imposed in (3.49) and (3.52), the averages:

$$v_a\,\vec{h}^M_{\mathrm{Li}} = \frac{1}{V}\left[\int_{V_a}\vec{h}^m_{\mathrm{Li}}\,\mathrm{d}\Omega - \int_{V_a}\dot{c}^m_{\mathrm{Li}}\,(\vec{x}-\vec{x}^{\,\mathsf{ref}})\,\mathrm{d}\Omega - \int_{\partial V_a\cap\partial V_e} h_{BV}\,(\vec{x}-\vec{x}^{\,\mathsf{ref}})\,\mathrm{d}\Gamma\right] \tag{3.76}$$

$$s = -\frac{1}{V}\int_{\partial V_a\cap\partial V_e} h_{BV}\,\mathrm{d}\Gamma \tag{3.77}$$

$$v_a\,\dot{c}^M_{\mathrm{Li}} = \frac{1}{V}\int_{V_a}\dot{c}^m_{\mathrm{Li}}\,\mathrm{d}\Omega \tag{3.78}$$

finally come out.

Averages (3.76, 3.77, 3.78) extend to Li-ions and their counter-ions, as well as to electrons. The path of reasoning here taken for neutral Lithium leads to the following identities:

$$v_e\,\vec{h}^M_{\mathrm{X}^-} = \frac{1}{V}\left[\int_{V_e}\vec{h}^m_{\mathrm{X}^-}\,\mathrm{d}\Omega - \int_{V_e}\dot{c}^m_{\mathrm{X}^-}\,(\vec{x}-\vec{x}^{\,\mathsf{ref}})\,\mathrm{d}\Omega\right] \tag{3.79}$$

$$v_e\,\dot{c}^M_{\mathrm{X}^-} = \frac{1}{V}\int_{V_e}\dot{c}^m_{\mathrm{X}^-}\,\mathrm{d}\Omega \tag{3.80}$$

$$v_e\,\vec{h}^M_{\mathrm{Li}^+} = \frac{1}{V}\left[\int_{V_e}\vec{h}^m_{\mathrm{Li}^+}\,\mathrm{d}\Omega - \int_{V_e}\dot{c}^m_{\mathrm{Li}^+}\,(\vec{x}-\vec{x}^{\,\mathsf{ref}})\,\mathrm{d}\Omega + \int_{\partial V_a\cap\partial V_e} h_{BV}\,(\vec{x}-\vec{x}^{\,\mathsf{ref}})\,\mathrm{d}\Gamma\right] \tag{3.81}$$

$$v_e\,\dot{c}^M_{\mathrm{Li}^+} = \frac{1}{V}\int_{V_e}\dot{c}^m_{\mathrm{Li}^+}\,\mathrm{d}\Omega \tag{3.82}$$

$$v_s\,\vec{h}^M_{\mathrm{e}^-} = \frac{1}{V}\left[\int_{V_s}\vec{h}^m_{\mathrm{e}^-}\,\mathrm{d}\Omega - \int_{V_s}\dot{c}^m_{\mathrm{e}^-}\,(\vec{x}-\vec{x}^{\,\mathsf{ref}})\,\mathrm{d}\Omega + \int_{\partial V_a\cap\partial V_e} h_{BV}\,(\vec{x}-\vec{x}^{\,\mathsf{ref}})\,\mathrm{d}\Gamma\right] \tag{3.83}$$

$$v_s\,\dot{c}^M_{\mathrm{e}^-} = \frac{1}{V}\int_{V_s}\dot{c}^m_{\mathrm{e}^-}\,\mathrm{d}\Omega \tag{3.84}$$

Migration contribution - For the *migration processes in the electrolyte* the micro to macro scale transition (3.70) implies:

$$\frac{1}{V}\left[-\int_{V_e}\nabla\left[\,\hat{\phi}^m_e\,\right]\cdot\left(\frac{\partial\vec{D}^m_e}{\partial t} + F\,(\vec{h}^m_{\mathrm{Li}^+}-\vec{h}^m_{\mathrm{X}^-})\right)\mathrm{d}\Omega + \int_{\partial V_s\cap\partial V_e}\lambda^m\,\hat{\phi}^m_e\mathrm{d}\Gamma\right] = -v_e\,\nabla\left[\,\hat{\phi}^M_e\,\right]\cdot\left(\frac{\partial\vec{D}^M_e}{\partial t} + F\,\left(\vec{h}^M_{\mathrm{Li}^+}-\vec{h}^M_{\mathrm{X}^-}\right)\right) + r\;\hat{\phi}^M_e$$

Linearization (3.44-a) specifies as:

$$\hat{\phi}^m_e(\vec{x}) = \hat{\phi}^m_e(\vec{x}^{\,\mathsf{ref}}) + \nabla\left[\,\hat{\phi}^M_e\,\right]\cdot(\vec{x}-\vec{x}^{\,\mathsf{ref}}) + \hat{\tilde{\phi}}^m_e(\vec{x})\;,\qquad \vec{x}\in V_e \tag{3.85}$$

Denoting with $\aleph_e^m = \left(\frac{\partial \vec{D}_e^m}{\partial t} + F\,(\vec{h}_{\mathrm{Li}^+}^m - \vec{h}_{\mathrm{X}^-}^m)\right)$ for the sake of shortness, for being

$$-\int_{V_e} \nabla\left[\hat{\tilde{\phi}}_e^m\right] \cdot \aleph_e^m \,\mathrm{d}\Omega = -\int_{\partial V_e} \underbrace{\hat{\tilde{\phi}}_e^m \,\aleph_e^m \cdot \vec{n}}_{=0 \text{ in view of (3.47)}} \mathrm{d}\Omega + \int_{V_e} \underbrace{\hat{\tilde{\phi}}_e^m \,\mathrm{div}\left[\aleph_e^m\right]}_{=0 \text{ in view of (3.5)}} \mathrm{d}\Omega = 0$$

it comes out:

$$\begin{aligned}
&-\int_{V_e} \left(\nabla\left[\hat{\phi}_e^M\right] + \nabla\left[\hat{\tilde{\phi}}_e^m\right]\right) \cdot \aleph_e^m \,\mathrm{d}\Omega + \\
&+\int_{\partial V_s \cap \partial V_e} \lambda^m \left(\hat{\phi}_e^m(\vec{x}^{\,\mathsf{ref}}) + \nabla\left[\hat{\phi}_e^M\right] \cdot (\vec{x} - \vec{x}^{\,\mathsf{ref}})\right) \mathrm{d}\Gamma + \\
&+\int_{\partial V_s \cap \partial V_e} \lambda^m \underbrace{\hat{\tilde{\phi}}_e^m(\vec{x})}_{=0 \text{ in view of (3.47)}} \mathrm{d}\Gamma = \\
&\hat{\phi}_e^m(\vec{x}^{\,\mathsf{ref}}) \int_{\partial V_s \cap \partial V_e} \lambda^m \,\mathrm{d}\Gamma + \\
&-\nabla\left[\hat{\phi}_e^M\right] \cdot \left[\int_{V_e} \aleph_e^m \,\mathrm{d}\Omega - \int_{\partial V_s \cap \partial V_e} \lambda^m \,(\vec{x} - \vec{x}^{\,\mathsf{ref}}) \mathrm{d}\Gamma\right]
\end{aligned}$$

In view of the constraint (3.49) in the form

$$\hat{\phi}_e^m(\vec{x}^{\,\mathsf{ref}}) = \hat{\phi}_e^M$$

the average

$$r = \frac{1}{V} \int_{\partial V_s \cap \partial V_e} \lambda^m \,\mathrm{d}\Gamma \tag{3.86}$$

comes out together with the following identity:

$$\begin{aligned}
&v_e \left(\frac{\partial \vec{D}_e^M}{\partial t} + F\,\left(\vec{h}_{\mathrm{Li}^+}^M - \vec{h}_{\mathrm{X}^-}^M\right)\right) = \\
&\frac{1}{V}\left[\int_{V_e} \left(\frac{\partial \vec{D}_e^m}{\partial t} + F\,(\vec{h}_{\mathrm{Li}^+}^m - \vec{h}_{\mathrm{X}^-}^m)\right) \mathrm{d}\Omega - \int_{\partial V_s \cap \partial V_e} \lambda^m \,(\vec{x} - \vec{x}^{\,\mathsf{ref}}) \mathrm{d}\Gamma\right]
\end{aligned}$$

The latter can be rearranged taking into account averages (3.79, 3.81) and identity (3.13) as

$$\begin{aligned}
&v_e \,\frac{\partial \vec{D}_e^M}{\partial t} = \\
&\frac{1}{V}\left[\int_{V_e} \frac{\partial \vec{D}_e^m}{\partial t} \,\mathrm{d}\Omega + F \int_{V_e} (\dot{c}_{\mathrm{Li}^+}^m - \dot{c}_{\mathrm{X}^-}^m)\,(\vec{x} - \vec{x}^{\,\mathsf{ref}})\,\mathrm{d}\Omega\right. \\
&\left.-F \int_{\partial V_a \cap \partial V_e} h_{BV}\,(\vec{x} - \vec{x}^{\,\mathsf{ref}}) \mathrm{d}\Gamma - \int_{\partial V_s \cap \partial V_e} \lambda^m \,(\vec{x} - \vec{x}^{\,\mathsf{ref}}) \mathrm{d}\Gamma\right]
\end{aligned} \tag{3.87}$$

The same path of reasoning can be applied to electrons. Average (3.86) again arises in view of constraint

$$\hat{\phi}_s^m(\vec{x}^{\,\mathsf{ref}}) = \hat{\phi}_s^M$$

Furthermore, it holds:

$$v_s \frac{\partial \vec{D}_s^M}{\partial t} = \frac{1}{V}\left[\int_{V_a\cup V_c} \frac{\partial \vec{D}_s^m}{\partial t}\,\mathrm{d}V - F\int_{V_a\cup V_c} \dot{c}_{\mathrm{e}^-}^m\,(\vec{x}-\vec{x}^{\,\mathsf{ref}})\,\mathrm{d}V + F\int_{\partial V_a\cap\partial V_e} h_{BV}\,(\vec{x}-\vec{x}^{\,\mathsf{ref}})\mathrm{d}\Gamma + \int_{\partial V_s\cap\partial V_e} \lambda^m\,(\vec{x}-\vec{x}^{\,\mathsf{ref}})\mathrm{d}\Gamma\right] \tag{3.88}$$

3.8 Appendix: The hypothesis of steady motion of charges at the interfaces

In battery modeling magnetic and electric problems are coupled by the interface conditions, as shown in equation (3.22). Electro-quasi-statics requires the evaluation of the magnetizing field along the interface between active particles and electrolyte. This drawback has been circumvented assuming that the curl of the magnetizing field is continuous across all interfaces when projected in the normal direction. In order to simplify further the model and *uncouple the differential problem for the magnetic field from the other partial differential equations*, the magnetic field *at the interface between active particles and electrolyte* can be estimated from the steady motion of charges (see [13], chapter 3). This approach is pursued in this appendix.

At the micro scale, Ampère's law without Maxwell's correction properly describe the magnetic field generated by a steady current.

$$\mathrm{curl}\left[\vec{H}^m\right]\cdot\vec{n} = \vec{i}^m\cdot\vec{n}$$

At the interface between electrolyte and conductive particles, as no flow of charges take place,

$$\frac{\partial \vec{D}^m}{\partial t}\cdot\vec{n} = 0 \qquad \vec{x}\in\partial V_c\cap\partial V_e \tag{3.89}$$

Noting that the direction of electric current is, by convention, opposite to the direction of electron flow, at the interface between electrolyte and active particles $\partial V_e\cap\partial V_a$, interface conditions read:

$$\left(\frac{\partial \vec{D}_s^m}{\partial t} + \vec{i}_{\mathrm{e}^-}^m\right)\cdot\vec{n}_a = i_{BV} \qquad \vec{x}\in\partial V_a\cap\partial V_e \tag{3.90a}$$

$$\left(\frac{\partial \vec{D}_e^m}{\partial t} + \vec{i}_e^m\right)\cdot\vec{n}_e = -i_{BV} \qquad \vec{x}\in\partial V_a\cap\partial V_e \tag{3.90b}$$

In view of the conditions above, the micro scale weak form is slightly modified. The micro and macro weak forms read:

Microscale:

Find $y^m\in\mathcal{V}^{[0,t_f]}$ such that

$$\frac{\mathrm{d}}{\mathrm{d}t} b^m\left(\hat{y}^m, z^m(t)\right) + a^m(\hat{y}^m, y^m(t)) = 0 \quad \forall \hat{y}^m \in \mathcal{V}$$

where

$$\begin{aligned}
b^m\left(\hat{y}^m, z^m\right) &= -\int_{V_a} \hat{\mu}^m_{\mathrm{Li}}\, c^m_{\mathrm{Li}}\,\mathrm{d}V - \int_{V_a\cup V_c} \hat{\mu}^m_{\mathrm{e}^-}\, c^m_{\mathrm{e}^-}\,\mathrm{d}V - \int_{V_e} \hat{\mu}^m_{\mathrm{Li}^+}\, c^m_{\mathrm{Li}^+} + \hat{\mu}^m_{\mathrm{X}^-}\, c^m_{\mathrm{X}^-}\,\mathrm{d}V \\
&\quad - \int_{V_a\cup V_c} \nabla\left[\,\hat{\phi}^m_s\,\right]\cdot \vec{D}^m_s\,\mathrm{d}V - \int_{V_e} \nabla\left[\,\hat{\phi}^m_e\,\right]\cdot \vec{D}^m_e\,\mathrm{d}V + \int_V \hat{\boldsymbol{\varepsilon}}^m : \boldsymbol{\sigma}^m\,\mathrm{d}V \\
a^m\left(\hat{y}^m, y^m\right) &= \int_{V_a} \nabla\left[\,\hat{\mu}^m_{\mathrm{Li}}\,\right]\cdot \vec{h}^m_{\mathrm{Li}}\,\mathrm{d}V + \int_{V_a\cup V_c} \nabla\left[\,\hat{\mu}^m_{\mathrm{e}^-}\,\right]\cdot \vec{h}^m_{\mathrm{e}^-}\,\mathrm{d}V \\
&+ \int_{V_e} \nabla\left[\,\hat{\mu}^m_{\mathrm{Li}^+}\,\right]\cdot \vec{h}^m_{\mathrm{Li}^+} + \nabla\left[\,\hat{\mu}^m_{\mathrm{X}^-}\,\right]\cdot \vec{h}^m_{\mathrm{X}^-}\,\mathrm{d}V \\
&- \int_{V_a\cup V_c} \nabla\left[\,\hat{\phi}^m_s\,\right]\cdot \vec{i}^m_{\mathrm{e}^-}\,\mathrm{d}V - \int_{V_e} \nabla\left[\,\hat{\phi}^m_e\,\right]\cdot \vec{i}^m_e\,\mathrm{d}V \\
&- \int_{\partial V_a\cap\partial V_e} h_{BV}\,\hat{\gamma}^m - i_{BV}\,\hat{\xi}^m\,\mathrm{d}\Gamma
\end{aligned}$$

with $y^m = \{\mu^m_{\mathrm{Li}}, \mu^m_{\mathrm{e}^-}, \mu^m_{\mathrm{Li}^+}, \mu^m_{\mathrm{X}^-}, \phi^m_s, \phi^m_e, \vec{u}^m\}$ and $i_{BV} = F\, h_{BV}$.

Macroscale:

Any $y^M \in \mathcal{V}^{[0,t_f]}$ such that

$$\frac{\mathrm{d}}{\mathrm{d}t}\, b_{el}\left(\hat{y}^M, z^M(t)\right) + a_{el}(\hat{y}^M, y^M(t)) = f_{el}(\hat{y}^M) + j_{el}(\hat{y}^M) \quad \forall \hat{y}^M \in \mathcal{V}$$

where

$$\begin{aligned}
b_{el}\left(\hat{y}^M, z^M\right) &= -\int_\Omega v_a\,\hat{\mu}^M_{\mathrm{Li}}\, c^M_{\mathrm{Li}} + v_s\,\hat{\mu}^M_{\mathrm{e}^-}\, c^M_{\mathrm{e}^-} + v_e\,\left(\hat{\mu}^M_{\mathrm{Li}^+}\, c^M_{\mathrm{Li}^+} + \hat{\mu}^M_{\mathrm{X}^-}\, c^M_{\mathrm{X}^-}\right)\mathrm{d}\Omega \\
&\quad - \int_\Omega v_s\,\nabla\left[\,\hat{\phi}^M_s\,\right]\cdot \vec{D}^M_s + v_e\,\nabla\left[\,\hat{\phi}^M_e\,\right]\cdot \vec{D}^M_e - \hat{\boldsymbol{\varepsilon}}^M : \boldsymbol{\sigma}^M \mathrm{d}\Omega \\
a_{el}\left(\hat{y}^M, \mathbf{y}^M\right) &= \int_\Omega v_a\,\nabla\left[\,\hat{\mu}^M_{\mathrm{Li}}\,\right]\cdot \vec{h}^M_{\mathrm{Li}} + v_s\,\nabla\left[\,\hat{\mu}^M_{\mathrm{e}^-}\,\right]\cdot \vec{h}^M_{\mathrm{e}^-} \\
&+ v_e\left(\nabla\left[\,\hat{\mu}^M_{\mathrm{Li}^+}\,\right]\cdot \vec{h}^M_{\mathrm{Li}^+} + \nabla\left[\,\hat{\mu}^M_{\mathrm{X}^-}\,\right]\cdot \vec{h}^M_{\mathrm{X}^-}\right)\mathrm{d}\Omega \\
&- \int_\Omega v_s\,\nabla\left[\,\hat{\phi}^M_s\,\right]\cdot \vec{i}^M_{\mathrm{e}^-} + v_e\,\nabla\left[\,\hat{\phi}^M_e\,\right]\cdot F\,\left(\vec{h}^M_{\mathrm{Li}^+} - \vec{h}^M_{\mathrm{X}^-}\right)\mathrm{d}\Omega \\
f_{el}\left(\hat{y}^M\right) &= -\int_\Omega s\,\hat{\gamma}^M - r\,\hat{\xi}^M \mathrm{d}\Omega
\end{aligned}$$

The adjustments in the weak forms impact on some of the scale transition averages, which now read:

$$r = -\frac{1}{V}\int_{\partial V_a\cap\partial V_e} i_{BV}\,\mathrm{d}\Gamma \tag{3.91a}$$

$$v_e\,\frac{\partial \vec{D}^M_e}{\partial t} = \frac{1}{V}\left[\int_{V_e} \frac{\partial \vec{D}^m_e}{\partial t}\,\mathrm{d}V + F\int_{V_e} \left(\dot{c}^m_{\mathrm{Li}^+} - \dot{c}^m_{\mathrm{X}^-}\right)\left(\vec{x} - \vec{x}^{\,\mathsf{ref}}\right)\mathrm{d}V\right] \tag{3.91b}$$

$$v_s\,\frac{\partial \vec{D}^M_s}{\partial t} = \frac{1}{V}\left[\int_{V_a\cup V_c} \frac{\partial \vec{D}^m_s}{\partial t}\,\mathrm{d}V - F\int_{V_a\cup V_c} \dot{c}^m_{\mathrm{e}^-}\,\left(\vec{x} - \vec{x}^{\,\mathsf{ref}}\right)\mathrm{d}V\right] \tag{3.91c}$$

In view of identity (3.13) and of average (3.58-f) - which does not change - terms r and s turn out to be related as

$$r = F\, s \tag{3.92}$$

and equations (3.30) and (3.31) are one and the same.

Part II

Constitutive equations and validation

Chapter 4
Electrolyte Formulation

The formulation presented in section 3.2 outlines a framework for the description of multiphase microstructures of Li-ion batteries composite electrodes. Each component occupying a subdomain of the overall microscale has been related to a proper set of balance equations. Appropriate interface conditions (section 3.2.3) account for interactions among phases.
Nevertheless, each set of balance equations is self consistent. The weak form can be derived (see (3.15), (3.16) and (3.17)) and solved independently if provided with suitable constitutive equations and boundary conditions.
In view of these considerations it is reasonable to validate the formulation disclosed in section 3.2 focusing on a specific set of equations a time. This is the purpose of the chapters 4 and 5 that respectively focus on the electrolyte and active material. A study case has been chosen for each of them that do not require a multiscale description and for which the set of balance equations (3.3-3.6) is suitable.
Reciprocal interactions between electrolyte and active material will be investigated in chapter 6 in which a complete battery cell will be considered.

To validate the modeling of ionic transport in the electrolyte is the purpose of the present chapter[1]. Diffusion and migration govern the process, while convection is disregarded. Maxwell's equations have been used, coupled to Faraday's law of electrochemical charge transfer. The set of continuity equations for mass and Maxwell equations lead to a consistent model, with distinctive energy characteristics.
The chapter does not focus on the double layer in which chemical reactions occur. The formulation is limited to small displacements and strains.

Liquid electrolyte will be first investigated. Attention will be restricted to binary electrolytes, that is, solutions of a binary salt, say LiX, plus a solvent, say a polymer. Both the elements composing the salt are ions, a cation Li^+ and an anion X^- (PF_6^- for instance).

Solid electrolyte will also be considered. Some minor, yet relevant, modifications to transport model are required due to the so-called *ionization reaction*, by which a certain amount of Li-ion is binded to other atoms and not free to flow any more.

General principles of non-equilibrium thermodynamics are presented in section 4.3 following the approach of [16, 17]. The electrochemical potential is defined based on the rate at which power is expended on a material region, including mechanical contributions as well as the power due to mass transport and electromagnetic interactions. All processes are taken to be isothermal. The entropy imbalance with the Coleman-Noll procedure provides thermodynamic restrictions, satisfied by the usual Fickian description of diffusion and migration in terms of the electrochemical potential, defined as in [18, 19]. Infinitely dilute solutions (section 4.4) and solutions close to saturation (section 4.8) are both addressed.

[1] This chapter extends contents of [128–130]

Two different one-dimensional models of ionic transport in the Li-ion batteries electrolyte, inspired by [10, 21], have been numerically simulated. The results published in [10, 21] in terms of concentrations and electric field are recovered, showing the robustness of the approach. The small imbalance of concentration between anions and cations (ten orders of magnitude smaller than the bulk concentration of salt in the electrolyte) is still capable to produce a strong electric field particularly near the electrodes, as already described in [131]. By modeling Maxwell's law explicitly, no theoretical contradictions arise.

4.1 Balance equations: liquid electrolyte

Diffusion is governed by transport of mass, which is a conserved quantity, and described by the mass continuity equation, which is linked to the two ionic concentrations c_{Li^+} and c_{X^-} and to the mass fluxes of Li^+ and X^-. Nevertheless, the set of two mass balance equations contains a further unknown, the electric field, because ionic transport entails movement of mass as well as of charge. For that reason, coupling with an additional relation is mandatory to model the migration process.

The most common selection for such an additional relation in battery modeling is the *electroneutrality* condition

$$c_{\mathrm{Li}^+} - c_{\mathrm{X}^-} = 0 \tag{4.1}$$

which implies that charge separation is impossible and neutrality is maintained in the solution.

In several studies, originated by Newman [6] and collectively gathered in the terminology "porous electrode theory", condition (4.1) is used *in lieu of Maxwell's law* - see among others [28, 49–51, 90, 132, 133]. Other Authors describe migration via equation (4.1), e.g. [10, 21, 134]. In all the aforementioned models, the electric field is not constrained in any way to satisfy Maxwell's equations. Remarkably, paradoxically as stated in [7], it does violate[2] Maxwell's equations (see for instance [10], fig. 3 and comments therein).

Equation (4.1) reflects physical properties of the processes in an average sense and has to be considered as an approximation as pointed out in [7]. An excellent discussion on the origin of equation (4.1) can also be found there in terms of the Debye length (see also section 2.3)

$$r_D = \sqrt{\frac{1}{2}\frac{\mathrm{\not\epsilon}}{c_{bulk}}\frac{RT}{F^2}}$$

It assesses a charge electrostatic effect in the electrolyte solution, and measures how far that effect persists. The Debye length is typically in the order of nanometers or even below in battery cells electrolyte (see section 4.6).

In the present chapter, equation (4.1) is not used as a fundamental law. Instead, the electro-magnetics is explicitly taken into account via the *electro-quasi-static* formulation [14] of Maxwell's equations, summarized in section 2.1. Inductive effects are not included, yet the effect of the magnetizing field is taken into account by means of Maxwell's correction within Ampère's law. This is major novelty of the proposed approach, in which electroneutrality is an outcome of the problem solution. The numerical simulations performed in section 4.6, where real battery data are considered, reveal that the deviation from electroneutrality is

[2] This is immediately accomplished in 1D, where in view of electroneutrality Gauss law reads $\frac{\partial D}{\partial x} = 0$, thus leading to a constant electric field.

as small as expected, ten orders of magnitude with respect to the equilibrium electrolyte concentration, in agreement with the literature (see [6], page 286 and [131]).

Electroneutrality is used to identify the relevance of external actions, in order to simplify the model (refer to section 2.3). For the balance of momentum, Lorentz's forces are indeed related to the deviation from electroneutrality. The effect of such forces appears to be of second order compared to the effects of surface tractions of mechanical origin.

The balance equations underlying the formulation are briefly recalled (compare with section 3.2.1).

The *mass balance* equations characterize the transport of Li^+ and X^- ions in the electrolyte.

$$\frac{\partial c_{\mathrm{Li}^+}}{\partial t} + \operatorname{div}\left[\,\vec{h}_{\mathrm{Li}^+}\,\right] = 0 \qquad \vec{x} \in V_e \tag{4.2a}$$

$$\frac{\partial c_{\mathrm{X}^-}}{\partial t} + \operatorname{div}\left[\,\vec{h}_{\mathrm{X}^-}\,\right] = 0 \qquad \vec{x} \in V_e \tag{4.2b}$$

Taking into account Faraday's law (2.3), the rate equation (2.14) govern the electric displacement field

$$\operatorname{div}\left[\,\frac{\partial \vec{D}_e}{\partial t} + F\,(\vec{h}_{\mathrm{Li}^+} - \vec{h}_{\mathrm{X}^-})\,\right] \;=\; 0 \qquad \vec{x} \in V_e \tag{4.2c}$$

Neglecting Lorentz forces in view of electroneutrality assumption, the balance of forces applies without any body forces:

$$\operatorname{div}\left[\,\boldsymbol{\sigma}\,\right] = \vec{0} \qquad \vec{x} \in V_e \tag{4.2d}$$

It is worth pointing out that equations (4.2) are defined for $\vec{x} \in V_e$ (compare with 3.2.1) to stress that only the electrolyte is taken into account in this context.

4.2 Weak form and boundary conditions

Following the approach pursued in section 3.2.3 the weak formulation is constructed in terms of chemical and electric potentials $y = \{\mu_{\mathrm{Li}^+}, \mu_{\mathrm{X}^-}, \phi\}$ in a time interval $[0, t_f]$, thus entailing the same energy meaning (consistent with [8, 9]). The contribution related to the mass balance equations (4.2) for cations and anions reads ($\alpha = \mathrm{Li}^+, \mathrm{X}^-$):

$$\begin{aligned}
&\int_{V_e} \hat{\mu}_\alpha \left\{ \frac{\partial c_\alpha}{\partial t} + \operatorname{div}\left[\,\vec{h}_\alpha\,\right] \right\} \mathrm{d}V = \\
&\quad = \int_{V_e} \hat{\mu}_\alpha \, \frac{\partial c_\alpha}{\partial t} \, \mathrm{d}V - \int_{V_e} \nabla\left[\,\hat{\mu}_\alpha\,\right] \cdot \vec{h}_\alpha \, \mathrm{d}V + \int_{\partial V_e} \hat{\mu}_\alpha \, \vec{h}_\alpha \cdot \vec{n} \, \mathrm{d}\Gamma = 0
\end{aligned} \tag{4.3}$$

The last term at the right hand side of (4.3) is a contribution defined at the boundary $\Gamma_{BV} \subseteq \partial V_e^N$ of the electrolyte. Γ_{BV} is the only portion of the boundary along which a non-zero Neumann term is present, i.e. the location where the oxidation/reduction reaction takes place within a battery cell. At that locus there is no intercalation of X^--anions, whereas Faradaic reaction (1.2) converts the oxidized Lithium to its neutral state before it diffuses into the electrodes or vice versa. Therefore, the electrolyte boundaries are discontinuity loci

for the electric and chemical potentials within a cell, (they represent the electric and the reaction Gibbs energies [118], respectively). As this chapter is restricted to the electrolyte only, electrode kinetics is not detailed and the mass flux at the boundary, termed h_{BV}, must be derived from a Butler-Volmer equation, which is here considered as given. Mass flux boundary conditions thus read:

$$\vec{h}_{\mathrm{Li^+}} \cdot \vec{n} = -h_{BV} \qquad \vec{x} \in \Gamma_{BV} \tag{4.4a}$$

$$\vec{h}_{\mathrm{Li^+}} \cdot \vec{n} = 0 \qquad \vec{x} \in \partial^N V_e \setminus \Gamma_{BV} \tag{4.4b}$$

$$\vec{h}_{\mathrm{X^-}} \cdot \vec{n} = 0 \qquad \vec{x} \in \partial^N V_e \tag{4.4c}$$

With a similar reasoning, balance law (4.2c) becomes

$$\begin{aligned} &\int_{V_e} \hat{\phi}_e \,\mathrm{div}\left[\frac{\partial \vec{D}_e}{\partial t} + F\left(\vec{h}_{\mathrm{Li^+}} - \vec{h}_{\mathrm{X^-}}\right)\right] \mathrm{d}V = \\ &\quad - \int_{V_e} \nabla\left[\hat{\phi}_e\right] \cdot \frac{\partial \vec{D}_e}{\partial t}\,\mathrm{d}V - F\int_{V_e} \nabla\left[\hat{\phi}_e\right] \cdot \left(\vec{h}_{\mathrm{Li^+}} - \vec{h}_{\mathrm{X^-}}\right) \mathrm{d}V + \\ &\quad + \int_{\partial V_e} \hat{\phi}_e \left\{\frac{\partial \vec{D}_e}{\partial t} + F\left(\vec{h}_{\mathrm{Li^+}} - \vec{h}_{\mathrm{X^-}}\right)\right\} \cdot \vec{n}\,\mathrm{d}\Gamma = 0 \end{aligned} \tag{4.5}$$

Ampère's law (2.9) allows to extract boundary conditions for the electric potential

$$\left\{\frac{\partial \vec{D}_e}{\partial t} + F\left(\vec{h}_{\mathrm{Li^+}} - \vec{h}_{\mathrm{X^-}}\right)\right\} \cdot \vec{n} = \mathrm{curl}\left[\vec{H}\right] \cdot \vec{n} \qquad \vec{x} \in \partial V_e \tag{4.6}$$

making the evaluation of the magnetizing field $\vec{H}$ unavoidable, as noticed in section 3.2.3. To circumvent such a drawback it will be assumed henceforth that $\vec{B}$ *along the boundary* can be estimated from the "steady current" theory (see [13], chapter 3 and appendix 3.8).

A different approach has been pursued in section 3.2.3 (according to [9]), where the curl of the magnetizing field was assumed to be continuous across all interfaces when projected in the normal direction. Such a continuity condition led to a formulation of the problem in terms of Lagrange multipliers, that unfortunately cannot be rephrased for the case where only the electrolyte is modeled. Ampère's law without Maxwell's correction describes the magnetic field generated by a steady current

$$\mathrm{curl}\left[\vec{H}\right] \cdot \vec{n} = -F\,h_{BV} \qquad \vec{x} \in \Gamma_{BV} \tag{4.7}$$

In view of (4.4) and (4.6), boundary conditions for the electric potential read:

$$\frac{\partial \vec{D}_e}{\partial t} \cdot \vec{n} = 0 \qquad \vec{x} \in \Gamma_{BV} \tag{4.8}$$

To make the solution of the problem unique, Dirichlet boundary conditions (usually homogeneous) for the potential need to be added.

Finally, for the equilibrium equations (4.2d) in rate form one writes

$$\int_{V_e} \vec{\hat{u}} \cdot\ \mathrm{div}\left[\frac{\partial \boldsymbol{\sigma}}{\partial t}\right] \mathrm{d}V \;=\; -\int_{V_e} \hat{\boldsymbol{\varepsilon}} : \frac{\partial \boldsymbol{\sigma}}{\partial t}\,\mathrm{d}V + \int_{\partial V_e} \vec{\hat{u}} \cdot\ \frac{\partial \boldsymbol{\sigma}}{\partial t} \cdot \vec{n}\,\mathrm{d}\Gamma = 0 \tag{4.9}$$

The given tractions along the Neumann part of the boundary $\partial^N V$ will be denoted with $\vec{\overline{p}}$

$$\boldsymbol{\sigma} \cdot \vec{n} = \vec{\overline{p}} \qquad \vec{x} \in \partial^N V_e \tag{4.10}$$

A Dirichlet boundary condition (usually homogeneous) for the displacements shall be added along the Dirichlet part $\partial^D V_e$.

The extension of Neumann boundaries are defined for each field and differ from field to field. In order to enlighten the notation however the field dependence has not been specified in writing $\partial^N V$ and has been left backward. Same arguments apply to Dirichlet boundaries.

In conclusion, the weak form of the balance equations can be written in terms of the potentials in time interval $[0, t_f]$ as

$$\text{Find } y \in \mathcal{V}^{[0,t_f]} \text{ such that} \qquad \frac{\mathrm{d}}{\mathrm{d}t} b\left(\hat{y}, z(t)\right) + a(\hat{y}, y(t)) = f(\hat{y}) \quad \forall \hat{y} \in \mathcal{V} \tag{4.11}$$

where

$$\begin{aligned}
b\left(\hat{y}, z\right) &= -\int_{V_e} \hat{\mu}_{\mathrm{Li}^+}\, c_{\mathrm{Li}^+} + \hat{\mu}_{\mathrm{X}^-}\, c_{\mathrm{X}^-}\, \mathrm{d}V - \int_{V_e} \nabla\left[\,\hat{\phi}_e\,\right] \cdot \vec{D}_e\, \mathrm{d}V + \int_{V_e} \hat{\boldsymbol{\varepsilon}} : \boldsymbol{\sigma}\, \mathrm{d}V \\
a\left(\hat{y}, y\right) &= \int_{V_e} \nabla\left[\,\hat{\mu}_{\mathrm{Li}^+}\,\right] \cdot \vec{h}_{\mathrm{Li}^+} + \nabla\left[\,\hat{\mu}_{\mathrm{X}^-}\,\right] \cdot \vec{h}_{\mathrm{X}^-}\, \mathrm{d}V + \\
&\quad - \int_{V_e} \nabla\left[\,\hat{\phi}_e\,\right] \cdot \left(F\,\left(\vec{h}_{\mathrm{Li}^+} - \vec{h}_{\mathrm{X}^-}\right)\right) \mathrm{d}V \\
f\left(\hat{y}\right) &= \int_{\Gamma_{BV}} \left(F\hat{\phi}_e - \hat{\mu}_{\mathrm{Li}^+}\right) h_{BV}\, \mathrm{d}\Gamma + \int_{\partial^N V_e} \vec{\hat{u}} \cdot\, \frac{\partial \vec{\overline{p}}}{\partial t}\, \mathrm{d}\Gamma
\end{aligned}$$

with $z = \{\, c_{\mathrm{Li}^+},\, c_{\mathrm{X}^-}\}$, $y = \{\mu_{\mathrm{Li}^+}, \mu_{\mathrm{X}^-}, \phi_e, \vec{u}\}$. Columns z and y collect the time-dependent unknown fields. Column $\hat{y}$ collects the steady-state test functions that correspond to the unknown fields in y. To computationally solve the (either weak or strong) problem, constitutive equations must be specified, which is the subject of sections 4.4 and 4.8. Ellipticity of operators, functional and numerical properties of the solution and of its approximation depend on the constitutive assumptions and on the choice of the correct functional spaces $\mathcal{V}^{[0,t_f]}, \mathcal{V}$, whose identification falls beyond the scope of the present paper.

Factor $F\hat{\phi}_e - \hat{\mu}_{\mathrm{Li}^+}$ on the right hand side represents the contribution of the electrolyte to Gibbs reaction energy at the interface.

The weak form (4.11) is remarkably different from the literature [48, 50, 51] and acquires the usual physical meaning of power expenditure: for this reason it is written in terms of chemical potentials rather than concentrations.

4.3 Thermodynamics: electrolyte

4.3.1 Energy balance

The first law of thermodynamics, in the assumption of *small displacements*, represents the balance of the interplay between the internal energy of a material region $\mathcal{P}$, the power expended on $\mathcal{P}$, the heat transferred in $\mathcal{P}$, and the power due to mass and electromagnetic

interactions exchanged on $\mathcal{P}$. The energy balance for the problem at hand, for *quasi-static interactions*, reads:

$$\frac{\partial \mathcal{U}(\mathcal{P})}{\partial t} = \mathcal{W}(\mathcal{P}) + \mathcal{Q}(\mathcal{P}) + \mathcal{T}(\mathcal{P}) + \mathcal{E}(\mathcal{P}) \tag{4.12}$$

with $\mathcal{U}$ the net internal energy of $\mathcal{P}$, $\mathcal{W}(\mathcal{P})$ the mechanical external power, $\mathcal{Q}$ the power due to heat transfer, $\mathcal{T}$ the power due to mass transfer, $\mathcal{E}$ the power due to electromagnetic interactions. It is assumed that any of these processes is accompanied with its own *separate energy contribution* in the balance, in particular *the energies due to charges and mass transfer are additively treated* as two separate processes. The individual contributions read:

$$\mathcal{W}(\mathcal{P}) = \int_{\mathcal{P}} \vec{b} \cdot \vec{v} \, \mathrm{d}\Omega + \int_{\partial\mathcal{P}} \vec{p} \cdot \vec{v} \, \mathrm{d}\Gamma \tag{4.13a}$$

$$\mathcal{Q}(\mathcal{P}) = \int_{\mathcal{P}} s_q \, \mathrm{d}\Omega - \int_{\partial\mathcal{P}} \vec{q} \cdot \vec{n} \, \mathrm{d}\Gamma \tag{4.13b}$$

$$\mathcal{T}(\mathcal{P}) = \sum_{\alpha} \left\{ \int_{\mathcal{P}} \mu_\alpha \, s_\alpha \, \mathrm{d}\Omega - \int_{\partial\mathcal{P}} \mu_\alpha \, \vec{h}_\alpha \cdot \vec{n} \, \mathrm{d}\Gamma \right\} \tag{4.13c}$$

$$\mathcal{E}(\mathcal{P}) = - \int_{\partial\mathcal{P}} (\vec{E} \times \vec{H}) \cdot \vec{n} \, \mathrm{d}\Gamma \tag{4.13d}$$

The time variation of net internal energy corresponds to the power expenditure of external agencies: a mechanical contribution due to body forces $\vec{b}$ and contact forces $\vec{p}$ that spend power against velocities $\vec{v}$; a heat contribution where the scalar s_q is the heat supplied by external agencies and $\vec{q}$ is the heat flux vector; a mass flux contribution with the scalar μ denoting the *chemical* potential, the scalar s_α the supply of species ($\alpha = \mathrm{Li}^+, \mathrm{X}^-$) and $\vec{h}_\alpha$ the mass flux vector; an electromagnetic contribution with the energy flux vector $\vec{E} \times \vec{H}$ generated by the electric and magnetizing fields. It is not trivial to recognize $\vec{E} \times \vec{H}$ as an energy flux vector, but it actually results from Poyinting's theorem (see also [17, 18]).

As usual in thermodynamics of continua one can write the local form of the first principle in terms of rates of the specific (i.e. per unit volume in the reference body, see [16]) internal energy u[3]

$$\mathcal{U}(\mathcal{P}) = \int_{\mathcal{P}} u \, \mathrm{d}\Omega$$

Standard application of the divergence theorem and of mass balances (4.2a-b) leads from (4.13) to

$$\mathcal{W}(\mathcal{P}) = \int_{\mathcal{P}} \boldsymbol{\sigma} : \frac{\partial \boldsymbol{\varepsilon}}{\partial t} \, \mathrm{d}\Omega \tag{4.14a}$$

$$\mathcal{Q}(\mathcal{P}) = \int_{\mathcal{P}} s_q - \mathrm{div}\,[\,\vec{q}\,] \, \mathrm{d}\Omega \tag{4.14b}$$

$$\mathcal{T}(\mathcal{P}) = \sum_{\alpha} \int_{\mathcal{P}} \mu_\alpha \frac{\partial c_\alpha}{\partial t} - \vec{h}_\alpha \cdot \nabla\,[\,\mu_\alpha\,] \, \mathrm{d}\Omega \tag{4.14c}$$

For the electromagnetic contribution one writes

$$\begin{aligned} \mathcal{E}(\mathcal{P}) &= - \int_{\partial\mathcal{P}} (\vec{E} \times \vec{H}) \cdot \vec{n} \, \mathrm{d}\Gamma = - \int_{\mathcal{P}} \mathrm{div} \left[\vec{E} \times \vec{H} \right] \mathrm{d}\Omega = \\ &= - \int_{\mathcal{P}} \vec{H} \cdot \mathrm{curl} \left[\vec{E} \right] - \mathrm{curl} \left[\vec{H} \right] \cdot \vec{E} \, \mathrm{d}\Omega \end{aligned} \tag{4.15}$$

[3] No source of confusion between the internal energy density u and the displacement vector $\vec{u}$ should arise.

After substitution of the curls from Maxwell's equations, Poynting's theorem comes out. In the assumption of electro-quasi-statics and in view of Ampère's-Maxwell's law (2.9)

$$\mathcal{E}(\mathcal{P}) = \int_{\mathcal{P}} \left(\frac{\partial \vec{D}}{\partial t} + \vec{i} \right) \cdot \vec{E} \, \mathrm{d}\Omega \tag{4.16}$$

The local form of the first principle in terms of rates of the internal energy u arises since the energy balance (4.12) must hold for all regions $\mathcal{P}$. It reads:

$$\frac{\partial u}{\partial t} = \boldsymbol{\sigma} : \frac{\partial \boldsymbol{\varepsilon}}{\partial t} + s_q - \operatorname{div}[\,\vec{q}\,] + \left(\frac{\partial \vec{D}}{\partial t} + \vec{i} \right) \cdot \vec{E} + \sum_{\alpha} \mu_\alpha \frac{\partial c_\alpha}{\partial t} - \vec{h}_\alpha \cdot \nabla[\,\mu_\alpha\,] \tag{4.17}$$

The electromagnetic contribution (4.16) to the energy balance can be given a different expression in the framework of electro-quasi-statics, keeping in mind that charges are conveyed together with mass and thus the processes of migration and diffusion are coupled. The link between the two processes is Faraday's laws of electrolysis (2.3). Exploiting it together with Gauss's law (2.8) and definition of $\vec{E}_e$ (2.13), (4.16) becomes

$$\begin{aligned}
\mathcal{E}(\mathcal{P}) &= -\int_{\mathcal{P}} \frac{\partial \vec{D}}{\partial t} \cdot \nabla[\,\phi\,] + \vec{i} \cdot \nabla[\,\phi\,] \, \mathrm{d}\Omega = \\
&= -\int_{\mathcal{P}} \operatorname{div}\left[\phi \frac{\partial \vec{D}}{\partial t} \right] - \phi \operatorname{div}\left[\frac{\partial \vec{D}}{\partial t} \right] + F \sum_{\alpha} z_\alpha \vec{h}_\alpha \cdot \nabla[\,\phi\,] \, \mathrm{d}\Omega = \\
&= \int_{\mathcal{P}} \phi \frac{\partial \zeta}{\partial t} - \sum_{\alpha} (F\, z_\alpha \nabla[\,\phi\,]) \cdot \vec{h}_\alpha \, \mathrm{d}\Omega - \int_{\partial\mathcal{P}} \phi \frac{\partial \vec{D}}{\partial t} \cdot \vec{n} \, \mathrm{d}\Gamma = \\
&= \sum_{\alpha} \int_{\mathcal{P}} (F\, z_\alpha\, \phi) \frac{\partial c_\alpha}{\partial t} - (F\, z_\alpha \nabla[\,\phi\,]) \cdot \vec{h}_\alpha \, \mathrm{d}\Omega - \int_{\partial\mathcal{P}} \phi \frac{\partial \vec{D}}{\partial t} \cdot \vec{n} \, \mathrm{d}\Gamma
\end{aligned} \tag{4.18}$$

From (4.14, 4.18), the power expenditure due to mass transfer and electromagnetic interactions specialize in the electrolyte as:

$$\begin{aligned}
&\mathcal{T}(\mathcal{P}) + \mathcal{E}(\mathcal{P}) = \\
&\sum_{\alpha} \int_{\mathcal{P}} (\mu_\alpha + F\, z_\alpha\, \phi) \frac{\partial c_\alpha}{\partial t} - \vec{h}_\alpha \cdot \nabla[\,\mu_\alpha + F\, z_\alpha\, \phi\,] \, \mathrm{d}\Omega - \int_{\partial\mathcal{P}} \phi \frac{\partial \vec{D}}{\partial t} \cdot \vec{n} \, \mathrm{d}\Gamma
\end{aligned} \tag{4.19}$$

In the absence of charged species, only diffusion takes place; the relevant constitutive theory can be found in [16], section 66. In its dual way, in the absence of gradients of chemical potential, diffusion cannot proceed and current is thus driven by migration only. When diffusion is present, a current density rises due to Faraday's law and both processes contribute to the charge flux. It is therefore clear that concentration gradients and electric field act contemporarily to generate ion mobility. This is the intimate nature of the energy contribution (4.19) and of the electrochemical potential $\overline{\mu}_\alpha$ that in the light of (4.19) will be *defined by the decomposition*

$$\overline{\mu}_\alpha = \mu_\alpha + F\, z_\alpha\, \phi \tag{4.20}$$

- see also [18], chapter XIII, section 3.4, formula (42). Accordingly, the local form of the first principle in terms of rates of the referential internal energy u reads also:

$$\frac{\partial u}{\partial t} = \boldsymbol{\sigma} : \frac{\partial \boldsymbol{\varepsilon}}{\partial t} + s_q - \operatorname{div}[\,\vec{q}\,] - \operatorname{div}\left[\phi \frac{\partial \vec{D}}{\partial t} \right] + \sum_{\alpha} \overline{\mu}_\alpha \frac{\partial c_\alpha}{\partial t} - \vec{h}_\alpha \cdot \nabla[\,\overline{\mu}_\alpha\,] \tag{4.21}$$

4.3.2 Entropy imbalance

A local form of the entropy imbalance can be derived from the Clausis-Duhem inequality in terms of the referential entropy η and of the absolute temperature T [16]:

$$\frac{\partial \eta}{\partial t} - \frac{q}{T} + \operatorname{div}\left[\frac{\vec{q}}{T}\right] \geq 0 \tag{4.22}$$

By noting that

$$\operatorname{div}\left[\frac{\vec{q}}{T}\right] = \frac{1}{T}\operatorname{div}[\vec{q}] - \frac{1}{T^2}\,\vec{q}\cdot\nabla[T]$$

the entropy imbalance can be expressed in terms of internal energy in the form (4.17)

$$\begin{aligned} T\,\frac{\partial \eta}{\partial t} - \left\{ \frac{\partial u}{\partial t} - \boldsymbol{\sigma} : \frac{\partial \boldsymbol{\varepsilon}}{\partial t} - \left(\frac{\partial \vec{D}}{\partial t} + \vec{i}\right)\cdot\vec{E} + \right. \\ \left. - \sum_{\alpha}\left(\mu_\alpha\,\frac{\partial c_\alpha}{\partial t} - \vec{h}_\alpha\cdot\nabla[\mu_\alpha]\right)\right\} - \frac{1}{T}\,\vec{q}\cdot\nabla[T] \geq 0 \end{aligned} \tag{4.23}$$

Consider the internal energy u to be function of the entropy η, the concentrations c_α, the electric displacement field $\vec{D}$, and the kinematic variables in terms of the small strain tensor $\boldsymbol{\varepsilon}$. One has therefore

$$\frac{\partial u}{\partial t} = \frac{\partial u}{\partial \eta}\,\frac{\partial \eta}{\partial t} + \frac{\partial u}{\partial \boldsymbol{\varepsilon}} : \frac{\partial \boldsymbol{\varepsilon}}{\partial t} + \frac{\partial u}{\partial \vec{D}}\cdot\frac{\partial \vec{D}}{\partial t} + \sum_{\alpha}\frac{\partial u}{\partial c_\alpha}\,\frac{\partial c_\alpha}{\partial t} \tag{4.24}$$

to be inserted in (4.23). The entropy imbalance yields

$$\begin{aligned} \frac{\partial \eta}{\partial t}\left(T - \frac{\partial u}{\partial \eta}\right) + \frac{\partial \boldsymbol{\varepsilon}}{\partial t} : \left(\boldsymbol{\sigma} - \frac{\partial u}{\partial \boldsymbol{\varepsilon}}\right) + \frac{\partial \vec{D}}{\partial t}\cdot\left(\vec{E} - \frac{\partial u}{\partial \vec{D}}\right) + \\ + \sum_{\alpha}\frac{\partial c_\alpha}{\partial t}\left(\mu_\alpha - \frac{\partial u}{\partial c_\alpha}\right) + \vec{i}\cdot\vec{E} - \sum_{\alpha}\vec{h}_\alpha\cdot\nabla[\mu_\alpha] - \frac{1}{T}\,\vec{q}\cdot\nabla[T] \geq 0 \end{aligned} \tag{4.25}$$

Term $\vec{i}\cdot\vec{E}$ is the Joule effect. In view of Faraday's law, easy algebra allows to write:

$$\begin{aligned} \vec{i}\cdot\vec{E} - \sum_{\alpha}\vec{h}_\alpha\cdot\nabla[\mu_\alpha] = -F\sum_{\alpha} z_\alpha\,\vec{h}_\alpha\cdot\nabla[\phi] - \sum_{\alpha}\vec{h}_\alpha\cdot\nabla[\mu_\alpha] = \\ - \sum_{\alpha}\vec{h}_\alpha\cdot(\nabla[\mu_\alpha] + z_\alpha\,F\,\nabla[\phi]) = -\sum_{\alpha}\vec{h}_\alpha\cdot\nabla[\overline{\mu}_\alpha] \end{aligned}$$

taking into account (4.20). By applying the Coleman-Noll procedure, one requires that inequality (4.25) holds for all constitutive processes [16, 135]. The following thermodynamic restrictions thus arise:

$$\begin{aligned} T - \frac{\partial u}{\partial \eta} = 0\,, \qquad \boldsymbol{\sigma} - \frac{\partial u}{\partial \boldsymbol{\varepsilon}} = 0\,, \qquad \mu_\alpha - \frac{\partial u}{\partial c_\alpha} = 0\,, \qquad \vec{E} - \frac{\partial u}{\partial \vec{D}} = 0\,, \\ \vec{h}_\alpha\cdot\nabla[\overline{\mu}_\alpha] \geq 0\,, \qquad \frac{1}{T}\,\vec{q}\cdot\nabla[T] \leq 0 \end{aligned} \tag{4.26}$$

Different thermodynamic potentials can be considered rather than the internal energy u. A classical one is the specific *Helmholtz free energy*

$$\psi(T, \boldsymbol{\varepsilon}, c_\alpha, \vec{E}) = u(\eta, \boldsymbol{\varepsilon}, c_\alpha, \vec{D}) - T\,\eta - \vec{E}\cdot\vec{D}$$

that will be used henceforth.

4.4 Constitutive theory: ideal solution

The constitutive specifications outlined in this section are essentially based on literature. Recent scientific investigations provided significant progresses on the mechanical constitutive behavior of energy storage materials. We here depart from these insights, aiming for simple, yet efficient, models.

As in [128] the Helmholtz free energy density ψ that describes the isothermal processes at hand is assumed to consist of three separate parts:

$$\psi(\boldsymbol{\varepsilon}, c_\alpha, \vec{E}) = \psi_{diff}(c_\alpha) + \psi_{el}(\vec{E}) + \psi_{mech}(\boldsymbol{\varepsilon}) \tag{4.27}$$

The mass transport process is described by ψ_{diff}, adopting species concentrations c_α as the state variables. The contribution ψ_{el} models the electromagnetic interactions, in terms of the electric field $\vec{E}$. Finally, ψ_{mech} is the mechanical energy density. Noteworthy, the processes are thermodynamically uncoupled: the electrolyte is made of materials whose properties are insensitive to the deformations, the electric field, and the ionic concentrations. This feature will not be replicated in the electrodes.

The electric displacement field is related to the electric field constitutively. In linear media

$$\psi_{el}(\vec{E}\,) = -\frac{1}{2}\mathfrak{E}\,\vec{E}\cdot\vec{E} \tag{4.28}$$

whence

$$\vec{D} = \mathfrak{E}\,\vec{E} = -\mathfrak{E}\,\nabla\,[\,\phi\,] \tag{4.29}$$

The chemical potential as well as the free energy $\psi_{diff}(c_\alpha)$ in a mixture depend on the composition of the mixture itself. In *ideal*, infinitely diluted conditions[4], the chemical interactions between solutes are neglected. The electrostatic potential ϕ is the result of moving idealized electric charges from one electrode to the other. Guided by restriction (4.26), Fickian-diffusion suggests a linear dependence of the mass flux of species α on the gradient of the electrochemical potential:

$$\vec{h}_\alpha = -\boldsymbol{M}_\alpha\,\nabla\,[\,\overline{\mu}_\alpha\,] \tag{4.30}$$

by means of a positive definite mobility tensor $\boldsymbol{M}_\alpha$.

A classical case of the mobility tensor $\boldsymbol{M}_\alpha$ for *dilute solutions far from saturation* is the isotropic, linear choice

$$\boldsymbol{M}_\alpha(c_\alpha) = \mathfrak{u}_\alpha\, c_\alpha\, \mathbb{1} \tag{4.31}$$

Definition (4.31) implies that the pure phase $c_\alpha = 0$ has a vanishing mobility. The amount $\mathfrak{u}_\alpha > 0$ is usually termed the *ion mobility* and represents the average velocity of species α in the solution when acted upon by a force of 1 N/mol independent of the origin of the force[5].

[4]Ideal conditions are conventionally met in infinitely dilute solutions [6]. Therefore, in writing constitutive theories one firmly distinguishes the items of dilute and concentrated solutions in order to specify the thermodynamic potentials.
The item of ideal diluted solutions will be considered in the following sections, while moderately non-ideal diluted solution and concentrated solution theory are summarized in appendices 4.14 and 4.15.

[5]As the free energy density ψ has been selected as the thermodynamic potential, no source of confusion between the ion mobility u_α and the internal energy density u will arise henceforth.

An *ideal solution model* (see [19]) provides the following free energy density for the continuum approximation of the mixing for dilute solutions far from saturation

$$\psi^{id}_{diff}(c_{\mathrm{Li}^+}, c_{\mathrm{X}^-}) = \mu^0_{\mathrm{Li}^+}\, c_{\mathrm{Li}^+} + \mu^0_{\mathrm{X}^-}\, c_{\mathrm{X}^-} + RT\,(c_{\mathrm{Li}^+}\,\ln[c_{\mathrm{Li}^+}] + c_{\mathrm{X}^-}\,\ln[c_{\mathrm{X}^-}]) \tag{4.32}$$

R is the universal gas constant; μ^0_α is a reference value of the chemical potential of diffusing species α; T is the absolute temperature. The chemical potential results in the form

$$\mu_\alpha = \mu^0_\alpha + RT\,(1 + \ln[c_\alpha]) \tag{4.33}$$

and Fick's law (4.30) equipped with definition (4.20) becomes

$$\vec{h}_\alpha = -\mathbb{D}_\alpha\, RT\, \nabla[\,c_\alpha\,] - z_\alpha\, F\, \mathbb{D}_\alpha\, c_\alpha\, \nabla[\,\phi\,] \tag{4.34}$$

which is the usual form for the flux density of species α in absence of convection (see for instance [6]) in dilute solutions far from saturation. The *diffusivity* $\mathbb{D}_\alpha$ is defined by $\mathbb{D}_\alpha = \mathbb{D}_\alpha\, RT$ (this equation is sometimes termed after Nernst-Einstein).

The simplest special case for the mechanical behavior of the separator/electrolyte system is isotropic, linear elastic (the total strain being coincident with the elastic strain):

$$\psi_{mech}(\boldsymbol{\varepsilon}) = \frac{1}{2}\,\boldsymbol{\varepsilon} : \mathbb{C} : \boldsymbol{\varepsilon} = \frac{1}{2}\left(K\,\mathrm{tr}[\,\boldsymbol{\varepsilon}\,]^2 + 2G\,||\,\mathrm{dev}[\,\boldsymbol{\varepsilon}\,]\,||^2\right) \tag{4.35}$$

K, G are the bulk and shear modulus respectively. Symbol $\mathrm{tr}[\,-\,]$ denotes the trace operator whereas $\mathrm{dev}[\,-\,]$ is the deviator operator. Thermodynamics restrictions (4.26) imply:

$$\boldsymbol{\sigma} = K\,\mathrm{tr}[\,\boldsymbol{\varepsilon}\,]\,\mathbb{1} + 2G\,\mathrm{dev}[\,\boldsymbol{\varepsilon}\,] \tag{4.36}$$

with the usual definition

$$\boldsymbol{\varepsilon} = \frac{1}{2}\left(\nabla[\,\vec{u}\,] + \nabla[\,\vec{u}\,]^T\right) \tag{4.37}$$

4.5 Governing equations and weak form: ideal solution

Governing equations can be derived by incorporating the constitutive equations (4.29), (4.34), and (4.36) into the balance equations. The variable fields controlling the problem result from the thermodynamic choices made, i.e. concentrations c_α, displacements $\vec{u}$, and the electric potential ϕ_e. Governing equations hold at all points $\vec{x} \in V$:

$$\frac{\partial c_{\mathrm{Li}^+}}{\partial t} + \mathrm{div}\,[\,-\mathbb{D}_{\mathrm{Li}^+}\,\nabla[\,c_{\mathrm{Li}^+}\,] - F\,\mathbb{D}_{\mathrm{Li}^+}\,c_{\mathrm{Li}^+}\,\nabla[\,\phi_e\,]\,] = 0 \tag{4.38a}$$

$$\frac{\partial c_{\mathrm{X}^-}}{\partial t} + \mathrm{div}\,[\,-\mathbb{D}_{\mathrm{X}^-}\,\nabla[\,c_{\mathrm{X}^-}\,] + F\,\mathbb{D}_{\mathrm{X}^-}\,c_{\mathrm{X}^-}\,\nabla[\,\phi_e\,]\,] = 0 \tag{4.38b}$$

$$\mathrm{div}\left[\,-\mathbb{C}\,\nabla\left[\,\frac{\partial \phi_e}{\partial t}\,\right] + F\,(\mathbb{D}_{\mathrm{X}^-}\,\nabla[\,c_{\mathrm{X}^-}\,] - \mathbb{D}_{\mathrm{Li}^+}\,\nabla[\,c_{\mathrm{Li}^+}\,] + \right. \tag{4.38c}$$

$$\left. -F\,(\mathbb{D}_{\mathrm{Li}^+}\,c_{\mathrm{Li}^+} + \mathbb{D}_{\mathrm{X}^-}\,c_{\mathrm{X}^-})\,\nabla[\,\phi_e\,])\,\right] = 0$$

$$\mathrm{div}\,[\,\mathbb{C} : \boldsymbol{\varepsilon}\,] = \vec{0} \tag{4.38d}$$

whereas conditions (4.4), (4.7) and (4.10) are applied along Neumann boundaries $\partial^N V_e$. To ensure uniqueness, Dirichlet boundary conditions have to be imposed along part $\partial^D V_e$, being $\partial V_e = \partial^D V_e \cup \partial^N V_e$. It is typical in batteries to fully impose Neumann conditions (4.4) for concentration, in terms of mass fluxes, during galvanostatic processes. Rigid body constraints and zero electric potential are enforced through the Dirichlet boundary conditions.

Initial conditions are usually imposed for concentration of ions $c_{\mathrm{Li}^+}(\vec{x}, t=0)$ and $c_{\mathrm{X}^-}(\vec{x}, t=0)$ in the electrolyte solution. To comply with equilibrium thermodynamics they are uniform in volume V_e; furthermore initial concentrations are equal, obeying the electroneutrality condition (4.1) exactly. Consistently, a positive constant c_{bulk} will be defined as

$$c_{bulk} = c_{\mathrm{Li}^+}(\vec{x}, t=0) = c_{\mathrm{X}^-}(\vec{x}, t=0) \tag{4.39}$$

and will be used to scale concentration variables further on.

Initial conditions for electric potential and displacements should match the boundary value problem at $t = 0$. In view of the perfect electroneutrality, at initial time Gauss law (2.8) and balance of momentum (4.2d) provide the necessary and sufficient equations to be solved for ϕ_e and $\vec{u}$:

$$\mathrm{div}\,[\,\mathbb{k}\,\nabla\,[\,\phi_e\,]\,] = 0 \qquad \vec{x} \in V_e,\ t=0 \tag{4.40a}$$

$$\mathrm{div}\,[\,\mathbb{C} : \boldsymbol{\varepsilon}\,] = \vec{0} \qquad \vec{x} \in V_e,\ t=0 \tag{4.40b}$$

together with homogeneous boundary conditions for potential and current, in view of thermodynamic equilibrium at initial time, and usual given boundary conditions for displacements and tractions.

The evolution problem can be formulated in a weak form as well. Following a Galerkin approach, weak forms are built using "variations" of the same set of variables that rule the problem[6], namely concentrations $\hat{c}_\alpha$, displacements $\hat{\vec{u}}$, and electric potential $\hat{\phi}_e$. By doing so however the energy interpretation of weak form (4.11) is lost. To give to the new weak form at least the physical dimension of a power expenditure, the mass balance equations will be scaled by suitable coefficients, inherited from constitutive equation (4.33). The following identities are derived straightforwardly:

$$\frac{RT}{c_{bulk}} \int_{V_e} \hat{c}_{\mathrm{Li}^+}\, \frac{\partial c_{\mathrm{Li}^+}}{\partial t} + \mathbb{D}_{\mathrm{Li}^+}\, \nabla\,[\,\hat{c}_{\mathrm{Li}^+}\,] \cdot \nabla\,[\,c_{\mathrm{Li}^+}\,] + F\, \mathbb{u}_{\mathrm{Li}^+}\, c_{\mathrm{Li}^+}\ \nabla\,[\,\hat{c}_{\mathrm{Li}^+}\,] \cdot \nabla\,[\,\phi_e\,]\, \mathrm{d}V +$$
$$- \frac{RT}{c_{bulk}} \int_{\Gamma_{BV}} \hat{c}_{\mathrm{Li}^+}\, h_{BV}\, \mathrm{d}\Gamma = 0 \tag{4.41a}$$

$$\frac{RT}{c_{bulk}} \int_{V_e} \hat{c}_{\mathrm{X}^-}\, \frac{\partial c_{\mathrm{X}^-}}{\partial t} + \mathbb{D}_{\mathrm{X}^-}\, \nabla\,[\,\hat{c}_{\mathrm{X}^-}\,] \cdot \nabla\,[\,c_{\mathrm{X}^-}\,] - F\, \mathbb{u}_{\mathrm{X}^-}\, c_{\mathrm{X}^-}\, \nabla\,[\,\hat{c}_{\mathrm{X}^-}\,] \cdot \nabla\,[\,\phi_e\,]\, \mathrm{d}V = 0 \tag{4.41b}$$

$$\int_{V_e} \nabla\left[\,\hat{\phi}_e\,\right] \cdot \left\{ \mathbb{k}\, \nabla\left[\,\frac{\partial \phi_e}{\partial t}\,\right] + F^2\, (\mathbb{u}_{\mathrm{Li}^+}\, c_{\mathrm{Li}^+} + \mathbb{u}_{\mathrm{X}^-}\, c_{\mathrm{X}^-})\, \nabla\,[\,\phi_e\,] \right\} \mathrm{d}V +$$
$$- F \int_{V_e} \nabla\left[\,\hat{\phi}_e\,\right] \cdot (\mathbb{D}_{\mathrm{X}^-}\, \nabla\,[\,c_{\mathrm{X}^-}\,] - \mathbb{D}_{\mathrm{Li}^+}\, \nabla\,[\,c_{\mathrm{Li}^+}\,])\ \mathrm{d}V - F \int_{\Gamma_{BV}} \hat{\phi}_e\, h_{BV}\, \mathrm{d}\Gamma = 0 \tag{4.41c}$$

[6]This is the approach usually pursued to set up numerical algorithm from the weak form. Weak forms written of sections 3.2.3 - 4.2 have a different purpose and entail an energy meaning (required within a computational homogenization framework, see section 3.4.2).

$$\int_{V_e} \hat{\boldsymbol{\varepsilon}} : \mathbb{C} : \frac{\partial \boldsymbol{\varepsilon}}{\partial t}\, \mathrm{d}V - \int_{\partial^N V_e} \hat{\vec{u}} \cdot \frac{\partial \vec{\overline{p}}}{\partial t}\, \mathrm{d}\Gamma = 0 \tag{4.41d}$$

Boundary conditions (4.4), (4.7) and (4.10) have been used.

It is convenient to derive a dimensionless expression for equations (4.41). To this aim, fields that govern the problem are scaled to dimension of unity - denoted with starred superscripts from now on - via suitable scaling factors, namely:

$$c_\alpha^* = \frac{c_\alpha}{c_{bulk}}, \qquad \phi_e^* = \frac{F}{RT}\,\phi_e, \qquad \vec{u}^* = \frac{\vec{u}}{L} \tag{4.42}$$

L standing for a given characteristic length. In view of (4.41), a weak form of governing equations (4.38) can be given in a time interval $[0, t_f]$ as

$$\begin{aligned} &\text{Find } y^*(\vec{x},t) \in \mathcal{V}^{[0,t_f]} \text{ such that} \\ &\frac{\partial}{\partial t} b^*\left(\hat{y}^*(\vec{x}), y^*(\vec{x},t)\right) + a^*\left(\hat{y}^*(\vec{x}), y^*(\vec{x},t)\right) = f^*\left(\hat{y}^*(\vec{x})\right) \quad \forall \hat{y}^*(\vec{x}) \in \mathcal{V} \end{aligned} \tag{4.43}$$

where

$$\begin{aligned} b^*&\left(\hat{y}^*(\vec{x}), y^*(\vec{x},t)\right) = \\ &RT\, c_{bulk} \int_{V_e} \hat{c}^*_{\mathrm{Li^+}}\, c^*_{\mathrm{Li^+}} + \hat{c}^*_{\mathrm{X^-}}\, c^*_{\mathrm{X^-}}\, \mathrm{d}V + \not\sharp \left(\frac{RT}{F}\right)^2 \int_{V_e} \nabla\left[\,\hat{\phi_e}^{\,*}\,\right] \cdot \nabla\left[\,\phi_e^*\,\right]\, \mathrm{d}V + \\ &\quad + L^2 \int_{V_e} \hat{\boldsymbol{\varepsilon}}^* : \mathbb{C} : \boldsymbol{\varepsilon}^*\, \mathrm{d}V \\ a^*&\left(\hat{y}^*(\vec{x}), y^*(\vec{x},t)\right) = \\ &RT\, c_{bulk}\, \mathbb{D}_{\mathrm{Li^+}} \int_{V_e} \nabla\left[\,\hat{c}^*_{\mathrm{Li^+}}\,\right] \cdot \nabla\left[\,c^*_{\mathrm{Li^+}}\,\right] + c^*_{\mathrm{Li^+}}\ \nabla\left[\,\hat{c}^*_{\mathrm{Li^+}}\,\right] \cdot \nabla\left[\,\phi_e^*\,\right]\, \mathrm{d}V + \\ &RT\, c_{bulk}\, \mathbb{D}_{\mathrm{X^-}} \int_{V_e} \nabla\left[\,\hat{c}^*_{\mathrm{X^-}}\,\right] \cdot \nabla\left[\,c^*_{\mathrm{X^-}}\,\right] - c^*_{\mathrm{X^-}}\, \nabla\left[\,\hat{c}^*_{\mathrm{X^-}}\,\right] \cdot \nabla\left[\,\phi_e^*\,\right]\, \mathrm{d}V + \\ &RT\, c_{bulk}\, \mathbb{D}_{\mathrm{Li^+}} \int_{V_e} \nabla\left[\,\hat{\phi}_e^*\,\right] \cdot \nabla\left[\,\phi_e^*\,\right]\, c^*_{\mathrm{Li^+}} + \nabla\left[\,\hat{\phi}_e^*\,\right] \cdot \nabla\left[\,c^*_{\mathrm{Li^+}}\,\right]\, \mathrm{d}V + \\ &RT\, c_{bulk}\, \mathbb{D}_{\mathrm{X^-}} \int_{V_e} \nabla\left[\,\hat{\phi}_e^*\,\right] \cdot \nabla\left[\,\phi_e^*\,\right]\, c^*_{\mathrm{X^-}} - \nabla\left[\,\hat{\phi}_e^*\,\right] \cdot \nabla\left[\,c^*_{\mathrm{X^-}}\,\right]\, \mathrm{d}V \\ f^*&\left(\hat{y}^*(\vec{x})\right) = RT \int_{\Gamma_{BV}} \left(\hat{\phi}_e^* + \hat{c}^*_{\mathrm{Li^+}}\right) h_{BV}\, \mathrm{d}\Gamma + L \int_{\partial^N V_e} \hat{\vec{u}}^* \cdot \frac{\partial \vec{\overline{p}}}{\partial t}\, \mathrm{d}\Gamma \end{aligned}$$

with $y^*(\vec{x},t) = \{c^*_{\mathrm{Li^+}}, c^*_{\mathrm{X^-}}, \phi_e^*, \vec{u}^*\}$. Ellipticity of operators, functional and numerical properties of the solution and of its approximation depend on the constitutive assumptions and on the choice of the correct functional spaces $\mathcal{V}^{[0,t_f]}, \mathcal{V}$, whose identification falls beyond the scope of the present paper.

4.6 One-dimensional modeling of ionic transport in a liquid electrolyte: ideal solution

4.6.1 Description

This section deals with the case study analysed in [10], namely a $LiPF_6$ electrolyte subject to a galvanostatic process of charge at 1 C-rate at a temperature of 25^oC, with current

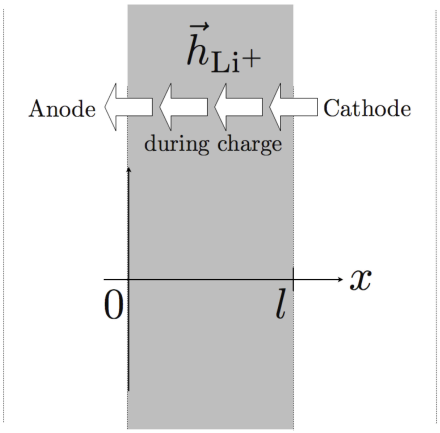

Figure 4.1: *A one-dimensional model of a Li-ion battery, with separator of size* $l = 2.8 \times 10^{-4}$m *highlighted in gray. The flux of* Li^+ *ions during charge is pointed out.*

$I_{1C} = 0.72$A corresponding to a storage capacity of 720mAh. In order to make initial and boundary conditions compatible with thermodynamic equilibrium at $t = 0$, the current $I(t)$ is tuned in time as

$$I(t) = (1 - e^{-t})\, I_{1C} \tag{4.44}$$

with t in seconds.

Boundary and initial conditions have been taken according to [10]. Initially (at $t = 0$) the concentrations of ions across the electrolyte are uniform as in equation (4.39), because no profiles have been developed yet.

$$c_\alpha(\vec{x}, 0) = c_{bulk} = 1500\,\mathrm{mol\,m^{-3}} \qquad \vec{x} \in V_e \tag{4.45}$$

With no side reactions, the flux of Lithium ions at the electrodes/separator interfaces (of net area $A = 2 \times 10^{-2}\mathrm{m}^2$) is related to the given current $I(t)$ flowing through the battery. A uniform ionic flow at the interfaces is considered, enabling a 1D description. Boundary conditions (4.4) thus read:

$$h_{BV}|_{(x=0)}\,(t) = h_{BV}|_{(x=l)}\,(t) = -\frac{I(t)}{FA} \tag{4.46a}$$

$$\vec{h}_{\mathrm{X}^-} \cdot \vec{n}\,\Big|_{(x=0)}\,(t) = \vec{h}_{\mathrm{X}^-} \cdot \vec{n}\,\Big|_{(x=l)}\,(t) = 0 \tag{4.46b}$$

see also Figure 4.1. From identity (4.44) it comes out that the "steady" mass flux at $t \gg 0$ reads

$$h_{1C} = -\frac{I_{1C}}{FA}$$

Diffusivities amount at $\mathbb{D}_{\mathrm{Li}^+} = 2 \times 10^{-11}\mathrm{m}^2\mathrm{s}^{-1}$, $\mathbb{D}_{\mathrm{PF}_6^-} = 3 \times 10^{-11}\mathrm{m}^2\mathrm{s}^{-1}$. The separator thickness is $l = 280\mu$m. All data are taken from [10] apart from the relative permittivity, assumed as $\mathbb{\epsilon}_r = 2.25$. The Debye length (2.19) is estimated to be $r_D = 4.20512 \times 10^{-11}$m.

4.6.2 Discretization and time advancing by finite differences

As in [10], mechanical effects are not described here. Balance equations are limited to mass (4.2a-b) and Maxwell's (4.2c). The weak form (4.43) can be transformed in a first order

Ordinary Differential Equation (ODE) in time if discretization is performed via separated variables, with spatial test $\varphi_i(x)$ and shape functions $\varphi_j(x)$ and nodal unknowns (collectively gathered in column y with component $y_j(t)$) that depend solely on time. For the sake of readability the star superscript is omitted from the dimensionless quantities: for example, in this section $c_j^{\mathrm{Li}^+}$ stands for the j-th nodal unknown for Li-ions dimensionless concentration at time t. The usual Einstein summation convention is taken henceforth for repeated indexes. The non linear ODE reads:

$$\text{Find } y(t) \text{ s.t.} \qquad b_i^* \cdot \frac{\partial y}{\partial t}(t) + a_i^*[\, y(t)\,] = f_i^*(t) \qquad \text{for } i = 1, 2, ..., N \tag{4.47}$$

where

$$\frac{1}{RT\, c_{bulk}}\, b_i^* \cdot \frac{\partial y}{\partial t}(t) = \int_0^l \varphi_i^{\mathrm{Li}^+}\, \varphi_j^{\mathrm{Li}^+}\, \mathrm{d}x\, \frac{\partial c_j^{\mathrm{Li}^+}}{\partial t} + \int_0^l \varphi_i^{\mathrm{X}^-}\, \varphi_j^{\mathrm{X}^-}\, \mathrm{d}x\, \frac{\partial c_j^{\mathrm{X}^-}}{\partial t} + \frac{\not{\mathbb{1}}}{c_{bulk}}\, \frac{RT}{F^2} \int_0^l \frac{\partial \varphi_i^\phi}{\partial x}\, \frac{\partial \varphi_j^\phi}{\partial x}\, \mathrm{d}x\, \frac{\partial \phi_j^e}{\partial t}$$

$$\begin{aligned}
\frac{a_i^*[\, y(t)\,]}{RT\, c_{bulk}} = {} & \mathbb{D}_{\mathrm{Li}^+} \int_0^l \frac{\partial \varphi_i^{\mathrm{Li}^+}}{\partial x}\, \frac{\partial \varphi_j^{\mathrm{Li}^+}}{\partial x}\, \mathrm{d}x\, c_j^{\mathrm{Li}^+} + \mathbb{D}_{\mathrm{Li}^+} \int_0^l \varphi_j^{\mathrm{Li}^+}\, \frac{\partial \varphi_i^{\mathrm{Li}^+}}{\partial x}\, \frac{\partial \varphi_k^\phi}{\partial x}\, \mathrm{d}x\, c_j^{\mathrm{Li}^+}\, \phi_k^e + \\
& + \mathbb{D}_{\mathrm{X}^-} \int_0^l \frac{\partial \varphi_i^{\mathrm{X}^-}}{\partial x}\, \frac{\partial\, \varphi_j^{\mathrm{X}^-}}{\partial x}\, \mathrm{d}x\, c_j^{\mathrm{X}^-} - \mathbb{D}_{\mathrm{X}^-} \int_0^l \varphi_j^{\mathrm{X}^-}\, \frac{\partial \varphi_i^{\mathrm{X}^-}}{\partial x}\, \frac{\partial \varphi_k^\phi}{\partial x}\, \mathrm{d}x\, c_j^{\mathrm{X}^-}\, \phi_k^e + \\
& + \mathbb{D}_{\mathrm{Li}^+} \int_0^l \frac{\partial \varphi_i^\phi}{\partial x}\, \frac{\partial \varphi_k^\phi}{\partial x}\, \varphi_j^{\mathrm{Li}^+}\, \mathrm{d}x\, c_j^{\mathrm{Li}^+}\, \phi_k^e + \mathbb{D}_{\mathrm{Li}^+} \int_0^l \frac{\partial \varphi_i^\phi}{\partial x}\, \frac{\partial \varphi_j^{\mathrm{Li}^+}}{\partial x}\, \mathrm{d}x\, c_j^{\mathrm{Li}^+} + \\
& + \mathbb{D}_{\mathrm{X}^-} \int_0^l \frac{\partial \varphi_i^\phi}{\partial x}\, \frac{\partial \varphi_k^\phi}{\partial x}\, \varphi_j^{\mathrm{X}^-}\, \mathrm{d}x\, c_j^{\mathrm{X}^-}\, \phi_k^e - \mathbb{D}_{\mathrm{X}^-} \int_0^l \frac{\partial \varphi_i^\phi}{\partial x}\, \frac{\partial \varphi_j^{\mathrm{X}^-}}{\partial x}\, \mathrm{d}x\, c_j^{\mathrm{X}^-}
\end{aligned}$$

$$\frac{f_i^*(t)}{RT\, c_{bulk}} = \frac{1}{c_{bulk}} \int_{\Gamma_{BV}} (\varphi_i^\phi + \varphi_i^{\mathrm{Li}^+})\, h_{BV}\, \mathrm{d}\Gamma$$

with $y_j(t) = \{c_j^{\mathrm{Li}^+}, c_j^{\mathrm{X}^-}, \phi_j,\, u_j\,\}$. Form $a_i^*[\, y(t)\,]$ is clearly non linear. It can be split into the sum of a non linear form ${}^n a_i^*[\, y(t)\,]$, which reads

$$\begin{aligned}
\frac{{}^n a_i^*[\, y(t)\,]}{RT\, c_{bulk}} = {} & \mathbb{D}_{\mathrm{Li}^+} \int_0^l \varphi_j^{\mathrm{Li}^+}\, \frac{\partial \varphi_i^{\mathrm{Li}^+}}{\partial x}\, \frac{\partial \varphi_k^\phi}{\partial x}\, \mathrm{d}x\, c_j^{\mathrm{Li}^+}\, \phi_k + \mathbb{D}_{\mathrm{Li}^+} \int_0^l \frac{\partial \varphi_i^\phi}{\partial x}\, \frac{\partial \varphi_k^\phi}{\partial x}\, \varphi_j^{\mathrm{Li}^+}\, \mathrm{d}x\, c_j^{\mathrm{Li}^+}\, \phi_k + \\
& - \mathbb{D}_{\mathrm{X}^-} \int_0^l \varphi_j^{\mathrm{X}^-}\, \frac{\partial \varphi_i^{\mathrm{X}^-}}{\partial x}\, \frac{\partial \varphi_k^\phi}{\partial x}\, \mathrm{d}x\, c_j^{\mathrm{X}^-}\, \phi_k + \mathbb{D}_{\mathrm{X}^-} \int_0^l \frac{\partial \varphi_i^\phi}{\partial x}\, \frac{\partial \varphi_k^\phi}{\partial x}\, \varphi_j^{\mathrm{X}^-}\, \mathrm{d}x\, c_j^{\mathrm{X}^-}\, \phi_k
\end{aligned} \tag{4.49}$$

and a bilinear counterpart ${}^l a_i^* \cdot y(t)$ defined by comparison.

A family of time-advancing methods based on the so-called θ-scheme can be set up for the discrete problem (4.47). Assume that solution $y(t)$ is given at time t, and that the algorithm

is triggered at the initial time $t = 0$ by means of equations (4.40). The scheme seeks for $y(t + \Delta t)$ such that

$$b_i^* \cdot \frac{y(t+\Delta t) - y(t)}{\Delta t} + a_i^*[\, \theta\, y(t+\Delta t) + (1-\theta) y(t)\,] = \theta\, f_i^*(t+\Delta t) + (1-\theta) f_i^*(t) \quad (4.50)$$

for $i = 1, 2, ..., N$, where $0 \leq \theta \leq 1$, $\Delta t = t_f / N_t$ is the time step, N_t is a positive integer. θ-scheme includes the forward Euler scheme ($\theta = 0$, linear in $y(t + \Delta t)$), backward Euler ($\theta = 1$), and Crank-Nicholson ($\theta = 1/2$). For bilinear forms $a_i^* = {}^l a_i^*$ unconditional stability is proved when $1/2 \leq \theta \leq 1$, whereas stability conditions when $0 \leq \theta < 1/2$ can be found for instance in [123].

In the numerical simulations that follow, backward Euler ($\theta = 1$) has been selected, thus searching for $y(t + \Delta t)$ such that

$$b_i^* \cdot \frac{y(t+\Delta t)}{\Delta t} + {}^l a_i^* \cdot y(t+\Delta t) + {}^n a_i^*[\, y(t+\Delta t)\,] = f_i^*(t+\Delta t) + b_i^* \cdot \frac{y(t)}{\Delta t} \quad (4.51)$$

For the sake of a better readability, a linear operator l_i, a non linear operator $n_i[-]$, and given terms ξ_i are defined as:

$$\begin{aligned} l_i &= \frac{b_i^*}{\Delta t} + {}^l a_i^* \\ n_i[\, y(t+\Delta t)\,] &= {}^n a_i^*[\, y(t+\Delta t)\,] \\ \xi_i &= f_i^*(t+\Delta t) + b_i^* \cdot \frac{y(t)}{\Delta t} \end{aligned}$$

so to write (4.51) as

$$l_i \cdot y(t+\Delta t) + n_i[\, y(t+\Delta t)\,] = \xi_i \quad (4.52)$$

4.6.3 Non linear algorithms

Two iterative schemes have been implemented to solve non-linear problem (4.51). Denoting with $\mathtt{q} = 1, 2, ...$ the iteration counter, the schemes proceed until a condition on the L_2 norm of the increment

$$\delta y = {}^{\mathtt{q}+1} y(t+\Delta t) - {}^{\mathtt{q}} y(t+\Delta t)$$

is satisfied. The *linearized updated* technique solves (4.51) for ${}^{\mathtt{q}+1} y(t + \Delta t)$ after having linearized operator n_i as $n_i[\, {}^{\mathtt{q}} c_j^{\mathrm{Li}^+}(t+\Delta t), {}^{\mathtt{q}} c_j^{\mathrm{X}^-}(t+\Delta t), {}^{\mathtt{q}}\phi_j(t+\Delta t)\,]$. The *Newton-Raphson* strategy seeks for δy such that

$$l_i \cdot \delta y + \frac{\mathrm{d}}{\mathrm{d}\epsilon} n_i[\, {}^{\mathtt{q}} y(t+\Delta t) + \epsilon\, \delta y\,]\Big|_{\epsilon=0} = \xi_i - l_i \cdot {}^{\mathtt{q}} y(t+\Delta t) + n_i[\, {}^{\mathtt{q}} y(t+\Delta t)\,] \quad (4.53)$$

The two numerical techniques have been implemented in a Wolfram Mathematica package script[7], provided solutions with 16 coincident digits and converged up to a tolerance of 10^{-9} in the L_2 norm of the (relative) increment.

[7]The algorithm extending the formulation at hand to 2D problems have been implemented by means of the Abaqus User Element (UEL) script. It is reported in appendix 4.16.

Stability analyses for the non linear problem at hand will be considered in further publications, but simple considerations on operator l_i highlight four dimensionless groups that govern the condition number of the "stiffness" matrix, namely:

$$\frac{\Delta t\, D_{\mathrm{Li}^+}}{L^2}\,, \qquad \frac{\Delta t\, D_{\mathrm{X}^-}}{L^2}\,, \qquad \frac{\sharp}{c_{bulk}}\,\frac{RT}{F^2}\,\frac{1}{\Delta t\, D_{\mathrm{Li}^+}}\,, \qquad \frac{\sharp}{c_{bulk}}\,\frac{RT}{F^2}\,\frac{1}{\Delta t\, D_{\mathrm{X}^-}}$$

where L is a characteristic length of the discretization, typically the element length for uniform meshes. The last two numbers are related to the Debye length r_D defined in (2.19). The parameters that govern stability are expected to be the following three ratios

$$\gamma_{\mathrm{Li}^+} = \frac{\Delta t\, D_{\mathrm{Li}^+}}{L^2}\,, \qquad \gamma_{\mathrm{X}^-} = \frac{\Delta t\, D_{\mathrm{X}^-}}{L^2}\,, \qquad \gamma_\phi = \frac{r_D}{L}$$

4.6.4 Simulations

Single discharge

Several simulations have been carried out with different time steps and number of elements. The outcomes here reported refer to 128 equal finite elements and a constant time step of 1 minute, for which

$$\gamma_{\mathrm{Li}^+} = 250.776\,, \qquad \gamma_{\mathrm{X}^-} = 376.163\,, \qquad \gamma_\phi = 1.92234 \times 10^{-5}$$

At the initial time $t = 0$, concentration for ions is given according to (4.39, 4.45). For being in thermodynamic equilibrium with neither current nor mass flowing, the electric potential satisfies equations (4.40) and has to be homogeneous

$$\phi_e(\vec{x}, 0) = 0 \qquad \vec{x} \in V_e \tag{4.54}$$

After a "sufficiently long" time has passed, the steady state configuration

$$c_\infty(x) = c_{bulk} - \frac{h_{1C}}{2D_{\mathrm{LI}^+}}(x - \frac{l}{2}) \tag{4.55}$$

is approached. As reported in Figure 4.2, both the solution provided in [10] and the steady asymptotic behavior are adequately recovered.

Figure 4.3 depicts the electric potential $\phi(x)$ as well as electric field $\vec{E}(x)$ and their evolution in time. The figure shows a fictitious jump between the initial, homogeneous condition and the first curve that refers to one minute. This is due to the chosen time step $\Delta t = 60s$ that is too large to follow the initial evolution in time of the current according to (4.44); indeed at one minute the current $I(t)$ basically amounts at I_{1C}. A refined analysis with time step $\Delta t = 0.05s$ has been carried out and $\phi_e(x)$ is depicted in the upper left corner of Figure 4.3. It is worth noting that the electric potential is one of the unknowns of the model at hand, whereas it is reconstructed a posteriori in the models based on the porous electrode theory.

The flux of ions is plotted in Figure 4.4. The flux near the electrode interfaces is dictated by the boundary conditions (4.46). The closer the regions to the electrodes the faster they reach the steady state. As discussed in [10] the Li^+ ionic current is mainly carried by migration at the beginning of the charging process, while under steady-state conditions diffusion and migration contribute equally. The anionic mass flux reaches its peak rapidly, and to

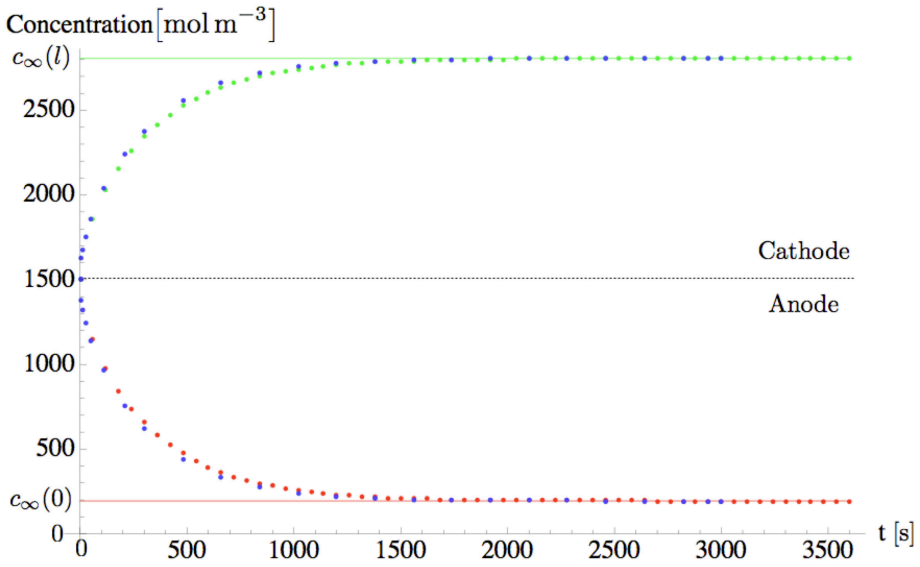

Figure 4.2: *Ionic concentration profile at Anode (red) and Cathode (green). Steady state solutions are reported for the Anode ($c_\infty(0)$) and for the Cathode ($c_\infty(l)$). Both are asymptotically achieved. The blue dots refer to the solution provided by [10].*

capture it correctly a small time step is required. Once the steady state is approached, the flux of PF_6^- tends to vanish, and no contribution is provided to the overall ionic conductivity.

Figure 4.5 assesses the electroneutrality condition (4.1), which is well approximated by the numerical solution, *in the sense that the difference in concentration is about nine to ten orders of magnitude smaller than the equilibrium electrolyte concentration* c_{bulk}. The direct difference of the two approximated fields however does *not* provide a reliable quantitative account of the deviation from electroneutrality [131]. In terms of the accuracy in concentrations c_{Li^+}, c_{X^-} and potential ϕ_e the outcome appears satisfactory. Nevertheless, it might be possible that the accuracy for c_{Li^+} and c_{X^-} is insufficient in terms of the difference $c_{\mathrm{Li}^+} - c_{\mathrm{X}^-}$. Indeed, the numerical approximations for c_{Li^+} and c_{X^-} coincide by eight digits or more, and the difference is obviously affected by numerical accuracy. Therefore, the obtained difference in concentrations $c_{\mathrm{Li}^+} - c_{\mathrm{X}^-}$ should be interpreted as an upper bound for the concentration unbalance.

A better estimate for the deviation from electroneutrality can be achieved from Gauss law (2.8). The electric charge ζ is related by equation (2.2) to the gap of concentration by Faraday's constant. Since the ratio of Faraday's constant and the permittivity amounts at $\frac{F}{\mathfrak{f}} \sim 1.1 \cdot 10^{17} \mathfrak{f}_r^{\natural}\,\mathrm{V\,m\,mol^{-1}}$, an extremely small deviation from electroneutrality may provide a significant electric field contribution in the battery cell. A finite difference approximation for the concentration imbalance shows

$$c_{\mathrm{Li}^+} - c_{\mathrm{X}^-} = -\frac{\mathfrak{f}}{F}\frac{\partial^2 \phi}{\partial x^2} \sim -\frac{\mathfrak{f}}{F}\frac{\phi(x+h) - 2\phi(x) + \phi(x-h)}{h^2} \tag{4.56}$$

with $h = l/128$ the "element length". Within the limit of its numerical accuracy[8], approach

[8] It is well known however that second derivative estimation via finite differences may result in poor accuracy.

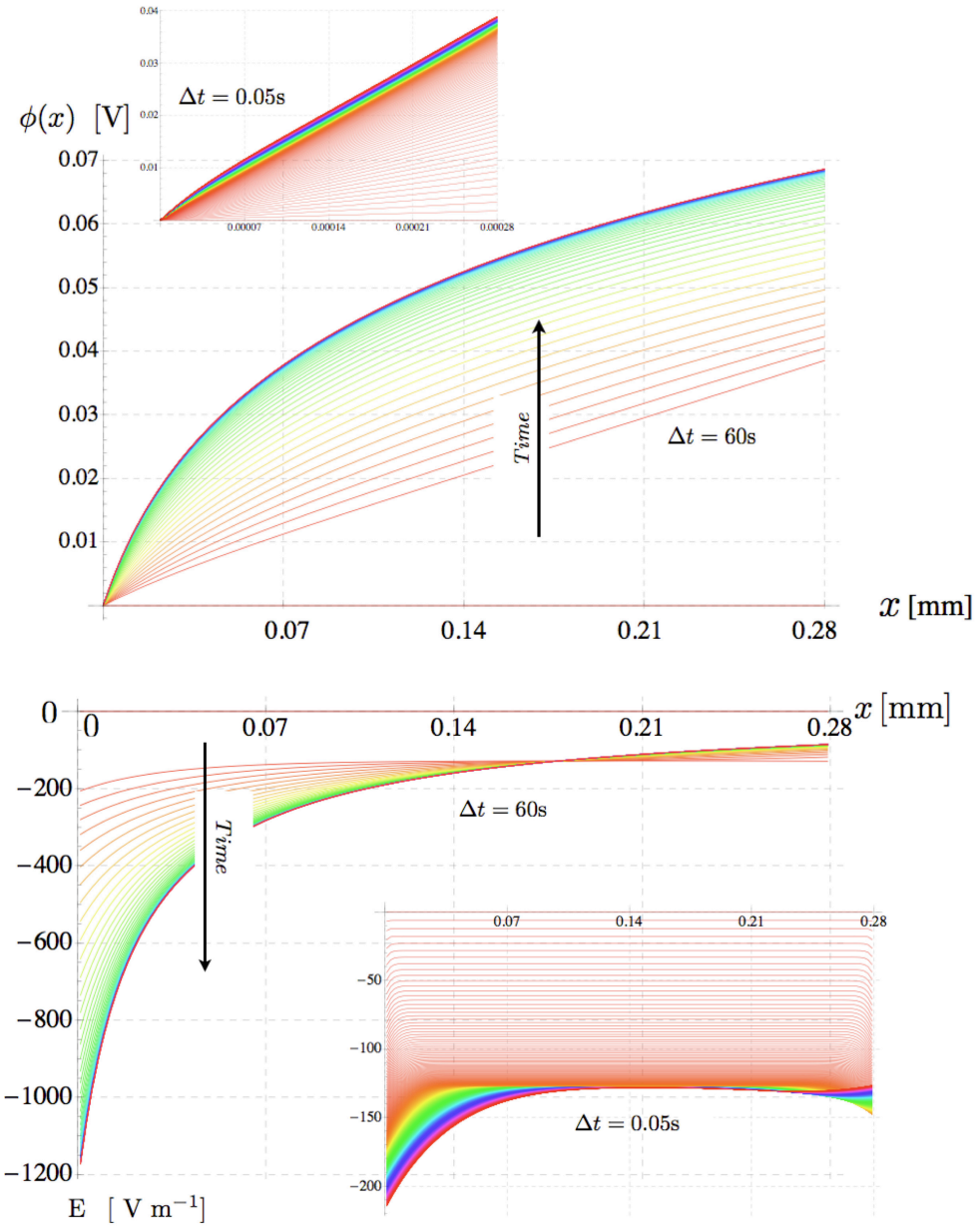

Figure 4.3: *The electric potential $\phi_e(x)$ and electric field $\vec{E}(x)$ parametrized in time. The electric charge is related to the unbalance of concentration by Faraday's constant. Since the ratio of Faraday's constant and the permittivity amounts at $\frac{F}{\epsilon} \sim 1.1 \cdot 10^{17} \epsilon_r$ V m mol^{-1}, the observed deviation from electroneutrality generates a non negligible electric field in the battery cell in view of Gauss's law.*

(4.56) provides estimations of deviation from electroneutrality two order of magnitudes less than the simple difference of concentrations (see figure 4.6).

Discharge/charge cycle

A second test was carried out by ending the simulation at $t_f = 7200$s and including a current reversal after one hour, without relaxation. The current $I(t)$ is therefore tuned in time as

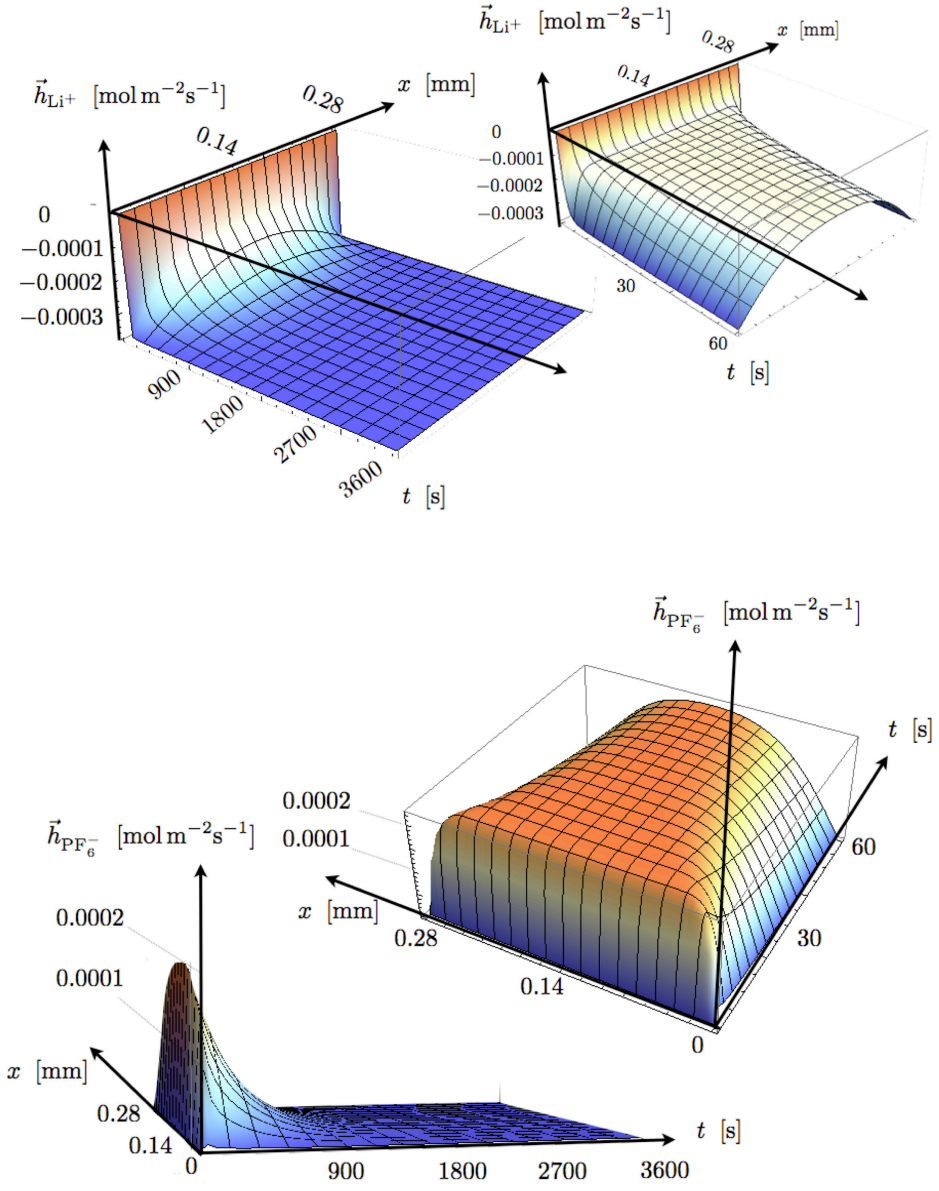

Figure 4.4: *Three dimensional plots of* $\vec{h}_{Li^+}(x,t)$, $\vec{h}_{PF_6^-}(x,t)$, *with their zoom about the first minute.*

follows:

$$I(t) = (1 - e^{-t})\, I_{1C} \times \begin{cases} 1 & \text{if } t \leq 3600 \text{ s} \\ -1 & \text{if } 3600 < t \leq 7200 \text{ s} \end{cases} \tag{4.57}$$

with t in seconds. Initial (4.45) and boundary (4.46) conditions are unaffected, as well as all material parameters, the time step and the number of finite elements.

After current reversal, the concentration eventually reaches a new steady state, which has an opposite sign with respect to the one right before $t = 3600$s, see Figure 4.7. A similar conclusion can be drawn for the electric potential.

Figure 4.8 allows to conclude that even under current reversal, electroneutrality condition

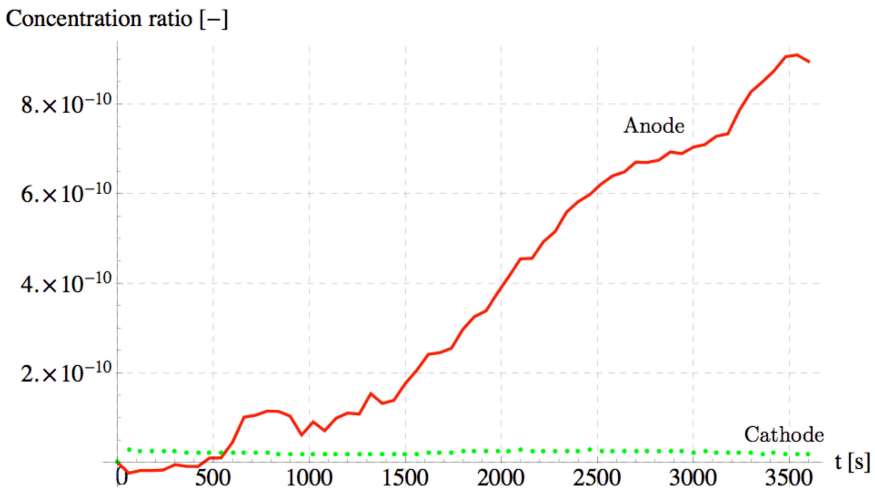

Figure 4.5: *Ionic concentration ratio* $\frac{c_{\mathrm{Li}^+} - c_{\mathrm{X}^-}}{c_{bulk}}$ *at Anode (continuous line) and Cathode (dotted line). The plot shows that the difference in concentration after the numerical solution is ten orders of magnitude smaller than the equilibrium electrolyte concentration. Electroneutrality (4.1) is thus well approximated.*

(4.1) is adequately approximated, i.e. nine to ten orders of magnitude smaller than the equilibrium electrolyte concentration as for monotonic current. The analysis shows also that a quantitative analysis cannot be performed by the direct difference $c_{\mathrm{Li}^+} - c_{\mathrm{X}^-}$ as already argued. Figure 4.8 indeed does not show any sort of sign inversion for the deviation from electroneutrality. On the contrary, making recourse to formula (4.56) appears to be more accurate and robust, as pointed out again in figure 4.8.

4.7 Dilute solution accounting for saturation

From Figure 4.2 it is clear that the steady state concentration at the electrodes is in the order of $2800\,\mathrm{mol\,m^{-3}}$. It can be argued from literature [136] that the saturation limit for $LiPF_6$ in the electrolyte solvent is between 4000 and $5000\,\mathrm{mol\,m^{-3}}$. The concentrations arising from numerical simulations do not correspond to a solution far from saturation, amounting about 50% of such a limiting value. The usual and widespread usage of a simplified form of the chemical Helmholtz free energy density due to mixing of the species (4.31-4.32) is not allowed. The modifications induced by the saturation contribution extensively are investigated in subsequent sections.

Balance laws (refer to section 4.1) are not at all affected by the saturation. Mass balance (4.1) is kept homogeneous even while modeling the influence of saturation, which means the degree of dissociation of the binary salt is still considered to be complete. The latter condition may not be satisfied in reality when concentrations get close to the saturation limit, thus requiring a bulk term in the mass balance equation of the ionic species accompanied with a further mass balance equation for the undissociated salt [10]. Nevertheless, the outcomes of the numerical analyses reported in section 4.6 (refer also to [128]) suggest that concentrations are too high to neglect the role of saturation, but still sufficiently far from saturation to exclude incomplete dissociation of the Li-salt.

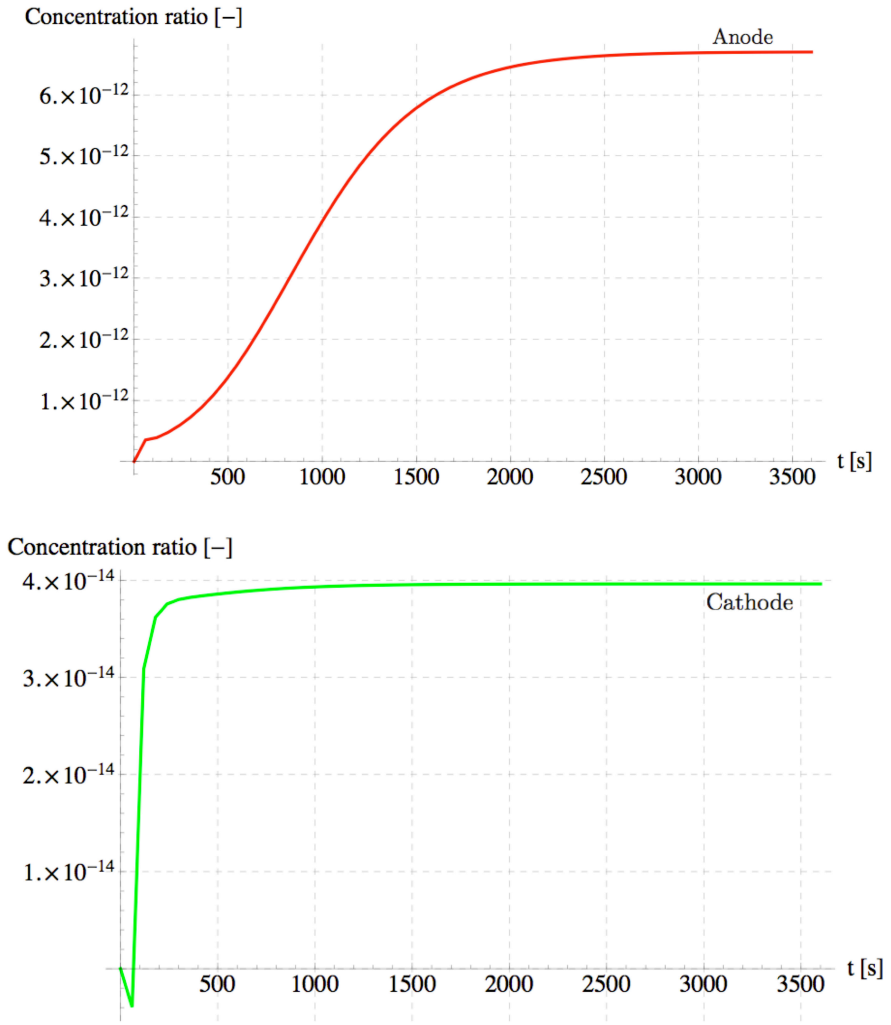

Figure 4.6: *Concentration ratio* $\frac{c_{\mathrm{Li}+} - c_{\mathrm{X}-}}{c_{bulk}}$ *at Anode (left) and Cathode (right) derived from equation (4.56).*

According to thermodynamic restrictions of section 4.3, the so called "dilute solutions" constitutive model has been implemented taking into account the saturation limit. The formulation also applies to mixing with interactions (regular solutions), to moderately diluted solutions in terms of activity coefficients and to concentrated solutions modeled by the Maxwell-Stefan equations of multicomponent diffusion.

One more time, a weak form has been derived for governing equations in terms of the selected thermodynamic fields and the one-dimensional application to ionic transport in Li-ion batteries electrolyte, illustrated in section 4.6, performed. Outcomes with and without saturation are compared, and the role of the latter clearly identified.

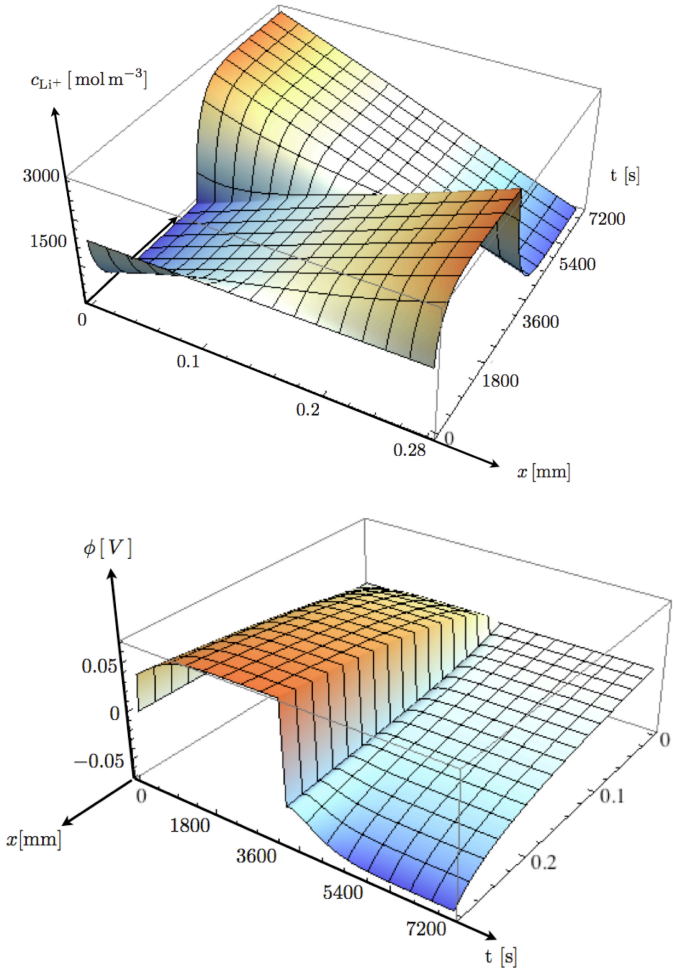

Figure 4.7: *A three dimensional plot of concentration* c_{Li^+} *and electric potential* ϕ.

4.8 Constitutive theory: diluted solution accounting for saturation

It is assumed the Helmholtz free energy density ψ can be decomposed in three separate parts, as in section 4.4:

$$\psi(\boldsymbol{\varepsilon}, c_\alpha, \vec{E}) = \psi_{diff}(c_\alpha) + \psi_{el}(\vec{E}) + \psi_{mech}(\boldsymbol{\varepsilon})$$

Definitions (4.28 - 4.29 - 4.35 - 4.36) still hold for ψ_{el}, $\vec{D}_e$, ψ_{mech} and $\boldsymbol{\sigma}$ respectively.

A classical [20] specialization of mobility tensor $\boldsymbol{M}_\alpha$ for *dilute solutions accounting for saturation* is isotropic yet non linear

$$\boldsymbol{M}_\alpha(c_{\mathrm{Li}^+}, c_{\mathrm{X}^-}) = \mathbb{1}_\alpha \, c_\alpha \, (1 - \theta_{\mathrm{Li}^+} - \theta_{\mathrm{X}^-}) \, \mathbb{1} \tag{4.58}$$

θ_α is defined as the ratio $\theta_\alpha = \frac{c_\alpha}{c^{max}}$, where c^{max} stands for the cumulative saturation limit for ions Li^+ and X^- in the solution, in condition of electroneutrality[9]. Definition (4.58) represents the physical requirement that both the pure ($c_\alpha = 0$) and the saturated ($\theta_{\mathrm{Li}^+} +$

[9] In the simulation it has been taken as twice the saturation limit of the salt LiX.

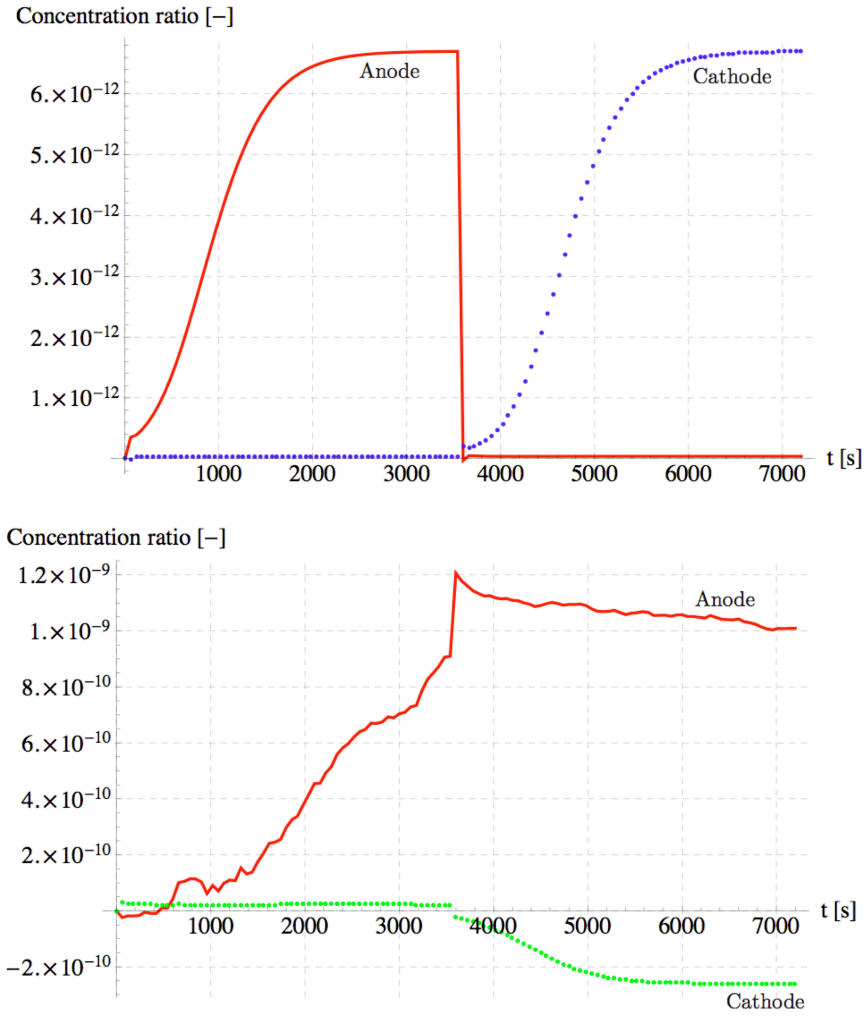

Figure 4.8: *Concentration ratio* $\frac{c_{\mathrm{Li}^+} - c_{\mathrm{X}^-}}{c_{bulk}}$ *at Anode (continuous line) and Cathode (dotted line) derived from equation (4.56) and from direct difference of numerical solutions for* c_{Li^+} *and* c_{X^-}.

$\theta_{\mathrm{X}^-} = 1$) phases have vanishing mobilities in the electrolyte. It can be seen as a special case of the Maxwell-Stefan approach (see appendix 4.15). Exploiting the electroneutrality condition[10] (4.1) largely discussed in section 2.3, the specialization for the mobility tensor simplifies as

$$\boldsymbol{M}_\alpha(c_\alpha) = \Cancel{\mathbb{1}}_\alpha \, c_\alpha \left(1 - 2\frac{c_\alpha}{c^{max}}\right) \mathbb{1} \tag{4.59}$$

Anions and cations are thus considered as non-interacting and no recourse is made to *regular solution*. The free energy comes out of an ideal solution model as:

$$\begin{aligned} &\psi^{id}_{diff}(c_{\mathrm{Li}^+}, c_{\mathrm{X}^-}) = \\ &\quad \mu^0_{\mathrm{Li}^+} \, c_{\mathrm{Li}^+} \; + \mu^0_{\mathrm{X}^-} \, c_{\mathrm{X}^-} \; + R\,T\,c^{max} \, (\theta_{\mathrm{Li}^+} \, \ln[\theta_{\mathrm{Li}^+}] + \theta_{\mathrm{X}^-} \, \ln[\theta_{\mathrm{X}^-}]) + \\ &\qquad + R\,T\,c^{max} \, (1 - \theta_{\mathrm{Li}^+} - \theta_{\mathrm{X}^-}) \, \ln[(1 - \theta_{\mathrm{Li}^+} - \theta_{\mathrm{X}^-})] \end{aligned} \tag{4.60}$$

[10] No contradictions arise using this simplification which entirely fits within the discussion of section 2.3.

By exploiting electroneutrality (4.1), the chemical potential results in the form

$$\mu_\alpha = \mu_\alpha^0 + RT \ln\left[\frac{c_\alpha}{c^{max} - 2c_\alpha}\right] \tag{4.61}$$

thus leading to the following expression for the mass flux:

$$\vec{h}_\alpha = -\mathbb{D}_\alpha \nabla[c_\alpha] - z_\alpha F \mathbb{\mu}_\alpha c_\alpha \left(1 - 2\frac{c_\alpha}{c^{max}}\right) \nabla[\phi_e] \tag{4.62}$$

By comparing (4.62) with the mass flux formula for infinitely diluted solutions (4.34) one concludes that saturation has no effect on the diffusivity: in fact, the impact of saturation on the mobility tensor (4.59) and on the chemical potential (4.61) act one against the other and the effects cancel out in the evaluation of diffusivity[11]. Saturation does affect the electric contribution in the mass flux (4.62) by changing the mobility, thus creating either a lower mass flux at a given potential gradient or a higher potential gradient at a given flux.

4.9 Governing equations and weak form: dilute solution accounting for saturation

Governing equations have been derived by incorporating constitutive equations (4.29), (4.62), and (4.36) into balance equations (4.2). The variable fields that rule the problem are the same as in section 4.5: concentrations c_α, displacements $\vec{u}$, and the electric potential ϕ_e. Governing equations hold at all points $\vec{x} \in V_e$ in all instants of interval $[0, t_f]$:

$$\frac{\partial c_{\mathrm{Li}^+}}{\partial t} + \operatorname{div}\left[-\mathbb{D}_{\mathrm{Li}^+} \nabla[c_{\mathrm{Li}^+}] - F \mathbb{\mu}_{\mathrm{Li}^+} c_{\mathrm{Li}^+} \left(1 - 2\frac{c_{\mathrm{Li}^+}}{c^{max}}\right) \nabla[\phi_e]\right] = 0 \tag{4.63a}$$

$$\frac{\partial c_{\mathrm{X}^-}}{\partial t} + \operatorname{div}\left[-\mathbb{D}_{\mathrm{X}^-} \nabla[c_{\mathrm{X}^-}] + F \mathbb{\mu}_{\mathrm{X}^-} c_{\mathrm{X}^-} \left(1 - 2\frac{c_{\mathrm{X}^-}}{c^{max}}\right) \nabla[\phi_e]\right] = 0 \tag{4.63b}$$

$$\begin{aligned}\operatorname{div}\left[-\mathbb{\varepsilon} \nabla\left[\frac{\partial \phi_e}{\partial t}\right] + F\left(\mathbb{D}_{\mathrm{X}^-} \nabla[c_{\mathrm{X}^-}] - \mathbb{D}_{\mathrm{Li}^+} \nabla[c_{\mathrm{Li}^+}]\right)\right] + \\ - F^2 \operatorname{div}\left[\left(\mathbb{\mu}_{\mathrm{Li}^+} c_{\mathrm{Li}^+} \left(1 - 2\frac{c_{\mathrm{Li}^+}}{c^{max}}\right) + \mathbb{\mu}_{\mathrm{X}^-} c_{\mathrm{X}^-} \left(1 - 2\frac{c_{\mathrm{X}^-}}{c^{max}}\right)\right) \nabla[\phi_e]\right] = 0\end{aligned} \tag{4.63c}$$

$$\operatorname{div}[\mathbb{C} : \boldsymbol{\varepsilon}] = \vec{0} \tag{4.63d}$$

The difference between equations (4.62) and (4.34) are echoed in the distinction between this set of governing equations and the ones in section 4.5. Boundary conditions

$$\vec{h}_{\mathrm{Li}^+} \cdot \vec{n} = -h_{BV} \qquad \vec{x} \in \partial^N V_e \tag{4.64a}$$

$$\vec{h}_{\mathrm{X}^-} \cdot \vec{n} = 0 \qquad \vec{x} \in \partial^N V_e \tag{4.64b}$$

$$\operatorname{curl}\left[\vec{H}\right] \cdot \vec{n} = -F\, h_{BV} \qquad \vec{x} \in \partial^N V_e \tag{4.64c}$$

$$\boldsymbol{\sigma} \cdot \vec{n} = \vec{\overline{p}} \qquad \vec{x} \in \partial^N V_e \tag{4.64d}$$

are imposed along Neumann boundaries[12] $\partial^N V_e$. To ensure solvability to the problem, Dirichlet boundary conditions have to be enforced along part $\partial^D V_e$ as in section 4.5, being $\partial V_e = \partial^D V_e \cup \partial^N V_e$.

[11] There is actually more to say: it is anticipated here that in view of electroneutrality the saturation has no influence on the concentration field.

[12] Boundary conditions (4.64) have been derived in section 4.2.

Initial conditions (4.39) are foisted on concentration of ions $c_{\mathrm{Li}^+}(\vec{x}, t=0)$ and $c_{\mathrm{X}^-}(\vec{x}, t=0)$ in the electrolyte solution and comply equilibrium thermodynamics and electroneutrality condition (4.1).

Gauss law and balance of momentum in form (4.40) provide the necessary and sufficient equations to be solved for ϕ and $\vec{u}$ at $t=0$. Together with boundary conditions for displacements and tractions and homogeneous boundary conditions for potential and current they lead to the initial distribution of electric potential and displacements.

The evolution problem can be formulated in a weak form by multiplying the governing equations (4.63) by a suitable set of test functions and performing an integration upon the domain. As for (4.41) "variations" of the same set of variables that rule the problem have been used. The mass balance equations have been scaled by coefficients inherited from constitutive equation (4.61) to give to the new weak form the physical dimension of a power expenditure. The following identities are derived straightforwardly:

$$\begin{aligned}
&\frac{RT}{c_{bulk}} \int_{V_e} \hat{c}_{\mathrm{Li}^+} \left\{ \frac{\partial c_{\mathrm{Li}^+}}{\partial t} + \operatorname{div}\left[\vec{h}_{\mathrm{Li}^+} \right] \right\} \mathrm{d}V = \qquad (4.65a)\\
&\quad \frac{RT}{c_{bulk}} \int_{V_e} \hat{c}_{\mathrm{Li}^+} \frac{\partial c_{\mathrm{Li}^+}}{\partial t} + \mathbb{D}_{\mathrm{Li}^+} \nabla[\hat{c}_{\mathrm{Li}^+}] \cdot \nabla[c_{\mathrm{Li}^+}] \, \mathrm{d}V +\\
&\qquad + \frac{RT}{c_{bulk}} \int_{V_e} F \, \mathbb{\psi}_{\mathrm{Li}^+} c_{\mathrm{Li}^+} \left(1 - 2\frac{c_{\mathrm{Li}^+}}{c^{max}}\right) \nabla[\hat{c}_{\mathrm{Li}^+}] \cdot \nabla[\phi_e] \, \mathrm{d}V +\\
&\qquad\quad - \frac{RT}{c_{bulk}} \int_{\Gamma_{BV}} \hat{c}_{\mathrm{Li}^+} \, h_{BV} \, \mathrm{d}\Gamma = 0
\end{aligned}$$

$$\begin{aligned}
&\frac{RT}{c_{bulk}} \int_{V_e} \hat{c}_{\mathrm{X}^-} \left\{ \frac{\partial c_{\mathrm{X}^-}}{\partial t} + \operatorname{div}\left[\vec{h}_{\mathrm{X}^-} \right] \right\} \mathrm{d}V = \qquad (4.65b)\\
&\quad \frac{RT}{c_{bulk}} \int_{V_e} \hat{c}_{\mathrm{X}^-} \frac{\partial c_{\mathrm{X}^-}}{\partial t} + \mathbb{D}_{\mathrm{X}^-} \nabla[\hat{c}_{\mathrm{X}^-}] \cdot \nabla[c_{\mathrm{X}^-}] \, \mathrm{d}V +\\
&\qquad - \frac{RT}{c_{bulk}} \int_{V_e} F \, \mathbb{\psi}_{\mathrm{X}^-} c_{\mathrm{X}^-} \left(1 - 2\frac{c_{\mathrm{X}^-}}{c^{max}}\right) \nabla[\hat{c}_{\mathrm{X}^-}] \cdot \nabla[\phi_e] \, \mathrm{d}V = 0
\end{aligned}$$

$$\begin{aligned}
&\int_{V_e} \hat{\phi}_e \operatorname{div}\left[\frac{\partial \vec{D}}{\partial t} + F\left(\vec{h}_{\mathrm{Li}^+} - \vec{h}_{\mathrm{X}^-}\right) \right] \mathrm{d}V = \qquad (4.65c)\\
&\quad \int_{V_e} \mathbb{\epsilon} \nabla\left[\hat{\phi}_e\right] \cdot \nabla\left[\frac{\partial \phi_e}{\partial t}\right] \mathrm{d}V +\\
&\qquad + \int_{V_e} F^2 \left(\mathbb{\psi}_{\mathrm{Li}^+} c_{\mathrm{Li}^+} \left(1 - 2\frac{c_{\mathrm{Li}^+}}{c^{max}}\right) + \mathbb{\psi}_{\mathrm{X}^-} c_{\mathrm{X}^-} \left(1 - 2\frac{c_{\mathrm{X}^-}}{c^{max}}\right) \right) \nabla\left[\hat{\phi}_e\right] \cdot \nabla[\phi_e] \, \mathrm{d}V +\\
&\qquad\quad - F \int_{V_e} \nabla\left[\hat{\phi}_e\right] \cdot \left(\mathbb{D}_{\mathrm{X}^-} \nabla[c_{\mathrm{X}^-}] - \mathbb{D}_{\mathrm{Li}^+} \nabla[c_{\mathrm{Li}^+}] \right) \mathrm{d}V - F \int_{\Gamma_{BV}} \hat{\phi}_e \, h_{BV} \, \mathrm{d}\Gamma = 0
\end{aligned}$$

$$- \int_{V_e} \vec{\hat{u}} \cdot \operatorname{div}\left[\frac{\partial \boldsymbol{\sigma}}{\partial t} \right] \mathrm{d}V = \int_{V_e} \hat{\boldsymbol{\varepsilon}} : \mathbb{C} : \frac{\partial \boldsymbol{\varepsilon}}{\partial t} \, \mathrm{d}V - \int_{\partial^N V_e} \vec{\hat{u}} \cdot \frac{\partial \vec{\overline{p}}}{\partial t} \, \mathrm{d}\Gamma = 0 \qquad (4.65d)$$

Boundary conditions (4.64) have been used.

By scaling the fields that govern the problems according to (4.42) a dimensionless weak

form can be given in a time interval $[0, t_f]$ as

$$\begin{aligned} &\text{Find } y^*(\vec{x},t) \in \mathcal{V}^{[0,t_f]} \text{ such that} \\ &\frac{\partial}{\partial t} b^*\left(\hat{y}^*(\vec{x}), y^*(\vec{x},t)\right) + a^*(\hat{y}^*(\vec{x}), y^*(\vec{x},t)) = f^*(\hat{y}^*(\vec{x})) \quad \forall \hat{y}^*(\vec{x}) \in \mathcal{V} \end{aligned} \tag{4.66}$$

where subequations

$$\begin{aligned} &b^*\left(\hat{y}^*(\vec{x}), y^*(\vec{x},t)\right) = \\ &\quad RT\, c_{bulk} \int_{V_e} \hat{c}^*_{\mathrm{Li^+}}\, c^*_{\mathrm{Li^+}} + \hat{c}^*_{\mathrm{X^-}}\, c^*_{\mathrm{X^-}}\, \mathrm{d}V + \\ &\quad + \mathfrak{f} \left(\frac{RT}{F}\right)^2 \int_{V_e} \nabla\left[\hat{\phi}^*_e\right] \cdot \nabla\left[\phi^*_e\right]\, \mathrm{d}V + L^2 \int_{V_e} \hat{\boldsymbol{\varepsilon}}^* : \mathbb{C} : \boldsymbol{\varepsilon}^*\, \mathrm{d}V \end{aligned}$$

$$\begin{aligned} &a^*\left(\hat{y}^*(\vec{x}), y^*(\vec{x},t)\right) = \\ &\quad RT\, c_{bulk}\, \mathbb{D}_{\mathrm{Li^+}} \int_{V_e} \nabla\left[\hat{c}^*_{\mathrm{Li^+}}\right] \cdot \nabla\left[c^*_{\mathrm{Li^+}}\right] + c^*_{\mathrm{Li^+}} \left(1 - 2\frac{c^*_{\mathrm{Li^+}}}{c^*_{max}}\right) \nabla\left[\hat{c}^*_{\mathrm{Li^+}}\right] \cdot \nabla\left[\phi^*_e\right] \mathrm{d}V + \\ &\quad + RT\, c_{bulk}\, \mathbb{D}_{\mathrm{X^-}} \int_{V_e} \nabla\left[\hat{c}^*_{\mathrm{X^-}}\right] \cdot \nabla\left[c^*_{\mathrm{X^-}}\right] - c^*_{\mathrm{X^-}} \left(1 - 2\frac{c^*_{\mathrm{X^-}}}{c^*_{max}}\right) \nabla\left[\hat{c}^*_{\mathrm{X^-}}\right] \cdot \nabla\left[\phi^*_e\right] \mathrm{d}V + \\ &\quad + RT\, c_{bulk}\, \mathbb{D}_{\mathrm{Li^+}} \int_{V_e} \nabla\left[\hat{\phi}^*_e\right] \cdot \nabla\left[\phi^*_e\right] \left(1 - 2\frac{c^*_{\mathrm{Li^+}}}{c^*_{max}}\right) c^*_{\mathrm{Li^+}} + \nabla\left[\hat{\phi}^*_e\right] \cdot \nabla\left[c^*_{\mathrm{Li^+}}\right] \mathrm{d}V + \\ &\quad + RT\, c_{bulk}\, \mathbb{D}_{\mathrm{X^-}} \int_{V_e} \nabla\left[\hat{\phi}^*_e\right] \cdot \nabla\left[\phi^*_e\right] \left(1 - 2\frac{c^*_{\mathrm{X^-}}}{c^*_{max}}\right) c^*_{\mathrm{X^-}} - \nabla\left[\hat{\phi}^*_e\right] \cdot \nabla\left[c^*_{\mathrm{X^-}}\right] \mathrm{d}V \end{aligned}$$

$$f^*\left(\hat{y}^*(\vec{x})\right) = RT \int_{\Gamma_{BV}} (\hat{\phi}^*_e + \hat{c}^*_{\mathrm{Li^+}})\, h_{BV}\, \mathrm{d}\Gamma + L \int_{\partial^N V_e} \vec{\hat{u}}^* \cdot \frac{\partial \vec{p}}{\partial t}\, \mathrm{d}\Gamma$$

subequations with $y^*(\vec{x},t) = \{c^*_{\mathrm{Li^+}}, c^*_{\mathrm{X^-}}, \phi^*_e, \vec{u}^*\}$.

4.10 One-dimensional modeling of ionic transport in a liquid electrolyte accounting for saturation

This section develops further the case studied in section 4.6. A battery with a storage capacity of 720mAh is dealt with, which undergoes a galvanostatic process of charge at different C-rates (0.25, 0.5, 1, 2, and 4). The electrolyte is supposed to have a saturation limit for $LiPF_6$ of $5000\mathrm{mol\,m^{-3}}$ (whence $c^{max} = 10^4\mathrm{mol\,m^{-3}}$). The impact of saturation on the modeling of battery performances is analyzed.

Temperature of 25^oC is kept constant. Initial and boundary conditions are one and the same as section 4.6. The current $I(t)$ (with t in seconds) is tuned in time as

$$I(t) = (1 - e^{-t})\, I_{nC} \tag{4.67}$$

I_{nC} stands for the steady current at a C-rate equal to n. The concentration of ions across the electrolyte is uniform at $t = 0$ and amounts at $c_{bulk} = 1500\,\mathrm{mol\,m^{-3}}$. All other material and geometrical parameters are left unchanged with respect to the ones in section 4.6.

4.10.1 Discretization and time advancing by finite differences

Discretization is performed via separated variables, with spatial test $\varphi_i(x)$ and shape functions $\varphi_j(x)$ and nodal unknowns (collectively gathered in column y with component $y_j(t)$) that depend solely on time. Weak form (4.66) is accordingly transformed in a first order Ordinary Differential Equation (ODE) in time[13], which reads:

$$\text{Find } y(t) \text{ s.t.} \qquad b_i^* \cdot \dot{y}(t) + {}^l a_i^* \cdot y(t) + {}^n a_i^*[\, y(t)\,] = f_i^*(t) \qquad \text{for } i = 1, 2, ..., N \quad (4.68)$$

Linear operators b_i^* and ${}^l a_i^*$ are not influenced by the saturation of the electrolyte and coincide with the same operators in section 4.6.2. Non linear form ${}^n a_i^*[\, y(t)\,]$ on the contrary must be updated. It reads

$$\begin{aligned}
\frac{{}^n a_i^*[\, y(t)\,]}{RT\, c_{bulk}} = {} & \mathbb{D}_{\mathrm{Li^+}} \int_0^l \varphi_j^{\mathrm{Li^+}} c_j^{\mathrm{Li^+}} \left(1 - \frac{2}{c_{max}} \varphi_n^{\mathrm{Li^+}} c_n^{\mathrm{Li^+}}\right) \frac{\partial \varphi_i^{\mathrm{Li^+}}}{\partial x} \frac{\partial \varphi_k^{\phi}}{\partial x} \phi_k^e \, \mathrm{d}x + \\
& + \mathbb{D}_{\mathrm{Li^+}} \int_0^l \varphi_j^{\mathrm{Li^+}} c_j^{\mathrm{Li^+}} \left(1 - \frac{2}{c_{max}} \varphi_n^{\mathrm{Li^+}} c_n^{\mathrm{Li^+}}\right) \frac{\partial \varphi_i^{\phi}}{\partial x} \frac{\partial \varphi_k^{\phi}}{\partial x} \phi_k^e \, \mathrm{d}x + \\
& - \mathbb{D}_{\mathrm{X^-}} \int_0^l \varphi_j^{\mathrm{X^-}} c_j^{\mathrm{X^-}} \left(1 - \frac{2}{c_{max}} \varphi_n^{\mathrm{X^-}} c_n^{\mathrm{X^-}}\right) \frac{\partial \varphi_i^{\mathrm{X^-}}}{\partial x} \frac{\partial \varphi_k^{\phi}}{\partial x} \phi_k^e \, \mathrm{d}x + \\
& + \mathbb{D}_{\mathrm{X^-}} \int_0^l \varphi_j^{\mathrm{X^-}} c_j^{\mathrm{X^-}} \left(1 - \frac{2}{c_{max}} \varphi_n^{\mathrm{X^-}} c_n^{\mathrm{X^-}}\right) \frac{\partial \varphi_i^{\phi}}{\partial x} \frac{\partial \varphi_k^{\phi}}{\partial x} \phi_k^e \, \mathrm{d}x
\end{aligned}$$

A family of time-advancing methods based on the so-called θ-scheme can be set up for the discrete problem (4.68). In the numerical simulations that follows, the backward Euler scheme ($\theta = 1$) has been selected, thus seeking for $y(t + \Delta t)$ such that

$$b_i^* \cdot \frac{y(t + \Delta t)}{\Delta t} + {}^l a_i^* \cdot y(t + \Delta t) + {}^n a_i^*[\, y(t + \Delta t)\,] = f_i^*(t + \Delta t) + b_i^* \cdot \frac{y(t)}{\Delta t} \qquad (4.69)$$

As in 4.6, the *linearized updated* and the *Newton-Raphson* strategies have been implemented to solve non-linear problem (4.69).

4.10.2 Simulations

Several simulations of a single charge process have been carried out with different time steps and number of elements. An account of outcomes that refer to 150 equal finite elements and a constant time step of 1 second is here given. At the initial time the electric potential solves equations (4.40) and has to be homogeneous for being in thermodynamic equilibrium with neither current nor mass flowing.

$$\phi_e(\vec{x}, 0) = 0 \qquad \vec{x} \in V_e \qquad (4.70)$$

A symmetric ionic concentration profile arose in the electrolyte, initiated at the bulk concentration c_{bulk} that reflects thermodynamic equilibrium at time $t = 0$. Such a symmetry, emerged in section 4.6 (see also [128]) at a unit C-rate, is clearly envisaged also at different charging speeds, as emphasized in Figure 4.9.

[13] As in section 4.6.2 the star superscript is omitted from the definition of dimensionless quantities and the usual Einstein convention of sum is taken for the sake of readability.

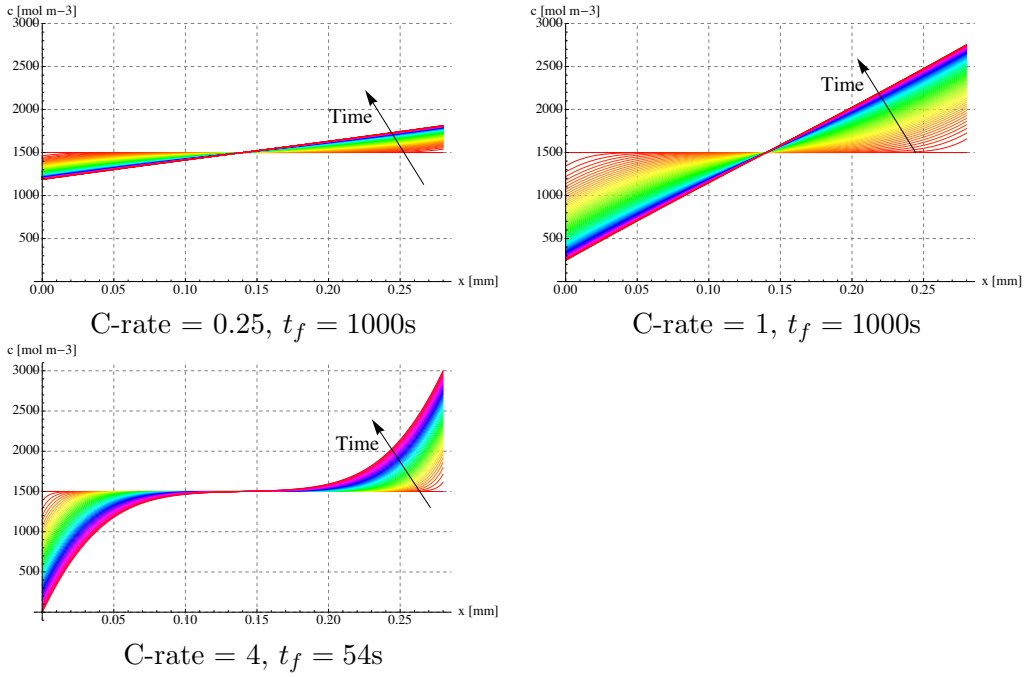

Figure 4.9: *Lithium ions concentration profiles $c_{\mathrm{Li}^+}(x,t)$ at different C-rates. In all cases the concentration at the initial time amounts at c_{bulk}, thus satisfying thermodynamic equilibrium.*

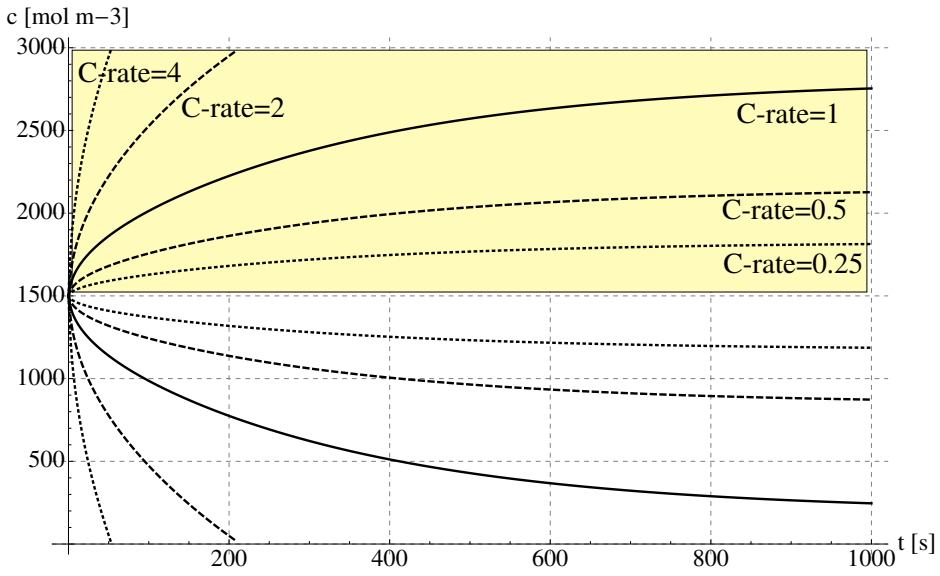

Figure 4.10: *Concentration profiles with saturation for a galvanostatic process at different C-rates at Cathode (upper, shadowed area) and Anode.*

After a "sufficiently long" time has passed, the steady state configuration has been approximated at C-rates less than 2. Analyses at higher C-rates have been quit before achieving the steady state configuration, because the limit concentration $c_{\mathrm{Li}^+} = 0$ was reached at the anode. In particular, for C-rate=2 the final time was $t_f = 210$s, whereas for C-rate=4 the analyses have been terminated at $t_f = 54$s. Concentration profiles in the presence of saturation at different C-rates are represented in Figure 4.10. The upper part of the picture, which

is shadowed, refers to the cathode, where concentration of Li^+ ions increase during charge processes. The lowest part of the same picture refers to the anode. The concentration profiles are symmetric respect to the bulk concentration $c_{bulk} = 1500\text{mol}\,\text{m}^{-3}$. As it was shown in Figure 4.2 for a unit C-rate, the steady asymptotic behaviors are recovered well, but steady state concentrations $c_\infty(0)$ and $c_\infty(l)$ have not been represented to the sake of readability.

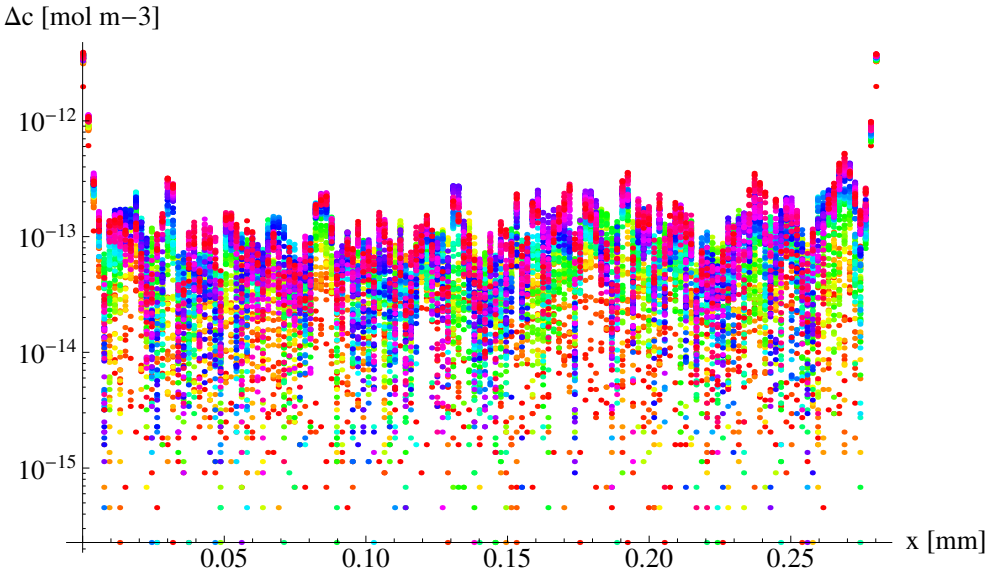

Figure 4.11: *Difference in concentration along the electrolyte between the solutions with and without saturation for a galvanostatic process at unit C-rate.*

Figure 4.11 depicts the difference in concentration $\Delta c(x,t)$ along the electrolyte $0 \le x \le 0.28$mm between the solutions with and without (section 4.6) saturation for a galvanostatic process at a unit C-rate. The difference ranges between $10^{-15} < \Delta c(x,t) < 10^{-12}\ \text{mol}\,\text{m}^{-3}$ depending on time $0 \le t \le t_f = 1000$s. It can be assessed from Figure 4.2 that ionic concentrations are in the order of $10^3\text{mol}\,\text{m}^{-3}$ along the electrolyte in the whole time frame. Accordingly, the impact of the saturation on concentration appears completely negligible. This effect has to be ascribed to electroneutrality.

To prove this assert, consider mass balance equations (4.63a) and (4.63b), here rewritten when electroneutrality condition (4.1) holds[14]

$$\frac{\partial c}{\partial t} + \text{div}\left[-\mathbb{D}_{\text{Li}^+} \nabla[c] - F\, \mathbb{t}_{\text{Li}^+}\, c \left(1 - 2\frac{c}{c^{max}}\right) \nabla[\phi_e] \right] = 0 \tag{4.71a}$$

$$\frac{\partial c}{\partial t} + \text{div}\left[-\mathbb{D}_{\text{X}^-} \nabla[c] + F\, \mathbb{t}_{\text{X}^-}\, c \left(1 - 2\frac{c}{c^{max}}\right) \nabla[\phi_e] \right] = 0 \tag{4.71b}$$

By multiplying the Li^+ balance equation for the mobility $\mathbb{t}_{\text{X}^-}$ and the X^- balance equation for the mobility $\mathbb{t}_{\text{Li}^+}$ the two equations (4.71) can be subtracted to form

$$(\mathbb{t}_{\text{X}^-} + \mathbb{t}_{\text{Li}^+})\frac{\partial c}{\partial t} - 2RT\, \mathbb{t}_{\text{X}^-}\, \mathbb{t}_{\text{Li}^+}\, \Delta[c] = 0 \tag{4.72}$$

Ionic concentrations in the assumption of electroneutrality are therefore independent upon the electric potential even in the case of saturation modeled via Fick's law (4.62). As the

[14] so to identify $c_{\text{Li}^+} = c_{\text{X}^-} = c$

deviation from electroneutrality is small (see discussions in 2.3) the analysis above provides an acceptable rationale to the numerically observed independence of ionic concentrations upon saturation.

Denote with $\phi_{nosat}(x,t)$ the solution for the electric potential when concentrations are far from saturation, i.e. assuming $c^{max} \to \infty$ in governing equations (4.63), and with $\phi_e(x,t)$ the solution for the electric potential of governing equations (4.63) with $c^{max} = 10000\text{mol}\,\text{m}^{-3}$. Electric potential profiles at the cathode whether in the presence of saturation or not at different C-rates are represented in figure 4.12.

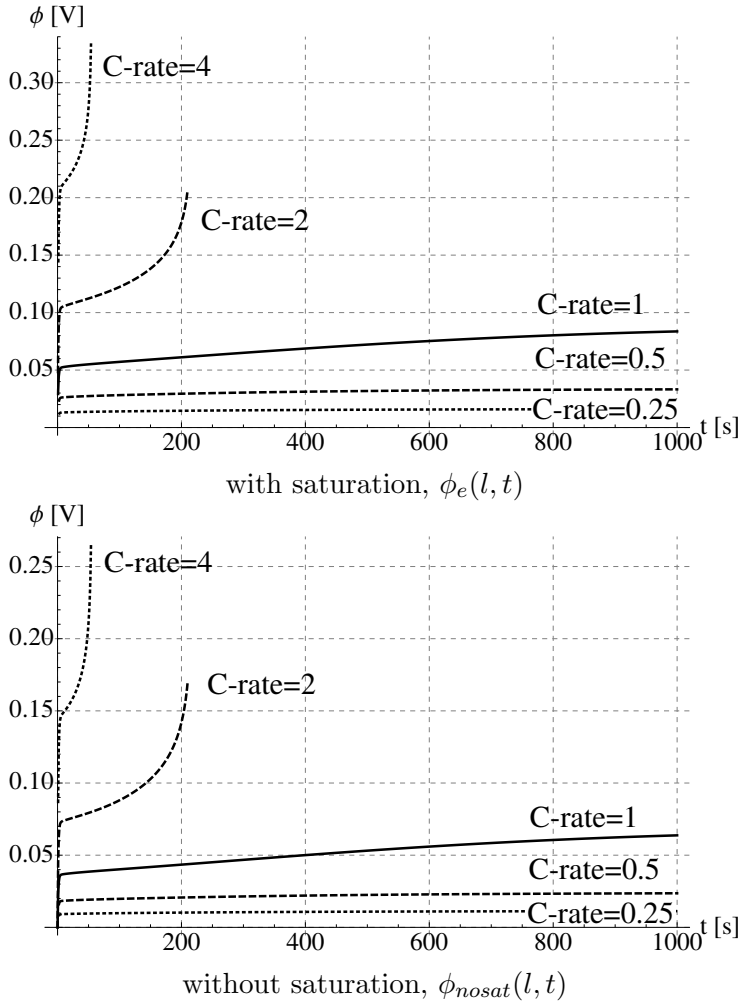

Figure 4.12: *Potential profile with and without saturation for a galvanostatic process at different C-rates at cathode. The electric potential at the anode is arbitrarily set to zero.*

Figure 4.13 depicts the evolution in time of the difference

$$\Delta\phi(x,t) = \phi_e(x,t) - \phi_{nosat}(x,t)$$

in the electric potential $\phi(x)$. The picture clearly shows that saturation does influence the electric potential and that the difference increases with time for all C-rates. The relative

difference

$$\Delta\phi(x,t) \times \phi_{nosat}^{-1}(x,t)$$

is plot in Figure 4.14. The latter shows that the saturation may increase the electric potential by about 40% near the cathode for all C-rates, and appears to be particularly significant at small C-rates even though in such cases concentrations may not be as close to the saturation limit at the end of the analyses t_f as they are for high C-rates.

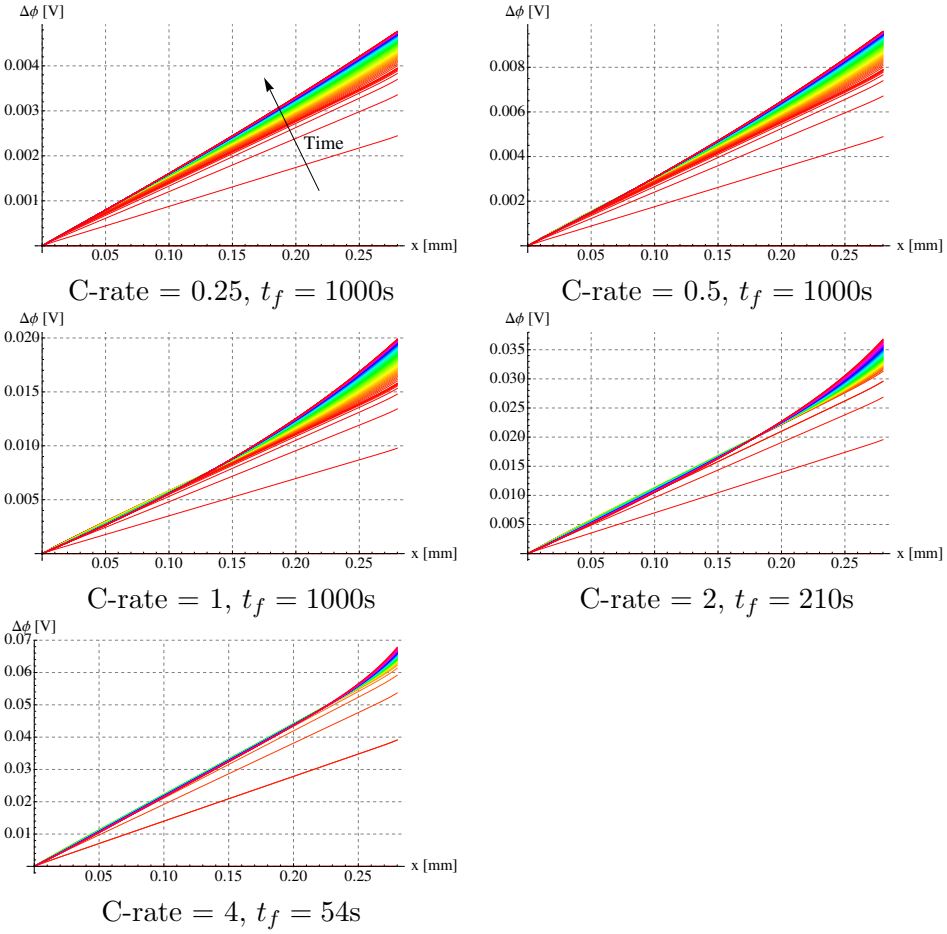

Figure 4.13: *Evolution in time of the difference* $\Delta\phi(x,t) = \phi(x,t) - \phi_{nosat}(x,t)$ *for several C-rates. The trend of the evolution in time is also depicted.*

Owing to Clausius-Planck inequality, the *internal entropy production* (shortened in IEP) cannot be negative. Following the approach of rational thermodynamics of Coleman and Noll, it can be written as:

$$\text{IEP}(x,t) = -\frac{1}{T}\sum_{\alpha}\vec{h}_{\alpha}\cdot\nabla\left[\,\overline{\mu}_{\alpha}\,\right] \geq 0 \tag{4.73}$$

for isothermal processes with no inelastic mechanical effects. After replacing Fick's law (4.30-4.59) into (4.73), the total internal entropy production amounts at

$$\frac{1}{T}\sum_{\alpha}\int_0^{t_f}\int_0^{L}\frac{1}{u_{\alpha}\,c_{\alpha}\,\left(1-2\frac{c_{\alpha}}{c^{max}}\right)}\vec{h}_{\alpha}\cdot\vec{h}_{\alpha}\,\mathrm{d}x\mathrm{d}t \tag{4.74}$$

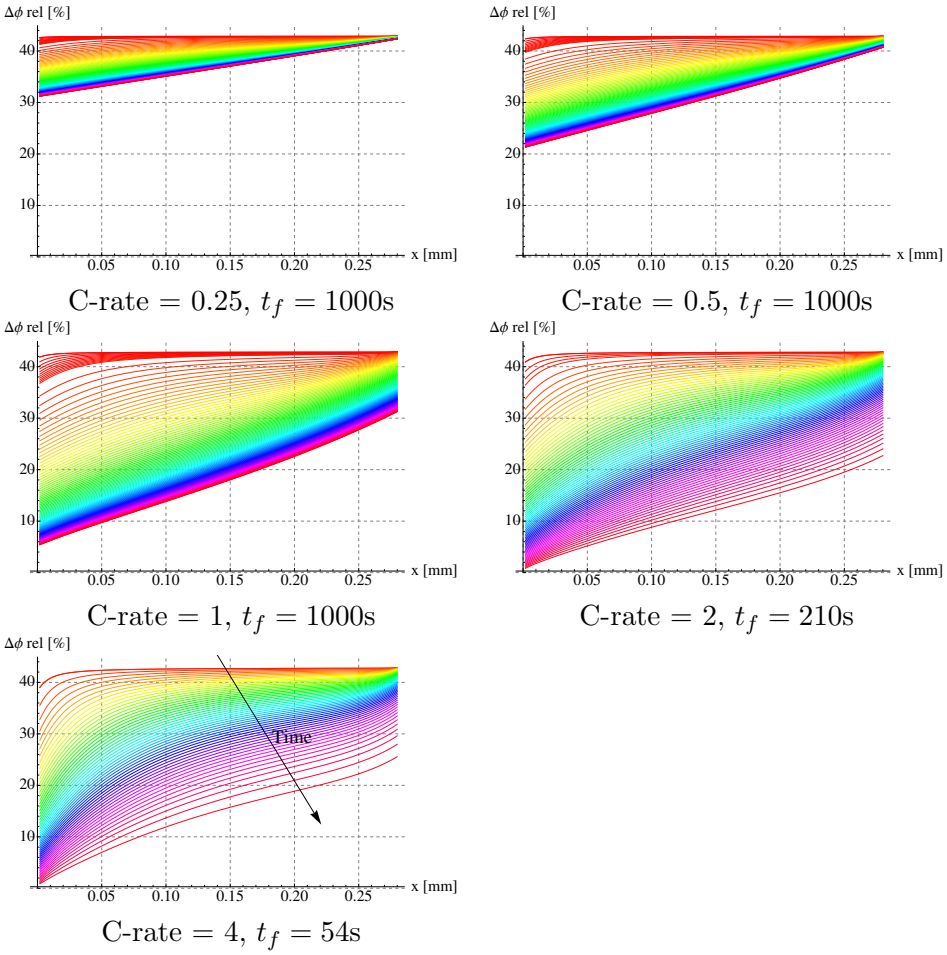

Figure 4.14: *Evolution in time of the ratio* $\Delta\phi(x,t) \times \phi^{-1}_{nosat}(x,t)$ *for several C-rates. The trend of the evolution in time is also depicted.*

with $\vec{h}_\alpha$ as in equation (4.62). Integration in time can be approximated in every time step by means of a trapezoidal rule. Furthermore, having used linear shape functions to approximate the concentration and potential fields, gradients result in constant amounts in each finite element. The scalar product $\vec{h}_\alpha \cdot \vec{h}_\alpha$ turns out to be a polynomial of degree four in the space variable x, which is of trivial integration. The amount

$$\frac{1}{T}\int_0^t \int_0^L \frac{1}{u_\alpha\, c_\alpha \left(1 - 2\frac{c_\alpha}{c^{max}}\right)} \vec{h}_\alpha \cdot \vec{h}_\alpha \, \mathrm{d}x\mathrm{d}\tau \tag{4.75}$$

is plotted in Figure 4.15 as a function of time t. It represents the buildup of internally generated entropy for Li^+ (continuous curve) and for PF_6^- (dashed curve), respectively, at different C-rates in the presence of saturation. At low C-rates, the flux of ions PF_6^- abates with time (Figure 4.4) and the slope of the IEP gets flatter and flatter with time[15]. Similarly,

[15]The flux near the electrode interfaces is dictated by the boundary conditions. The closer the regions to the electrodes the faster they reach the steady state - see Figure 5 in [128]). As discussed in [10] the Li^+ ionic current is mainly carried by migration at the beginning of the charging process, while under steady-state conditions diffusion and migrations contribute equally. The anionic mass flux reaches its peak very rapidly, and once the steady state is approached, the flux of PF_6^- tends to vanish, and no contribution is provided further to the overall ionic conductivity.

the flux of ions Li^+ tends to a constant while approaching the steady state conditions. The two effects combined providing to the IEP a linear trend with time at low C-rates. A similar behavior would be expected at higher C-rates, but the limit concentration is reached well before the steady state configuration.

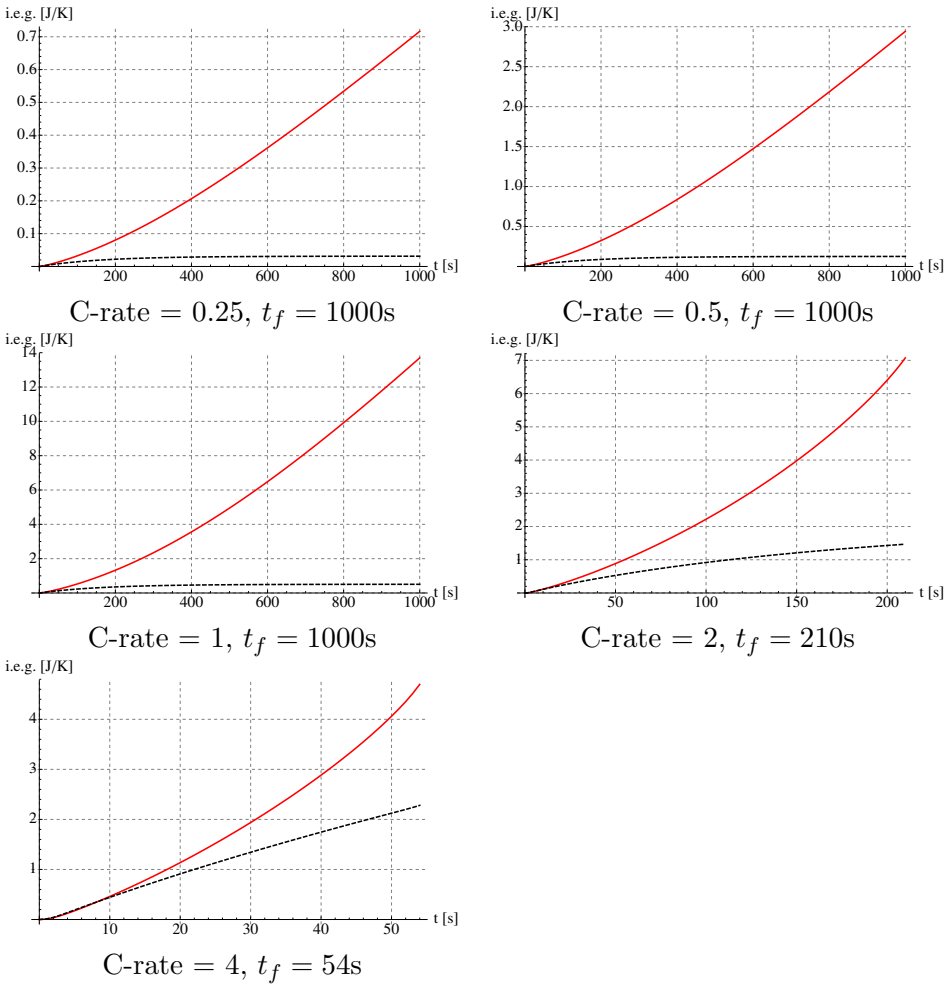

Figure 4.15: *Buildup of internally generated entropy for* Li^+ *(continuous curve) and for* PF_6^- *(dashed curve) at different C-rates in the presence of saturation.*

Figure 4.16 compares the total internal entropy production (4.74) with and without saturation. The increment of internally generated entropy due to the saturation is in the order of 40% of the unsaturated electrolyte IEP. The higher the C-rate the higher the rate of internally generated entropy. Nevertheless, as the limit concentration is reached at high charge rates, it is not allowed to conclude that the total accumulation of IEP is larger at high C-rates.

4.10.3 Remarks: liquid electrolyte

Either when C-rates are high (say 2 or more), or when the charge duration allows to reach a steady-state configuration at moderate C-rates (say about 1), the concentration near the electrodes gets close to the limit concentration $c_{Li^+} = 0$ at one side and close to the symmetric concentration $c_{Li^+} = 2c_{bulk}$ at the other electrode. In real batteries the latter concentration

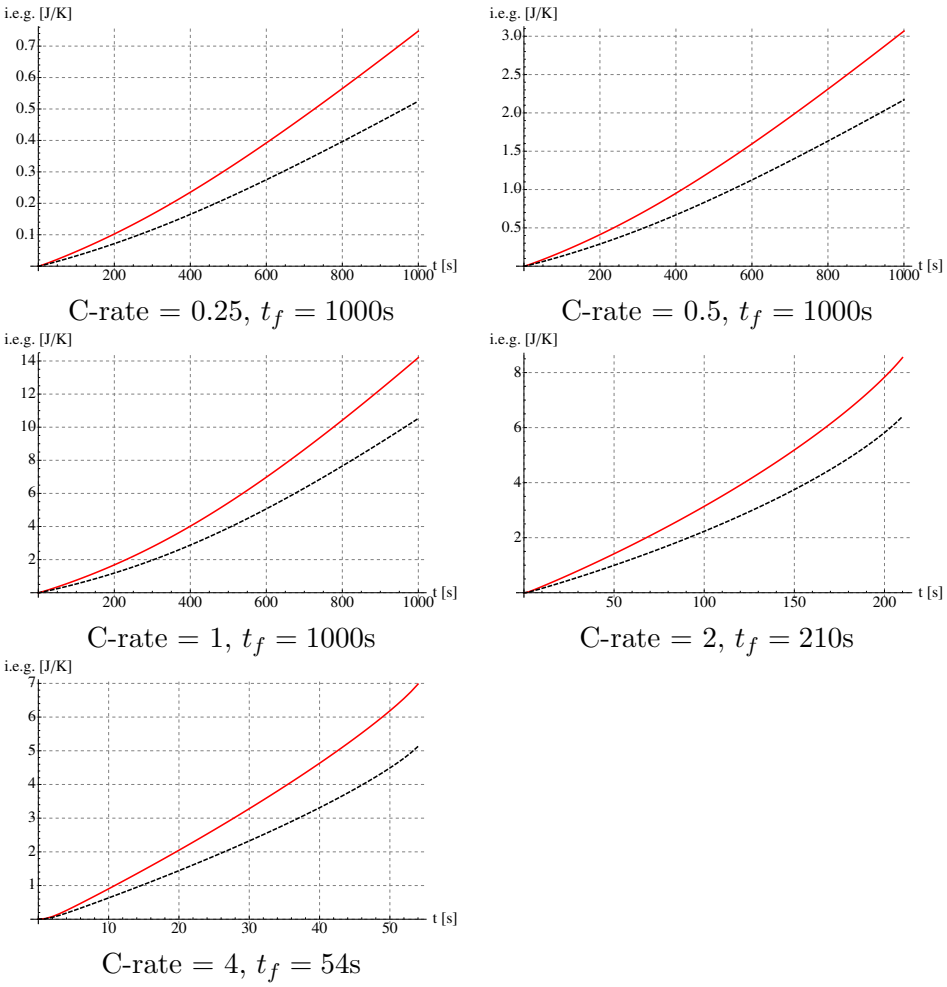

Figure 4.16: *Total internal entropy production (4.74) with (continuous curve) and without (dashed curve) saturation.*

can be higher than half of the saturation limit of the Li salt in the electrolyte solvent. Accordingly, it calls into question the assumption of ideal solutions far from saturation.

Such an assumption as been investigated in the further hypothesis that concentrations are too high to neglect the role of saturation but still sufficiently low to exclude incomplete dissociation of the Li-salt. This conjecture is confirmed indeed by the data and the numerical simulations on real batteries.

Constitutive specification (4.62) accounts for the saturation contribution. By comparing it with the mass flux constitutive equation adopted in [128], here reprinted in formula (4.62), one notices that saturation has no effect on the diffusivity. Under the assumption of electroneutrality, it can be assessed that saturation does not impact the concentration profiles either. Indeed, the electroneutrality condition (4.1) is well approximated during the simulations and the influence of saturation on the concentration profiles is actually negligible, see Figure 4.11.

Saturation does affect the electric potential in view of the mass flux equation (4.62) because it acts as to modify the ionic mobility, in turn inducing a higher potential gradient in the carried out simulations. Figures 4.13-4.14 confirm that the saturation may increase the electric potential by about 40% near the cathode for all C-rates. Saturation impacts by

a similar magnitude in the internal entropy production, as conveyed in Figure 4.16.

In conclusion, saturation appears to be an unavoidable feature in a multi scale and multi physics approach to battery modeling [8, 9]. Furthermore, the fully three-dimensional formulation proposed herein (see [8, 9, 128, 129]) and the numerical algorithms that emanate from the consequent weak forms have shown to be robust and capable to include the new constitutive specifications required to take into account of the saturation.
Moreover, the weak forms (4.43-4.66) are three-dimensional in nature, i.e. no 1D character influence the modeling at all: a 2D simulation will be provided in chapter 7. Nevertheless, one dimensional models can be formulated as a restriction of the general framework, as for example shown in sections 4.6-4.10.

Computations, based on Backward Euler and Newton Raphson schemes, show that the proposed methodology is efficient and reliable. Outcomes match the ones derived in [10].

4.11 Solid electrolyte

All-solid-state battery have a large beneficial impact on many applications, such as autonomous devices for ambient intelligence and medical implants [21].
The ionically conductive solid-state electrolytes play an important role in the solid-state battery design [21]. Construction of a consistent mathematical model describing the conductivity in the solid-state electrolyte therefore forms an essential component.
To this end, the novel approach presented, considering Maxwell's law explicitly, will be reshaped in the following sections to account for peculiar phenomena of solid-state electrolytes.

4.11.1 Balance equations

In Li_3PO_4 based solid-state electrolyte, Lithium atoms may occupy two states in the hosting matrix, namely immobile, oxygen-binded Lithium (denoted with Li^0) and mobile Li^+ ions. The total concentration of Lithium atoms in the solid electrolyte hosting material will be defined by c_{Li}^{tot} and will henceforth assumed to be independent upon position $\vec{x}$ and time t. Whereas c_{Li}^{tot} is a given amount assigned once for all for the electrolyte, ionic concentration c_{Li^+} changes during the process with position $\vec{x}$ and time t. So does the oxygen-binded Lithium, according to balance

$$c_{\mathrm{Li}^0}(\vec{x},t) = c_{\mathrm{Li}}^{tot} - c_{\mathrm{Li}^+}(\vec{x},t) \tag{4.76}$$

The ionization reaction

$$\mathrm{Li}^0 \underset{\mathrm{k_r}}{\overset{\mathrm{k_d}}{\rightleftarrows}} \mathrm{Li}^+ + \mathrm{X}^- \tag{4.77}$$

describes the transfer process of oxygen-binded Lithium to mobile Li^+ ions leaving uncompensated negative charges X^- behind, which are chemically associated with the closest nonbridging oxygen atoms. In isothermal processes, as the ones that are assumed to take place in the present work, factors $\mathrm{k_d}$ and $\mathrm{k_r}$ are taken to be constant during the whole process. They are not independent: *under equilibrium conditions* the rates of the forward and backward reactions are equal. By equating the two rate equations for the chemical reaction (4.77) it comes out

$$\mathrm{k_d}\, c_{\mathrm{Li}^0}^{eq} = \mathrm{k_r}\, c_{\mathrm{Li}^+}^{eq}\, c_{\mathrm{X}^-}^{eq} \tag{4.78}$$

Equilibrium concentrations $c^{eq}_{\mathrm{Li^0}}$, $c^{eq}_{\mathrm{Li^+}}$, and $c^{eq}_{\mathrm{X^-}}$ do not depend on the state of charge of the electrodes and are constant during the battery operation: therefore equation (4.78) is indeed a relationship between $\mathrm{k_d}$ and $\mathrm{k_r}$. To further stress this statement, the two constants can be related to the total amount of Lithium atoms in the solid electrolyte hosting material c^{tot}_{Li} by a constant $0 \leq \delta \leq 1$, which is calibrated against experimental analysis.

$$c^{eq}_{\mathrm{Li^+}} = c^{eq}_{\mathrm{X^-}} = \delta\, c^{tot}_{\mathrm{Li}}\ , \qquad c^{eq}_{\mathrm{Li^0}} = (1-\delta)\, c^{tot}_{\mathrm{Li}} \tag{4.79}$$

Statement (4.79) stems from eq. (4.76) and from observing that under equilibrium conditions electroneutrality holds strictly. Eq. (4.78) relates $\mathrm{k_d}$ to $\mathrm{k_r}$, c^{tot}_{Li} and δ as

$$\mathrm{k_d} = \mathrm{k_r}\, c^{tot}_{\mathrm{Li}}\, \frac{\delta^2}{1-\delta} \tag{4.80}$$

Equilibrium does *not* take place in batteries during charge, discharge or relaxation. It is in fact a limit condition. Accordingly equation (4.78) does not hold when actual concentrations replace equilibrium concentrations. During batteries operation reaction (4.77) is therefore unbalanced and $\mathrm{Li^+}$ ions are either generated or consumed. The ionization reaction acts as a rate controller: at all points $\vec{x}$ where $\mathrm{Li^+}$ accumulates during battery operations (see for instance the simulations in [10, 21, 128, 129]) more immobile, oxygen-binded Lithium is created, and vice versa. This results in a mass supply/sink within the mass balance equation (2.1) for ionic species. The amount of generated ions (either $\mathrm{Li^+}$ or $\mathrm{X^-}$) is:

$$s_{\mathrm{Li^+}}(\vec{x},t) = s_{\mathrm{X^-}}(\vec{x},t) = \mathrm{k_d}\, c_{\mathrm{Li^0}}(\vec{x},t) - \mathrm{k_r}\, c_{\mathrm{Li^+}}(\vec{x},t)\, c_{\mathrm{X^-}}(\vec{x},t) \tag{4.81}$$

By making use of equation (4.76), the *mass balance* equations that characterize the transport of $\mathrm{Li^+}$ ions and $\mathrm{X^-}$ uncompensated negative charges in the electrolyte read:

$$\frac{\partial c_{\mathrm{Li^+}}}{\partial t} + \mathrm{div}\left[\,\vec{h}_{\mathrm{Li^+}}\,\right] + \mathrm{k_d}\, c_{\mathrm{Li^+}} + \mathrm{k_r}\, c_{\mathrm{Li^+}}\, c_{\mathrm{X^-}} = \mathrm{k_d}\, c^{tot}_{\mathrm{Li}} \qquad \vec{x} \in V_e \tag{4.82a}$$

$$\frac{\partial c_{\mathrm{X^-}}}{\partial t} + \mathrm{div}\left[\,\vec{h}_{\mathrm{X^-}}\,\right] + \mathrm{k_d}\, c_{\mathrm{Li^+}} + \mathrm{k_r}\, c_{\mathrm{Li^+}}\, c_{\mathrm{X^-}} = \mathrm{k_d}\, c^{tot}_{\mathrm{Li}} \qquad \vec{x} \in V_e \tag{4.82b}$$

The electric displacement field is governed by the rate equation

$$\mathrm{div}\left[\,\frac{\partial \vec{D}_e}{\partial t} + F\,(\vec{h}_{\mathrm{Li^+}} - \vec{h}_{\mathrm{X^-}})\,\right] \;=\; 0 \qquad \vec{x} \in V_e \tag{4.82c}$$

The balance of forces is taken homogeneous

$$\begin{aligned} \mathrm{div}\,[\,\boldsymbol{\sigma}\,] &= \vec{0} \qquad \vec{x} \in V_e \\ \mathrm{skw}[\,\boldsymbol{\sigma}\,] &= \mathbf{0} \qquad \vec{x} \in V_e \end{aligned} \tag{4.82d}$$

4.11.2 Weak form and boundary conditions

The weak formulation of balance equations (4.82) results from multiplication by a suitable set of test functions and from an integration upon the domain, exploiting Green's formula

to reduce the order of differentiation. Take the mass balance equation (4.82a, 4.82b) in the following abstract formalism ($\alpha = \mathrm{Li}^+, \mathrm{X}^-$):

$$\begin{aligned}
\int_{V_e} \hat{\mu}_\alpha \left\{ \frac{\partial c_\alpha}{\partial t} + \operatorname{div}\left[\, \vec{h}_\alpha \,\right] + \mathrm{k_d}\, c_{\mathrm{Li}^+} + \mathrm{k_r}\, c_{\mathrm{Li}^+}\, c_{\mathrm{X}^-} \right\} \mathrm{d}V = \qquad (4.83)\\
= \int_{V_e} \hat{\mu}_\alpha \, \frac{\partial c_\alpha}{\partial t} \, \mathrm{d}V + \int_{V_e} \operatorname{div}\left[\, \hat{\mu}_\alpha \, \vec{h}_\alpha \,\right] - \nabla\left[\, \hat{\mu}_\alpha \,\right] \cdot \vec{h}_\alpha \, \mathrm{d}V + \\
+ \int_{V_e} \mathrm{k_d}\, \hat{\mu}_\alpha \, c_{\mathrm{Li}^+} + \mathrm{k_r}\, \hat{\mu}_\alpha \, c_{\mathrm{Li}^+}\, c_{\mathrm{X}^-} \, \mathrm{d}V \\
= \int_{V_e} \hat{\mu}_\alpha \, \frac{\partial c_\alpha}{\partial t} \, \mathrm{d}V - \int_{V_e} \nabla\left[\, \hat{\mu}_\alpha \,\right] \cdot \vec{h}_\alpha \, \mathrm{d}V + \int_{V_e} \mathrm{k_d}\, \hat{\mu}_\alpha \, c_{\mathrm{Li}^+} + \mathrm{k_r}\, \hat{\mu}_\alpha \, c_{\mathrm{Li}^+}\, c_{\mathrm{X}^-} \, \mathrm{d}V \\
+ \int_{\Gamma_{BV}} \hat{\mu}_\alpha \, \vec{h}_\alpha \cdot \vec{n}_e \, \mathrm{d}\Gamma \\
= \int_{V_e} \hat{\mu}_\alpha \, \mathrm{k_d}\, c_{\mathrm{Li}}^{tot} \, \mathrm{d}V
\end{aligned}$$

Within (4.83) a contribution is defined at the boundary $\Gamma_{BV} \subseteq \partial V_e^N$ of the electrolyte, i.e. at the location Γ_{BV} where the oxidation/reduction reaction takes place. At that locus there is no intercalation of X^- charges, whereas a Faradaic reaction converts the oxidized Lithium to its neutral state before its diffusion into the electrode lattice or vice versa. The mass flux at the interface Γ_{BV} satisfies the following boundary conditions:

$$\vec{h}_{\mathrm{Li}^+} \cdot \vec{n}_e = -h_{BV} \qquad \vec{x} \in \Gamma_{BV} \tag{4.84a}$$

$$\vec{h}_{\mathrm{Li}^+} \cdot \vec{n}_e = 0 \qquad \vec{x} \in \partial^N V_e \setminus \Gamma_{BV} \tag{4.84b}$$

$$\vec{h}_{\mathrm{X}^-} \cdot \vec{n}_e = 0 \qquad \vec{x} \in \partial^N V_e \tag{4.84c}$$

As in section 4.2 the mass flux at the boundary h_{BV} is here considered as given.

With a similar path of reasoning one deals with balance law (4.82c)

$$\begin{aligned}
\int_{V_e} \hat{\phi}_e \operatorname{div}\left[\frac{\partial \vec{D}_e}{\partial t} + F\left(\vec{h}_{\mathrm{Li}^+} - \vec{h}_{\mathrm{X}^-} \right) \right] \mathrm{d}V = \\
- \int_{V_e} \nabla\left[\hat{\phi}_e \right] \cdot \frac{\partial \vec{D}_e}{\partial t} \, \mathrm{d}V - F \int_{V_e} \nabla\left[\hat{\phi}_e \right] \cdot \left(\vec{h}_{\mathrm{Li}^+} - \vec{h}_{\mathrm{X}^-} \right) \mathrm{d}V + \qquad (4.85)\\
+ \int_{\Gamma_{BV}} \hat{\phi}_e \left\{ \frac{\partial \vec{D}_e}{\partial t} + F\left(\vec{h}_{\mathrm{Li}^+} - \vec{h}_{\mathrm{X}^-} \right) \right\} \cdot \vec{n}_e \, \mathrm{d}\Gamma = 0
\end{aligned}$$

Ampère's law

$$\left\{ \frac{\partial \vec{D}}{\partial t} + F\, \vec{h}_{\mathrm{Li}^+} \right\} \cdot \vec{n}_e = \operatorname{curl}\left[\vec{H}_e \right] \cdot \vec{n}_e \qquad \vec{x} \in \Gamma_{BV} \tag{4.86}$$

allows to devise boundary conditions for the electric potential in terms of the projection of the curl of magnetizing field across the interface. They will be considered later in section 6.1.3.

Finally, for the equilibrium equations (4.82d) in rate form, one writes

$$\int_{V_e} \vec{\hat{u}} \cdot \operatorname{div}\left[\frac{\partial \boldsymbol{\sigma}}{\partial t} \right] \mathrm{d}V = -\int_{V_e} \hat{\boldsymbol{\varepsilon}} : \frac{\partial \boldsymbol{\sigma}}{\partial t} \, \mathrm{d}V + \int_{\Gamma_{BV}} \vec{\hat{u}} \cdot \frac{\partial \boldsymbol{\sigma}}{\partial t} \cdot \vec{n}_e \, \mathrm{d}\Gamma = 0 \tag{4.87}$$

Tractions across the interface are supposed to be continuous, and no displacement jumps are taken into account.

4.11.3 Thermodynamics and constitutive theory: solid electrolyte

Thermodynamic restrictions, formulated as in (4.26), still apply. The first and the second law of thermodynamics are in fact unaffected by the nature of the source terms s_{Li^+} and s_{X^-} in the balance equations (4.82). Since internal energy balance (4.12), entropy imbalance (4.22) and Coleman-Noll will procedure would present no novelties with respect to section 4.3 they will not be repeated here.

By considering dilute solutions accounting for saturation, under the assumption of non-interacting species (refer to section 4.8), constitutive relation for $\vec{D}_e$, $\vec{h}_\alpha$ and $\boldsymbol{\sigma}$ in terms of $\{c_\alpha, \phi_e, \vec{u}\}$ read

$$\vec{D}_e = -\mathbb{\phi} \, \nabla [\, \phi_e \,] \tag{4.88a}$$

$$\vec{h}_\alpha = -\mathbb{D}_\alpha \, \nabla [\, c_\alpha \,] - z_\alpha \, F \, \mathbb{\psi}_\alpha \, c_\alpha \, \left(1 - 2 \frac{c_\alpha}{c^{max}} \right) \, \nabla [\, \phi_e \,] \tag{4.88b}$$

$$\boldsymbol{\sigma} = K \, \mathrm{tr} [\, \boldsymbol{\varepsilon} \,] \, \mathbb{1} + 2G \, \mathrm{dev} [\, \boldsymbol{\varepsilon} \,] \tag{4.88c}$$

4.11.4 Governing equations: solid electrolyte

Governing equations can be derived by incorporating the constitutive equations (4.88) into balance equations (4.82). The variable fields that rule the problem, resulting from the choice made for thermodynamic prescriptions, are concentrations c_α, displacements $\vec{u}$, and the electric potential ϕ_e. Governing equations hold at all points $\vec{x} \in V_e$ at all instants:

$$\frac{\partial c_{\mathrm{Li}^+}}{\partial t} + \mathrm{div} \left[-\mathbb{D}_{\mathrm{Li}^+} \, \nabla [\, c_{\mathrm{Li}^+} \,] - F \, \mathbb{\psi}_{\mathrm{Li}^+} \, c_{\mathrm{Li}^+} \, \left(1 - 2 \frac{\partial c_{\mathrm{Li}^+}}{\partial c^{max}} \right) \, \nabla [\, \phi_e \,] \right] + \\ + \mathrm{k_d} \, c_{\mathrm{Li}^+} + \mathrm{k_r} \, c_{\mathrm{Li}^+} \, c_{\mathrm{X}^-} = \mathrm{k_d} \, c_{\mathrm{Li}}^{tot} \tag{4.89a}$$

$$\frac{\partial c_{\mathrm{X}^-}}{\partial t} + \mathrm{div} \left[-\mathbb{D}_{\mathrm{X}^-} \, \nabla [\, c_{\mathrm{X}^-} \,] + F \, \mathbb{\psi}_{\mathrm{X}^-} \, c_{\mathrm{X}^-} \, \left(1 - 2 \frac{\partial c_{\mathrm{X}^-}}{\partial c^{max}} \right) \, \nabla [\, \phi_e \,] \right] + \\ + \mathrm{k_d} \, c_{\mathrm{Li}^+} + \mathrm{k_r} \, c_{\mathrm{Li}^+} \, c_{\mathrm{X}^-} = \mathrm{k_d} \, c_{\mathrm{Li}}^{tot} \tag{4.89b}$$

$$\mathrm{div} \left[-\mathbb{\phi} \, \nabla \left[\frac{\partial \phi_e}{\partial t} \right] + F \, (\mathbb{D}_{\mathrm{X}^-} \, \nabla [\, c_{\mathrm{X}^-} \,] - \mathbb{D}_{\mathrm{Li}^+} \, \nabla [\, c_{\mathrm{Li}^+} \,]) \right] + \\ - F^2 \, \mathrm{div} \left[\left\{ \mathbb{\psi}_{\mathrm{Li}^+} \, c_{\mathrm{Li}^+} \left(1 - 2 \frac{c_{\mathrm{Li}^+}}{c^{max}} \right) + \mathbb{\psi}_{\mathrm{X}^-} \, c_{\mathrm{X}^-} \left(1 - 2 \frac{c_{\mathrm{X}^-}}{c^{max}} \right) \right\} \nabla [\, \phi_e \,] \right] = 0 \tag{4.89c}$$

$$\mathrm{div} [\, \mathbb{C} \, : \, \boldsymbol{\varepsilon} \,] = \vec{0} \tag{4.89d}$$

Initial conditions are usually imposed for concentration of ions $c_{\mathrm{Li}^+}(\vec{x}, t = 0)$ and $c_{\mathrm{X}^-}(\vec{x}, t = 0)$ in the electrolyte solution. To comply with equilibrium thermodynamics they are constant in volume V_e; furthermore initial concentrations are equal, obeying the electroneutrality condition. Consistently, a positive constant c_{bulk} will be defined as

$$c_{bulk} = c_{\mathrm{Li}^+}(\vec{x}, t = 0) = c_{\mathrm{X}^-}(\vec{x}, t = 0) \tag{4.90}$$

and will be used to scale concentration variables henceforth.

Initial conditions for electric potential and displacements solve a boundary value problem at $t = 0$. In view of the perfect electroneutrality, at initial time Gauss law (2.8) and balance of momentum (2.11) provide the necessary and sufficient equations to be solved for ϕ_e and $\vec{u}$:

$$\operatorname{div}[\,\not\in\nabla[\,\phi_e\,]\,] = 0 \qquad \vec{x} \in V_e,\ t = 0 \tag{4.91a}$$

$$\operatorname{div}[\,\mathbb{C} : \boldsymbol{\varepsilon}\,] = \vec{0} \qquad \vec{x} \in V_e,\ t = 0 \tag{4.91b}$$

together with homogeneous boundary conditions for current, in view of thermodynamic equilibrium at initial time, and usual given boundary conditions for displacements and tractions.

4.12 Weak form: solid electrolyte

Following the same path of reasoning of sections 4.5 and 4.9 the evolution problem can be formulated in a weak form. In Galerkin approaches weak forms are built using "variations" of the same set of variables that rule the problem, namely "virtual" concentrations $\hat{c}_{\mathrm{Li^+}}$, $\hat{c}_{\mathrm{X^-}}$, displacements $\hat{\vec{u}}$, electric potential $\hat{\phi}_e$. By doing so however the energy meaning of (4.83), (4.85) and (4.87) is lost. To give to the new weak form at least the physical dimension of a power expenditure, equations will be scaled by suitable coefficients, that follow from constitutive equations. A weak form of governing equations can be given in a time interval $[0, t_f]$ as

$$\begin{aligned} &\text{Find } y(\vec{x},t) \in \mathcal{V}^{[0,t_f]} \text{ such that} \\ &\frac{\partial}{\partial t} b(\,\hat{y}(\vec{x}), y(\vec{x},t)\,) + a(\,\hat{y}(\vec{x}), y(\vec{x},t)\,) = f(\,\hat{y}(\vec{x})\,) \quad \forall \hat{y}(\vec{x}) \in \mathcal{V} \end{aligned} \tag{4.92}$$

where

$$\begin{aligned}
b(\hat{y}, y) &= -\frac{RT}{c_{bulk}} \int_{V_e} \hat{c}_{\mathrm{Li^+}}\, c_{\mathrm{Li^+}} + \hat{c}_{\mathrm{X^-}}\, c_{\mathrm{X^-}}\, \mathrm{d}V \\
&+ \not\in \int_{V_e} \nabla\left[\,\hat{\phi}_e\,\right] \cdot \nabla[\,\phi_e\,]\, \mathrm{d}V + \int_{V_e} \hat{\boldsymbol{\varepsilon}} : \boldsymbol{\sigma}(\boldsymbol{\varepsilon})\, \mathrm{d}V \\
a(\hat{y}, y) &= -\frac{RT}{c_{bulk}} \int_{V_e} \mathbb{D}_{\mathrm{Li^+}} \nabla[\,\hat{c}_{\mathrm{Li^+}}\,] \cdot \nabla[\,c_{\mathrm{Li^+}}\,] + \mathbb{D}_{\mathrm{X^-}} \nabla[\,\hat{c}_{\mathrm{X^-}}\,] \cdot \nabla[\,c_{\mathrm{X^-}}\,]\, \mathrm{d}V + \\
&- \frac{RT}{c_{bulk}} \int_{V_e} F \,\mathbb{\mu}_{\mathrm{Li^+}}\, c_{\mathrm{Li^+}} \left(1 - 2\frac{c_{\mathrm{Li^+}}}{c^{max}}\right) \nabla[\,\hat{c}_{\mathrm{Li^+}}\,] \cdot \nabla[\,\phi_e\,]\, \mathrm{d}V + \\
&+ \frac{RT}{c_{bulk}} \int_{V_e} F \,\mathbb{\mu}_{\mathrm{X^-}}\, c_{\mathrm{X^-}} \left(1 - 2\frac{c_{\mathrm{X^-}}}{c^{max}}\right) \nabla[\,\hat{c}_{\mathrm{X^-}}\,] \cdot \nabla[\,\phi_e\,]\, \mathrm{d}V + \\
&- \frac{RT}{c_{bulk}} \int_{V_e} \mathrm{k_d}\, \hat{c}_{\mathrm{Li^+}}\, c_{\mathrm{Li^+}} + \mathrm{k_r}\, \hat{c}_{\mathrm{Li^+}}\, c_{\mathrm{Li^+}}\, c_{\mathrm{X^-}}\, \mathrm{d}V + \\
&- \frac{RT}{c_{bulk}} \int_{V_e} \mathrm{k_d}\, \hat{c}_{\mathrm{X^-}}\, c_{\mathrm{Li^+}} + \mathrm{k_r}\, \hat{c}_{\mathrm{X^-}}\, c_{\mathrm{Li^+}}\, c_{\mathrm{X^-}}\, \mathrm{d}V + \\
&+ F \int_{V_e} \nabla\left[\,\hat{\phi}_e\,\right] \cdot (\mathbb{D}_{\mathrm{Li^+}} \nabla[\,c_{\mathrm{Li^+}}\,] - \mathbb{D}_{\mathrm{X^-}} \nabla[\,c_{\mathrm{X^-}}\,])\, \mathrm{d}V + \\
&+ F^2 \int_{V_e} \mathbb{\mu}_{\mathrm{Li^+}}\, c_{\mathrm{Li^+}} \left(1 - 2\frac{c_{\mathrm{Li^+}}}{c^{max}}\right) \nabla\left[\,\hat{\phi}_e\,\right] \cdot \nabla[\,\phi_e\,]\, \mathrm{d}V +
\end{aligned}$$

$$
\begin{aligned}
&+ \quad F^2 \int_{V_e} \psi_{\mathrm{X}^-}\, c_{\mathrm{X}^-} \left(1 - 2\frac{c_{\mathrm{X}^-}}{c^{max}}\right) \nabla\left[\,\hat{\phi}_e\,\right] \cdot \nabla\left[\,\phi_e\,\right] \mathrm{d}V + \\
f\left(\hat{y}\right) &= \int_{\Gamma_{BV}} \left(F\,\hat{\phi}_e - \frac{RT}{c_{bulk}}\,\hat{c}_{\mathrm{Li}^+}\right) h_{BV}\mathrm{d}\Gamma + L\int_{\partial^N V_e} \vec{\hat{u}} \cdot \frac{\partial\vec{\overline{p}}}{\partial t}\,\mathrm{d}\Gamma + \\
&- \quad \int_{V_e} \hat{c}_{\mathrm{Li}^+}\,\mathrm{k_d}\,c_{\mathrm{Li}}^{tot}\,\mathrm{d}V - \int_{V_e} \hat{c}_{\mathrm{X}^-}\,\mathrm{k_d}\,c_{\mathrm{Li}}^{tot}\,\mathrm{d}V
\end{aligned}
$$

with list $y(\vec{x},t) = \{c_{\mathrm{Li}^+}, c_{\mathrm{X}^-}, \phi_e, \vec{u}\,\}$. Owing to the scaling, a characteristic length L and a characteristic time Δt appear in the weak form. They will be given a neat identification in what follows. The proof descends from the same path of reasoning of the weak form for the balance equations provided in appendix 3.5 and will not be replicated.

4.13 One-dimensional modeling of ionic transport in a solid electrolyte

4.13.1 Description

This Section deals with the sole solid electrolyte of the case study analyzed in [21], namely a $1.5\mu m$ thick Li_3PO_4 solid electrolyte of a $10\mu Ah$ planar thin film all solid state Li-ion battery. The cell was charged and discharged according to the following regime: constant current with a 51.2 C-rate, followed by a 60 s relaxation period; a galvanostatic discharge and charge at 51.2 C-rate follows and a final relaxation period of 30 s have been left at the end. The reader may also refer to equation (4.98) for a schematic of the path. Several discharge rates were applied in [21] to reproduce experimental evidences. With the aim of validating the model here proposed, only a discharge rate of 51.2C is considered at temperature of 25^oC, with current density $I_{51.2C} = 5.12\mathrm{Am}^{-2}$.

As this Section is restricted to the electrolyte only, interfaces and electrode kinetics do not enter the governing equations. The interface Γ_{BV} becomes a Neumann boundary for the mass flux, which is taken as a given datum yet is still termed h_{BV} to point out that in principle it must derive from a Butler-Volmer equation. Mass flux boundary conditions thus read:

$$\vec{h}_{\mathrm{Li}^+} \cdot \vec{n} = -h_{BV} \qquad \vec{x} \in \partial^N V \tag{4.93a}$$

$$\vec{h}_{\mathrm{X}^-} \cdot \vec{n} = 0 \qquad \vec{x} \in \partial^N V \tag{4.93b}$$

In order to make initial and boundary conditions compatible with thermodynamic equilibrium at $t = 0$, the mass flux at the boundary h_{BV} is tuned in time as

$$
\begin{aligned}
h_{BV}|_{(x=0)}\left(t\right) = h_{BV}|_{(x=l)}\left(t\right) &= \left(1 - e^{-10t}\right)\frac{I_{51.2C}}{F} \\
&= \left(1 - e^{-10t}\right) 5.306 \times 10^{-5} \mathrm{mol\,m^{-2}s^{-1}}
\end{aligned}
\tag{4.94}
$$

with t in seconds.

Initially (at $t = 0$) the system is in thermodynamic equilibrium and the concentration of ions in the electrolyte is uniform and corresponds to equation (4.79). Data have been taken according to [21], namely

$$\delta = 0.18\,, \quad c_{\mathrm{Li}}^{tot} = 6.01 \times 10^4\,\mathrm{mol\,m^{-3}}\,, \quad c_\alpha(\vec{x},0) = c_{bulk} = 10818\,\mathrm{mol\,m^{-3}} \quad \vec{x} \in V_e \tag{4.95}$$

Diffusivities amount at $D_{\mathrm{Li}^+} = 9 \times 10^{-16}\mathrm{m^2s^{-1}}$, $D_{\mathrm{X}^-} = 5.1 \times 10^{-15}\mathrm{m^2s^{-1}}$. Relative permittivity has been assumed as $\xi_r = 2.25$.

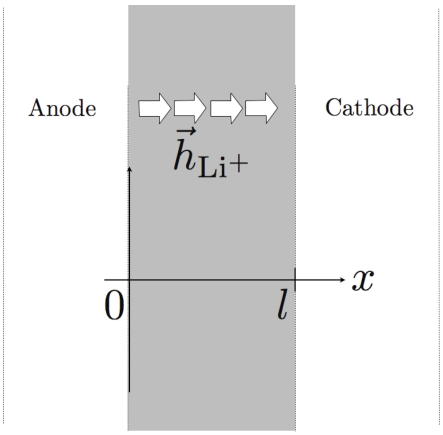

Figure 4.17: *A one-dimensional model of a Li-ion battery, with a* $1.5\mu m$ *thick* Li_3PO_4 *solid electrolyte layer highlighted in gray. The flux of* Li^+ *ions during discharge is pointed out.*

4.13.2 Discretization and time advancing by finite differences

It is convenient to derive a dimensionless expression for weak form (4.92). To this aim, fields that govern the problem are made quantity of dimension one - denoted with starred superscripts from now on - via suitable scaling factors, namely:

$$c_\alpha^* = \frac{c_\alpha}{c_{bulk}}, \qquad \phi_e^* = \frac{F}{RT}\,\phi_e, \qquad \vec{u}^* = \frac{\vec{u}}{L} \tag{4.96}$$

L standing for a given characteristic length.

Weak form (4.92) can be transformed in a first order Ordinary Differential Equation (ODE) in time if discretization is performed via separated variables, with spatial test $\varphi_i(x)$ and shape functions $\varphi_j(x)$ and nodal unknowns (collectively gathered in column y with component $y_j(t)$) that depend solely on time. For the sake of readability the star superscript is omitted from the definition of dimensionless quantities (4.96) and of c^{max}: for example, in this section $c_j^{\mathrm{Li}^+}$ stands for the j-th nodal unknown for Li-ions dimensionless concentration at time t. The usual Einstein convention of sum is taken henceforth: when an index variable appears twice in a single term it implies summation of that term over all the values of the index. The non linear ODE reads:

$$\text{Find } y(t) \text{ s.t.} \qquad b_i^* \cdot \dot{y}(t) + a_i^*[\, y(t)\,] = f_i^*(t) \qquad \text{for } i = 1, 2, ..., N \tag{4.97}$$

where

$$\begin{aligned}
\frac{b_i^* \cdot \dot{y}(t)}{RT\; c_{bulk}} &= -\int_0^l \varphi_i^{\mathrm{Li}^+}\, \varphi_j^{\mathrm{Li}^+}\, \mathrm{d}x\; \dot{c}_j^{\mathrm{Li}^+} - \int_0^l \varphi_i^{\mathrm{X}^-}\, \varphi_j^{\mathrm{X}^-}\, \mathrm{d}x\; \dot{c}_j^{\mathrm{X}^-} + \\
&\quad + \frac{\not{\epsilon}}{c_{bulk}}\, \frac{RT}{F^2} \int_0^l \frac{\partial \varphi_i^\phi}{\partial x}\, \frac{\partial \varphi_j^\phi}{\partial x}\, \mathrm{d}x\; \dot{\phi}_j \\
\frac{a_i^*[\, y(t)\,]}{RT\; c_{bulk}} &= -D_{\mathrm{Li}^+} \int_0^l \frac{\partial \varphi_i^{\mathrm{Li}^+}}{\partial x}\, \frac{\partial \varphi_j^{\mathrm{Li}^+}}{\partial x}\, \mathrm{d}x\; c_j^{\mathrm{Li}^+} + \\
&\quad - D_{\mathrm{Li}^+} \int_0^l \varphi_j^{\mathrm{Li}^+}\, \frac{\partial \varphi_i^{\mathrm{Li}^+}}{\partial x}\, \frac{\partial \varphi_k^\phi}{\partial x} \left(1 - 2\frac{\varphi_n^{\mathrm{Li}^+}\, c_n^{\mathrm{Li}^+}}{c^{max}}\right) \mathrm{d}x\; c_j^{\mathrm{Li}^+}\, \phi_k +
\end{aligned}$$

$$
\begin{aligned}
&- D_{\mathrm{X}^-} \int_0^l \frac{\partial \varphi_i^{\mathrm{X}^-}}{\partial x} \frac{\partial\, \varphi_j^{\mathrm{X}^-}}{\partial x} \,\mathrm{d}x\; c_j^{\mathrm{X}^-} \;+ \\
&+ D_{\mathrm{X}^-} \int_0^l \varphi_j^{\mathrm{X}^-} \frac{\partial \varphi_i^{\mathrm{X}^-}}{\partial x} \frac{\partial \varphi_k^{\phi}}{\partial x} \left(1 - 2\frac{\varphi_n^{\mathrm{X}^-}\, c_n^{\mathrm{X}^-}}{c^{max}}\right) \mathrm{d}x\; c_j^{\mathrm{X}^-}\, \phi_k \;+ \\
&- \mathrm{k_d} \int_{V_{el}} \varphi_i^{\mathrm{Li}^+} \varphi_j^{\mathrm{Li}^+} \,\mathrm{d}x\; c_j^{\mathrm{Li}^+} - \mathrm{k_r}\, c_{bulk} \int_{V_{el}} \varphi_i^{\mathrm{Li}^+}\, \varphi_j^{\mathrm{Li}^+}\, \varphi_n^{\mathrm{X}^-} \,\mathrm{d}x\; c_n^{\mathrm{X}^-}\; c_j^{\mathrm{Li}^+} \;+ \\
&- \mathrm{k_d} \int_{V_{el}} \varphi_i^{\mathrm{X}^-} \varphi_j^{\mathrm{Li}^+} \,\mathrm{d}x\; c_j^{\mathrm{Li}^+} - \mathrm{k_r}\, c_{bulk} \int_{V_{el}} \varphi_i^{\mathrm{X}^-}\, \varphi_j^{\mathrm{Li}^+}\, \varphi_n^{\mathrm{X}^-} \,\mathrm{d}x\; c_n^{\mathrm{X}^-}\; c_j^{\mathrm{Li}^+} + \\
&+ D_{\mathrm{Li}^+} \int_0^l \frac{\partial \varphi_i^{\phi}}{\partial x} \frac{\partial \varphi_k^{\phi}}{\partial x} \varphi_j^{\mathrm{Li}^+} \left(1 - 2\frac{\varphi_n^{\mathrm{Li}^+}\, c_n^{\mathrm{Li}^+}}{c^{max}}\right) \mathrm{d}x\; c_j^{\mathrm{Li}^+}\, \phi_k \;+ \\
&+ D_{\mathrm{Li}^+} \int_0^l \frac{\partial \varphi_i^{\phi}}{\partial x} \frac{\partial \varphi_j^{\mathrm{Li}^+}}{\partial x} \,\mathrm{d}x\; c_j^{\mathrm{Li}^+} \;+ \\
&+ D_{\mathrm{X}^-} \int_0^l \frac{\partial \varphi_i^{\phi}}{\partial x} \frac{\partial \varphi_k^{\phi}}{\partial x} \varphi_j^{\mathrm{X}^-} \left(1 - 2\frac{\varphi_n^{\mathrm{X}^-}\, c_n^{\mathrm{X}^-}}{c^{max}}\right) \mathrm{d}x\; c_j^{\mathrm{X}^-}\, \phi_k \;+ \\
&- D_{\mathrm{X}^-} \int_0^l \frac{\partial \varphi_i^{\phi}}{\partial x} \frac{\partial \varphi_j^{\mathrm{X}^-}}{\partial x} \,\mathrm{d}x\; c_j^{\mathrm{X}^-} \\
\frac{f_i^*(t)}{RT\; c_{bulk}} &= -\frac{\mathrm{k_d}}{c_{bulk}} \int_0^l \varphi_i^{\mathrm{Li}^+}\, c_{\mathrm{Li}}^{tot} \,\mathrm{d}V \;- \frac{\mathrm{k_d}}{c_{bulk}} \int_0^l \varphi_i^{\mathrm{X}^-}\, c_{\mathrm{Li}}^{tot} \,\mathrm{d}V \;+ \\
&+ \frac{1}{c_{bulk}} \left(\varphi_i^{\phi} - \varphi_i^{\mathrm{Li}^+}\right) h_{BV} \Big|_0^l
\end{aligned}
$$

Note that c_{Li}^{tot} and h_{BV} have not been scaled.

Form $a_i^*[\, y(t)\,]$ is clearly non linear. It can be split into the sum of a non linear form ${}^n a_i^*[\, y(t)\,]$, which reads

$$
\begin{aligned}
\frac{{}^n a_i^*[\, y(t)\,]}{RT\; c_{bulk}} &= - D_{\mathrm{Li}^+} \int_0^l \varphi_j^{\mathrm{Li}^+} \frac{\partial \varphi_i^{\mathrm{Li}^+}}{\partial x} \frac{\partial \varphi_k^{\phi}}{\partial x} \left(1 - 2\frac{\varphi_n^{\mathrm{Li}^+}\, c_n^{\mathrm{Li}^+}}{c^{max}}\right) \mathrm{d}x\; c_j^{\mathrm{Li}^+}\, \phi_k \;+ \\
&+ D_{\mathrm{X}^-} \int_0^l \varphi_j^{\mathrm{X}^-} \frac{\partial \varphi_i^{\mathrm{X}^-}}{\partial x} \frac{\partial \varphi_k^{\phi}}{\partial x} \left(1 - 2\frac{\varphi_n^{\mathrm{X}^-}\, c_n^{\mathrm{X}^-}}{c^{max}}\right) \mathrm{d}x\; c_j^{\mathrm{X}^-}\, \phi_k \;+ \\
&- \mathrm{k_r}\, c_{bulk} \int_{V_{el}} \varphi_i^{\mathrm{Li}^+}\, \varphi_j^{\mathrm{Li}^+}\, \varphi_n^{\mathrm{X}^-} \,\mathrm{d}x\; c_n^{\mathrm{X}^-}\; c_j^{\mathrm{Li}^+} \;+ \\
&- \mathrm{k_r}\, c_{bulk} \int_{V_{el}} \varphi_i^{\mathrm{X}^-}\, \varphi_j^{\mathrm{Li}^+}\, \varphi_n^{\mathrm{X}^-} \,\mathrm{d}x\; c_n^{\mathrm{X}^-}\; c_j^{\mathrm{Li}^+} + \\
&+ D_{\mathrm{Li}^+} \int_0^l \frac{\partial \varphi_i^{\phi}}{\partial x} \frac{\partial \varphi_k^{\phi}}{\partial x} \varphi_j^{\mathrm{Li}^+} \left(1 - 2\frac{\varphi_n^{\mathrm{Li}^+}\, c_n^{\mathrm{Li}^+}}{c^{max}}\right) \mathrm{d}x\; c_j^{\mathrm{Li}^+}\, \phi_k \;+ \\
&+ D_{\mathrm{X}^-} \int_0^l \frac{\partial \varphi_i^{\phi}}{\partial x} \frac{\partial \varphi_k^{\phi}}{\partial x} \varphi_j^{\mathrm{X}^-} \left(1 - 2\frac{\varphi_n^{\mathrm{X}^-}\, c_n^{\mathrm{X}^-}}{c^{max}}\right) \mathrm{d}x\; c_j^{\mathrm{X}^-}\, \phi_k
\end{aligned}
$$

and a bilinear counterpart ${}^l a_i^* \cdot y(t)$ defined by comparison.

Following the same procedure pursued in sections 4.6.2 and 4.6.3 a backward Euler time-advancing method as been set up. Both linearized update and Newton-Raphson iterative

schemes have been implemented to solve the numerical problem at hand. The two numerical techniques have been implemented in a Wolfram Mathematica package script, and provided the same solution up to the given accuracy threshold.

The same considerations raised in section 4.6.3 lead to the identification of six dimensionless groups that govern the condition number of the "stiffness" matrix, namely:

$$\frac{\Delta t\, D_{\mathrm{Li}^+}}{L^2}\,, \qquad \frac{\Delta t\, D_{\mathrm{X}^-}}{L^2}\,, \qquad \frac{\sharp}{c_{bulk}}\,\frac{RT}{F^2}\,\frac{1}{\Delta t\, D_{\mathrm{Li}^+}}$$
$$\frac{\sharp}{c_{bulk}}\,\frac{RT}{F^2}\,\frac{1}{\Delta t\, D_{\mathrm{X}^-}}\,, \qquad \mathrm{k_d}\,\Delta t\,, \qquad \frac{\mathrm{k_r}\, c_{bulk}}{\mathrm{k_d}}$$

where L is a characteristic length of the discretization, typically the element length for uniform mesh. The last two numbers are related to the Debye length r_D defined in (2.19). The parameters that govern stability are expected to be the following ratios

$$\gamma_{\mathrm{Li}^+} = \frac{\Delta t\, D_{\mathrm{Li}^+}}{L^2}\,, \qquad \gamma_{\mathrm{X}^-} = \frac{\Delta t\, D_{\mathrm{X}^-}}{L^2}\,, \qquad \gamma_\phi = \frac{r_D}{L}$$
$$\gamma_{\mathrm{d}} = \mathrm{k_d}\,\Delta t\,, \qquad \gamma_{\mathrm{r}} = \frac{\mathrm{k_r}\, c_{bulk}}{\mathrm{k_d}}$$

4.13.3 Simulations

Several simulations have been carried out with different time steps and number of elements. The outcomes here reported refer to 150 equal finite elements and a constant time step of 0.01 seconds, for which

$$\gamma_{\mathrm{Li}^+} = 0.09\,, \qquad \gamma_{\mathrm{X}^-} = 0.51\,, \qquad \gamma_\phi = 0.00156585\,,$$
$$\gamma_{\mathrm{d}} = 2.13721 \times 10^{-7}\,, \qquad \gamma_{\mathrm{r}} = 4.55556$$

Discharge/charge cycle

The test was carried out by imposing the following charge/discharge path:

$$I(t) = (1 - e^{-t})\, I_{51,2C} \times \begin{cases} 1 & \text{if } t \le 60 \text{ s} \\ 0 & \text{if } 60 < t \le 120 \text{ s} \\ -1 & \text{if } 120 < t \le 180 \text{ s} \\ 1 & \text{if } 180 < t \le 240 \text{ s} \\ 0 & \text{if } 240 < t \le 270 \text{ s} \end{cases} \tag{4.98}$$

with t in seconds. A current reversal have been imposed after 180s without relaxation, here identified by $I(t) = 0$. The simulation was ended at $t_f = 270$s.

Figure 4.18 represents both the mobile c_{Li^+} and the oxigen-binded c_{Li^0} Lithium distribution along the solid electrolyte domain, respectively fluctuating around the values $c_{bulk} = 10818\mathrm{molm}^{-3}$ and $c_{\mathrm{Li}}^{tot} - c_{bulk} = 49282\mathrm{molm}^{-3}$. All the steps of charge/discharge path (4.98) have been represented. From the picture it is apparent that c_{Li^+} and c_{Li^0} satisfy restriction (4.76).

Figure 4.18 also shows that a symmetric ionic concentration profile, with respect to the initial distribution, arose in the electrolyte during all the processes. The same behavior was observed from the outcomes of simulations concerning liquid electrolyte (refer to sections 4.6.4 and 4.10.2).

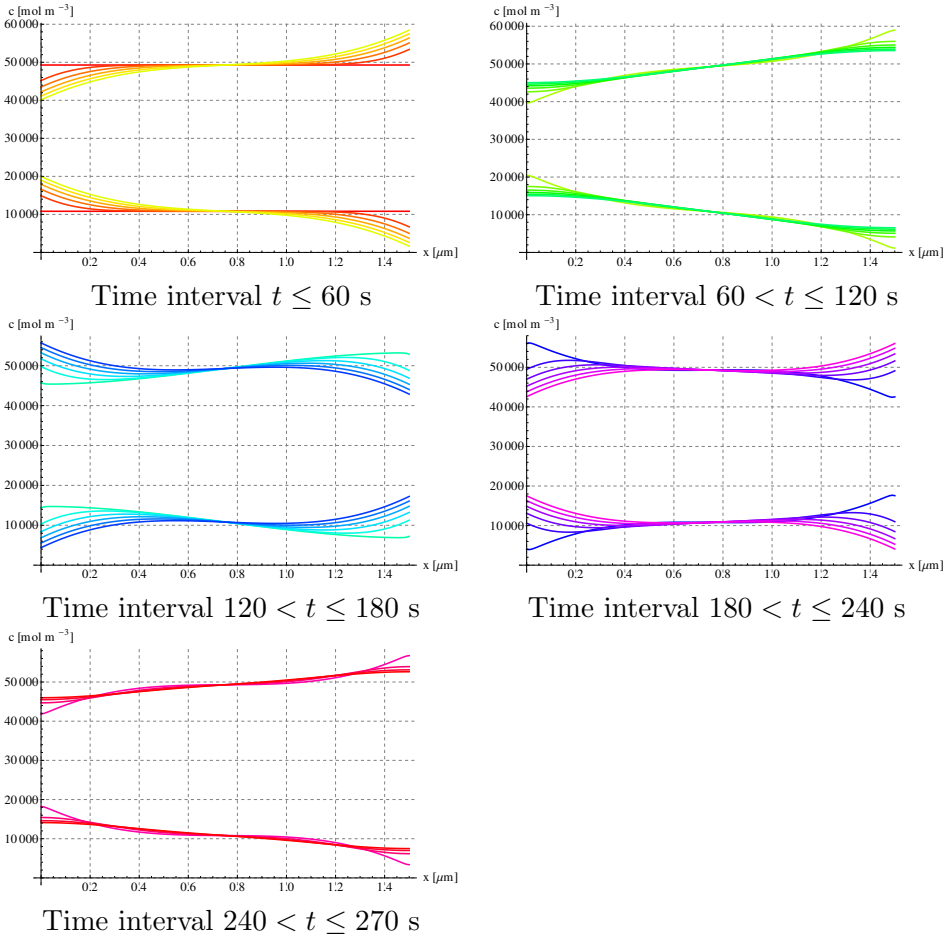

Figure 4.18: *Concentration distribution for mobile* c_{Li^+} *and oxigen-binded* c_{Li^0} *Lithium along the solid electrolyte.* c_{Li^+} *fluctuating around the value* $c_{bulk} = 10818\mathrm{molm}^{-3}$ *and* c_{Li^0} *fluctuating around the value* $c_{\mathrm{Li}}^{tot} - c_{bulk} = 49282\mathrm{molm}^{-3}$.

A good agreement is found between ionic distribution in the solid electrolyte during discharge at 51,2 C-rate, time interval $120 < t \leq 180$ s of Figure 4.18, and the results reported in *Danilov et al.* [21], Figure 12.

Concentration profiles at the anode (red) and cathode (green) are represented in Figure 4.19. Symmetry of the concentration profiles with respect to the bulk concentration $c_{bulk} = 10818\mathrm{molm}^{-3}$ is testified one more time.

As it was for the liquid electrolyte models (sections 4.6.4 and 4.10.2), an electroneutral regime is always established, as testified by Figure 4.20, being the difference among Li^+ and X^- concentrations about six order of magnitude smaller with respect to the initial value c_{bulk}.

4.13.4 Remarks: solid electrolyte

Also in the case of solid-state-electrolyte, the formulation adopted appears a reliable choice for modeling the processes driving the ionic conduction.
It is here anticipated that an all-solid-state battery will be the focus of chapter 6, inspired by [21], for which the formulation detailed from section 4.11 would be suitable. Nevertheless, due to lack of time, simulations have been carried therein using a liquid electrolyte. The

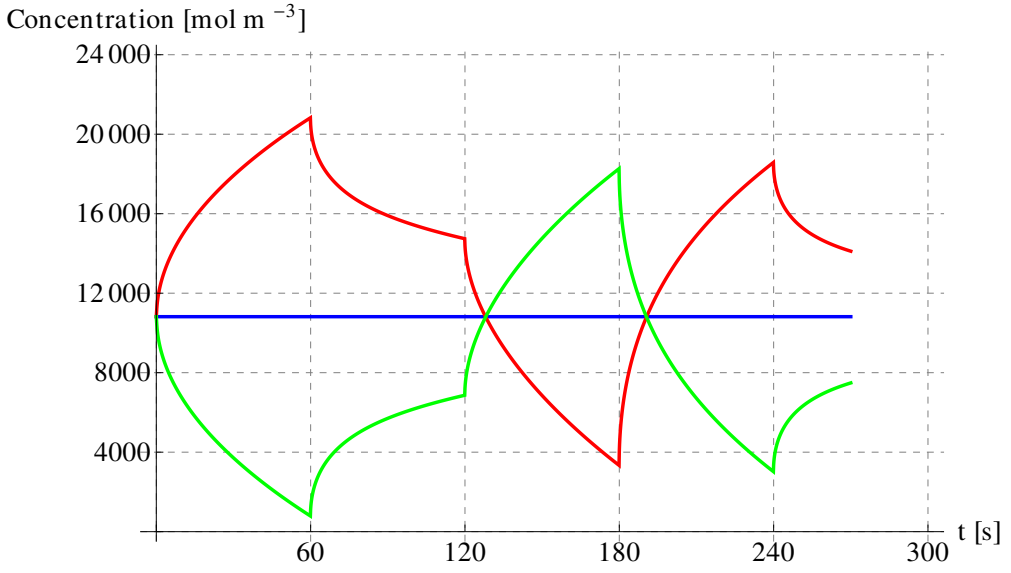

Figure 4.19: *Ionic concentration profile at anode (red) and cathode (green). The blue line refer to the initial concentration distribution.*

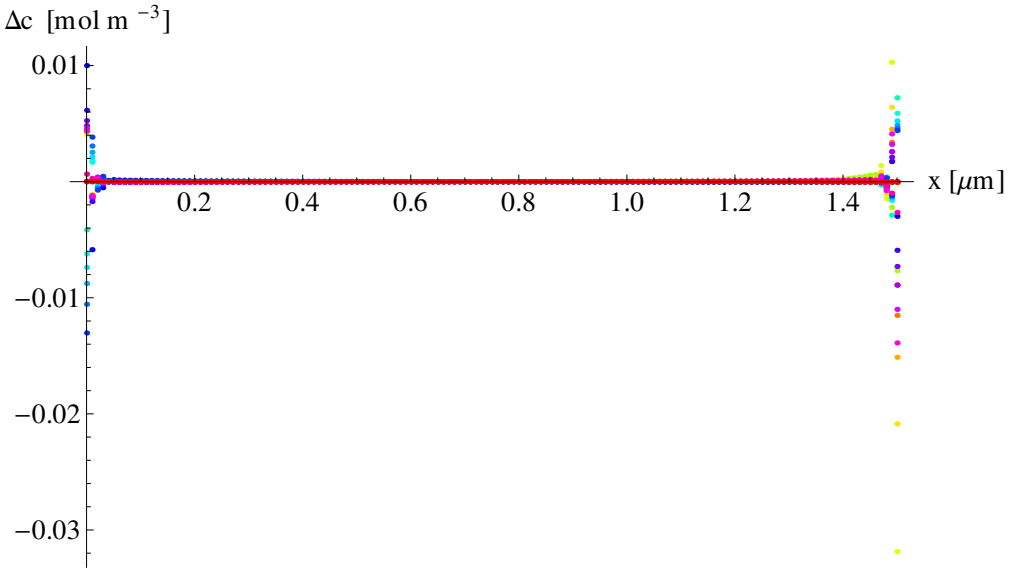

Figure 4.20: *Difference in concentration along the electrolyte between c_{Li^+} and c_{X^-} for a galvanostatic process at 52 C-rate.*

same numerical analysis will be replicated in the future by using a solid-state electrolyte model to guarantee more accurate comparison with the results in *Danilov et al.* [21].

4.14 Appendix: Moderately diluted solutions

In non ideal yet moderately diluted solutions it is assumed a linear dependency of the mass flux of species α upon the gradient of the electrochemical potential of the same species, as in (4.30), ignoring cross-effects.

The main advantage of the splitting

$$\overline{\mu}_\alpha = \mu_\alpha + F\, z_\alpha\, \phi \tag{4.99}$$

stands in its ability to characterize the electric state of a phase by means of an electric potential ϕ, that has the usual meaning of an electrostatic potential. According to Newman, see [6] section 3.5, to characterize the electrical state of a phase several definitions can be adopted for the electrical potential. In the simplest way, one assumes that a term $\psi_{dev}(c_\alpha)$ is added to the ideal free energy density for moderately diluted solutions:

$$\psi_{diff}(c_\alpha) = \psi^{id}_{diff}(c_\alpha) + \psi_{dev}(c_\alpha)$$

as in [6] section 3.5 formula (3.16). The contribution $\psi_{dev}(c_\alpha)$ expresses a deviation from ideality, in terms of the so called *ionic activity coefficient* f_α. Assuming as customary the following definition of activity coefficients:

$$\frac{\partial \psi_{dev}}{\partial c_\alpha} = RT \ln[f_\alpha]$$

easy algebra leads to the following expression for Fick's law:

$$\vec{h}_\alpha = -D_\alpha\, \nabla\,[\,c_\alpha\,] - z_\alpha\, F\, u_\alpha\, c_\alpha\, \left(1 - 2\frac{c_\alpha}{c^{max}}\right)\, \nabla\,[\,\phi\,] - D_\alpha\, c_\alpha\, \nabla\,[\ln[\,f_\alpha(c_\alpha)\,]\,] \tag{4.100}$$

that extends (4.62) to moderately diluted solutions. It is evident that it is the activity coefficient that expresses the deviation from ideality of the chemical interactions. A proper definition of the free energy ψ_{dev} can be given after the activity coefficients and their dependency upon the concentration are constitutively defined.

4.15 Appendix: Concentrated solutions

According to Ficks law (4.30) there is no influence of other phases on the flux of species α, i.e. cross-effects are ignored although they may appear in reality. To account for interactions between phases, the standard approach [137] within the theory of Irreversible Thermodynamics replaces Fickian fluxes by linear combinations of the gradients of all involved electrochemical potentials. In the case of binary electrodes:

$$\vec{h}_\alpha = -\sum_{\beta=1}^{2} \boldsymbol{M}_{\alpha\beta}(c_1, c_2)\, \nabla\left[\,\overline{\mu}_\beta\,\right] \qquad \alpha = 1, 2 \tag{4.101}$$

Mobility tensors $\boldsymbol{M}_{\alpha\beta}(c_1, c_2)$ on turn depend on the concentration of all phases. A classical specialization of such mobility tensors is an isotropic choice

$$\boldsymbol{M}_{\alpha\beta}(c_1, c_2) = M_{\alpha\beta}(c_1, c_2)\, c_\alpha\, \mathbb{1}$$

whereas linearity is not usually assumed for $M_{\alpha\beta}(c_1, c_2)$. The full matrix of mobility coefficients $M_{\alpha\beta}$ has to be positive semi-definite in order to be consistent with thermodynamic restriction (4.26) and symmetric due to the Onsager reciprocal relations. The approach that provides specifications for $M_{\alpha\beta}$ is usually known as Maxwell-Stefan approach [138].

4.16 Appendix: Implemented formulation for 2D electrolyte

The semi-discrete weak form for a liquid electrolyte (ideal solution model without the effect of saturation) outlined in section 4.6 is here extended to two dimensional case. Explicit expressions for the residual force vectors and consistent tangents for the Newton–Raphson iteration, inspired by [75], are listed below.

$$\begin{aligned} &K_{ab}^{\mathrm{Li}^+\,\mathrm{Li}^+}\,\delta c_{\mathrm{Li}^+}^b + K_{ab}^{\mathrm{Li}^+\,\phi_e}\,\delta\phi_e^b \;=\; R_a^{\mathrm{Li}^+} \\ &K_{ab}^{\mathrm{X}^-\,\mathrm{X}^-}\,\delta c_{\mathrm{X}^-}^b + K_{ab}^{\mathrm{X}^-\,\phi_e}\,\delta\phi_e^b \;=\; R_a^{\mathrm{X}^-} \\ &K_{ab}^{\phi_e\,\phi_e}\,\delta\phi_e^b + K_{ab}^{\phi_e\,\mathrm{Li}^+}\,\delta c_{\mathrm{Li}^+}^b + K_{ab}^{\phi_e\,\mathrm{X}^-}\,\delta c_{\mathrm{X}^-}^b \;=\; R_a^{\phi_e} \end{aligned} \tag{4.102}$$

In what follows, the variables within the integrals represent the values updated with the outcomes of the previous iteration, for example $c_{\mathrm{Li}^+}^b$ represent ${}^{\mathfrak{q}}c_{\mathrm{Li}^+}^b(t+\Delta t)$ according to formula (4.53). The usual Einstein summation convention is taken for repeated indexes i and apexes a, b.

$$\begin{aligned} R_a^{\mathrm{Li}^+} &= -\frac{1}{L}\int_V N^a\left(N^b\,c_{\mathrm{Li}^+}^b\right)\mathrm{d}V + \frac{\Delta t\,\mathbb{D}_{\mathrm{Li}^+}}{L^2}\int_V \frac{\partial N^a}{\partial x_i}\left(\frac{\partial N^b}{\partial x_i}c_{\mathrm{Li}^+}^b\right)\mathrm{d}V + \\ &+ \frac{\Delta t\,\mathbb{D}_{\mathrm{Li}^+}}{L^2}\int_V \frac{\partial N^a}{\partial x_i}\left(\frac{\partial N^d}{\partial x_i}\phi_e^d\right)\left(N^b c_{\mathrm{Li}^+}^b\right)\mathrm{d}V + \frac{\Delta t}{c_{bulk}\,L^2}\int_V N^a\,h_{BV}\,\mathrm{d}V \\ R_a^{\mathrm{X}^-} &= -\frac{1}{L}\int_V N^a\left(N^b\,c_{\mathrm{X}^-}^b\right)\mathrm{d}V + \frac{\Delta t\,\mathbb{D}_{\mathrm{X}^-}}{L^2}\int_V \frac{\partial N^a}{\partial x_i}\left(\frac{\partial N^b}{\partial x_i}c_{\mathrm{X}^-}^b\right)\mathrm{d}V + \\ &+ \frac{\Delta t\,\mathbb{D}_{\mathrm{X}^-}}{L^2}\int_V \frac{\partial N^a}{\partial x_i}\left(\frac{\partial N^d}{\partial x_i}\phi_e^d\right)\left(N^b c_{\mathrm{X}^-}^b\right)\mathrm{d}V \\ R_a^{\phi_e} &= -\frac{\mathfrak{f}\,RT}{c_{bulk}\,F^2\,L^2}\int_V \frac{\partial N^a}{\partial x_i}\left(\frac{\partial N^b}{\partial x_i}\phi_e^b\right)\mathrm{d}V + \\ &- \frac{\Delta t\,\mathbb{D}_{\mathrm{Li}^+}}{L^2}\int_V \frac{\partial N^a}{\partial x_i}\left(\frac{\partial N^b}{\partial x_i}c_{\mathrm{Li}^+}^b\right)\mathrm{d}V + \\ &+ \frac{\Delta t\,\mathbb{D}_{\mathrm{X}^-}}{L^2}\int_V \frac{\partial N^a}{\partial x_i}\left(\frac{\partial N^b}{\partial x_i}c_{\mathrm{X}^-}^b\right)\mathrm{d}V + \\ &- \frac{\Delta t\,\mathbb{D}_{\mathrm{Li}^+}}{L^2}\int_V \frac{\partial N^a}{\partial x_i}\left(\frac{\partial N^d}{\partial x_i}\phi_e^d\right)\left(N^b c_{\mathrm{Li}^+}^b\right)\mathrm{d}V \\ &- \frac{\Delta t\,\mathbb{D}_{\mathrm{X}^-}}{L^2}\int_V \frac{\partial N^a}{\partial x_i}\left(\frac{\partial N^d}{\partial x_i}\phi_e^d\right)\left(N^b c_{\mathrm{X}^-}^b\right)\mathrm{d}V \end{aligned}$$

$$\begin{aligned} K_{ab}^{\mathrm{Li}^+\,\mathrm{Li}^+} &= -\frac{1}{L}\int_V N^b N^a\mathrm{d}V - \frac{\Delta t\,\mathbb{D}_{\mathrm{Li}^+}}{L^2}\int_V \frac{\partial N^b}{\partial x_i}\frac{\partial N^a}{\partial x_i}\,\mathrm{d}V + \\ &- \frac{\Delta t\,\mathbb{D}_{\mathrm{Li}^+}}{L^2}\int_V \frac{\partial N^a}{\partial x_i}\left(\frac{\partial N^b}{\partial x_i}\,\phi_e^b\right)N^d\,\mathrm{d}V \\ K_{ab}^{\mathrm{Li}^+\,\phi_e} &= -\frac{\Delta t\,\mathbb{D}_{\mathrm{Li}^+}}{L^2}\int_V \frac{\partial N^b}{\partial x_i}\frac{\partial N^a}{\partial x_i}\,\left(N^d\,c_{\mathrm{Li}^+}^d\right)\mathrm{d}V \\ K_{ab}^{\mathrm{X}^-\,\mathrm{X}^-} &= -\frac{1}{L}\int_V N^b N^a\mathrm{d}V - \frac{\Delta t\,\mathbb{D}_{\mathrm{X}^-}}{L^2}\int_V \frac{\partial N^b}{\partial x_i}\frac{\partial N^a}{\partial x_i}\,\mathrm{d}V + \end{aligned}$$

$$
\begin{aligned}
&- \frac{\Delta t\, \mathbb{D}_{\mathrm{X}^-}}{L^2} \int_V \frac{\partial N^a}{\partial x_i} \left(\frac{\partial N^b}{\partial x_i}\, \phi_e^b \right) N^d \, \mathrm{d}V \\
K_{ab}^{\mathrm{X}^- \phi_e} &= - \frac{\Delta t\, \mathbb{D}_{\mathrm{X}^-}}{L^2} \int_V \frac{\partial N^b}{\partial x_i} \frac{\partial N^a}{\partial x_i} \left(N^d\, c_{\mathrm{X}^-}^d \right) \mathrm{d}V \\
K_{ab}^{\phi_e \phi_e} &= \frac{\mathbb{F}\, RT}{c_{bulk}\, F^2\, L^2} \int_V \frac{\partial N^b}{\partial x_i} \frac{\partial N^a}{\partial x_i} \, \mathrm{d}V \\
&+ \frac{\Delta t\, \mathbb{D}_{\mathrm{Li}^+}}{L^2} \int_V \frac{\partial N^b}{\partial x_i} \frac{\partial N^a}{\partial x_i} \left(N^d\, c_{\mathrm{Li}^+}^d \right) \mathrm{d}V \\
&+ \frac{\Delta t\, \mathbb{D}_{\mathrm{X}^-}}{L^2} \int_V \frac{\partial N^b}{\partial x_i} \frac{\partial N^a}{\partial x_i} \left(N^d\, c_{\mathrm{X}^-}^d \right) \mathrm{d}V \\
K_{ab}^{\phi_e\, \mathrm{Li}^+} &= \frac{\Delta t\, \mathbb{D}_{\mathrm{Li}^+}}{L^2} \int_V \frac{\partial N^b}{\partial x_i} \frac{\partial N^a}{\partial x_i} \, \mathrm{d}V \\
&+ \frac{\Delta t\, \mathbb{D}_{\mathrm{Li}^+}}{L^2} \int_V \frac{\partial N^a}{\partial x_i} \left(\frac{\partial N^b}{\partial x_i}\, \phi_e^b \right) N^d \, \mathrm{d}V \\
K_{ab}^{\phi_e\, \mathrm{X}^-} &= - \frac{\Delta t\, \mathbb{D}_{\mathrm{X}^-}}{L^2} \int_V \frac{\partial N^b}{\partial x_i} \frac{\partial N^a}{\partial x_i} \, \mathrm{d}V \\
&+ \frac{\Delta t\, \mathbb{D}_{\mathrm{X}^-}}{L^2} \int_V \frac{\partial N^a}{\partial x_i} \left(\frac{\partial N^b}{\partial x_i}\, \phi_e^b \right) N^d \, \mathrm{d}V
\end{aligned}
$$

4.17 Appendix: Steady state solutions

The porous electrode theory developed by Newman and coworkers [6] stems from the mass balance equation (4.2a,b) and from electroneutrality condition

$$c_{\mathrm{Li}^+} = c_{\mathrm{X}^-} = c$$

It has been indeed an easy exercise to derive equation (4.72,) which is independent upon the electric potential even in the case of saturation modeled via Fick's law (4.62). At steady state, the laplacian vanishes thus leading to a linear form $c_\infty(x) = ax + b$ for the concentration in 1D problems. The two parameters a and b can be determined by imposing the galvanostatic flux h_{1C} at $x = 0$ and by imposing the mass conservation through time, namely

$$\int_0^l c(x,t)\mathrm{d}x = \int_0^l c(x,0)\mathrm{d}x$$

that at steady state leads to

$$a\frac{l^2}{2} + b\, l = c_{bulk}\, l$$

and finally to the steady state concentration

$$c_\infty(x) = c_{bulk} - \frac{h_{1C}}{2D_{\mathrm{LI}^+}}(x - \frac{l}{2}) \tag{4.105}$$

Steady state solution is useful to envisage the role played by the non linear mobility tensor and by the free energy density at saturation in modeling Fick's law (4.62). If one, for instance, takes the linear isotropic mobility tensor

$$\boldsymbol{M}_\alpha(c_\alpha) = u_\alpha\, c_\alpha\, \mathbb{1} \tag{4.106}$$

together with the ideal solution model (4.60), mass balance equation (4.72) restates in 1D as:

$$(u_{\mathrm{X}^-} + u_{\mathrm{Li}^+})\frac{\partial c}{\partial t} - 2RT\, u_{\mathrm{X}^-}\, u_{\mathrm{Li}^+}\ \left\{ f(c)\ \Delta\left[c\right] + f'(c)\left(c'(x)\right)^2 \right\} = 0 \tag{4.107}$$

having defined

$$f(c) = 1 + \frac{c}{c^{max}} \frac{2}{1 - 2\frac{c}{c^{max}}}$$

At steady state, one is left with the non linear ordinary differential equation

$$f(c)\ \Delta\left[c\right] + f'(c)\left(c'(x)\right)^2 = 0$$

which admits the following solution:

$$c_\infty(x) = \frac{e^{2a(b+x)} + a\ c^{max}}{2a}$$

with parameters a and b to be evaluated again by imposing the galvanostatic flux h_{1C} at $x = 0$ and by imposing the mass conservation through time. The effect of the saturation within the free energy density is clearly envisaged in figure 4.21. It corresponds to a higher diffusivity, in turn dependent upon the concentration, which favors the diffusion into the electrolyte and decreases both the concentration at the electrodes and the concentration gradient within the electrolyte. On the contrary, the non linear isotropic mobility tensor itself causes a decrease of the diffusivity, with opposite effects. Indeed, they cancel out in the final Fick's law (4.62).

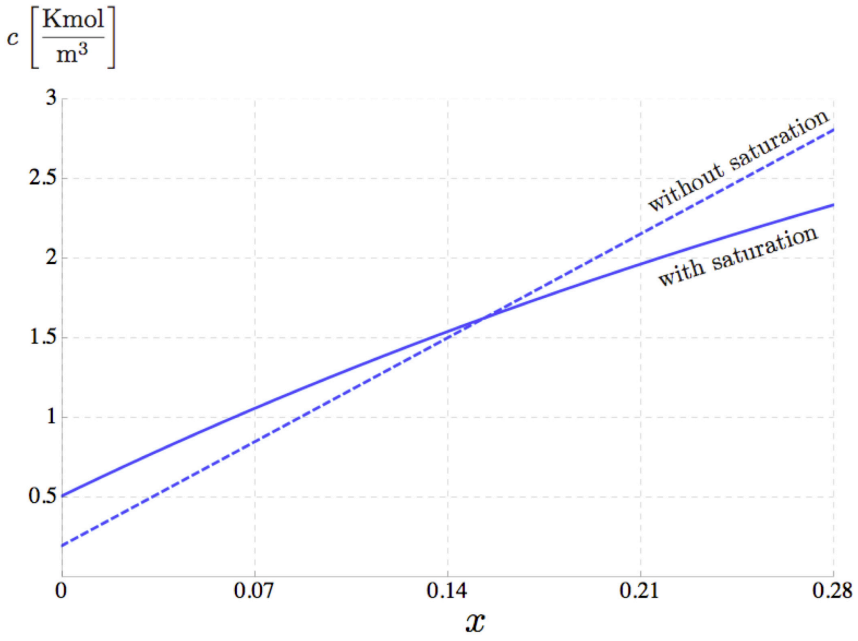

Figure 4.21: *The effect of the saturation within the free energy density resolves in favoring the diffusion into the electrolyte and decreasing both the deployment of concentration at the electrodes and the concentration gradient.*

Chapter 5
Active material formulation

To validate the modeling of electro-chemo-mechanical interaction in the electrodes is the purpose of the present chapter[1]. Thermodynamical coupling arise between neutral Lithium diffusion and stress distribution. Time independent Ohm's law govern the electric potential distribution in the electrodes, under the assumption they are perfect conductive materials.

Active particles embedded in lithium batteries composite electrodes will be investigated. Conductive particles and binders (refer to chapter 3) will not be detailed in this thesis.

General principles of non-equilibrium thermodynamics are presented in section 5.3 following the approach of [16, 17]. The chemical potential is defined based on the rate at which power is expended on a material region, including mechanical contributions as well as the power due to mass transport and electromagnetic interactions. All processes are taken to be isothermal. The entropy imbalance with the Coleman-Noll procedure provides thermodynamic restrictions, satisfied by the usual Fickian description of diffusion in terms of the chemical potential.

Hydrogen diffusion modeling is also considered in the present chapter. Similarities with the item of neutral Lithium diffusion in the electrodes arise for the balance equations involved and the constitutive theory selected.

A two-dimensional model of mass transport within a solid material have been numerically simulated. The analytical solutions both in terms of concentrations and displacements are recovered, showing the robustness of the approach.

5.1 Balance equations: active material

One *mass balance* equation is required to model the transport of neutral Li in the active materials. The following is selected:

$$\frac{\partial c_{\mathrm{Li}}}{\partial t} + \operatorname{div}\left[\vec{h}_{\mathrm{Li}}\right] = 0 \qquad \vec{x} \in V_a \tag{5.1a}$$

The lithiation mechanism in active materials is extremely complex and the selection of the mass balance equation reflects the modeling assumptions. In the equation above, no mass supply due to chemical reactions in the bulk of the active materials appears. This view is shared with several approaches (to quote but a few: [139–141]). Perhaps though the model that intrigues Authors the most [80] considers that part of the neutral Li flowing into the electrodes becomes immobilized, making alloys with the hosting atoms in the lattice and transforming the crystal structure into an amorphous phase. The proper model for this

[1] This chapter extends contents of [130]

process is in fact adopted from hydrogen embrittlement [82, 142] and considers a mass supply that corresponds to the Lithium that looses its mobility. As the target of the present thesis is to present a whole cell paradigm based on an alternative model for electroneutrality, which is well suited to welcome mutliphysics contributions within a rigorous multiscale technique, a simple model for lithiation is consciously taken via equation (5.1a).
Some insight on Hydrogen transport within a solid material will be also given in sections 5.6 and 5.7.

Although alternative descriptions have been proposed [121], the electron flow in electrodes is here modeled by Ohm's law as in several publications ([28, 48, 50, 143]).

$$\operatorname{div}\left[\,\vec{i}_{\mathrm{e}^-}\,\right] = 0 \qquad \vec{x} \in V_a \tag{5.1b}$$

with $\vec{i}_{\mathrm{e}^-}$ denoting the electric current in the electrodes.

The balance of forces is taken as homogeneous,

$$\begin{aligned} \operatorname{div}[\,\boldsymbol{\sigma}\,] &= \vec{0} \qquad \vec{x} \in V_a \\ \operatorname{skw}[\,\boldsymbol{\sigma}\,] &= \mathbf{0} \qquad \vec{x} \in V_a \end{aligned} \tag{5.1c}$$

The restriction $\vec{x} \in V_a$ emphasize that equations (5.1) refer to active material only, according to 3.2.1. A description of conductive particles (occupying V_c, section 3.2.1) would require the removal of equation (5.1a) from the set of balance equations, but it will not be carried out in this work.

5.2 Weak form and boundary conditions

The weak formulation of the mass balance equation (5.1a) can be achieved following the same path of reasoning used for the electrolyte in 4.2. It comes out

$$\begin{aligned} &\int_{V_a} \hat{\mu}_{\mathrm{Li}} \left\{ \frac{\partial c_{\mathrm{Li}}}{\partial t} + \operatorname{div}\left[\,\vec{h}_{\mathrm{Li}}\,\right] \right\} \mathrm{d}V = \\ &\quad = \int_{V_a} \hat{\mu}_{\mathrm{Li}} \, \frac{\partial c_{\mathrm{Li}}}{\partial t} \, \mathrm{d}V - \int_{V_a} \nabla\left[\,\hat{\mu}_{\mathrm{Li}}\,\right] \cdot \vec{h}_{\mathrm{Li}} \, \mathrm{d}V + \int_{\partial V_a} \hat{\mu}_{\mathrm{Li}} \, \vec{h}_{\mathrm{Li}} \cdot \vec{n} \, \mathrm{d}\Gamma = 0 \end{aligned} \tag{5.2}$$

The boundary of the electrode[2] is the union of the interface Γ_{BV}, of the Neumann part ∂V_a^N, and of the Dirichlet part ∂V_a^D. The mass flux across the interface satisfies the following condition:

$$\vec{h}_{\mathrm{Li}} \cdot \vec{n}_a = h_{BV} \qquad \vec{x} \in \Gamma_{BV} \tag{5.3}$$

where $\Gamma_{BV} \subseteq \partial V_a^N$ represents the location where oxidation/reduction reaction takes place. No Lithium flows across the remaining boundaries

$$\vec{h}_{\mathrm{Li}} \cdot \vec{n} = 0 \qquad \vec{x} \in \partial V_a^N \setminus \Gamma_{BV} \tag{5.4}$$

[2]The splitting of the boundary in Dirichlet and Neumann parts applies to each field separately. The Neumann part where tractions are imposed is generally different from the Neumann part where fluxes are given. As for 4.2, it is just to simplify the notation that it is assumed here that the Dirichlet and Neumann parts are one and the same for all fields. The extension to separated boundaries is just a useful yet boring exercise.

With a similar path of reasoning one deals with balance law (5.1b)

$$\int_{V_a} \hat{\phi}_s \operatorname{div}\left[\vec{i}_{\mathrm{e}^-}\right] \mathrm{d}V \;=\; -\int_{V_a} \nabla\left[\hat{\phi}_s\right] \cdot \vec{i}_{\mathrm{e}^-}\, \mathrm{d}V + \int_{\partial V_a} \hat{\phi}_s\, \vec{i}_{\mathrm{e}^-} \cdot \vec{n}\, \mathrm{d}\Gamma = 0$$

The usage of ϕ_s for the identification of the electric potential is consistent with section 3.2, in which the subscript $_s$ was used for any solid component of the porous electrode.

The current density at the interface satisfies the following boundary condition:

$$\vec{i}_{\mathrm{e}^-} \cdot \vec{n} = i_{BV} \qquad \vec{x} \in \Gamma_{BV} \tag{5.5}$$

Current density i_{BV} and mass flux h_{BV} have been studied in detail and related constitutively, formula 3.13. Across the remaining part of the Neumann boundaries the current flux is generally given

$$\vec{i}_{\mathrm{e}^-} \cdot \vec{n} = \overline{i_{\mathrm{e}^-}} \qquad \vec{x} \in \partial^N V_a \setminus \Gamma_{BV} \tag{5.6}$$

and a Dirichlet boundary condition that sets the location of the zero of the electric potential is mandatory to the problem definite.

Finally, for the equilibrium equations (5.1c) in rate form, one simply rewrites (4.9) with respect to V_a

$$\int_{V_a} \vec{\hat{u}} \cdot \operatorname{div}\left[\frac{\partial \boldsymbol{\sigma}}{\partial t}\right] \mathrm{d}V \;=\; -\int_{V_a} \hat{\boldsymbol{\varepsilon}} : \frac{\partial \boldsymbol{\sigma}}{\partial t}\, \mathrm{d}V + \int_{\partial V_a} \vec{\hat{u}} \cdot \frac{\partial \boldsymbol{\sigma}}{\partial t} \cdot \vec{n}\, \mathrm{d}\Gamma = 0 \tag{5.7}$$

Tractions-type boundary conditions are given along $\partial^N V_a$ and displacements are imposed on the Dirichlet part $\partial^D V_a$.

$$\boldsymbol{\sigma} \cdot \vec{n} = \vec{\overline{p}} \qquad \vec{x} \in \partial^N V_a \tag{5.8a}$$

$$\vec{u} = \vec{\overline{u}} \qquad \vec{x} \in \partial^D V_a \tag{5.8b}$$

In conclusion, a weak form can be given in a time interval $[0, t_f]$ as:

$$\text{Find } y \in \mathcal{V}^{[0,t_f]} \text{ such that } \frac{\mathrm{d}}{\mathrm{d}t}\, b\left(\hat{y}, z(t)\right) + a(\hat{y}, y(t)) = f(\hat{y}) \quad \forall \hat{y} \in \mathcal{V} \tag{5.9}$$

where

$$\begin{aligned}
b\left(\hat{y}, z\right) &= -\int_{V_a} \hat{\mu}_{\mathrm{Li}}\, c_{\mathrm{Li}}\, \mathrm{d}V + \int_{V_a} \hat{\boldsymbol{\varepsilon}} : \boldsymbol{\sigma}\, \mathrm{d}V \\
a\left(\hat{y}, y\right) &= \int_{V_a} \nabla\left[\hat{\mu}_{\mathrm{Li}}\right] \cdot \vec{h}_{\mathrm{Li}}\, \mathrm{d}V - \int_{V_a} \nabla\left[\hat{\phi}_s\right] \cdot \vec{i}_{\mathrm{e}^-}\, \mathrm{d}V \\
f\left(\hat{y}\right) &= \int_{\Gamma_{BV}} \hat{\mu}_{\mathrm{Li}}\, h_{BV}\, \mathrm{d}\Gamma - \int_{\Gamma_{BV}} \hat{\phi}_s\, i_{BV}\, \mathrm{d}\Gamma - \int_{\partial V_a^N \setminus \Gamma_{BV}} \hat{\phi}_s\, \overline{\vec{i}_{\mathrm{e}^-}}\, \mathrm{d}\Gamma \\
&+ \int_{\partial V_a^N} \vec{\hat{u}} \cdot \frac{\partial \vec{\overline{p}}}{\partial t}\, \mathrm{d}\Gamma
\end{aligned}$$

with $z = \{c_{\mathrm{Li}}\}$, $y = \{\mu_{\mathrm{Li}}, \phi_s, \vec{u}\}$. The right hand side $f\left(\hat{y}\right)$ is a functional on $\mathcal{V}^{[0,t_f]}$ that accounts for non-homogeneous Neumann boundary conditions.

Weak form (5.9) entails the physical meaning of power expenditure, which will be kept also in the weak form of the governing equations, after the specification of the constitutive equations.

5.3 Thermodynamics: active material

5.3.1 Energy balance

The energy balance (4.12) detailed for the electrolyte applies with slight modifications to the electrodes as well. Material region $\mathcal{P}$ now refers to active materials within the electrodes, and as such it still experiments the interactions energetically described by equations (4.13). Power $\mathcal{T}(\mathcal{P})$ is due to mass transfer of neutral Lithium, that is either oxidized or reduced at the interface Γ_{BV} before intercalation. Power due to electromagnetic interactions $\mathcal{E}(\mathcal{P})$ is due to electrons flow in the actve particles, assumed to be conductive materials. The main difference therefore is the separation between transport of mass and transport of charges, that take place with two different carriers. Equation (4.14c) refers to a single species

$$\mathcal{T}(\mathcal{P}) \;=\; \int_{\mathcal{P}} \mu_{\mathrm{Li}} \frac{\partial c_{\mathrm{Li}}}{\partial t} - \vec{h}_{\mathrm{Li}} \cdot \nabla\left[\,\mu_{\mathrm{Li}}\,\right] \mathrm{d}\Omega \tag{5.10a}$$

and Ampère's-Maxwell's law (4.16) simplifies as

$$\mathcal{E}(\mathcal{P}) = \int_{\mathcal{P}} \vec{i} \cdot \vec{E}\, \mathrm{d}\Omega \tag{5.11}$$

finally leading to the following local form of the first principle

$$\frac{\partial u}{\partial t} = \boldsymbol{\sigma} : \frac{\partial \boldsymbol{\varepsilon}}{\partial t} + s_q - \mathrm{div}\left[\,\vec{q}\,\right] + \vec{i} \cdot \vec{E} + \mu_{\mathrm{Li}} \frac{\partial c_{\mathrm{Li}}}{\partial t} - \vec{h}_{\mathrm{Li}} \cdot \nabla\left[\,\mu_{\mathrm{Li}}\,\right] \tag{5.12}$$

5.3.2 Additive decomposition of strains

As customary, the total strain $\boldsymbol{\varepsilon}$ will be additively decomposed in three contributions: an elastic recoverable part after unloading $\boldsymbol{\varepsilon}^{el}$, a swelling contribution due to the intercalation of Lithium in the hosting material $\boldsymbol{\varepsilon}^{s}$ and a distortion, usually of plastic nature $\boldsymbol{\varepsilon}^{p}$:

$$\boldsymbol{\varepsilon} = \frac{1}{2}\left(\nabla\left[\,\vec{u}\,\right] + \nabla\left[\,\vec{u}\,\right]^{T}\right) \tag{5.13a}$$

$$\boldsymbol{\varepsilon} = \boldsymbol{\varepsilon}^{el} + \boldsymbol{\varepsilon}^{s} + \boldsymbol{\varepsilon}^{p} \tag{5.13b}$$

The swelling contribution is taken as proportional to the concentration, by means of factors ω_{Li} termed chemical expansion coefficients of Lithium in the host material, which equal one third of the partial molar volumes of Lithium in the host material at a given temperature:

$$\boldsymbol{\varepsilon}^{s} = \omega_{\mathrm{Li}}\, c_{\mathrm{Li}}\, \mathbb{1} \tag{5.14}$$

denoting with $\mathbb{1}$ the identity matrix.

5.3.3 Entropy imbalance

As for equation (4.23), entropy imbalance may be derived in its local form as usual from energy balance (5.12):

$$\begin{aligned} T\frac{\partial \eta}{\partial t} - \Bigg\{ \frac{\partial u}{\partial t} - \boldsymbol{\sigma} : \left(\frac{\partial \boldsymbol{\varepsilon}^{el}}{\partial t} + \frac{\partial \boldsymbol{\varepsilon}^{p}}{\partial t}\right) - \omega_{\mathrm{Li}} \frac{\partial c_{\mathrm{Li}}}{\partial t}\,\mathrm{tr}\left[\,\boldsymbol{\sigma}\,\right] - \vec{i} \cdot \vec{E} + \\ - \mu_{\mathrm{Li}} \frac{\partial c_{\mathrm{Li}}}{\partial t} - \vec{h}_{\mathrm{Li}} \cdot \nabla\left[\,\mu_{\mathrm{Li}}\,\right] \Bigg\} - \frac{1}{T}\,\vec{q} \cdot \nabla\left[\,T\,\right] \geq 0 \end{aligned} \tag{5.15}$$

in view of definition (5.14).

Thermodynamic prescriptions will be expressed in terms of the Helmholtz free energy $\psi() = u() - T\,\eta$ rather than internal energy u. The selection of the free energy density reflects the assumptions made to model lithiation mechanism in electrodes. In the model proposed in [80], for instance, it is necessary to split the Lithium concentration in the mobile and immobilized parts, and for each of them a proper free energy density contribution has to be defined. As already remarked in section 5.1 a simple model for lithiation is consciously taken.

Collect in vector $\vec{\xi}$ a set of internal variables that account for the past history [144]. The Helmholtz free energy per unit volume is selected as follows:

$$\psi(T, c_{\mathrm{Li}}, \boldsymbol{\varepsilon}^{el}, \vec{\xi}) = \psi_{temp}(T) + \psi_{diff}(c_{\mathrm{Li}}) + \psi_{mech}(c_{\mathrm{Li}}, \boldsymbol{\varepsilon}^{el}, \vec{\xi}) \tag{5.16}$$

with the mechanical free energy density that is further split in an elastic and in an inelastic part following [145]

$$\psi_{mech}(c_{\mathrm{Li}}, \boldsymbol{\varepsilon}^{el}, \vec{\xi}) = \psi^{el}_{mech}(c_{\mathrm{Li}}, \boldsymbol{\varepsilon}^{el}) + \psi^{p}_{mech}(\vec{\xi}) \tag{5.17}$$

It finally holds

$$\begin{aligned} &\frac{\partial \psi(T, c_{\mathrm{Li}}, \boldsymbol{\varepsilon}^{el}, \vec{\xi})}{\partial t} = \\ &\frac{\partial \psi_{temp}}{\partial T}\frac{\partial T}{\partial t} + \left(\frac{\partial \psi_{diff}}{\partial c_{\mathrm{Li}}} + \frac{\partial \psi^{el}_{mech}}{\partial c_{\mathrm{Li}}}\right)\frac{\partial c_{\mathrm{Li}}}{\partial t} + \frac{\partial \psi^{el}_{mech}}{\partial \boldsymbol{\varepsilon}^{el}} : \frac{\partial \boldsymbol{\varepsilon}^{el}}{\partial t} + \frac{\partial \psi^{p}_{mech}}{\partial \vec{\xi}} \cdot \frac{\partial \vec{\xi}}{\partial t} \end{aligned} \tag{5.18}$$

By means of (5.18), the entropy imbalance yields:

$$\begin{aligned} &-\left(\eta + \frac{\partial \psi}{\partial T}\right)\frac{\partial T}{\partial t} + \left(\boldsymbol{\sigma} - \frac{\partial \psi^{el}_{mech}}{\partial \boldsymbol{\varepsilon}^{el}}\right) : \frac{\partial \boldsymbol{\varepsilon}^{el}}{\partial t} + \\ &+ \left(\mu_{\mathrm{Li}} + \omega_{\mathrm{Li}}\,\mathrm{tr}\,[\,\boldsymbol{\sigma}\,] - \frac{\partial \psi_{diff}}{\partial c_{\mathrm{Li}}} - \frac{\partial \psi^{el}_{mech}}{\partial c_{\mathrm{Li}}}\right)\frac{\partial c_{\mathrm{Li}}}{\partial t} + \qquad (5.19) \\ &+ \vec{i} \cdot \vec{E} - \vec{h}_{\mathrm{Li}} \cdot \nabla\,[\,\mu_{\mathrm{Li}}\,] - \frac{1}{T}\,\vec{q} \cdot \nabla\,[\,T\,] + \boldsymbol{\sigma} : \frac{\partial \boldsymbol{\varepsilon}^{p}}{\partial t} - \frac{\partial \psi^{p}_{mech}}{\partial \vec{\xi}} \cdot \frac{\partial \vec{\xi}}{\partial t} \geq 0 \qquad (5.20) \end{aligned}$$

After applying the Coleman-Noll procedure, the following thermodynamic prescriptions come out taking into account of assumption (2.13):

$$\begin{aligned} &\eta + \frac{\partial \psi_{temp}}{\partial T} = 0\,, \qquad \boldsymbol{\sigma} - \frac{\partial \psi^{el}_{mech}}{\partial \boldsymbol{\varepsilon}^{el}} = 0\,, \qquad \mu_{\mathrm{Li}} + \omega_{\mathrm{Li}}\,\mathrm{tr}\,[\,\boldsymbol{\sigma}\,] - \frac{\partial \psi_{diff}}{\partial c_{\mathrm{Li}}} - \frac{\partial \psi^{el}_{mech}}{\partial c_{\mathrm{Li}}} = 0\,, \\ &\vec{i} \cdot \nabla\,[\,\phi\,] \leq 0\,, \quad \vec{h}_{\mathrm{Li}} \cdot \nabla\,[\,\mu_{\mathrm{Li}}\,] \leq 0\,, \quad \vec{q} \cdot \nabla\,[\,T\,] \leq 0\,, \quad \boldsymbol{\sigma} : \frac{\partial \boldsymbol{\varepsilon}^{p}}{\partial t} + \vec{\chi} \cdot \frac{\partial \vec{\xi}}{\partial t} \geq 0 \end{aligned} \tag{5.21}$$

where

$$\vec{\chi} = -\frac{\partial \psi^{p}_{mech}}{\partial \vec{\xi}} \tag{5.22}$$

is the thermodynamic force vector conjugated to internal variables $\vec{\xi}$.

5.4 Constitutive theory: active material

The constitutive specifications outlined in this section bestow no novelties with respect to the up-to-date literature on the field. Remarkable advances have been brought forth by recent investigations [55, 58, 67, 73, 75–77] on the constitutive behavior of energy storage materials, with respect to which some assumptions are here consciously taken as simplistic. More elaborated prescriptions will be considered in the future.

Guided by Joule effect in restriction (5.21) a linear law is set as usual for the electron flow, by means of a material property termed conductivity $\kappa > 0$.

$$\vec{i} = \kappa\, \vec{E} = -\kappa\, \nabla\, [\, \phi\,] \tag{5.23}$$

Restriction (5.21) is satisfied by a linear Fickian-diffusion law, which is drew up for the Lithium diffusion in the electrodes by means of a positive definite mobility tensor $\boldsymbol{M}_{\mathrm{Li}}$

$$\vec{h}_{\mathrm{Li}} = -\boldsymbol{M}_{\mathrm{Li}}\, \nabla\, [\, \mu_{\mathrm{Li}}\,] \tag{5.24}$$

In the presence of high C-rates, which are indeed expected in real batteries or super capacitors, the Lithium concentration in the electrodes is often locally high. Recourse to saturation specialization of mobility tensor $\boldsymbol{M}_{\mathrm{Li}}$ is mandatory, in the still isotropic yet non linear form $\boldsymbol{M}_{\mathrm{Li}}(c_{\mathrm{Li}}) = \Psi_{\mathrm{Li}}\, \mathsf{M}_{\mathrm{Li}}(c_{\mathrm{Li}})\, \mathbb{1}$, with

$$\mathsf{M}_{\mathrm{Li}}(c_{\mathrm{Li}}) = c_{\mathrm{Li}}\, \left(1 - \frac{c_{\mathrm{Li}}}{c_{\mathrm{Li}}^{max}} \right) \tag{5.25}$$

As for (4.58), definition (5.25) represents the physical requirement that both the pure and the saturated phases have vanishing mobilities.

The Helmholtz free energy density that model the isothermal processes at hand entails the separate contributions ψ_{diff} and ψ_{mech} summarized in equation (5.16). Mass transport is described by ψ_{diff}, adopting the neutral Lithium concentrations as the state variable. The mechanical energy density ψ_{mech} is made dependent upon the neutral Lithium concentrations, the elastic tensor, and a set of internal variables. Differently from the electrolyte, the processes are thermodynamically coupled both in terms of constitutive prescriptions (5.21) and of free energy density, as the mechanical properties may vary with the concentration.

The mechanical free energy density $\psi^{el}_{mech}(c_{\mathrm{Li}}, \boldsymbol{\varepsilon}^{el})$ is taken as

$$\psi^{el}_{mech}(c_{\mathrm{Li}}, \boldsymbol{\varepsilon}^{el}) = \frac{1}{2}\, \left(K(c_{\mathrm{Li}})\, \mathrm{tr}\, \left[\, \boldsymbol{\varepsilon}^{el}\, \right]^2 + 2G(c_{\mathrm{Li}})\, ||\, \mathrm{dev}\, \left[\, \boldsymbol{\varepsilon}^{el}\, \right]\, ||^2 \right) \tag{5.26}$$

where K, G are the bulk and shear modulus respectively. Thermodynamics restrictions (5.21) yield the stress tensor as the gradient of the free energy density with respect to the elastic tensor, namely:

$$\boldsymbol{\sigma} = K(c_{\mathrm{Li}})\, \mathrm{tr}\, \left[\, \boldsymbol{\varepsilon}^{el}\, \right]\, \mathbb{1} + 2\, G(c_{\mathrm{Li}})\, \mathrm{dev}\, \left[\, \boldsymbol{\varepsilon}^{el}\, \right] \tag{5.27}$$

Owing to the additive decomposition of strains (5.13) and under the usual assumption of plastic incompressibility $\mathrm{tr}\, [\, \boldsymbol{\varepsilon}^{p}\,] = 0$, the identities

$$\mathrm{tr}\, \left[\, \boldsymbol{\varepsilon}^{el}\, \right] \;\; = \;\; \mathrm{tr}\, [\, \boldsymbol{\varepsilon}\,] - 3\, \omega_{\mathrm{Li}}\, c_{\mathrm{Li}}$$

$$\mathrm{dev}\left[\boldsymbol{\varepsilon}^{el}\right] \;=\; \mathrm{dev}\left[\boldsymbol{\varepsilon}\right] + \mathrm{dev}\left[\boldsymbol{\varepsilon}^{p}\right]$$

ensue, to be further inserted into (5.27) to finally derive the stress tensor in terms of the total strain and the concentration as

$$\boldsymbol{\sigma} = K(c_{\mathrm{Li}})\,\mathrm{tr}\left[\boldsymbol{\varepsilon}\right]\,\mathbb{1} + 2\,G(c_{\mathrm{Li}})\,\mathrm{dev}\left[\boldsymbol{\varepsilon}\right] - 3\,K(c_{\mathrm{Li}})\,\omega_{\mathrm{Li}}\,c_{\mathrm{Li}}\,\mathbb{1} + 2\,G(c_{\mathrm{Li}})\,\boldsymbol{\varepsilon}^{p} \tag{5.28a}$$

In what follows a standard J_2 flow theory with isotropic hardening is used. Accordingly, only one internal variable $\breve{\xi}$ is used and it has been taken $K^p \geq 0$ and

$$\psi^{p}_{mech}(\xi) = \frac{1}{2}K^{p}\breve{\xi}^{2} \tag{5.28b}$$

together with a von Mises yield criterion

$$\varphi(\boldsymbol{\sigma},\breve{\chi}) = ||\,\mathrm{dev}\left[\boldsymbol{\sigma}\right]\,|| - \sqrt{\frac{2}{3}}\sigma_Y + \breve{\chi} \tag{5.28c}$$

and associative flow rule

$$\dot{\boldsymbol{\varepsilon}}^{p} = \frac{\partial\varphi}{\partial\boldsymbol{\sigma}}\,\dot{\lambda}\,, \qquad \dot{\breve{\xi}} = \frac{\partial\varphi}{\partial\breve{\chi}}\,\dot{\lambda} \tag{5.28d}$$

Definition (5.22) of thermodynamic force $\breve{\chi}$ and Kuhn-Tucker conditions

$$\lambda \geq 0\,, \qquad \varphi \leq 0\,, \qquad \lambda\,\varphi = 0 \tag{5.28e}$$

complete the incremental form of the mechanical constitutive equations. The thermodynamic consistency of J_2 flow theory with isotropic hardening can be proved as usual

$$\boldsymbol{\sigma} \,:\, \dot{\boldsymbol{\varepsilon}}^{p} + \vec{\chi}\cdot\dot{\vec{\xi}} \overset{\varphi=0}{=} (||\,\mathrm{dev}\left[\boldsymbol{\sigma}\right]\,|| + \breve{\chi})\,\dot{\lambda} \overset{\varphi=0}{=} \sqrt{\frac{2}{3}}\sigma_Y\,\dot{\lambda} \;\geq 0$$

as it is not influenced by the diffusive contributions to $\boldsymbol{\sigma}$.

Free energy density (per unit volume) of mobile guest atoms interacting with a host medium is described by a regular solution model [19, 20], which provides the following free energy density for the continuum approximation to mixing

$$\psi_{diff}(c_{\mathrm{Li}}) = \mu^{0}_{\mathrm{Li}}\,c_{\mathrm{Li}} \;+ RT\,c^{max}\;\{\theta_{\mathrm{Li}}\,\ln[\theta_{\mathrm{Li}}] + (1-\theta_{\mathrm{Li}})\,\ln[(1-\theta_{\mathrm{Li}})] + \chi\!\!\!^{-}\,\theta_{\mathrm{Li}}(1-\theta_{\mathrm{Li}})\} \tag{5.29}$$

having defined $\theta_{\mathrm{Li}} = \frac{c_{\mathrm{Li}}}{c^{max}_{\mathrm{Li}}}$ and c^{max}_{Li} the saturation limit for neutral Li. Real valued $\chi\!\!\!^{-}$ - termed *exchange parameter* - characterizes energy of interaction between mobile guest atoms and empty intercalation sites. If all of the interactions between mobile atoms and empty sites are the same, then $\chi\!\!\!^{-} = 0$ and there is no energy of mixing: mixing is ideal and purely entropic in nature. The contribution $\chi\!\!\!^{-}\,\theta_{\mathrm{Li}}(1-\theta_{\mathrm{Li}})$ provides the free energy density with a non convex behavior with respect to c_{Li} for $\chi\!\!\!^{-} > 2$, which in turn may lead to phase segregation [80, 141].

From the thermodynamic restriction (5.21), the chemical potential results in the form

$$\mu_{\mathrm{Li}} = \mu^{0}_{\mathrm{Li}} \;+ RT\;\{\ln[\theta_{\mathrm{Li}}] - \ln[1-\theta_{\mathrm{Li}}] + \chi\!\!\!^{-}\,(1-2\theta_{\mathrm{Li}})\} +$$

$$+\frac{1}{2}\frac{\partial K(c_{\mathrm{Li}})}{\partial c_{\mathrm{Li}}}\,\mathrm{tr}\left[\,\boldsymbol{\varepsilon}^{el}\,\right]^2+\frac{\partial G(c_{\mathrm{Li}})}{\partial c_{\mathrm{Li}}}\,||\,\mathrm{dev}\left[\,\boldsymbol{\varepsilon}^{el}\,\right]\,||^2+$$
$$-\,\omega_{\mathrm{Li}}\,\mathrm{tr}\,[\,\boldsymbol{\sigma}\,] \tag{5.30}$$

Even in the simple theory here dealt with, the chemical potential is quite complex and consist in three separate contributions. The first arises from $\frac{\partial \psi_{diff}}{\partial c_{\mathrm{Li}}}$, is non-convex in general and has a purely transport origin. The second contribution has a mechanical nature and conveys the effect of the mechanical parameters on the chemical potential. Finally, the last contribution measures the effects of the swelling deformation on the chemical potential.

By defining as usual the *diffusivity* by $\mathbb{D}_{\mathrm{Li}} = \mathbb{M}_{\mathrm{Li}}\,RT$, Fick's law (5.24) becomes

$$\begin{aligned}\vec{h}_{\mathrm{Li}} = -\mathbb{D}_{\mathrm{Li}}&\left(1-\frac{2\chi}{c_{\mathrm{Li}}^{max}}\,\mathsf{M}_{\mathrm{Li}}(c_{\mathrm{Li}})\right)\,\nabla\,[\,c_{\mathrm{Li}}\,]+\\
&-\mathbb{M}_{\mathrm{Li}}\,\mathsf{M}_{\mathrm{Li}}(c_{\mathrm{Li}})\,\nabla\left[\frac{1}{2}\frac{\partial K(c_{\mathrm{Li}})}{\partial c_{\mathrm{Li}}}\,\mathrm{tr}\left[\,\boldsymbol{\varepsilon}^{el}\,\right]^2+\frac{\partial G(c_{\mathrm{Li}})}{\partial c_{\mathrm{Li}}}\,||\,\mathrm{dev}\left[\,\boldsymbol{\varepsilon}^{el}\,\right]\,||^2\right]\\
&+\omega_{\mathrm{Li}}\,\mathbb{M}_{\mathrm{Li}}\,\mathsf{M}_{\mathrm{Li}}(c_{\mathrm{Li}})\,\nabla\,[\,\mathrm{tr}\,[\,\boldsymbol{\sigma}\,]\,]\end{aligned} \tag{5.31}$$

with the trace of the stress tensor to be evaluated stemming from equation (5.28a) and the elastic strain tensor from decomposition (5.13) in terms of total strain and concentration of Lithium.

5.5 Governing equations and weak form: active material

Numerical simulations in this thesis do not include phase segregation. Therefore, governing equations will be deployed in the easier case of material parameters independent upon c_{Li} when $\chi = 0$. The general framework is postponed in appendix 5.10. Governing equations can be derived by incorporating the constitutive equations (5.23), (5.28), and (5.31) into balance equations. They will be written in terms of the following new field:

$$\overline{\mu_{\mathrm{Li}}^{mech}}(c_{\mathrm{Li}},\boldsymbol{\varepsilon}) = -\omega_{\mathrm{Li}}\,\mathrm{tr}\,[\,\boldsymbol{\sigma}\,] = -3\,K\,\omega_{\mathrm{Li}}\,\left(\mathrm{tr}\,[\,\boldsymbol{\varepsilon}\,] - 3\,\omega_{\mathrm{Li}}\,c_{\mathrm{Li}}\right) \tag{5.32}$$

that designates how the chemical potential (5.30) depends upon mechanical factors. The variables that rule the problem are thus concentrations c_{Li}, displacements $\vec{u}$, the electric potential ϕ_s, and μ_{Li}^{mech}. Governing equations hold at all points $\vec{x} \in V_a$ at all instants, and write

$$\frac{\partial c_{\mathrm{Li}}}{\partial t}\;+\;\mathrm{div}\,[\,-\mathbb{D}_{\mathrm{Li}}\,\nabla\,[\,c_{\mathrm{Li}}\,]\,]+\;\mathrm{div}\left[\,-\mathbb{M}_{\mathrm{Li}}\,\mathsf{M}_{\mathrm{Li}}(c_{\mathrm{Li}})\;\nabla\left[\,\mu_{\mathrm{Li}}^{mech}\,\right]\,\right]=0 \tag{5.33a}$$
$$\mathrm{div}\,[\,-\kappa\,\nabla\,[\,\phi_s\,]\,]=0 \tag{5.33b}$$
$$\mathrm{div}\,[\,\boldsymbol{\sigma}\,]=\vec{0} \tag{5.33c}$$
$$\mu_{\mathrm{Li}}^{mech}-\overline{\mu_{\mathrm{Li}}^{mech}}(c_{\mathrm{Li}},\boldsymbol{\varepsilon})=0 \tag{5.33d}$$

with $\boldsymbol{\sigma}$ defined constitutively by equations (5.28).

Boundary conditions (5.3), (5.4), (5.5), (5.6) and (5.8) are applied along Neumann boundaries $\partial^N V_a$. To ensure solvability to the problem, Dirichlet boundary conditions have to be imposed along part $\partial^D V_a$, being $\partial V_a = \partial^D V_a \cup \partial^N V_a$. Rigid body motion inhibition and zero electric potential have to be included amidst Dirichlet boundary conditions.

Initial conditions are usually imposed for concentration of neutral Lithium $c_{\mathrm{Li}}(\vec{x}, t=0)$. To comply with equilibrium thermodynamics it is constant in volume V_a. Initial conditions for electric potential and displacements solve a boundary value problem at $t = 0$, made of equations (5.33b-c-d) together with homogeneous boundary conditions for current, in view of thermodynamic equilibrium at initial time, and usual given boundary conditions for displacements and tractions.

Following the same path of reasoning of sections 4.5 and 4.9, the evolution problem can be formulated in a weak form. In Galerkin approaches weak forms are built using "variations" of the same set of variables that rule the problem, namely "virtual" concentrations $\hat{c}_{\mathrm{Li}}$, displacements $\vec{\hat{u}}$, electric potential $\hat{\phi}_s$, chemical potential $\hat{\mu}^{mech}_{\mathrm{Li}}$. By doing so however the energy meaning of weak form (5.9) is lost. To give to the new weak form at least the physical dimension of a power expenditure, the mass balance equations and definition (5.32) will be scaled by suitable coefficients, that follow from constitutive equations. A weak form of governing equations can be given in a time interval $[0, t_f]$ as

$$\frac{RT}{c_{bulk}} \int_{V_a} \hat{c}_{\mathrm{Li}} \, \frac{\partial c_{\mathrm{Li}}}{\partial t} + \mathbb{D}_{\mathrm{Li}} \, \nabla [\, \hat{c}_{\mathrm{Li}} \,] \cdot \nabla [\, c_{\mathrm{Li}} \,] + \mathbb{M}_{\mathrm{Li}} (c_{\mathrm{Li}}) \; \nabla [\, \hat{c}_{\mathrm{Li}} \,] \cdot \nabla \left[\, \mu^{mech}_{\mathrm{Li}} \, \right] \, \mathrm{d}V + \\ + \frac{RT}{c_{bulk}} \int_{\Gamma_{BV}} \hat{c}_{\mathrm{Li}} \, h_{BV} \, \mathrm{d}\Gamma = 0 \tag{5.34a}$$

$$\kappa \int_{V_a} \nabla \left[\, \hat{\phi}_s \, \right] \cdot \nabla [\, \phi_s \,] \, \mathrm{d}V + \int_{\Gamma_{BV}} F \, \hat{\phi}_s \, h_{BV} \, \mathrm{d}\Gamma + \int_{\partial^N V_a \setminus \Gamma_{BV}} \hat{\phi}_s \, \overline{i_{\mathrm{e}^-}} \, \mathrm{d}\Gamma = 0 \tag{5.34b}$$

$$\int_{V_a} \hat{\boldsymbol{\varepsilon}} : \frac{\partial \boldsymbol{\sigma}}{\partial t} \, \mathrm{d}V - \int_{\partial^N V_a} \vec{\hat{u}} \cdot \frac{\partial \vec{p}}{\partial t} \, \mathrm{d}\Gamma = 0 \tag{5.34c}$$

$$\frac{c_{bulk}}{RT \, \Delta t} \int_{V_a} \hat{\mu}^{mech}_{\mathrm{Li}} \, \left(\mu^{mech}_{\mathrm{Li}} - \overline{\mu^{mech}_{\mathrm{Li}}}(c_{\mathrm{Li}}, \boldsymbol{\varepsilon}) \right) \mathrm{d}V = 0 \tag{5.34d}$$

Boundary conditions (5.3), (5.4), (5.5) ,(5.6),(5.8) and relation (3.13) have been used.

It is convenient to derive a dimensionless expression for equations (5.34). To this aim, fields that govern the problem are scaled to dimension of unity, denoted with starred superscripts from now on, via suitable scaling factors, namely:

$$c^*_{\mathrm{Li}} = \frac{c_{\mathrm{Li}}}{c_{bulk}}, \qquad \phi^*_s = \frac{F}{RT} \, \phi_s, \qquad \mu^{mech\,*}_{\mathrm{Li}} = \frac{\mu^{mech}_{\mathrm{Li}}}{RT}, \qquad \vec{u}^* = \frac{\vec{u}}{L} \tag{5.35}$$

L standing for a given characteristic length. In view of (5.34), a weak form of governing equations (5.33) can be given in a time interval $[0, t_f]$ as

$$\begin{aligned} &\text{Find } y(\vec{x}, t) \in \mathcal{V}^{[0,t_f]} \text{ such that} \\ &\frac{\partial}{\partial t} b\,(\, \hat{y}(\vec{x}), y(\vec{x}, t)\,) + a(\, \hat{y}(\vec{x}), y(\vec{x}, t)\,) = f(\, \hat{y}(\vec{x})\,) \quad \forall \hat{y}(\vec{x}) \in \mathcal{V} \end{aligned} \tag{5.36}$$

where

$$\begin{aligned} b\,(\hat{y}, y) &= RT \, c_{bulk} \int_{V_a} \hat{c}^*_{\mathrm{Li}} \, c^*_{\mathrm{Li}} \, \mathrm{d}V + L \int_{V_a} \hat{\boldsymbol{\varepsilon}}^* : \boldsymbol{\sigma}(c_{\mathrm{Li}}, \boldsymbol{\varepsilon}) \, \mathrm{d}V \\ a\,(\hat{y}, y) &= RT \, c_{bulk} \, \mathbb{D}_{\mathrm{Li}} \int_{V_a} \nabla [\, \hat{c}^*_{\mathrm{Li}} \,] \cdot \nabla [\, c^*_{\mathrm{Li}} \,] \, \mathrm{d}V + \end{aligned}$$

$$
\begin{aligned}
&+ \quad RT\,\mathrm{D}_{\mathrm{Li}} \int_{V_a} \mathsf{M}_{\mathrm{Li}}(c_{\mathrm{Li}})\ \nabla\left[\,\hat{c}^{*}_{\mathrm{Li}}\,\right] \cdot \nabla\left[\,\mu^{mech\,*}_{\mathrm{Li}}\,\right]\,\mathrm{d}V \\
&+ \quad \kappa\left(\frac{RT}{F}\right)^{2} \int_{V_a} \nabla\left[\,\hat{\phi}^{*}_{s}\,\right] \cdot \nabla\left[\,\phi^{*}_{s}\,\right]\,\mathrm{d}V \\
&+ \quad \frac{c_{bulk}}{RT\,\Delta t} \int_{V_a} \hat{\mu}^{mech\,*}_{\mathrm{Li}}\ \left(\mu^{mech\,*}_{\mathrm{Li}} - \overline{\mu^{mech}_{\mathrm{Li}}}^{*}(c_{\mathrm{Li}},\boldsymbol{\varepsilon})\right)\,\mathrm{d}V \\
f\,(\hat{y}) \quad &= \quad -RT \int_{\Gamma_{BV}} \left(\hat{c}^{*}_{\mathrm{Li}} + \hat{\phi}^{*}_{s}\right) h_{BV}\,\mathrm{d}\Gamma - \frac{RT}{F} \int_{\partial^{N}V_a \setminus \Gamma_{BV}} \hat{\phi}^{*}_{s}\,\overline{i_{\mathrm{e}^-}}\,\mathrm{d}\Gamma \\
&+ \quad L \int_{\partial^{N}V_a} \vec{u}^{*} \cdot \frac{\partial \vec{p}}{\partial t}\,\mathrm{d}\Gamma
\end{aligned}
$$

with list $y(\vec{x},t) = \{c_{\mathrm{Li}}, \phi_s, \vec{u}, \mu^{mech}_{\mathrm{Li}}\}$. Owing to the scaling, a characteristic length L and a characteristic time Δt appear in the weak form. Within finite elements analysis they can be taken as the characteristic length of the element of the mesh and the interval of time adopted for the time stepping procedure.

5.6 Hydrogen embrittlement

There are noticeable analogies between neutral Lithium and Hydrogen diffusion through a solid lattice.
Within the wide literature on Hydrogen-embrittlement, some publications propose models for Hydrogen transport in metals assuming it diffuses without interactions with the defects of the hosting material lattice (refer for example to [146]). In this case, balance equations (5.1a) and (5.1c) and constitutive equations (5.28), (5.24) and (5.30) can be used to describe the phenomena. If such an approach is adopted, the Hydrogen and Lithium diffusion models in hosting materials only differs because of Ohm's law (5.1b), required in batteries electrodes to account for the presence of the electric current $\vec{i}_{\mathrm{e}^-}$. Moreover, it is worth noting that the electric potential ϕ_s is uncoupled from the other thermodynamic variables c_{Li^+} , $\vec{u}$ and μ^{mech}, section 5.4, thus making the impact of such an equation minor within a numerical framework.

Other approaches have been pursued [82, 83, 142] in which the total Hydrogen concentration in the hosting material has been split into immobile *trapped Hydrogen* and mobile *interstitial lattice Hydrogen* to account for energetic binding of atoms. The so-called *Oriani's approach* [119] is usually used to relate the above-mentioned quantities.

The immobilization of diffusing species has been experimentally observed [147] also for Lithium atoms into Silicon electrode, that causes changes in the elastic moduli of the host medium.
Moving from these considerations, separation of guest atoms into mobile and immobilized, according to the models of [82, 83, 142], has been recently pursed for neutral Lithium diffusion modeling into electrodes [81, 148] as well. The mechanical response of active particles subjected to propagation of a sharp interphase between regions rich and poor in Lithium guest atoms have been analysed therein.

The model of *Krom et al.* [82], accounting for concentration splitting, is summarized in the following sections.

5.7 Krom's model in brief

The Hydrogen transport model of *Krom ey al.* [82] emanates from the previous work of *Sofronis and McMeeking* [142]. Both models investigate the effect of the hydrostatic stress and trapping on the Hydrogen distribution in a plastically deforming steel, assuming that Hydrogen atoms diffuse through lattice sites and that trap sites are filled by lattice diffusion.

Krom's model enhances [142] by including a strain rate factor in the Hydrogen transport equation. It stems on the equilibrium theory presented by *Oriani* [119]. The latter assumes that traps[3] are isolated, i.e. do not form an extended network. For this reason, on any subpart V_H of a system, the flux of Hydrogen $\vec{h}_H$ across the boundary ∂V_H is assumed to be purely interstitial, following *Larchè and Cahn* [15, 149]. Part of the Hydrogen (say s_H) flowing into V_H is trapped in the bulk and cannot contribute to Hydrogen transport by lattice diffusion. Only saturable and reversible traps are considered, such as dislocation cores.

5.7.1 Balance equations: Krom's model

Based on the above, the local mass balance equation at point $\vec{x}$ reads

$$\frac{\partial c_L}{\partial t} + \operatorname{div}\left[\,\vec{h}_{\mathrm{H}}\,\right] = s_{\mathrm{H}} \qquad \vec{x} \in V_{\mathrm{H}} \tag{5.37}$$

where: c_L is the *molarity* (i.e. the number of moles per unit volume) of lattice hydrogen; $\vec{h}_H$ is the mass flux in terms of moles, i.e. the number of moles of hydrogen measured per unit area per unit time; s_H is the mass trapped, i.e. the number of moles of hydrogen trapped per unit volume and unit time.

The trapped hydrogen obeys a trivial equation, stating that its concentration c_T is altered by the mass supply s_H:

$$\frac{\partial c_T}{\partial t} = -s_{\mathrm{H}} \qquad \vec{x} \in V_{\mathrm{H}} \tag{5.38}$$

The principle of virtual power (with the two requirements: Power balance $\mathcal{W}_{\mathrm{ext}} = \mathcal{W}_{\mathrm{int}}$ in any sub part, frame indifference for $\mathcal{W}_{\mathrm{int}}$ in any sub part for any virtual velocity) leads to the usual balance of forces, in absence of body forces:

$$\operatorname{div}\left[\,\boldsymbol{\sigma}\,\right] = \vec{0} \qquad \vec{x} \in V_{\mathrm{H}} \tag{5.39}$$

and to the symmetry of tensor $\boldsymbol{\sigma}$ in the framework of small displacements and strains, in which this work stands.

5.7.2 Additive decomposition of strains

As customary, the total strain $\boldsymbol{\varepsilon}$ will be additively decomposed in three contributions: an elastic recoverable part after unloading $\boldsymbol{\varepsilon}^{el}$, a swelling contribution due to the intercalation of hydrogen in the hosting material $\boldsymbol{\varepsilon}^{s}$ and a distortion, usually of plastic nature $\boldsymbol{\varepsilon}^{p}$:

$$\boldsymbol{\varepsilon} = \frac{1}{2}\left(\nabla\left[\,\vec{u}\,\right] + \nabla\left[\,\vec{u}\,\right]^{T}\right) \tag{5.40a}$$

$$\boldsymbol{\varepsilon} = \boldsymbol{\varepsilon}^{el} + \boldsymbol{\varepsilon}^{s} + \boldsymbol{\varepsilon}^{p} \tag{5.40b}$$

The swelling contribution is taken as proportional to the concentration, by means of factors ω_L and ω_T termed chemical expansion coefficients of hydrogen in the host material, which

[3]The subscript L refers to lattice (interstitial) sites and the subscript T to trap sites from now on.

equal one third of the partial molar volumes of hydrogen in the host material at a given temperature:

$$\boldsymbol{\varepsilon}^s = (\omega_L\, c_L + \omega_T\, c_T)\, \mathbb{1} \tag{5.41}$$

denoting with $\mathbb{1}$ the identity matrix.

5.7.3 Essentials of thermodynamics

The balance of energy, in its local form, can be readily written as (see [16] for details)

$$\frac{\partial u}{\partial t} = \boldsymbol{\sigma} : \frac{\partial \boldsymbol{\varepsilon}}{\partial t} + s_q - \operatorname{div}[\,\vec{q}\,] + \mu_L \frac{\partial c_L}{\partial t} - \vec{h}_{\mathrm{H}} \cdot \nabla[\,\mu_L\,] + \mu_T \frac{\partial c_T}{\partial t} \tag{5.42}$$

In the formula above, s_q is the heat supply and $\vec{q}$ the heat flux. The lack of a "trapping" flux $\vec{h}_T$ descends from the assumption of traps not forming a network, so rather then $\vec{h}_L$ the flux of Hydrogen will be henceforth simply denoted with $\vec{h}_H$. Fickian-diffusion conjectures a linear dependency of such a mass flux from the gradient of the chemical potential of the Hydrogen in the lattice sites μ_L:

$$\vec{h}_{\mathrm{H}} = -\boldsymbol{M}_{\mathrm{H}}\, \nabla[\,\mu_L\,] \tag{5.43}$$

A classical specialization of mobility tensor $\boldsymbol{M}_{\mathrm{H}}(c_L)$ is the isotropic, yet non linear choice

$$\boldsymbol{M}_{\mathrm{H}}(c_L) = \mathbb{\mu}_L\, c_L \left(1 - \frac{c_L}{c_L^{max}}\right) \mathbb{1} \tag{5.44}$$

denoting with $\mathbb{\mu}_L$ the mobility of the Hydrogen in lattice sites.

Entropy η imbalance may be derived in its local form as usual from energy balance (5.42):

$$\begin{aligned} T\frac{\partial \eta}{\partial t} - \frac{\partial u}{\partial t} + \boldsymbol{\sigma} : \left(\frac{\partial \boldsymbol{\varepsilon}^{el}}{\partial t} + \frac{\partial \boldsymbol{\varepsilon}^{s}}{\partial t} + \frac{\partial \boldsymbol{\varepsilon}^{p}}{\partial t}\right) + \\ + \mu_L \frac{\partial c_L}{\partial t} - \vec{h}_{\mathrm{H}} \cdot \nabla[\,\mu_L\,] + \mu_T \frac{\partial c_T}{\partial t} - \frac{1}{T}\, \vec{q} \cdot \nabla[\,T\,] \geq 0 \end{aligned} \tag{5.45a}$$

taking into account of decomposition (5.40). In view of definition (5.41), imbalance (5.45) rewrites as

$$\begin{aligned} T\frac{\partial \eta}{\partial t} - \frac{\partial u}{\partial t} + \boldsymbol{\sigma} : \left(\frac{\partial \boldsymbol{\varepsilon}^{el}}{\partial t} + \frac{\partial \boldsymbol{\varepsilon}^{p}}{\partial t}\right) + \left(\omega_L \frac{\partial c_L}{\partial t} + \omega_T \frac{\partial c_T}{\partial t}\right) \operatorname{tr}[\,\boldsymbol{\sigma}\,] + \\ + \mu_L \frac{\partial c_L}{\partial t} - \vec{h}_{\mathrm{H}} \cdot \nabla[\,\mu_L\,] + \mu_T \frac{\partial c_T}{\partial t} - \frac{1}{T}\, \vec{q} \cdot \nabla[\,T\,] \geq 0 \end{aligned} \tag{5.46a}$$

Thermodynamic prescriptions are usually expressed in terms of the Helmholtz free energy $\psi() = u() - T\,\eta$ rather than internal energy u. Collecting in vector $\vec{\xi}$ the set of internal variables, the free energy density accounts additively for hardening contribution as

$$\psi(T, c_L, c_T, \varepsilon^{el}, \xi) = \psi_{temp}(T) + \psi_{diff}(c_L, c_T) + \psi^{el}_{mech}(\boldsymbol{\varepsilon}^{el}) + \psi^{p}_{mech}(\vec{\xi}) \tag{5.47}$$

and it holds

$$\frac{\partial \psi(T, c_L, c_T, \varepsilon^{el}, \xi)}{\partial t} = \frac{\partial \psi_{temp}}{\partial T}\frac{\partial T}{\partial t} + \frac{\partial \psi_{diff}}{\partial c_L}\frac{\partial c_L}{\partial t} + \frac{\partial \psi_{diff}}{\partial c_T}\frac{\partial c_T}{\partial t} + \frac{\partial \psi^{el}_{mech}}{\partial \boldsymbol{\varepsilon}^{el}} : \frac{\partial \boldsymbol{\varepsilon}^{el}}{\partial t} + \frac{\partial \psi^{p}_{mech}}{\partial \vec{\xi}} \cdot \frac{\partial \vec{\xi}}{\partial t} \tag{5.48}$$

By means of (5.48), the entropy imbalance yields:

$$\begin{aligned} &- \left(\eta + \frac{\partial \psi_{temp}}{\partial T}\right)\frac{\partial T}{\partial t} + \left(\boldsymbol{\sigma} - \frac{\partial \psi^{el}_{mech}}{\partial \boldsymbol{\varepsilon}^{el}}\right) : \frac{\partial \boldsymbol{\varepsilon}^{el}}{\partial t} + \left(\mu_L + \omega_L \operatorname{tr}[\boldsymbol{\sigma}] - \frac{\partial \psi_{diff}}{\partial c_L}\right)\frac{\partial c_L}{\partial t} + \\ &+ \left(\mu_T + \omega_T \operatorname{tr}[\boldsymbol{\sigma}] - \frac{\partial \psi_{diff}}{\partial c_T}\right)\frac{\partial c_T}{\partial t} + \\ &+ \vec{h}_{\mathrm{H}} \cdot \nabla[\mu_L] + \boldsymbol{\sigma} : \frac{\partial \boldsymbol{\varepsilon}^{p}}{\partial t} - \frac{\partial \psi^{p}_{mech}}{\partial \vec{\xi}} \cdot \frac{\partial \vec{\xi}}{\partial t} - \frac{1}{T}\vec{q} \cdot \nabla[T] \geq 0 \end{aligned} \tag{5.49}$$

After applying the Coleman-Noll procedure, the following thermodynamic prescriptions come out:

$$\begin{aligned} &\eta + \frac{\partial \psi_{temp}}{\partial T} = 0\,, \qquad \boldsymbol{\sigma} - \frac{\partial \psi^{el}_{mech}}{\partial \boldsymbol{\varepsilon}^{el}} = 0\,, \\ &\mu_L + \omega_L \operatorname{tr}[\boldsymbol{\sigma}] - \frac{\partial \psi_{diff}}{\partial c_L} = 0\,, \qquad \mu_T + \omega_T \operatorname{tr}[\boldsymbol{\sigma}] - \frac{\partial \psi_{diff}}{\partial c_T} = 0\,, \\ &\vec{h}_{\mathrm{H}} \cdot \nabla[\mu_L] \geq 0\,, \qquad \vec{q} \cdot \nabla[T] \leq 0\,, \qquad \boldsymbol{\sigma} \cdot \frac{\partial \boldsymbol{\varepsilon}^{p}}{\partial t} + \vec{\chi} \cdot \frac{\partial \vec{\xi}}{\partial t} \geq 0 \end{aligned} \tag{5.50}$$

where

$$\vec{\chi} = -\frac{\partial \psi^{p}_{mech}}{\partial \vec{\xi}} \tag{5.51}$$

is the internal force vector, conjugated to $\vec{\xi}$.

A regular solution model [19] provides the following free energy density for the ideal continuum approximation to mixing

$$\psi_{diff}(c_\alpha) = \mu^0_\alpha\, c_\alpha + R\,T\, c^{max}_\alpha\, (\theta_\alpha \ln[\theta_\alpha] + (1-\theta_\alpha)\ln[1-\theta_\alpha]) \tag{5.52}$$

having defined $\theta_\alpha = \frac{c_\alpha}{c^{max}_\alpha}$ and c^{max}_α the saturation limit for species $\alpha = L\,,\, T$. Specialization (5.52) of Helmholtz' free energy density represents the entropy of mixing for an ideal solution, with no energetic interactions. μ^0_α is a reference value of the chemical potential of species α.

The chemical potential results in the form

$$\mu_\alpha = \frac{\partial \psi}{\partial c_\alpha} = \frac{\partial \psi_{diff}}{\partial c_\alpha} - \omega_\alpha \operatorname{tr}[\boldsymbol{\sigma}] = \mu^0_\alpha + R\,T\,(\ln[\theta_\alpha] - \ln[1-\theta_\alpha]) - \omega_\alpha \operatorname{tr}[\boldsymbol{\sigma}] \tag{5.53}$$

with ω_α denoting the coefficient of chemical expansion of Hydrogen in the host material, which equals one third of the partial molar volume of Hydrogen in the host material at a given temperature.

The second logarithmic contribution in (5.53) is usually neglected far from saturation, when $\theta_\alpha << 1$. This is generally the case for the interstitial Hydrogen, for which Fick's law (5.43) becomes

$$\vec{h}_{\mathrm{H}} = -\mathbb{D}_L \, \nabla [\, c_L \,] + \omega_L \, \mathbb{k}_L \, c_L \, \nabla [\, \mathrm{tr} [\, \boldsymbol{\sigma} \,] \,] \tag{5.54}$$

by substituting $\mathbb{D}_L = \mathbb{k}_L \, R \, T$.

As it was assumed that traps do not form an extended network, there is no flux of trapped Hydrogen. The kinetics of trapped Hydrogen has to be described on a different basis. Oriani postulated that within a continuum-level material point the microstructure affects the local distribution of Hydrogen keeping the Hydrogen in trapping sites in thermodynamic equilibrium with lattice sites. This implies

$$\mu_L = \mu_T \tag{5.55}$$

i.e. under the *usual* assumption of $\omega_L = \omega_T$

$$\mu_L^0 \; - \; \mu_T^0 \; = R \, T \; (\ln[\theta_T] - \ln[1 - \theta_T]) - R \, T \; (\ln[\theta_L] - \ln[1 - \theta_L]) \tag{5.56}$$

The left hand side is related to the trap binding energy $-\Delta E_\tau$ with respect to the lattice site, and in turn related to the *equilibrium constant* K^{eq}:

$$\mu_L^0 \; - \; \mu_T^0 \; = -\Delta E_\tau = R \, T \, \ln[K^{eq}] \tag{5.57}$$

Easy algebra leads to:

$$K^{eq} = \frac{\theta_T}{\theta_L} \frac{1}{1 - \theta_T} \tag{5.58}$$

which can easily inverted for θ_T

$$\theta_T = \frac{1}{1 + \frac{1}{K^{eq} \theta_L}} \tag{5.59}$$

Equation (5.59) governs the problem together with (5.37, 5.38, 5.39, and 5.54). By inserting (5.38) into (5.37)

$$\begin{aligned} &\frac{\partial c_L}{\partial t} + \frac{\partial c_T}{\partial t} + \mathrm{div} \left[\vec{h}_{\mathrm{H}} \right] = \frac{\partial c_L}{\partial t} + \frac{\partial c_T^{max}}{\partial t} \theta_T + \frac{\partial \theta_T}{\partial t} c_T^{max} + \mathrm{div} \left[\vec{h}_{\mathrm{H}} \right] = \\ &\quad \frac{\partial c_L}{\partial t} + \frac{1}{1 + \frac{1}{K \theta_L}} \frac{\partial c_T^{max}}{\partial t} + c_T^{max} \, \frac{\partial \theta_T}{\partial \theta_L} \frac{\partial \theta_L}{\partial t} + \mathrm{div} \left[\vec{h}_{\mathrm{H}} \right] = \\ &\quad \frac{\partial c_L}{\partial t} + \frac{1}{1 + \frac{1}{K \theta_L}} \frac{\partial c_T^{max}}{\partial t} + \frac{c_T^{max}(t)}{c_L^{max}} \, \frac{K}{(1 + K \theta_L)^2} \frac{\partial c_L}{\partial t} + \mathrm{div} \left[\vec{h}_{\mathrm{H}} \right] = 0 \end{aligned} \tag{5.60}$$

The term $\frac{\partial c_T^{max}}{\partial t}$ was not taken into account in the model of *Sofronis and McMeeking* [142]. *Krom et al.* [82] adopt a fit of data from *Kumnick and Johnson* [150] to follow the history variation of traps. The latter carried out permeation tests on pure iron with Hydrogen gas charging and found that the trap density in iron increases sharply with deformations at low deformation levels and then increases more gradually with further deformation. They also estimated a trap binding energy of -60kJ/mol independent of deformation level within the range of $0 - 80\%$ cold work and independent of temperature within the range of $288 - 343$K

suggesting one type of trap. A fit of the number of trap sites against the equivalent plastic strain $\bar{\varepsilon}^p$

$$\bar{\varepsilon}^p = \int_0^t \sqrt{\frac{2}{3}\,\dot{\boldsymbol{\varepsilon}}^p : \dot{\boldsymbol{\varepsilon}}^p}\,\mathrm{d}t \tag{5.61}$$

which is close to their experimental observations is

$$\log[c_T^{max}\,N_A] = 23.26 - 2.33e^{-5.5\bar{\varepsilon}^p} \tag{5.62}$$

with N_A denoting Avogadro's number. From equation (5.62) one gets

$$\frac{\partial c_T^{max}}{\partial t} = \ln[10]\,c_T^{max}(t)\;(\log[c_T^{max}\,N_A] - 23.26)\,(-5.5)\frac{\partial \bar{\varepsilon}^p}{\partial t} \tag{5.63}$$

Substitution of equation (5.63) and of constitutive law (5.54) into mass balance (5.60) provides a new equation that governs the problem together with (5.39) in terms of Hydrogen concentration c_L and displacements $\vec{u}$ after a suitable constitutive law

$$\boldsymbol{\sigma} = \mathbb{C} : (\boldsymbol{\varepsilon} - (\omega_L\,c_L + \omega_T\,c_T)\,\mathbb{1} - \boldsymbol{\varepsilon}^p) \tag{5.64}$$

is selected for the elastoplastic behavior of the hosting metal. Equations (5.28b-e) complete the formulation if standard J_2 flow theory with isotropic hardening is used.

5.8 Two-dimensional modeling of species diffusion

In the sections that follow, a two dimensional example accounting for mechanical/diffusion coupling will be used to validate the numerical algorithm descending from the formulations detailed in the present chapter. Strong simplifying assumptions have been introduced. An analytical solution for the steady state is available for comparison against the numerical outcomes.

The formulations detailed in sections 5.5 and 5.7 only differ because of the Ohm's law (5.1b), peculiar of the electrode model, and the splitting between *trapped*, c_T, and *lattice*, c_L, species peculiar of Hydrogen models, equations (5.37-5.38).

A simplified version of Krom's model 5.7 is here considered by making the assumption that Hydrogen trapping does not occur. Since all the Hydrogen is available for diffusion at any instant of time, the source term in equation (5.37) and the equation (5.38) itself do not come into play [146]. The set of equations governing the problem is thus the same of section 5.5 without (5.33b).

From weak form (5.34) it is apparent that Ohm's law is uncoupled from the other equations and therefore ϕ_s does not impact the remaining unknowns. Being the main goal of the present section to validate the numerical algorithm dealing with (simple) mechanical/diffusion coupling, it seems an acceptable choice to focus on a numerical benchmark tailored on Hydrogen diffusion problems.

Validation of the active material formulation described in 5.5 accounting for Ohm's law is postponed to chapter 6.

5.8.1 Description

Geometry and boundary conditions have been chosen so that the problems is suitable for an axisymmetric description. This allows to test the *two-dimensional* numerical algorithm[4]

[4] A general two-dimensional formulation has been used for the numerical algorithm which does not take advantage of axisymmetry.

(implemented within an *Abaqus User element script*) and to compare the results against an analytical solution. The problem can indeed be rephrased as a first order non-linear ODE allowing for explicit solution.

Geometry, material parameters and constants

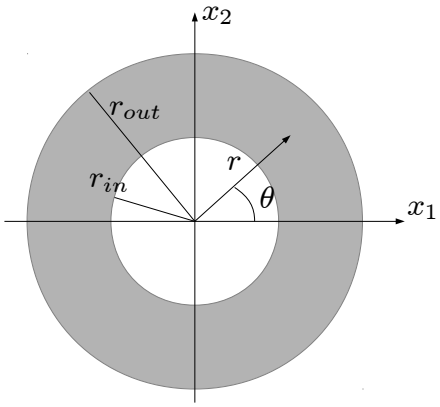

Figure 5.1: Cross section of a tube and related nomenclature

The body is a cylinder of inner radius $r_{in} = 1 \times 10^{-2}\,\mathrm{m}$ and outer radius $r_{out} = 1,2 \times 10^{-2}\,\mathrm{m}$, Figure 5.1, containing gaseous Hydrogen. Empty space surrounds the cylinder.
A linear elastic constitutive model is used to characterize the material composing the cylinder. A Young's modulus $E = 207 \times 10^{9}\,\mathrm{Nm}^{-2}$, Poisson's ratio $\nu = 0,3$ and chemical expansion coefficient $\omega_H = 6,67 \times 10^{-5}\,\mathrm{m}^3\mathrm{mol}^{-1}$ have been adopted. It is assumed that the transport of Hydrogen is characterized by a diffusivity coefficient $\mathbb{D}_H = 1,27 \times 10^{-8}\,\mathrm{m}^2\mathrm{s}^{-1}$ and that the processes take place at a constant temperature $T = 300\,\mathrm{K}$. Material parameters and constants have been taken according to [82, 83, 142].

Initial and boundary conditions

It is assumed the cylinder is initially unaffected by the presence of Hydrogen

$$c_{\mathrm{H}}(r, t = 0) \;=\; 0 \qquad r \;\in [r_{in}, r_{out}] \tag{5.65}$$

Expansion of the cylinder along the radial direction (subscript r) is constrained at any time $t \in [0, t_f]$

$$u_r(r_{in}, t) \;=\; u_r(r_{out}, t) \;=\; 0 \qquad t \;\in [0, t_f] \tag{5.66a}$$

Hydrogen concentration along the external radius r_{out} has also been kept constant

$$c_{\mathrm{H}}(r_{out}, t) \;=\; 0 \qquad t \;\in [0, t_f] \tag{5.66b}$$

while along the inner radius r_{in} concentration has been tuned, using a linear ramp[5], from $c_{\mathrm{H}}(r_{in}) = 0$ to a non-zero value

$$c_{\mathrm{H}}(r_{in}) \;=\; c_{bound} = 3,46 \;\times\; 10^{-3}\frac{\mathrm{mol}}{\mathrm{m}^3} \tag{5.66c}$$

[5]This allows to avoid a sharp discontinuity from $t = 0$ and the next time step.

and kept constant.

The author is aware conditions (5.66) are somehow simplistic. More realistic boundary conditions for the Hydrogen concentration would require constraints on chemical potential at both edges. This would reflect the thermodynamic equilibrium condition [83] achieved among intercalated Hydrogen and gaseous Hydrogen on one side and intercalated Hydrogen and empty space on the other.
A *stress free* boundary condition would also be more suitable in correspondence of the outer edge.

Once again, the intent of this section is to identify an example allowing for analytical solution. The set of boundary conditions (5.66) has been chosen to this purpose and used for comparison against the outcomes of numerical analyses (section 5.9.3).

5.9 Simplified governing equations

Governing equations will be deployed without Hydrogen concentration splitting. It is assumed that the whole amount of Hydrogen is available for diffusion within the lattice, here shortly denoted with c_{H}. Neither saturation nor energetic interaction ($\chi = 0$) are accounted for.

The governing equations that rule the problem are summarized as follows

$$\frac{\partial c_{\mathrm{H}}}{\partial t} - \operatorname{div}\left[\, \mathbb{D}_{\mathrm{H}} \, \nabla \left[\, c_{\mathrm{H}} \,\right]\right] - \operatorname{div}\left[\, \mathbb{M}_{\mathrm{H}} \, c_{\mathrm{H}} \, \nabla \left[\, \mu_{\mathrm{H}}^{mech} \,\right]\right] = 0 \tag{5.67a}$$

$$\operatorname{div}\left[\, \boldsymbol{\sigma} \,\right] = \vec{0} \tag{5.67b}$$

$$\mu_{\mathrm{H}}^{mech} = -3\, K\, \omega_{\mathrm{H}} \, \left(\operatorname{tr}\left[\, \boldsymbol{\varepsilon} \,\right] - 3\, \omega_{\mathrm{H}}\, c_{\mathrm{H}}\right) \tag{5.67c}$$

with

$$\boldsymbol{\sigma} = \mathbb{C}^{ps} : \left(\boldsymbol{\varepsilon} - \omega_{\mathrm{H}}\, c_{\mathrm{H}}\, \mathbb{1}\right)$$

where $\mathbb{C}^{ps}$ identifies the *elastic modulus tensor* tailored for the *plane strain* case.

The weak form descending from equations (5.67) can be transformed in a first order ODE in time if discretization is performed via separated variables, with spatial test $N_i(x)$ and shape functions $N_j(x)$ and nodal unknowns (collectively gathered in column y with component $y_j(t)$) that depend solely on time[6].
Adimensionalization of variables has been pursued according to (5.35). For the sake of readability the star superscript is omitted from the dimensionless quantities as in section 4.6.2. The usual Einstein summation convention is taken henceforth for repeated indexes.

The non linear ODE reads:

$$\text{Find } y(t) \text{ such that} \quad b_i^* \cdot \frac{\partial y}{\partial t}(t) + a_i^*[\, y(t) \,] = 0 \qquad \text{for } i = 1, 2, ..., N \tag{5.68}$$

where

$$b_i^* \cdot \frac{\partial y}{\partial t}(t) =$$

[6] Test and shape function are denoted with N instead of φ (refer to 4.6.2, 4.10.1 and 4.13.2) to emphasize that the weak form refers to a two-dimensional problem [151]. The m-th component of vector $\vec{u}$ is here discretized as $\sum_j N_j^{u_m}\, u_{mj}$

$$
\begin{aligned}
& RT\, c_{bulk} \int_{V_{\mathrm{H}}} N_i^{\mathrm{H}}\, N_j^{\mathrm{H}}\, \mathrm{d}V\, \frac{\partial c_j^{\mathrm{H}}}{\partial t} + \\
& \quad - L^2 \int_{V_{\mathrm{H}}} C_{klmn}^{ps}\, \frac{\partial N_i^{u_k}}{\partial x_l}\, \frac{\partial N_j^{u_m}}{\partial x_n}\, \mathrm{d}V\, \frac{\partial u_{mj}}{\partial t} + \\
& \quad + 3\, K\, \omega_{\mathrm{H}}\, c_{bulk}\, L \int_{V_{\mathrm{H}}} \frac{\partial N_i^{u_k}}{\partial x_k}\, N_j^{\mathrm{H}}\, \mathrm{d}V\, \frac{\partial c_j^{\mathrm{H}}}{\partial t}
\end{aligned}
$$

$$
\begin{aligned}
& a_i^*[\, y(t)\,] = \\
& \quad RT\, c_{bulk}\, \mathbb{D}_{\mathrm{H}} \int_{V_{\mathrm{H}}} \frac{\partial N_i^{\mathrm{H}}}{\partial x_k}\, \frac{\partial N_j^{\mathrm{H}}}{\partial x_k}\, \mathrm{d}V\, c_j^{\mathrm{H}} + \\
& \quad + RT\, c_{bulk}\, \mathbb{D}_{\mathrm{H}} \int_{V_{\mathrm{H}}} N_j^{\mathrm{H}}\, \frac{\partial N_i^{\mathrm{H}}}{\partial x_k}\, \frac{\partial N_d^{\mu}}{\partial x_k}\, \mathrm{d}V\, c_j^{\mathrm{H}}\, \mu_d^{mech} + \\
& \quad + \frac{RT\, c_{bulk}}{\Delta t} \int_{V_{\mathrm{H}}} N_i^{\mu}\, N_j^{\mu}\, \mathrm{d}V\, \mu_j^{mech} + \\
& \quad + \frac{3\, K\, \omega_{\mathrm{H}}\, c_{bulk}\, L}{\Delta t} \int_{V_{\mathrm{H}}} N_i^{\mu}\, \frac{\partial N_j^{u_k}}{\partial x_k}\, \mathrm{d}V\, u_{kj} + \\
& \quad - \frac{9\, K\, \omega_{\mathrm{H}}^2\, c_{bulk}^2}{\Delta t} \int_{V_{\mathrm{H}}} N_i^{\mu}\, N_j^{\mathrm{H}}\, \mathrm{d}V\, c_j^{\mathrm{H}}
\end{aligned}
$$

with $y_j(t) = \{c_j^{\mathrm{H}}, \mu_j^{mech}, \vec{u}_j\}$ and for $k, l, m, n = 1, 2$. The fourth order tensor C_{ijkl}^{ps} reads

$$
\begin{cases}
C_{1111}^{ps} = C_{2222}^{ps} = \frac{E\,(1-\nu)}{(1+\nu)\,(1-2\nu)} \\
C_{1122}^{ps} = C_{2211}^{ps} = \frac{E\,\nu}{(1+\nu)\,(1-2\nu)} \\
C_{1212}^{ps} = C_{1221}^{ps} = C_{2112}^{ps} = C_{2121}^{ps} = \frac{E}{2\,(1+\nu)} \\
0 \qquad \text{elsewhere}
\end{cases}
\tag{5.70}
$$

where E identifies the Young's modulus and ν the Poisson's ratio.

The ODE (5.68) is homogeneous since only Dirichlet boundary conditions (5.66) have been set.
Form $a_i^*[\, y(t)\,]$ is clearly non linear. It can be split into the sum of a non linear form ${}^n a_i^*[\, y(t)\,]$, which reads

$$
{}^n a_i^*[\, y(t)\,] = RT\, c_{bulk}\, \mathbb{D}_{\mathrm{H}} \int_{V_{\mathrm{H}}} N_j^{\mathrm{H}}\, \frac{\partial N_i^{\mathrm{H}}}{\partial x_k}\, \frac{\partial N_d^{\mu}}{\partial x_k}\, \mathrm{d}V\, c_j^{\mathrm{H}}\, \mu_d^{mech} \tag{5.71}
$$

and a bilinear counterpart ${}^l a_i^* \cdot y(t)$ defined by comparison.

A backward Euler scheme have been chosen as time-advancing method. Due to nonlinearity, a Newton-Raphson iterative scheme have been implemented to solve the problem at hand, analogously to sections 4.6.2-4.6.3.

The same considerations raised in section 4.6.3 lead to the identification of three dimensionless groups that govern the condition number of the "stiffness" matrix, namely:

$$
\gamma_{\mathrm{H}} = \frac{\Delta t\, D_{\mathrm{H}}}{L^2}\,, \qquad \gamma_{\mu\, u} = \frac{K\, \omega_{\mathrm{H}}}{RT}\,, \qquad \gamma_{\mu\, c_{\mathrm{H}}} = \omega_{\mathrm{H}}\, c_{bulk}
$$

where L is a characteristic length of the discretization and K is the bulk modulus. These parameters are expected to govern the stability of the numerical system.

5.9.1 Polar Coordinates Formulation: Axisymmetry

The features of the example allows to rewrite the governing equations (5.67) by using polar coordinates r and θ (refer to Figure 5.1). Subscripts $_r$ and $_\theta$ will be used from now on to identify the radial and tangential components of vectors accordingly.
Due to axisymmetry, the displacements field along tangential direction $u_\theta = 0$, shear strain $\varepsilon_{r\theta} = 0$ and stresses $\sigma_{r\theta} = 0$ have to vanish. For the same reason, the mass flux $\vec{h}_{\mathrm{H}}$ has non-zero radial component only, being $h_{\mathrm{H}_\theta} = 0$.

The equations governing the problem can be rewritten as follows:

Strain tensor

$$\begin{aligned} \varepsilon_r &= \frac{\partial u_r}{\partial r} \\ \varepsilon_\theta &= \frac{1}{r} u_r \\ \varepsilon_z &= \varepsilon_{r\theta} = 0 \end{aligned} \tag{5.72}$$

Elastic strain

$$\begin{aligned} \varepsilon_r^{el} &= \varepsilon_r - c_{\mathrm{H}}\,\omega_{\mathrm{H}} \\ \varepsilon_\theta^{el} &= \varepsilon_\theta - c_{\mathrm{H}}\,\omega_{\mathrm{H}} \\ \varepsilon_z^{el} &= -c_{\mathrm{H}}\,\omega_{\mathrm{H}} \\ \varepsilon_{r\theta}^{el} &= 0 \end{aligned} \tag{5.73}$$

Balance equations

force

$$\frac{\partial \sigma_r}{\partial r} + \frac{\sigma_r - \sigma_\theta}{r} = 0 \tag{5.74}$$

mass

$$\frac{\partial c_{\mathrm{H}}}{\partial t} + \frac{1}{r}\left(h_{\mathrm{H_r}} + r\frac{\partial h_{\mathrm{H_r}}}{\partial r}\right) = 0 \tag{5.75}$$

Constitutive equations

stresses

$$\begin{aligned} \sigma_r &= \frac{E}{(1+\nu)(1-2\nu)}[(1-\nu)\varepsilon_r + \nu\varepsilon_\theta] - \frac{E}{(1-2\nu)} c_{\mathrm{H}}\,\omega_{\mathrm{H}} \\ \sigma_\theta &= \frac{E}{(1+\nu)(1-2\nu)}[(1-\nu)\varepsilon_\theta + \nu\varepsilon_r] - \frac{E}{(1-2\nu)} c_{\mathrm{H}}\,\omega_{\mathrm{H}} \\ \sigma_z &= \frac{E\nu}{(1+\nu)(1-2\nu)}\left(\varepsilon_r + \varepsilon_\theta - \frac{1+\nu}{\nu} c_{\mathrm{H}}\,\omega_{\mathrm{H}}\right) \\ \tau_{r\theta} &= 0 \end{aligned} \tag{5.76}$$

molar flux

$$h_{\mathrm{H_r}} = -\mathbb{D}_H \frac{\partial c_{\mathrm{H}}}{\partial r} - \frac{\mathbb{D}_{\mathrm{H}}}{RT} c_{\mathrm{H}} \frac{\partial}{\partial r}\left[-3K\omega_{\mathrm{H}}\left(\frac{\partial u_r}{\partial r} + \frac{1}{r}u_r\right) + 9\,K\,\omega_{\mathrm{H}}^2\,c_{\mathrm{H}}\right] \tag{5.77}$$

Once expressed in polar coordinates, it is apparent that all the variables merely depend on the radial coordinate r.

From equations (5.72), (5.74) and (5.76) easy algebra leads to a relation between the trace of strain tensor $\varepsilon_r + \varepsilon_\theta$ and concentration c_{H}

$$\frac{\partial}{\partial r}(\varepsilon_r + \varepsilon_\theta) = \frac{1+\nu}{1-\nu}\omega_{\mathrm{H}}\frac{\partial c_{\mathrm{H}}}{\partial r} \tag{5.78}$$

By defining

$$\phi = 2\frac{\mathbb{D}_{\mathrm{H}}}{RT}\frac{E}{1-\nu}\omega_a^2 \tag{5.79}$$

mass conservation equation (5.75) becomes

$$\frac{\partial c_{\mathrm{H}}}{\partial t} - \mathbb{D}_{\mathrm{H}}\left(\frac{1}{r}\frac{\partial c_{\mathrm{H}}}{\partial r} + \frac{\partial^2 c_{\mathrm{H}}}{\partial r^2}\right) - \phi\left[\frac{1}{r}c_{\mathrm{H}}\frac{\partial c_{\mathrm{H}}}{\partial r} + \frac{\partial}{\partial r}\left(c_{\mathrm{H}}\frac{\partial c_{\mathrm{H}}}{\partial r}\right)\right] = 0 \tag{5.80}$$

The concentration c_{H} is the only unknown of the problem. Once its distribution along r and evolution in time t are know, other variables ($\vec{u}$, $\boldsymbol{\varepsilon}$ and $\boldsymbol{\sigma}$) can be easily detected.

5.9.2 Steady state analytical solution

From equation (5.80) one gets that the *steady state concentration distribution* satisfies the second order non-linear ordinary differential equation in c_{H}

$$\mathbb{D}_{\mathrm{H}}\left(\frac{\partial c_{\mathrm{H}}}{\partial r} + r\,\frac{\partial^2 c_{\mathrm{H}}}{\partial r^2}\right) + \phi\left[c_{\mathrm{H}}\,\frac{\partial c_{\mathrm{H}}}{\partial r} + r\,\frac{\partial}{\partial r}\left(c_{\mathrm{H}}\frac{\partial c_{\mathrm{H}}}{\partial r}\right)\right] = 0 \qquad r \in [r_{in}, r_{out}] \tag{5.81}$$

Solutions to equation (5.81) are not unique, but the only one admissible for the problem considered, according to boundary conditions (5.66b-c) and for $c_{bulk} \geq 0$, reads

$$c_{\mathrm{H}}(r) = \sqrt{\left(\frac{\mathbb{D}_{\mathrm{H}}}{\phi}\right)^2 + \left(2\,\frac{\mathbb{D}_{\mathrm{H}}}{\phi} + c_{bound}\right)c_{bound}\frac{\log r - \log r_{out}}{\log r_{in} - \log r_{out}}} - \frac{\mathbb{D}_{\mathrm{H}}}{\phi} \qquad r \in [r_{in}, r_{out}] \tag{5.82}$$

The radial displacement u_r can be determined straightforwardly from equations (5.78), (5.72) and (5.82) by seeking for the solution of the non-homogeneous ODE

$$\frac{\partial u_r}{\partial r} + \frac{1}{r}u_r = \frac{1+\nu}{1-\nu}\omega_{\mathrm{H}}\,c_{\mathrm{H}}(r) + k_1 \tag{5.83}$$

satisfying boundary conditions (5.66a)

Solution to equation (5.83) has been determined using the analytical solver *Wolfram Mathematica*, its plot within the range $[r_{in}, r_{out}]$ is shown in Figure 5.5.
The distribution of stresses, computed using equations (5.72) and (5.76), are reported in Figures 5.6-5.8.

5.9.3 Simulations

Several simulations have been carried out with different time steps and number of elements. The outcomes here reported refer to the 1200 elements mesh depicted in Figure 5.2. Taking advantage of axisymmetry, the numerical analyses have been carried out by restricting the attention on one fourth of the overall cross section. A constant time step of 10 seconds has been used, for which:

$$\gamma_{\mathrm{H}} = 12.7\,, \qquad \gamma_{\mu\, u} = 4612.75\,, \qquad \gamma_{\mu\, c_{\mathrm{H}}} = 2.30782 \times 10^{-7}$$

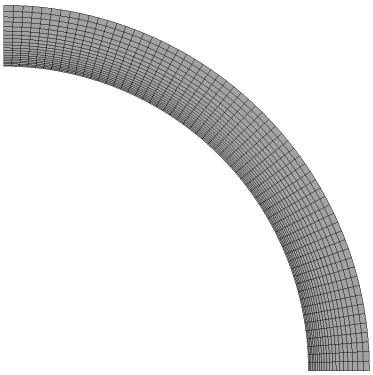

Figure 5.2: One fourth of the tube cross section used for numerical analyses. The mesh depicted here is made up by 1200 elements.

The numerical analyses have been run for an interval of time $t \in [0\,,\, 300\,\mathrm{sec}]$, during which the steady state condition is reached.

In Figure 5.3 the outcomes of numerical analyses in terms of Hydrogen concentration c_H and radial displacements u_r at the steady state are reported. It is worth pointing out that although the finite element algorithm implemented accounts for general 2D problems, axisymmetric solutions are perfectly recovered in both cases. The contour have been plotted on the undeformed configuration.

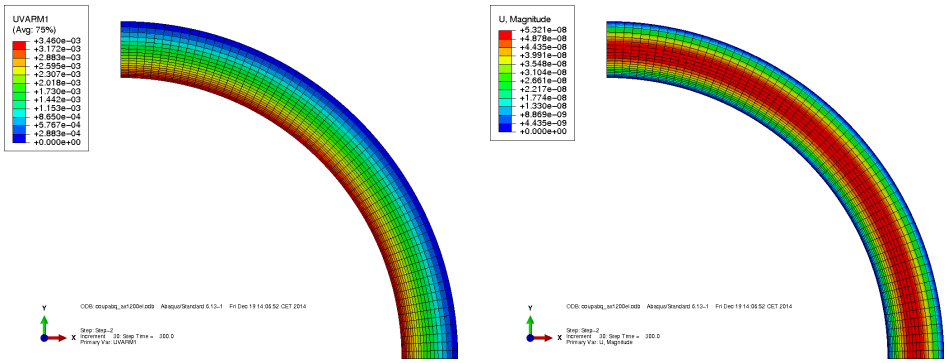

c_H steady state $\qquad$ u_r steady state

Figure 5.3: *Contour plot of Hydrogen concentration c_H and radial displacement u_r at the steady state within the cross section.*

The steady state c_H distribution determined from numerical analyses has been compared in Figure 5.4 with the analytical solution corresponding to equation (5.82). The good agree-

ment achieved denote the robustness of the algorithm implemented.
The trend of the radial displacements u_r is also recovered, as the overlapping of the numerical results and the analytical solution testifies in Figure 5.5.

Also the numerical outcomes in terms of stresses have been compared against the analytical solution - descending from equations (5.72) and (5.76) - for completeness. They have been depicted in Figures 5.6-5.8.

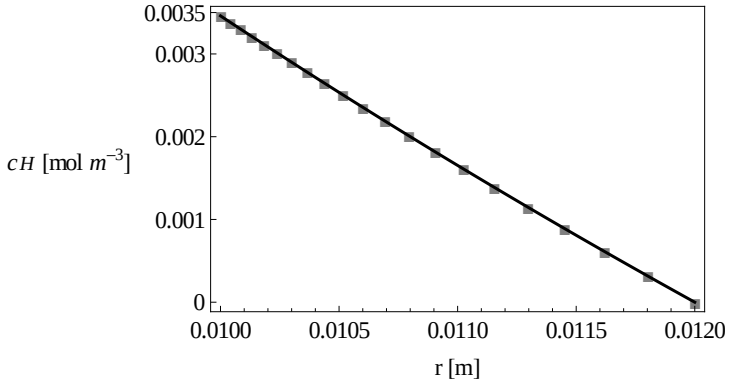

Figure 5.4: *Analytical (continuus) and numerical (squared) solutions for the steady state concentration distribution c_{H} along the radius r.*

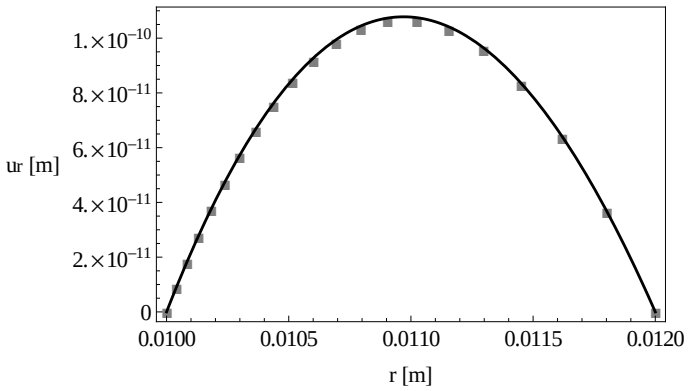

Figure 5.5: *Analytical (continuus) and numerical (squared) solutions for the steady state radial displacement distribution u_r along the radius r.*

5.9.4 Remarks

In this chapter, balance equations for active materials, discussed in 3.2, have been completed by a set of constitutive equations fulfilling thermodynamic restrictions (5.21).

The numerical algorithm that descend form the weak form (5.36) leads to satisfactory results, see 5.9.3. The constitutive theory implemented for two-dimensional problems may appear simplistic, but it has to be intended as a step forward into a complex numerical framework that descends from the model described in chapter 3. In chapter 6 an all-solid-state battery cell will be simulated. To this end, the formulation that describes the electrolyte

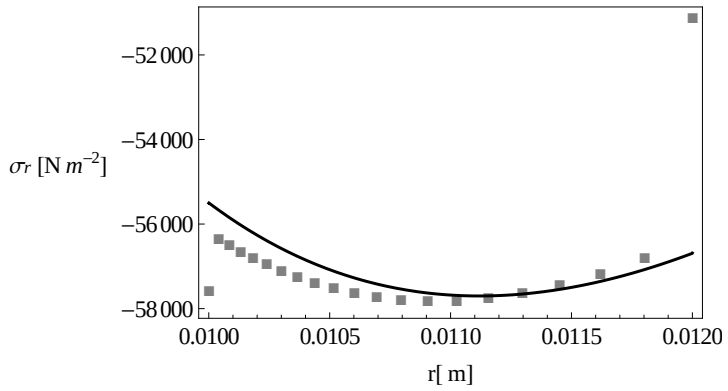

Figure 5.6: *Analytical (continuus) and numerical (squared) solutions for the steady state radial stress distribution σ_r along the radius r.*

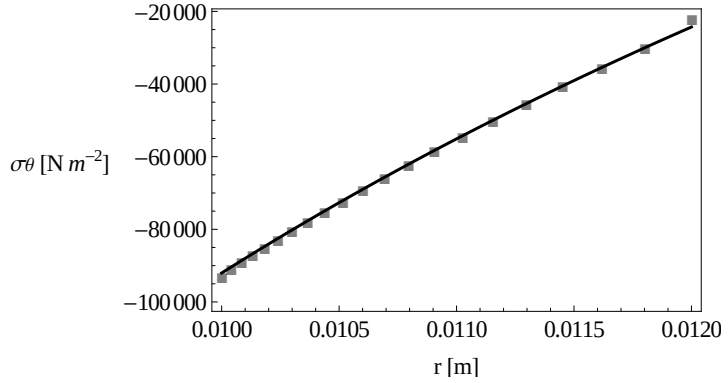

Figure 5.7: *Analytical (continuus) and numerical (squared) solutions for the steady state tangential stress distribution σ_θ along the radius r.*

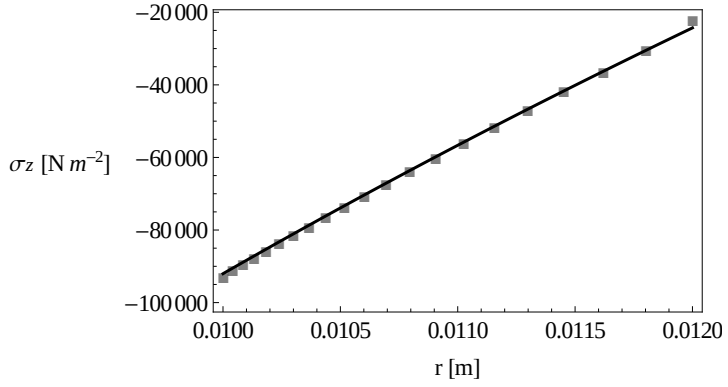

Figure 5.8: *Analytical (continuus) and numerical (squared) solutions for the steady state out of plane stress distribution σ_z along the radius r.*

(chapter 4) and the electrodes (active materials, chapter 5) will be coupled through the interface reactions (see 3.2.2), giving rise to further complications.
The one-dimensional simulation that will be discussed in chapter 6 will anyway take into

account inelastic effects.

Thanks to the analogy between neutral Lithium diffusion within electrodes material and Hydrogen diffusion in metal lattice, the possibility of pursuing different approaches in future works is envisaged [81, 148].

5.10 Appendix: General form of governing equations for electrodes

Governing equations can be derived by incorporating the constitutive equations (5.23), (5.28), and (5.31) into balance equations. They will be written as usual in terms of $\overline{\mu_{\rm Li}^{mech}}$ as

$$\overline{\mu_{\rm Li}^{mech}}(c_{\rm Li},\boldsymbol{\varepsilon}) = \frac{1}{2}\frac{\partial K(c_{\rm Li})}{\partial c_{\rm Li}}\left(\mathrm{tr}\,[\,\boldsymbol{\varepsilon}\,]-3\,\omega_{\rm Li}\,c_{\rm Li}\right)^2+\frac{\partial G(c_{\rm Li})}{\partial c_{\rm Li}}\,||\,\mathrm{dev}\,[\,\boldsymbol{\varepsilon}\,]+\mathrm{dev}\,[\,\boldsymbol{\varepsilon}^p\,]\,||^2-\omega_{\rm Li}\,\mathrm{tr}\,[\,\boldsymbol{\sigma}\,] \tag{5.84a}$$

that designates how the chemical potential (5.30) depends upon mechanical factors. The variables that rule the problem are thus concentrations $c_{\rm Li}$, displacements $\vec{u}$, the electric potential ϕ, and $\mu_{\rm Li}^{mech}$. Governing equations hold at all points $\vec{x}\in V_a$ at all instants, and write

$$\frac{\partial c_{\rm Li}}{\partial t}+\mathrm{div}\left[-\mathbb{D}_{\rm Li}\left(1-\frac{2\chi}{c_{\rm Li}^{max}}\,\mathsf{M}_{\rm Li}(c_{\rm Li})\right)\nabla\,[\,c_{\rm Li}\,]\right]+\mathrm{div}\left[-\mathbb{t}_{\rm Li}\,\mathsf{M}_{\rm Li}(c_{\rm Li})\;\nabla\left[\overline{\mu_{\rm Li}^{mech}}\right]\right]=0 \tag{5.84b}$$

$$\mathrm{div}\,[\,-\kappa\,\nabla\,[\,\phi\,]\,]=0 \tag{5.84c}$$

$$\mathrm{div}\,[\,\boldsymbol{\sigma}\,]=\vec{0} \tag{5.84d}$$

with $\boldsymbol{\sigma}$ defined constitutively by equations (5.28).

Following the same path of reasoning of (5.9), the evolution problem can be formulated in a general weak form in a time interval $[0,t_f]$ as

$$\begin{array}{l}\text{Find } y(\vec{x},t)\in\mathcal{V}^{[0,t_f]} \text{ such that}\\ \quad \dfrac{\mathrm{d}}{\mathrm{d}t}b\,(\,\hat{y}(\vec{x}),y(\vec{x},t)\,)+a(\,\hat{y}(\vec{x}),y(\vec{x},t)\,)=f(\,\hat{y}(\vec{x})\,)\qquad\forall\hat{y}(\vec{x})\in\mathcal{V}\end{array} \tag{5.85}$$

where

$$\begin{aligned}
b\,(\hat{y},y) &= \frac{RT}{c_{bulk}}\int_{V_a}\hat{c}_{\rm Li}\,c_{\rm Li}\,\mathrm{d}V+\int_{V_a}\hat{\boldsymbol{\varepsilon}}:\boldsymbol{\sigma}(c_{\rm Li},\boldsymbol{\varepsilon})\,\mathrm{d}V\\
a\,(\hat{y},y) &= \frac{RT}{c_{bulk}}\int_{V_a}\mathbb{D}_{\rm Li}\left(1-\frac{2\chi}{c_{\rm Li}^{max}}\,\mathsf{M}_{\rm Li}(c_{\rm Li})\right)\nabla\,[\,\hat{c}_{\rm Li}\,]\cdot\nabla\,[\,c_{\rm Li}\,]\,\mathrm{d}V+\\
&+ \frac{RT}{c_{bulk}}\int_{V_a}\mathbb{t}_{\rm Li}\,\mathsf{M}_{\rm Li}(c_{\rm Li})\;\nabla\,[\,\hat{c}_{\rm Li}\,]\cdot\nabla\left[\mu_{\rm Li}^{mech}\right]\mathrm{d}V+\\
&+ \frac{c_{bulk}}{RT\,\Delta t}\int_{V_a}\hat{\mu}_{\rm Li}^{mech}\left(\mu_{\rm Li}^{mech}-\overline{\mu_{\rm Li}^{mech}}(c_{\rm Li},\boldsymbol{\varepsilon})\right)\mathrm{d}V\\
&+ \kappa\int_{V_s}\nabla\left[\hat{\phi}_a\right]\cdot\nabla\,[\,\phi_s\,]\,\mathrm{d}V+\\
f\,(\hat{y}) &= -\int_{\Gamma_{BV}}\left(\frac{RT}{c_{bulk}}\,\hat{c}_{\rm Li}+F\,\hat{\phi}_s\right)h_{BV}\,\mathrm{d}\Gamma-\int_{\partial V_a^N\setminus\Gamma_{BV}}\hat{\phi}_s\,\overline{i_{\rm e}}\,\mathrm{d}\Gamma+\int_{\partial^N V_a}\hat{\vec{u}}\cdot\frac{\partial\vec{\overline{p}}}{\partial t}\,\mathrm{d}\Gamma
\end{aligned}$$

with list $y(\vec{x},t)=\{c_{\rm Li},\mu_{\rm Li}^{mech},\phi_s,\vec{u}\}$. Owing to the scaling, a characteristic length L and a characteristic time Δt appear in the weak form.

Chapter 6
Complete cell: Microscale formulation validation

The purpose of the present chapter is to validate the model detailed in chapter 3 for the microscale[1].
To this end, the case of an all-solid-state battery studied in *Danilov et al.* [21], also depicted in Figure 6.1, will be considered. The battery is made up by three layers: a Lithium anode, a solid-electrolyte, and a $LiCoO_2$ cathode. This simple geometry makes it is suitable for a one-dimensional modeling.

The formulation describing the electro-chemo-mechanical processes in the active material exposed in chapter 5 is adopted for both the homogeneous electrodes.
The liquid electrolyte model of chapter 4 is here used to model ionic transport within the electrolyte. This approach is an approximation to simplify the numerical burden. The solid electrolyte model described in section 4.11 would lead to more accurate evaluations and will be considered for future works.
Interface reactions are explicitly modeled, extending the formulation anticipated in section 3.2.2.

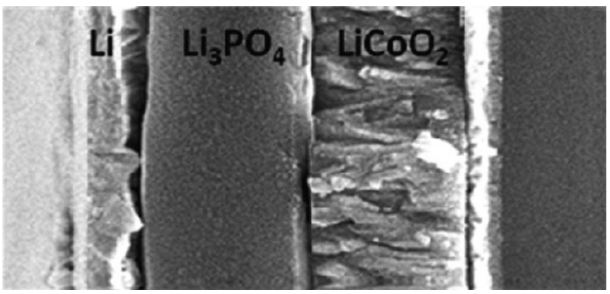

Figure 6.1: *An example of SEM image of an as-produced solid-state Li-ion battery [21].*

6.1 Electroneutral formulation

6.1.1 Electrolyte

The framework detailed in chapter 4 for liquid electrolyte modeling is here adopted. The same set of balance equations and weak forms of sections 4.1 and 4.2 have been used. Subscript $_e$ denotes quantities that refer to the electrolyte.

The boundary of the electrolyte is the union of the Neumann part $\partial^N V_e$ and of the Dirichlet part $\partial^D V_e$. According to section 4.2, $\Gamma_{BV} \subseteq \partial^N V_e$ is the location where the

[1] This chapter extends contents of [130]

oxidation/reduction reaction takes place. At that locus there is no intercalation of X^- charges, whereas a Faradaic reaction converts the oxidized Lithium to its neutral state before its diffusion into the electrode lattice or vice versa. The mass flux along the boundary $\partial^N V_e$ satisfies the following conditions:

$$\vec{h}_{\mathrm{Li}^+} \cdot \vec{n}_e = -h_{BV} \qquad \vec{x} \in \Gamma_{BV} \tag{6.1a}$$

$$\vec{h}_{\mathrm{Li}^+} \cdot \vec{n}_e = 0 \qquad \vec{x} \in \partial^N V_e \setminus \Gamma_{BV} \tag{6.1b}$$

$$\vec{h}_{\mathrm{X}^-} \cdot \vec{n}_e = 0 \qquad \vec{x} \in \partial^N V_e \tag{6.1c}$$

Electrode kinetics detailed in section 3.2.2 will be recalled in 6.1.3, where h_{BV} will be defined as the mass flux in the outward normal direction at the surface of an electrode. It will be constitutively defined in terms of Butler-Volmer equation in formulae (6.10, 6.14), as its suffix asserts.

Ampère's law

$$\left\{ \frac{\partial \vec{D}_e}{\partial t} + F\, \vec{h}_{\mathrm{Li}^+} \right\} \cdot \vec{n}_e = \mathrm{curl}\left[\vec{H}_e \right] \cdot \vec{n}_e \qquad \vec{x} \in \Gamma_{BV} \tag{6.2}$$

allows to devise boundary conditions for the electric potential in terms of the projection of the curl of magnetizing field across the interface. They will be considered later in section 6.1.3.

Tractions across the electrode/electrolyte interface are supposed to be continuous, no displacement jumps are taken into account.

6.1.2 Electrodes

In this section and henceforth, to shorten notation, the subscript $_a$ will stand collectively for the anode and the cathode[2]. When necessary, the subscripts $_{an}$ and $_{cath}$ will identify anode and cathode, respectively.

The framework detailed in chapter 5 for the active material modeling will be adopted in the following for homogeneous material electrodes interested by neutral Lithium intercalation. The same set of balance equations and weak forms of sections 5.1 and 5.2 will be used, they are thus not reported here.

The boundary of the electrode is the union of the Neumann part $\partial^N V_a$ and of the Dirichlet part $\partial^D V_a$. The mass flux across the interface $\Gamma_{BV} \subseteq \partial^N V_a$ satisfies the following condition:

$$\vec{h}_{\mathrm{Li}} \cdot \vec{n}_a = h_{BV} \qquad \vec{x} \in \Gamma_{BV} \tag{6.3}$$

whereas no Lithium flows across the remaining boundaries

$$\vec{h}_{\mathrm{Li}} \cdot \vec{n}_a = 0 \qquad \vec{x} \in \partial^N V_a \setminus \Gamma_{BV} \tag{6.4}$$

The current density at the interface satisfies the following boundary condition:

$$\vec{i}_{\mathrm{e}^-} \cdot \vec{n}_a = i_{BV} \qquad \vec{x} \in \Gamma_{BV} \tag{6.5}$$

[2]The subscript $_a$ is a reminiscence of chapters 3 and 5 where the formulation here used for homogeneous electrodes was suitable for *active material* only.

Current density i_{BV} and mass flux h_{BV} have been studied in detail and related constitutively in section 3.2.2. Across the remaining part of the Neumann boundaries the current flux is generally given

$$\vec{i}_{e^-} \cdot \vec{n} = \overline{i_{e^-}} \qquad \vec{x} \in \partial^N V_a \setminus \Gamma_{BV} \tag{6.6}$$

and a Dirichlet boundary condition that sets the location of the zero of the electric potential is mandatory to the problem definite.

Tractions-type boundary conditions are given along $\partial^N V_a$ and displacements are imposed on the Dirichlet part $\partial^D V_a$

$$\boldsymbol{\sigma} \cdot \vec{n}_{an} = \vec{\bar{p}}_{an} \qquad \vec{x} \in \partial^N V_{an} \,, \qquad \boldsymbol{\sigma} \cdot \vec{n}_{cath} = \vec{\bar{p}}_{cath} \qquad \vec{x} \in \partial^N V_{cath} \tag{6.7a}$$

$$\vec{u} = \overline{\vec{u}_{an}} \qquad \vec{x} \in \partial^D V_{an} \,, \qquad \vec{u} = \overline{\vec{u}_{cath}} \qquad \vec{x} \in \partial^D V_{cath} \tag{6.7b}$$

6.1.3 Interfaces

The following reaction of Lithium deposition/dissolution

$$\mathrm{Li} \rightleftarrows \mathrm{Li}^+ + \mathrm{e}^- \tag{6.8}$$

is assumed to take place at the two sharp electrode/electrolyte interfaces. In reaction (6.8) electrical charge is created or consumed. These events are accompanied by an electrostatic potential difference between the solid electrolyte and electrode, that will be modeled as a discontinuity $\xi = [\![\phi]\!]$ that arises across a zero-thickness interface denoted with Γ_{BV} (see also 3.2.2).

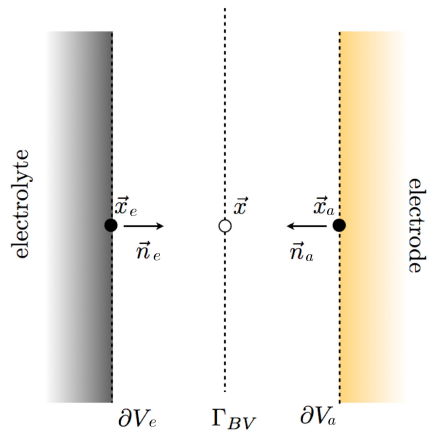

Figure 6.2: *A model of the interface between electrolyte and electrode as a discontinuity locus.*

As depicted in Figure 6.2 a one-to-one mapping is set between interface Γ_{BV} and boundaries ∂V_e and ∂V_a. At any point $\vec{x}$ along Γ_{BV} two points correspond along boundaries ∂V_e and ∂V_a. At point $\vec{x}_e$ the outer normal $\vec{n}_e$ is associated, and analogously to point $\vec{x}_a$. In the light of the small displacement assumption, during the deformation process the normals identity $\vec{n}_e = -\vec{n}_a$ is kept.

The Nernst potential ξ^{Nernst} (refer to 3.2.2) is a function of the state of charge of the battery, which will be taken as a given (i.e. extrapolated from experimental measures as in [21]) function of an internal variable $\natural$. The net mass flux flowing between electrode and electrolyte is related to the *surface over-potential*, expressed by the difference

$$\chi = \xi - \xi^{Nernst}(\natural) \tag{6.9}$$

The mass flux projected *in the outward normal direction at the surface of an electrode*, has already been denoted by h_{BV}, refer again to 3.2.2. The relationship between averaged mass flux and surface over-potential is usually described by means of the *Butler-Volmer equation* [6, 11, 88, 118]:

$$h_{BV}(\chi) = \frac{\mathrm{i}_0}{F} \left\{ \exp\left[\frac{(1-\beta)}{RT} F\,\chi\right] - \exp\left[-\frac{\beta}{RT} F\,\chi\right] \right\} \tag{6.10}$$

There are two kinetic parameters in equation (6.10), namely i_0 and β. Experimental data are required to estimate these parameters. Factor i_0, termed *exchange current density*, depends on the microscopic state of the system nearby the physical interface between electrolyte and electrode. Parameter β is a *symmetry factor* and represents the fraction of the surface over-potential that promotes cathodic reaction. It is widely assumed to be $\beta = 1/2$ and as such was taken in the simulations.

It will be assumed that the interface is not capable to store neither charge nor mass. Accordingly, the inflow shall equal the outflow (refer to Figure 6.3 for notation):

$$\vec{h}_{\mathrm{Li}^+} \cdot \vec{n}_e + \vec{h}_{\mathrm{Li}} \cdot \vec{n}_{an} = 0 \quad \vec{x} \in \Gamma_{BV}^{an}\,, \quad \vec{h}_{\mathrm{Li}^+} \cdot \vec{n}_e + \vec{h}_{\mathrm{Li}} \cdot \vec{n}_{cath} = 0 \quad \vec{x} \in \Gamma_{BV}^{cath} \tag{6.11a}$$

$$F\,\vec{h}_{\mathrm{Li}^+} \cdot \vec{n}_e + \vec{i}_{an} \cdot \vec{n}_{an} = 0 \quad \vec{x} \in \Gamma_{BV}^{an}\,, \quad F\,\vec{h}_{\mathrm{Li}^+} \cdot \vec{n}_e + \vec{i}_{cath} \cdot \vec{n}_{cath} = 0 \quad \vec{x} \in \Gamma_{BV}^{cath} \tag{6.11b}$$

In terms of the Butler-Volmer flux defined in (6.10) the conservation equations above reads:

$$\vec{h}_{\mathrm{Li}^+} \cdot \vec{n}_e + h_{BV}^{an}(\chi) = 0 \quad \vec{x} \in \Gamma_{BV}^{an}\,, \quad \vec{h}_{\mathrm{Li}^+} \cdot \vec{n}_e + h_{BV}^{cath}(\chi) = 0 \quad \vec{x} \in \Gamma_{BV}^{cath} \tag{6.12}$$

The current density projected *in the outward normal direction at the surface of an electrode* $\vec{i}_{\mathrm{e}^-} \cdot \vec{n}_a$ has been denoted by i_{BV} in equation (6.5). Faraday's law induces a constraint along the interface between the mass flux and current in view of the continuity of current density across the interface (6.11b):

$$F\,\vec{h}_{\mathrm{Li}^+} \cdot \vec{n}_e + i_{BV} = 0 \qquad \vec{x} \in \Gamma_{BV}^{an}\,, \qquad F\,\vec{h}_{\mathrm{Li}^+} \cdot \vec{n}_e + i_{BV} = 0 \qquad \vec{x} \in \Gamma_{BV}^{cath} \tag{6.13}$$

By comparison of formulae (6.12) and (6.13) it turns out that Faraday's law extends to the current density and mass fluxes across interfaces Γ_{BV}^{an} and Γ_{BV}^{cath}, in the following form:

$$i_{BV}(\chi) = F\,h_{BV}(\chi) \tag{6.14}$$

Boundary conditions (6.2) are the mere link between the magnetic and electric fields due to the electro-quasi-static assumption. To account for the projection of the curl of the

magnetizing field on the normal at the boundary in equation (6.2), the differential problem (2.5) for $\vec{B}$ should be deployed. Rather than attempting at that, in order to simplify the formulation the assumption is made[3] that along the interface Γ_{BV}

$$\operatorname{curl}\left[\vec{H}_e\right]\cdot\vec{n}_e = -i_{BV} \tag{6.15}$$

which is an acceptable assumption as long as

$$\frac{\partial\vec{D}_e}{\partial t}\cdot\vec{n}_e \ll \vec{i}_e\cdot\vec{n}_e \qquad \vec{x}\in\Gamma_{BV} \tag{6.16}$$

with $\vec{i}_e = F\,\vec{h}_{\mathrm{Li}^+}$ in view of Faraday's law (2.2-2.3) and boundary conditions (6.1b-c). Continuity of the electric current across the interface at each point $\vec{x}\in\Gamma_{BV}$ therefore allows to identify also the projection of the curl of the magnetizing field on the normal at the boundary.

Tractions as well as displacements across the interface are supposed to be continuous:

$$\boldsymbol{\sigma}_e\cdot\vec{n}_e + \boldsymbol{\sigma}_{an}\cdot\vec{n}_{an} = 0 \quad \vec{x}\in\Gamma_{BV}^{an}\,, \quad \boldsymbol{\sigma}_e\cdot\vec{n}_e + \boldsymbol{\sigma}_{cath}\cdot\vec{n}_{cath} = 0 \quad \vec{x}\in\Gamma_{BV}^{cath} \tag{6.17a}$$

$$\vec{u}_{el} - \vec{u}_{an} = 0 \quad \vec{x}\in\Gamma_{BV}^{an}\,, \quad \vec{u}_{el} - \vec{u}_{cath} = 0 \quad \vec{x}\in\Gamma_{BV}^{cath} \tag{6.17b}$$

Weak form

The constraint (6.14) will be imposed via Lagrange multipliers λ, that inherit the physical meaning of a current density across the interface Γ_{BV}. The weak form reads:

$$\int_{\Gamma_{BV}} -\hat{\xi}\,\lambda + \hat{\gamma}\,h_{BV}(\chi) + \hat{\lambda}\,(\lambda - F\,h_{BV}(\chi))\;\mathrm{d}\Gamma \tag{6.18}$$

The symbol γ denotes the virtual counterpart of the reaction Gibbs energy

$$\gamma = \mu_{\mathrm{Li}} - \mu_{\mathrm{Li}^+} \tag{6.19}$$

and the symbol $\hat{\lambda}$ denotes the field energetically conjugated to λ.

6.1.4 Weak form

In conclusion, a weak form can be given in a time interval $[0, t_f]$ as:

$$\text{Find } y\in\mathcal{V}^{[0,t_f]} \text{ such that } \frac{\mathrm{d}}{\mathrm{d}t}\,b\,(\hat{y}, z(t)) + a(\hat{y}, y(t)) = f(\hat{y}) \quad \forall\hat{y}\in\mathcal{V} \tag{6.20}$$

where

$$\begin{aligned} b\,(\hat{y}, z) \;=\; & -\int_{V_a}\hat{\mu}_{\mathrm{Li}}\,c_{\mathrm{Li}}\,\mathrm{d}V - \int_{V_e}\hat{\mu}_{\mathrm{Li}^+}\,c_{\mathrm{Li}^+} + \hat{\mu}_{\mathrm{X}^-}\,c_{\mathrm{X}^-}\,\mathrm{d}V + \\ & -\int_{V_e}\nabla\left[\hat{\phi}_e\right]\cdot\vec{D}_e\,\mathrm{d}V + \int_V\hat{\boldsymbol{\varepsilon}}:\boldsymbol{\sigma}\,\mathrm{d}V \end{aligned}$$

[3] i.e. $\vec{B}$ *along the boundary* can be estimated from the "steady current" theory (see appendix 3.8 and[13], chapter 3).

$$
\begin{aligned}
a\left(\hat{y}, y\right) &= \int_{V_a} \nabla\left[\,\hat{\mu}_{\mathrm{Li}}\,\right] \cdot \vec{h}_{\mathrm{Li}}\,\mathrm{d}V + \int_{V_e} \nabla\left[\,\hat{\mu}_{\mathrm{Li}^+}\,\right] \cdot \vec{h}_{\mathrm{Li}^+} + \nabla\left[\,\hat{\mu}_{\mathrm{X}^-}\,\right] \cdot \vec{h}_{\mathrm{X}^-}\,\mathrm{d}V + \\
&- \int_{V_a} \nabla\left[\,\hat{\phi}_s\,\right] \cdot \vec{i}_{\mathrm{e}^-}\,\mathrm{d}V - \int_{V_e} \nabla\left[\,\hat{\phi}_e\,\right] \cdot \left(F\,\left(\vec{h}_{\mathrm{Li}^+} - \vec{h}_{\mathrm{X}^-}\right)\right)\,\mathrm{d}V + \\
&- \int_{\Gamma_{BV}} -\hat{\xi}\,\lambda + \,\hat{\gamma}\,h_{BV}(\chi)\, + \hat{\lambda}\left(\lambda - F\,h_{BV}(\chi)\right)\,\mathrm{d}\Gamma
\end{aligned}
$$

with $z = \{c_{\mathrm{Li}},\, c_{\mathrm{Li}^+},\, c_{\mathrm{X}^-}\},\ y = \{\mu_{\mathrm{Li}}, \mu_{\mathrm{Li}^+}, \mu_{\mathrm{X}^-}, \phi_a, \phi_e, \vec{u}, \lambda\}$. The unknown field λ along the interface acts as a Lagrange multiplier. Gibbs' reaction energy is defined according to equations (6.19) as

$$\hat{\gamma} = \hat{\mu}_{\mathrm{Li}} - \hat{\mu}_{\mathrm{Li}^+} \tag{6.21}$$

the potential jump as

$$\hat{\xi} = \hat{\phi}_s - \hat{\phi}_e$$

Mass flux across the interface $h_{BV}(\chi)$ obeys to Butler-Volmer equation (6.10). The right hand side

$$f\left(\hat{y}\right) = -\int_{\partial^N V_a \setminus \Gamma_{BV}} \hat{\phi}_s\,\overline{i_{\mathrm{e}^-}}\,\mathrm{d}\Gamma + \int_{\partial^N V_a} \hat{\vec{u}}_a \cdot \vec{\overline{p}}_a\,\mathrm{d}\Gamma$$

is a functional on $\mathcal{V}^{[0,t_f]}$ that accounts for non-homogeneous Neumann boundary conditions as well as for the bulk terms of the balance equations.

The weak form (6.20) is written in terms of potentials rather than concentrations. Through this choice, the weak form maintains the usual physical meaning of power expenditure, which will be kept also in the weak form of the governing equations, after the specification of the constitutive equations.

6.2 Thermodynamics and constitutive theory

6.2.1 Electrolyte

Thermodynamic restrictions, formulated as in (4.26), apply. Dilute solutions accounting for saturation, under the assumption of non-interacting species will be considered

6.2.2 Electrodes

The procedure detailed in chapter 5, sections 5.3 and 5.4, while discussing about active materials applies here.

6.2.3 Interfaces

As interfaces are here assumed as mere zero-thickness discontinuity locus, with all thermodynamic interactions taking place in the electrodes and electrolyte, no thermodynamic restrictions arise for interfaces.

6.3 Governing equations.

6.3.1 Electrolyte

Governing equations can be derived as in 4.9 by incorporating the constitutive equations (4.29), (4.62) and (4.36) into balance equations (4.2). The variable fields that rule the problem, resulting from the choice made for thermodynamic prescriptions, are concentrations c_α, displacements $\vec{u}$, and the electric potential ϕ_e. Governing equations hold at all points $\vec{x} \in V_e$ at all instants:

$$\frac{\partial c_{\mathrm{Li}^+}}{\partial t} + \operatorname{div}\left[-\mathbb{D}_{\mathrm{Li}^+} \nabla [\, c_{\mathrm{Li}^+} \,] - F \,\mathbb{\mu}_{\mathrm{Li}^+} c_{\mathrm{Li}^+} \left(1 - 2\frac{c_{\mathrm{Li}^+}}{c^{max}}\right) \nabla [\, \phi_e \,] \right] = 0 \tag{6.22a}$$

$$\frac{\partial c_{\mathrm{X}^-}}{\partial t} + \operatorname{div}\left[-\mathbb{D}_{\mathrm{X}^-} \nabla [\, c_{\mathrm{X}^-} \,] + F \,\mathbb{\mu}_{\mathrm{X}^-} c_{\mathrm{X}^-} \left(1 - 2\frac{c_{\mathrm{X}^-}}{c^{max}}\right) \nabla [\, \phi_e \,] \right] = 0 \tag{6.22b}$$

$$\begin{aligned} &\operatorname{div}\left[-\mathbb{\varepsilon} \nabla \left[\frac{\partial \phi_e}{\partial t} \right] + F \left(\mathbb{D}_{\mathrm{X}^-} \nabla [\, c_{\mathrm{X}^-} \,] - \mathbb{D}_{\mathrm{Li}^+} \nabla [\, c_{\mathrm{Li}^+} \,] \right) \right] + \\ &\quad - F^2 \operatorname{div}\left[\left(\mathbb{\mu}_{\mathrm{Li}^+} c_{\mathrm{Li}^+} \left(1 - 2\frac{c_{\mathrm{Li}^+}}{c^{max}}\right) + \mathbb{\mu}_{\mathrm{X}^-} c_{\mathrm{X}^-} \left(1 - 2\frac{c_{\mathrm{X}^-}}{c^{max}}\right) \right) \nabla [\, \phi_e \,] \right] = 0 \end{aligned} \tag{6.22c}$$

$$\operatorname{div}[\, \mathbb{C} : \boldsymbol{\varepsilon} \,] = \vec{0} \tag{6.22d}$$

Initial conditions are usually imposed for concentration of ions $c_{\mathrm{Li}^+}(\vec{x}, t = 0)$ and $c_{\mathrm{X}^-}(\vec{x}, t = 0)$ in the electrolyte solution. To comply with equilibrium thermodynamics they are uniform on volume V_e; furthermore initial concentrations are equal, obeying the electroneutrality condition. Consistently, a positive constant c_{bulk} will be defined as

$$c_{bulk} = c_{\mathrm{Li}^+}(\vec{x}, t = 0) = c_{\mathrm{X}^-}(\vec{x}, t = 0) \tag{6.23}$$

and will be used to scale concentration variables henceforth.

Initial conditions for electric potential and displacements solve a boundary value problem at $t = 0$. In view of the perfect electroneutrality, at initial time Gauss law (2.8) and balance of momentum (2.11) provide the necessary and sufficient equations to be solved for ϕ_e and $\vec{u}$:

$$\operatorname{div}[\, \mathbb{\varepsilon} \nabla [\, \phi_e \,] \,] = 0 \qquad \vec{x} \in V_e,\ t = 0 \tag{6.24a}$$

$$\operatorname{div}[\, \mathbb{C} : \boldsymbol{\varepsilon} \,] = \vec{0} \qquad \vec{x} \in V_e,\ t = 0 \tag{6.24b}$$

together with homogeneous boundary conditions for current, in view of thermodynamic equilibrium at initial time, and usual given boundary conditions for displacements and tractions.

6.3.2 Electrodes

As in 5.5 governing equations will be deployed considering material parameters independent upon c_{Li} and without energetic interactions, $\chi = 0$. Governing equations can be derived by incorporating the constitutive equations (5.23), (5.28), and (5.31) into balance equations (5.1) and completed by the definition (5.32) of μ^{mech}_{Li}.
The variables that rule the problem are thus concentrations c_{Li}, displacements $\vec{u}$, the electric

potential ϕ_a, and μ_{Li}^{mech}. Governing equations hold at all points $\vec{x} \in V_a$ at all instants, and write

$$\frac{\partial c_{\mathrm{Li}}}{\partial t} + \operatorname{div}\left[-\mathbb{D}_{\mathrm{Li}} \nabla\left[c_{\mathrm{Li}} \right] \right] + \operatorname{div}\left[-\mathbb{M}_{\mathrm{Li}}(c_{\mathrm{Li}}) \nabla\left[\mu_{\mathrm{Li}}^{mech} \right] \right] = 0 \tag{6.25a}$$

$$\operatorname{div}\left[-\kappa \nabla\left[\phi_s \right] \right] = 0 \tag{6.25b}$$

$$\operatorname{div}\left[\boldsymbol{\sigma} \right] = \vec{0} \tag{6.25c}$$

$$\mu_{\mathrm{Li}}^{mech} - \overline{\mu_{\mathrm{Li}}^{mech}}(c_{\mathrm{Li}}, \boldsymbol{\varepsilon}) = 0 \tag{6.25d}$$

with $\boldsymbol{\sigma}$ defined constitutively by equations (5.28).

Boundary conditions (6.3), (6.4), (6.5), (6.6) and (6.7) are applied along Neumann boundaries $\partial^N V_a$. To ensure solvability to the problem, Dirichlet boundary conditions have to be imposed along part $\partial^D V_a$, being $\partial V_a = \partial^D V_a \cup \partial^N V_a$. Rigid body motion inhibition and zero electric potential have to be included amidst Dirichlet boundary conditions.

Initial conditions are usually imposed for concentration of neutral Lithium $c_{\mathrm{Li}}(\vec{x}, t = 0)$. To comply with equilibrium thermodynamics it is constant in volume V_a. Initial conditions for electric potential and displacements solve a boundary value problem at $t = 0$, made of equations (6.25b-c-d) together with homogeneous boundary conditions for current, in view of thermodynamic equilibrium at initial time, and usual given boundary conditions for displacements and tractions.

6.4 Weak form: complete cell

Following the same path of reasoning of sections 4.5, 4.9 and 5.5, the evolution problem can be formulated in a weak form. In Galerkin approaches weak forms are built using "variations" of the same set of variables that rule the problem, namely "virtual" concentrations $\hat{c}_{\mathrm{Li}^+}$, $\hat{c}_{\mathrm{X}^-}$, $\hat{c}_{\mathrm{Li}}$, displacements $\vec{\hat{u}}$, electric potential $\hat{\phi}$, chemical potential $\hat{\mu}_{\mathrm{Li}}^{mech}$, and Lagrange multipliers $\hat{\lambda}$. By doing so however the energy meaning of weak form (6.20) is lost. To give to the new weak form at least the physical dimension of a power expenditure, the mass balance equations and definition (5.32) will be scaled by suitable coefficients, that follow from constitutive equations. A weak form of governing equations can be given in a time interval $[0, t_f]$ as

$$\begin{aligned} &\text{Find } y(\vec{x}, t) \in \mathcal{V}^{[0,t_f]} \text{ such that} \\ &\frac{\partial}{\partial t} b\left(\hat{y}(\vec{x}), y(\vec{x}, t) \right) + a\left(\hat{y}(\vec{x}), y(\vec{x}, t) \right) = f\left(\hat{y}(\vec{x}) \right) \quad \forall \hat{y}(\vec{x}) \in \mathcal{V} \end{aligned} \tag{6.26}$$

where

$$\begin{aligned} b\left(\hat{y}, y\right) &= -\frac{RT}{c_{bulk}} \int_{V_a} \hat{c}_{\mathrm{Li}}\, c_{\mathrm{Li}} \,\mathrm{d}V - \frac{RT}{c_{bulk}} \int_{V_e} \hat{c}_{\mathrm{Li}^+}\, c_{\mathrm{Li}^+} + \hat{c}_{\mathrm{X}^-}\, c_{\mathrm{X}^-} \,\mathrm{d}V \\ &+ \oint_{V_e} \nabla\left[\hat{\phi}_e \right] \cdot \nabla\left[\phi_e \right] \mathrm{d}V + \int_{V_e} \hat{\boldsymbol{\varepsilon}} : \boldsymbol{\sigma}(\boldsymbol{\varepsilon}) \,\mathrm{d}V + \int_{V_a} \hat{\boldsymbol{\varepsilon}} : \boldsymbol{\sigma}(c_{\mathrm{Li}}, \boldsymbol{\varepsilon}) \,\mathrm{d}V \\ a\left(\hat{y}, y\right) &= -\frac{RT}{c_{bulk}} \int_{V_a} \mathbb{D}_{\mathrm{Li}} \nabla\left[\hat{c}_{\mathrm{Li}} \right] \cdot \nabla\left[c_{\mathrm{Li}} \right] \mathrm{d}V + \\ &- \frac{RT}{c_{bulk}} \int_{V_a} \mathbb{M}_{\mathrm{Li}}(c_{\mathrm{Li}}) \nabla\left[\hat{c}_{\mathrm{Li}} \right] \cdot \nabla\left[\mu_{\mathrm{Li}}^{mech} \right] \mathrm{d}V + \end{aligned}$$

$$
\begin{aligned}
&+ \quad \frac{c_{bulk}}{RT\,\Delta t}\int_{V_a} \hat{\mu}_{\mathrm{Li}}^{mech}\ \left(\mu_{\mathrm{Li}}^{mech} - \overline{\mu_{\mathrm{Li}}^{mech}}(c_{\mathrm{Li}},\boldsymbol{\varepsilon})\right)\,\mathrm{d}V \\
&- \quad \frac{RT}{c_{bulk}}\int_{V_e} \mathbb{D}_{\mathrm{Li^+}}\,\nabla\left[\,\hat{c}_{\mathrm{Li^+}}\,\right]\cdot\nabla\left[\,c_{\mathrm{Li^+}}\,\right] + \mathbb{D}_{\mathrm{X^-}}\,\nabla\left[\,\hat{c}_{\mathrm{X^-}}\,\right]\cdot\nabla\left[\,c_{\mathrm{X^-}}\,\right]\,\mathrm{d}V + \\
&- \quad \frac{RT}{c_{bulk}}\int_{V_e} F\,\mathbb{t}_{\mathrm{Li^+}}\,c_{\mathrm{Li^+}}\ \left(1-2\frac{c_{\mathrm{Li^+}}}{c^{max}}\right)\ \nabla\left[\,\hat{c}_{\mathrm{Li^+}}\,\right]\cdot\nabla\left[\,\phi_e\,\right]\mathrm{d}V + \\
&+ \quad \frac{RT}{c_{bulk}}\int_{V_e} F\,\mathbb{t}_{\mathrm{X^-}}\,c_{\mathrm{X^-}}\ \left(1-2\frac{c_{\mathrm{X^-}}}{c^{max}}\right)\ \nabla\left[\,\hat{c}_{\mathrm{X^-}}\,\right]\cdot\ \nabla\left[\,\phi_e\,\right]\mathrm{d}V + \\
&+ \quad \kappa\int_{V_a} \nabla\left[\,\hat{\phi}_s\,\right]\cdot\nabla\left[\,\phi_s\,\right]\,\mathrm{d}V + \\
&+ \quad F\int_{V_e} \nabla\left[\,\hat{\phi}_e\,\right]\cdot\left(\mathbb{D}_{\mathrm{Li^+}}\,\nabla\left[\,c_{\mathrm{Li^+}}\,\right] - \mathbb{D}_{\mathrm{X^-}}\,\nabla\left[\,c_{\mathrm{X^-}}\,\right]\right)\,\mathrm{d}V + \\
&+ \quad F^2\int_{V_e}\left(\mathbb{t}_{\mathrm{Li^+}}\,c_{\mathrm{Li^+}}\ \left(1-2\frac{c_{\mathrm{Li^+}}}{c^{max}}\right) + \mathbb{t}_{\mathrm{X^-}}\,c_{\mathrm{X^-}}\ \left(1-2\frac{c_{\mathrm{X^-}}}{c^{max}}\right)\right)\nabla\left[\,\hat{\phi}_e\,\right]\cdot\nabla\left[\,\phi_e\,\right]\,\mathrm{d}V + \\
&- \quad \int_{\Gamma_{BV}} \frac{RT}{c_{bulk}}\left(\hat{c}_{\mathrm{Li}} - \hat{c}_{\mathrm{Li^+}}\right)h_{BV}(\chi)\ -\ \left(\hat{\phi}_s - \hat{\phi}_e\right)\lambda + \frac{L}{\kappa}\,\hat{\lambda}\,\left(\lambda - F\,h_{BV}(\chi)\right)\,\mathrm{d}\Gamma \\
f\left(\hat{y}\right) \quad &= \quad -\int_{\partial^N V_a}\hat{\phi}_s\,\overline{i_{\mathrm{e^-}}}\,\mathrm{d}\Gamma + \int_{\partial^N V_a}\hat{\vec{u}}_a\ \cdot\ \vec{\bar{p}}_a\,\mathrm{d}\Gamma
\end{aligned}
$$

with list $y(\vec{x},t) = \{c_{\mathrm{Li^+}}, c_{\mathrm{X^-}}, c_{\mathrm{Li}}, \mu_{\mathrm{Li}}^{mech}, \phi_a, \phi_e, \vec{u}_a, \vec{u}_e, \lambda\,\}$. Owing to the scaling, a characteristic length L and a characteristic time Δt appear in the weak form. They will be given a neat identification in what follows. The proof descends from the same path of reasoning of the weak form for the balance equations provided in appendix 3.5 and will not be replicated.

6.5 One-dimensional modeling of an all-solid-state Li-ion battery.

6.5.1 Description

This section deals with the case study analysed in [21], namely a 10 μAh planar thin film all-solid-state Li-ion battery, also depicted in Figure 6.1. It is composed by a metallic Lithium anode, an amorphous Li_3PO_4 solid electrolyte and a $LiCoO_2$ cobaltate Lithium cathode. The sizes of each component are reported in Figure 6.3.
Several discharge rates were applied in [21] to reproduce experimental evidences. With the aim of validating the model here proposed, only a discharge rate of 51.2 C-rate is considered at temperature of 25^{o}C, with current density $I_{51.2C} = 5.12\mathrm{Am}^{-2}$.

In order to make initial and boundary conditions compatible with thermodynamic equilibrium at $t = 0$, the current $I(t)$ is tuned in time as

$$I(t) = (1 - e^{-t})\,I_{51.2C} \tag{6.27}$$

with t in seconds.

A uniform ionic flow at the interfaces is considered, enabling a 1D description. Due to charge conservation, the value of the specific current per unit area along the outer boundaries of both electrodes is given by the ratio between the current $I(t)$ flowing through the battery and the net area $A = 1 \times 10^{-2}\mathrm{m}^2$. Boundary conditions (6.5) thus read:

$$\vec{i}_{\mathrm{e^-}}\cdot\vec{n}_{an}\Big|_{\Gamma_{an}}(t) \;=\; \vec{i}_{\mathrm{e^-}}\cdot\vec{n}_{cath}\Big|_{\Gamma_{cath}}(t) \;=\; \frac{I(t)}{A} \tag{6.28}$$

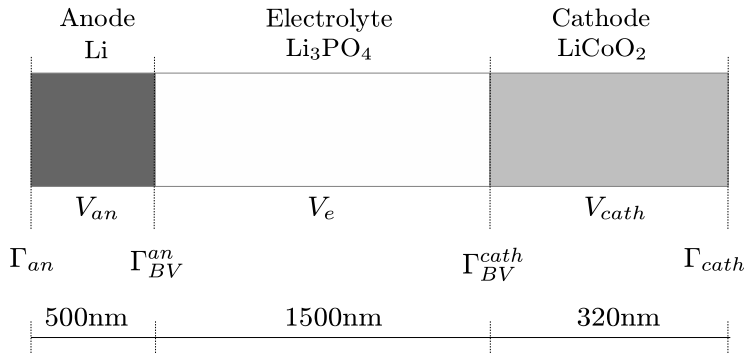

Figure 6.3: *Skematic of an all-solid-state Li-ion battery, nomenclature and dimensions.*

It is here assumed that the expansion of the battery cell is prevented, refer to Figure 6.3 for notation

$$\vec{u}^{an}(\vec{x},t) = 0 \qquad \vec{x} \in \Gamma_{an} \tag{6.29a}$$

$$\vec{u}^{cath}(\vec{x},t) = 0 \qquad \vec{x} \in \Gamma_{cath} \tag{6.29b}$$

The current collectors have not been modeled, boundary conditions (6.28) and (6.29) are used in their place.

The pure Lithium foil has been chosen as reference electrode. The electric potential in correspondence of the outer boundary has been set to zero accordingly

$$\phi_s^{an}(\vec{x},t) = 0 \qquad \vec{x} \in \Gamma_{an} \tag{6.30}$$

Initial conditions have been taken according to [21]. The cell is assumed to be in thermodynamic equilibrium and fully charged at time $t = 0$. The concentrations of both neutral and ionic Lithium across the electrodes and the electrolyte are uniform

$$c_{\mathrm{Li}}(\vec{x},0) = 4.61 \times 10^6 \,\mathrm{mol\,m^{-3}} \qquad \vec{x} \in V_{an} \tag{6.31a}$$

$$c_{\mathrm{Li^+}}(\vec{x},0) = c_{\mathrm{X^-}}(x,0) = 1.1 \times 10^4 \,\mathrm{mol\,m^{-3}} \qquad \vec{x} \in V_{el} \tag{6.31b}$$

$$c_{\mathrm{Li}}(\vec{x},0) = 1.2 \times 10^4 \,\mathrm{mol\,m^{-3}} \qquad \vec{x} \in V_{cath} \tag{6.31c}$$

It is worth pointing out that no boundary conditions have been imposed on the electrolyte domain V_e, they arise from interface conditions (6.11), (6.12), (6.13) and (6.17). This represents a difference against the inspiring work of *Danilov et al.* [21], in which a Lithium flux h_{BV} (i.e. an electric current) is imposed in correspondence of Γ_{BV}^{an} and Γ_{BV}^{cath}.

6.5.2 Material parameters and constants

Assumption is made that all processes take place at temperature $T == 298.15\mathrm{K}$. Material parameters have been taken according to [21, 48, 70, 152].

Anode

Young's modulus $E_{an} = 4.9 \times 10^9\ \mathrm{N\,m^{-2}}$, Poisson's ratio $\nu^{an} = 0,3$, Yield stress $\sigma_Y^{an} = 2.58 \times 10^8 \mathrm{N\,m^{-2}}$, $K^p = 4.0 \times 10^{10}\ \mathrm{N\,m^{-2}}$ have been used for the pure Lithium. A value $\kappa^{an} = 1.08 \times 10^7\ \mathrm{S\,m^{-1}}$ has been taken for the electric conductivity.
It is here assumed that pure Lithium is actually unaffected by the delithiation process, diffusivity[4] coefficient $\mathbb{D}_{\mathrm{Li}}^{an}$ and chemical expansion coefficient $\omega_{\mathrm{Li}}^{an}$ have been set to zero accordingly.

Cathode

Young's modulus $E_{cath} = 8 \times 10^{10}\ \mathrm{N\,m^{-2}}$, Poisson's ratio $\nu^{cath} = 0,3$, Yield stress $\sigma_Y^{cath} = 2.58 \times 10^8\ \mathrm{N\,m^{-2}}$, $K^p = 4.0 \times 10^{10}\ \mathrm{N\,m^{-2}}$ have been used for the $LiCoO_2$. A value $\kappa^{cath} = 10^4\ \mathrm{S\,m^{-1}}$ has been taken for the electric conductivity.
A diffusivity $\mathbb{D}_{\mathrm{Li}}^{cath} = 1.76 \times 10^{-15}\ \mathrm{m^2\,s^{-1}}$ and a chemical expansion coefficient $\omega_{\mathrm{Li}}^{cath} = 3.497 \times 10^{-6}\ \mathrm{m^2\,mol^{-1}}$ have been adopted.

Electrolyte

The Li_3PO_4 electrolyte is here regarded as an incompressible fluid according to the adoption of the *liquid electrolyte model*. It is then regarded as a linear elastic material characterized by a huge[5] Young's modulus. A value $\mathbb{\epsilon}^{el} = 2.25\,\mathbb{\epsilon}_0\ \mathrm{F\,m^{-1}}$ has been assumed for the electric permittivity[6].
Diffusivities amount at $\mathbb{D}_{\mathrm{Li}^+} = 0.9 \times 10^{-15}\mathrm{m^2\,s^{-1}}$, $\mathbb{D}_{\mathrm{X}^-} = 5.1 \times 10^{-15}\mathrm{m^2\,s^{-1}}$.

6.5.3 Adimensional weak form: complete cell

Weak form (6.26) can be transformed in a first order ODE in time if discretization is performed via separated variables, with spatial test $\varphi_i(x)$ and shape functions $\varphi_j(x)$ and nodal unknowns (collectively gathered in column y with component $y_j(t)$) that depend solely on time. A dimensionless expression is derived by making fields in list $y(x,t)$ quantity of dimension one via suitable scaling factors, namely:

$$c_\alpha^* = \frac{c_\alpha}{c_{bulk}}, \qquad \mu_{\mathrm{Li}}^{mech*} = \frac{\mu_{\mathrm{Li}}^{mech}}{RT}, \qquad \phi^* = \frac{F}{RT}\,\phi, \qquad \vec{u}^* = \frac{\vec{u}}{L}, \qquad \lambda^* = \frac{L}{\kappa}\,\frac{F}{RT}\,\lambda, \quad (6.32)$$

The star superscript is omitted for the sake of readability. The usual Einstein convention of sum is taken henceforth.

A one-dimensional domain is considered, nevertheless integration boundaries will be identified by V, ∂V and Γ to easily recognize different domains. Explicit distinction should be made among anode and cathode, but this would require the introduction of further terms in

[4]The opposite strategy has been adopted in numerical analyses. Being the goal to have the Lithium concentration unaffected by the delithiation process, an extremely large value (theree order of magnitudes larger than the ones used for other components) has been adopted. In this way a sort of steady state distribution is always achieved.

[5]From a numerical point of view, a *sufficiently large* number compared with the Young's modulus of the other components.

[6]The same value was used in section 4.6

the weak form. In order to avoid introduction of additional terms, both the electrodes and the material parameters related to them will be identified with subscript $_a$. Subscript $_e$ will denote material parameters that refer to the electrolyte.

Within the one-dimensional setting, equations (5.27) and (5.32) specify as follows:

$$\sigma_a = E_a \left(\frac{\partial u}{\partial x} - \varepsilon^p - \omega_a \, c_{\mathrm{Li}} \right) \tag{6.33a}$$

$$\overline{\mu_{\mathrm{Li}}^{mech}}_{\,a} = - E_a \, \omega_a \left(\frac{\partial u}{\partial x} - \varepsilon^p - \omega_a \, c_{\mathrm{Li}} \right) \tag{6.33b}$$

The shape functions referring to ϕ_s and ϕ_e will be identified by φ^{ϕ_s} and φ^{ϕ_e} along the interface Γ_{BV}, where both the electric potentials are present. They will shortly be denoted by φ^{ϕ} elsewhere, since the connection either to ϕ_s or ϕ_e should be apparent from the context.

In the present section, the effect of saturation has not been taken into account for any of the components.

The non linear ODE reads:

$$\text{Find } y(t) \text{ such taht} \qquad b_i^* \cdot \frac{\partial y}{\partial t}(t) + a_i^*[\, y(t) \,] = f_i^*(t) \qquad \text{for } i = 1, 2, ..., N \tag{6.34}$$

where

$$\begin{aligned}
\frac{b_i^*}{RT \; c_{bulk}} \cdot \frac{\partial y}{\partial t}(t) = & - \int_{V_a} \varphi_i^{\mathrm{Li}} \; \varphi_j^{\mathrm{Li}} \, \mathrm{d}V \; \frac{\partial c_j^{\mathrm{Li}}}{\partial t} + \\
& - \int_{V_e} \varphi_i^{\mathrm{Li}^+} \; \varphi_j^{\mathrm{Li}^+} \, \mathrm{d}V \; \frac{\partial c_j^{\mathrm{Li}^+}}{\partial t} - \int_{V_e} \varphi_i^{\mathrm{X}^-} \; \varphi_j^{\mathrm{X}^-} \, \mathrm{d}V \; \frac{\partial c_j^{\mathrm{X}^-}}{\partial t} + \\
& + \frac{\not{\varepsilon}}{c_{bulk}} \; \frac{RT}{F^2} \; \int_{V_e} \frac{\partial \varphi_i^{\phi}}{\partial x} \, \frac{\partial \varphi_j^{\phi}}{\partial x} \, \mathrm{d}V \; \frac{\partial \phi_j^e}{\partial t} + \\
& + \frac{E_e \, L^2}{RT c_{bulk}} \; \int_{V_e} \frac{\partial \varphi_i^{u}}{\partial x} \, \frac{\partial \varphi_j^{u}}{\partial x} \, \mathrm{d}V \; \frac{\partial u_j}{\partial t} + \\
& + \frac{L^2}{RT c_{bulk}} \; \int_{V_a} \frac{\partial \varphi_i^{u}}{\partial x} \, \frac{1}{L} \, \frac{\partial \sigma(c_{\mathrm{Li}}, \varepsilon)}{\partial t} \, \mathrm{d}V
\end{aligned}$$

$$\begin{aligned}
\frac{a_i^*[\, y(t) \,]}{RT \; c_{bulk}} = & - \mathbb{D}_{\mathrm{Li}} \; \int_{V_a} \frac{\partial \varphi_i^{\mathrm{Li}}}{\partial x} \, \frac{\partial \varphi_j^{\mathrm{Li}}}{\partial x} \, \mathrm{d}V \; c_j^{\mathrm{Li}} + \\
& - \mathbb{D}_{\mathrm{Li}} \; \int_{V_a} \varphi_j^{\mathrm{Li}} \, \frac{\partial \varphi_i^{\mathrm{Li}}}{\partial x} \, \frac{\partial \varphi_k^{\mu}}{\partial x} \, \mathrm{d}V \; c_j^{\mathrm{Li}} \, \mu_k^{mech} + \\
& + \frac{1}{\Delta t} \; \int_{V_a} \varphi_i^{\mu} \; \varphi_j^{\mu} \, \mathrm{d}V \; \mu_j^{mech} + \\
& - \frac{1}{\Delta t} \; \int_{V_a} \varphi_i^{\mu} \; \overline{\mu_{\mathrm{Li}}^{mech}}(c_{\mathrm{Li}}, \varepsilon) \, \mathrm{d}V + \\
& - \mathbb{D}_{\mathrm{Li}^+} \; \int_{V_e} \frac{\partial \varphi_i^{\mathrm{Li}^+}}{\partial x} \, \frac{\partial \varphi_j^{\mathrm{Li}^+}}{\partial x} \, \mathrm{d}V \; c_j^{\mathrm{Li}^+} + \\
& - \mathbb{D}_{\mathrm{Li}^+} \; \int_{V_e} \varphi_j^{\mathrm{Li}^+} \, \frac{\partial \varphi_i^{\mathrm{Li}^+}}{\partial x} \, \frac{\partial \varphi_k^{\phi}}{\partial x} \, \mathrm{d}V \; c_j^{\mathrm{Li}^+} \, \phi_k^e +
\end{aligned}$$

$$
\begin{aligned}
&- \mathbb{D}_{\mathrm{X}^-} \int_{V_e} \frac{\partial \varphi_i^{\mathrm{X}^-}}{\partial x} \frac{\partial\, \varphi_j^{\mathrm{X}^-}}{\partial x} \,\mathrm{d}V\; c_j^{\mathrm{X}^-} \;+ \\
&+ \mathbb{D}_{\mathrm{X}^-} \int_{V_e} \varphi_j^{\mathrm{X}^-} \frac{\partial \varphi_i^{\mathrm{X}^-}}{\partial x} \frac{\partial \varphi_k^{\phi}}{\partial x} \,\mathrm{d}V\; c_j^{\mathrm{X}^-}\; \phi_k^e \;+ \\
&+ \frac{RT\,\kappa}{c_{bulk}\,F^2} \int_{V_a} \frac{\partial \varphi_i^{\phi}}{\partial x} \frac{\partial \varphi_j^{\phi}}{\partial x} \,\mathrm{d}V\; \phi_j^s \;+ \\
&+ \mathbb{D}_{\mathrm{Li}^+} \int_{V_e} \frac{\partial \varphi_i^{\phi}}{\partial x} \frac{\partial \varphi_k^{\phi}}{\partial x}\, \varphi_j^{\mathrm{Li}^+} \,\mathrm{d}V\; c_j^{\mathrm{Li}^+}\; \phi_k^e \;+ \\
&+ \mathbb{D}_{\mathrm{Li}^+} \int_{V_e} \frac{\partial \varphi_i^{\phi}}{\partial x} \frac{\partial \varphi_j^{\mathrm{Li}^+}}{\partial x} \,\mathrm{d}V\; c_j^{\mathrm{Li}^+} \;+ \\
&+ \mathbb{D}_{\mathrm{X}^-} \int_{V_e} \frac{\partial \varphi_i^{\phi}}{\partial x} \frac{\partial \varphi_k^{\phi}}{\partial x}\, \varphi_j^{\mathrm{X}^-} \,\mathrm{d}V\; c_j^{\mathrm{X}^-}\; \phi_k^s \;+ \\
&- \mathbb{D}_{\mathrm{X}^-} \int_{V_e} \frac{\partial \varphi_i^{\phi}}{\partial x} \frac{\partial \varphi_j^{\mathrm{X}^-}}{\partial x} \,\mathrm{d}V\; c_j^{\mathrm{X}^-} \;+ \\
&- \frac{1}{c_{bulk}} \int_{\Gamma_{BV}} \varphi_i^{\mathrm{Li}}\, h_{BV}(\chi) \,\mathrm{d}\Gamma + \frac{1}{c_{bulk}} \int_{\Gamma_{BV}} \varphi_i^{\mathrm{Li}^+}\, h_{BV}(\chi) \,\mathrm{d}\Gamma \;+ \\
&+ \frac{RT\kappa}{F^2\, c_{bulk}\, L} \int_{\Gamma_{BV}} \varphi_i^{\phi_s}\, \varphi_j^{\lambda} \,\mathrm{d}\Gamma\; \lambda_j \;- \frac{RT\kappa}{F^2\, c_{bulk}\, L} \int_{\Gamma_{BV}} \varphi_i^{\phi_e}\, \varphi_j^{\lambda} \,\mathrm{d}\Gamma \;+\; \lambda_j \\
&- \frac{RT\kappa}{F^2\, c_{bulk}\, L} \int_{\Gamma_{BV}} \varphi_i^{\lambda}\, \varphi_j^{\lambda} \,\mathrm{d}\Gamma\; \lambda_j \;+ \frac{1}{c_{bulk}} \int_{\Gamma_{BV}} \varphi_i^{\lambda}\, h_{BV}(\chi) \,\mathrm{d}\Gamma
\end{aligned}
$$

$$
\frac{f_i^*(t)}{RT\; c_{bulk}} = - \frac{1}{c_{bulk}\, F} \int_{\partial^N V_a} \varphi_i^{\phi}\, \overline{i_{\mathrm{e}^-}} \,\mathrm{d}\Gamma \;+ \frac{L}{RT\, c_{bulk}} \int_{\partial^N V_a} \varphi_i^{u}\, \frac{\partial \bar{p}_a}{\partial t} \,\mathrm{d}\Gamma +
$$

Note that h_{BV}, $\bar{p}$ and $\overline{i_{\mathrm{e}^-}}$ have not been scaled.

Form $a_i^*[y(t)]$ is clearly non-linear. The novelties with respect to discrete weak forms derived previous chapters (refer to sections 4.6.2, 4.10.1, 4.13.2 and 5.9) are represented by inelastic deformation ε^p and the boundary term h_{BV}, which is not given for the problem at hand.

J_2 *plasticity* is standard argument in solid mechanics and will not be detailed here. The *radial return* technique have been used for implementation, the reader may refer to [145, 153] for details.

The term h_{BV} depends on the electric potential discontinuity

$$
\xi \;= \phi_s \;- \;\phi_e \tag{6.35}
$$

across the electrode/electrolyte interface and on the Nernst potential ξ^{Nernst}, equation (6.9). The latter is generally not constant, it depends on the *state of charge* (SOC), i.e. number of charges measured per unit area identified by $\natural$, which represents the amount of charge that crosses the electrode/electrolyte interface in correspondence of a specific location, during a charge and discharge processes [21]. In this example, the location is unique because of the one-dimensional feature.

As the Lithium metal anode is used as ground electrode the open circuit potential ξ^{Nernst} in correspondence of the Γ_{BV}^{an} is set to zero [48, 132].

A relation between ξ^{Nernst} and the SOC $\natural$ has been experimentally determined by *Danilov et al.* [21] for the Γ_{BV}^{cath} interface. The outcomes of those experimental fitting are depicted in Figure 6.4 and have been used in the numerical computations at hand.

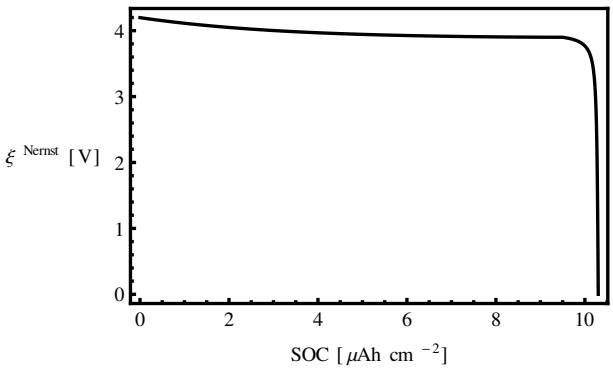

Figure 6.4: *Experimental fitting of the relation among ξ^{Nernst} and the state of charge $\natural$ [21].*

By pursuing the same path of reasoning used in section 4.6.2, backward Euler scheme has been selected as time-advancing method for the numerical simulations that follow.

Search $y(t+\Delta t)$ such that

$$b_i^* \cdot \frac{y(t+\Delta t)}{\Delta t} + {}^l a_i^* \cdot y(t+\Delta t) \; + {}^n a_i^*[\, y(t+\Delta t)\,] = \; f_i^*(t+\Delta t) + b_i^* \cdot \frac{y(t)}{\Delta t} \tag{6.36}$$

after having decomposed $a_i^*[y(t)]$ in the linear ${}^l a_i^* \cdot y(t)$ and non-linear ${}^n a_i^*[\, y(t+\Delta t)\,]$ forms.

By defining the generic component of ${}^n a_i^*[\, y(t+\Delta t)\,]$ containing the term h_{BV} as follows:

$$n_i^{BV}[y(t+\Delta t)] = \int_{\Gamma_{BV}} \varphi_i \; h_{BV}\,(\chi)\,\mathrm{d}\Gamma \tag{6.37}$$

the correspondent contribution to Newton-Raphson strategy of the form (4.53) reads:

$$\begin{aligned}
&\frac{\mathrm{d}}{\mathrm{d}\epsilon} n_i^{BV}[\, {}^{\mathfrak{q}}y(t+\Delta t) + \epsilon\,\delta y\,]\Big|_{\epsilon=0} = \\
&\quad = \frac{\mathrm{i}_0}{L^2} \int_{\Gamma_{BV}} \varphi_i \left\{ (1-\beta)\, \exp\left[(1-\beta) \left({}^{\mathfrak{q}}\xi^* - \frac{F}{RT}\, \xi^{Nernst}\,(t+\Delta t) \right) \right] + \right. \\
&\qquad \left. + \beta\, \exp\left[-\beta \left({}^{\mathfrak{q}}\xi^* - \frac{F}{RT}\, \xi^{Nernst}\,(t+\Delta t) \right) \right] \right\} \left(\varphi_k^{\phi_s}\; {}^{\mathfrak{q}}\delta\phi_k^{s\,*} - \varphi_m^{\phi_e}\; {}^{\mathfrak{q}}\delta\phi_m^{e\,*} \right) \mathrm{d}\Gamma
\end{aligned} \tag{6.38}$$

where

$${}^{\mathfrak{q}}\xi^* = \left(\varphi_k^{\phi_s}\; {}^{\mathfrak{q}}\phi_k^{s*} \right) - \left(\varphi_k^{\phi_e}\; {}^{\mathfrak{q}}\phi_k^{e*} \right) - \xi^{Nernst}\left(\natural(t+\Delta t) \right) \tag{6.39}$$

and ${}^{\mathfrak{q}}\phi_k^{s*}$, ${}^{\mathfrak{q}}\phi_k^{e*} \in {}^{\mathfrak{q}}y$ according to section 4.6.3.
In order to avoid additional iterations, ξ^{Nernst} has been calculated using the value of $\natural$ at the beginning of the Newton-Raphson loop, and has been kept constant for the whole time step.

The numerical technique (4.53) that refers to problem (6.34) have been implemented in a Wolfram Mathematica package script.

Several dimensionless groups arise that numerically connote the multi-physics processes concurrently taking place. The parameters expected to rule the stability of the numerical solution are:

$$\gamma_\alpha = \frac{\Delta t\, D_\alpha}{L^2}\,, \qquad \gamma_{bulk} = \omega_{\mathrm{Li}} c_{bulk}\,, \quad \gamma_{\phi_1} = \frac{r_D}{L}\,, \qquad \gamma_{\phi_2} = \frac{\kappa\, \Delta t}{\mathfrak{f}}\,,$$
$$\gamma_{BV_1} = \frac{\mathrm{i}_0}{\kappa}\,\frac{F}{RT}\,L\,, \qquad \gamma_{BV_2} = \frac{\mathrm{i}_0}{c_{bulk} F}\,\frac{\Delta t}{L}\,, \qquad \gamma_\sigma = \frac{K\,\omega_{\mathrm{Li}}}{RT}\,,$$

r_D being the Debye length defined in (2.19).

6.5.4 Simulation: complete cell

Several simulations have been carried out with different time steps and number of elements. The outcomes here reported refer to finite elements of equal length $L = 10^{-8}$m (50 elements for the anode, 150 for the electrolyte ad 32 for the cathode) and a constant time step $\Delta t = 0.01$ s. The value $c^{an}_{bulk} = 11000\mathrm{mol\,m^{-3}}$ has been used for adimensionalization (6.32) for all the components.
The simulation was ended at time $t_f = 90$s. The steady state is not achieved for high discharge rate as the one at hand, 51.2 C-rate. The amount of charge transferred at the interface Γ^{cath}_{BV} is such that the open circuit potential collapse, Figure 6.4, and the electric current flow is suddenly interrupted.

The Lithium concentration distribution obtained from the numerical analyses is given in Figure 6.5 for all the components of the battery. Two different pictures overlap in that representation.
In the first graph the concentration ranges from 0 to roughly $4 \times 10^6\mathrm{mol\,m^{-3}}$. This allows to appreciate the huge difference in Lithium content between the pure Lithium anode and the other components. Within the latter the concentration seems to lie along the x-coordinate. The neutral Lithium concentration in anode is unchanged with respect to the initial value $c_{\mathrm{Li}}(\vec{x}, 0) = 4.61 \times 10^6\,\mathrm{mol\,m^{-3}}$.
In the second part the concentration ranges from 0 to $3.5 \times 10^4\mathrm{mol\,m^{-3}}$, which means it is two orders of magnitude smaller then the previous. This allows to appreciate the time evolution of Lithium distribution, both ionic and neutral, within the electrolyte and the cathode (the anode concentration content is out of the range of the plot) and the jump across the Γ^{cath}_{BV} interface. As expected, the concentration profiles depart from the initial uniform values of $c_{\mathrm{Li}^+}(\vec{x}, 0) = 1.1 \times 10^4\,\mathrm{mol\,m^{-3}}$ and $c_{\mathrm{Li}}(\vec{x}, 0) = 1.2 \times 10^4\,\mathrm{mol\,m^{-3}}$ toward non-uniform distributions. The time evolution is in good agreement with data published in [21], Figure 12.

Figure 6.6 depicts the electric potential and its evolution in time. Linear distribution of ϕ develops in both the electrodes (difficult to appreciate due to the small gradient) according to the assumption of *conductive materials*. The electric potential discontinuity (6.35), apparent between electrolyte and cathode, arises at both interfaces Γ^{an}_{BV} and Γ^{cath}_{BV}. The galvanostatic regime imposes, through equations (6.10) and (6.14), that the overpotential (6.9) has to be constant in one-dimensional processes. This implies that the discontinuity (6.35) has to follow the evolution of ξ^{Nernst}, which can be envisaged from the time evolution of ϕ_s along the cathode. The latter reproduces in fact the trend of Figure 6.4, being the time parametrization of Figure 6.6 correspondent to a constant time step.

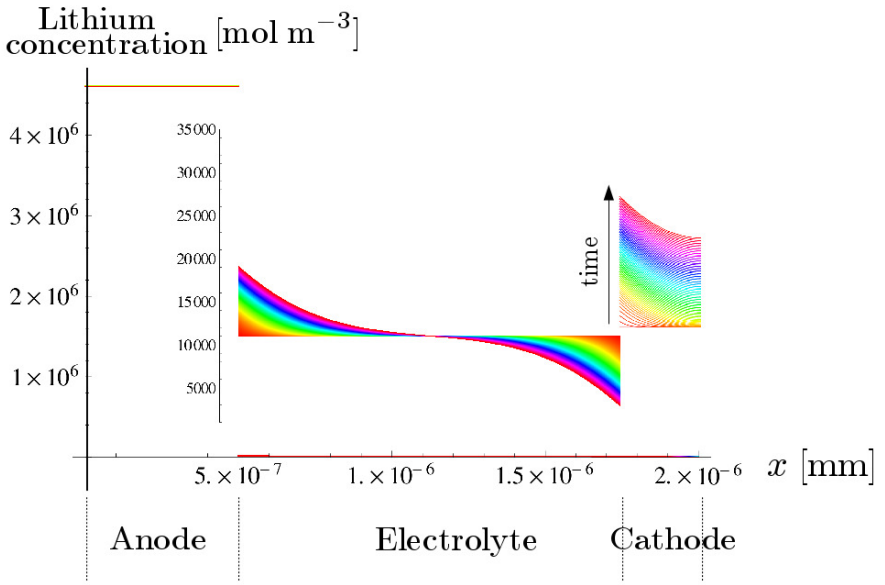

Figure 6.5: *Lithium concentration distribution paramaterized in time along the solid-state battery. Two different intervals are depicted for the concentratio-axis. The range* 0 *to* $4\times10^6\,\mathrm{mol\,m^{-3}}$ *refers to all the components; the range* 0 *to* $3.5\times10^4\,\mathrm{mol\,m^{-3}}$ *is restricted to electrolyte and the cathode. The x-axis is shared.*

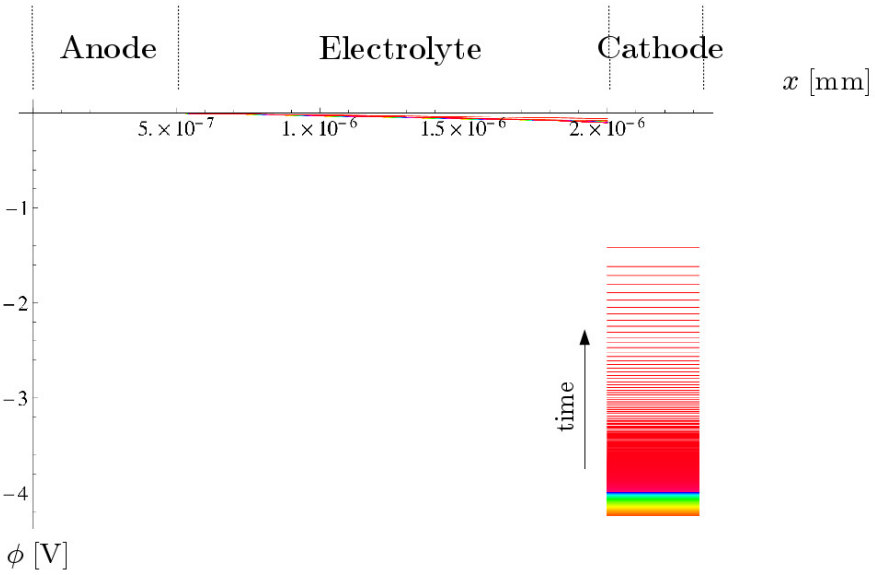

Figure 6.6: *Plot of the electric potential* ϕ *parametrized in time along the solid-state battery.*

Displacements and stresses are plotted in Figure 6.7 and 6.8 respectively. Due to the hypothesis made, refer to section 6.5.2, the chemo-mechanical coupling only affects the cathode. The constrained swelling, Figure 6.7, of the $LiCoO_2$ under lithiation give rise to compression stresses in both the electrodes, Figure 6.8, in agreement with the assumption of incompressible electrolyte. Since the latter has been modeled as a rigid body no stresses arise.
The outcomes of the numerical analyses show that no plastic deformation develops being the achieved values of stresses far below the yield stress σ_Y.

No comparison are available for the mechanical part, not investigated by *Danilov et al.* [21].

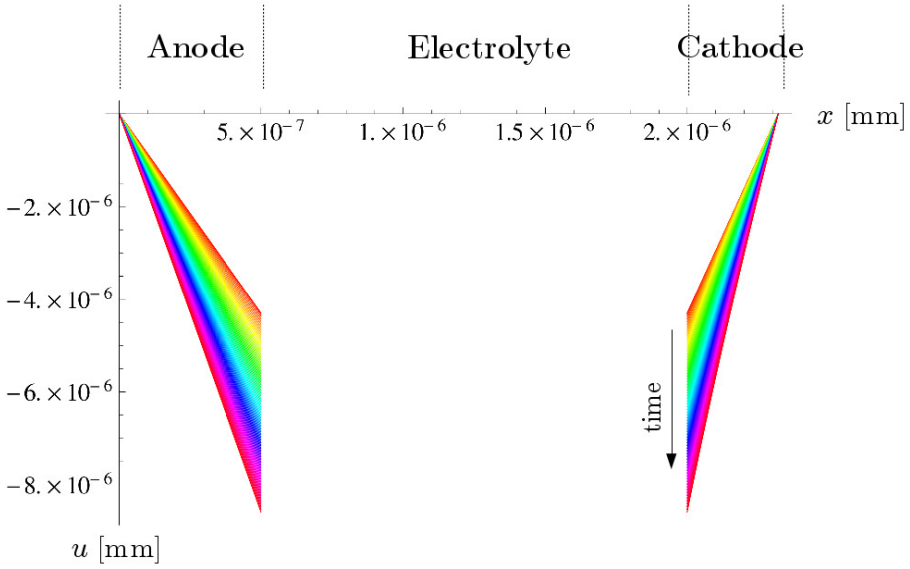

Figure 6.7: *Plot of the displacement u parametrized in time along the solid-state battery.*

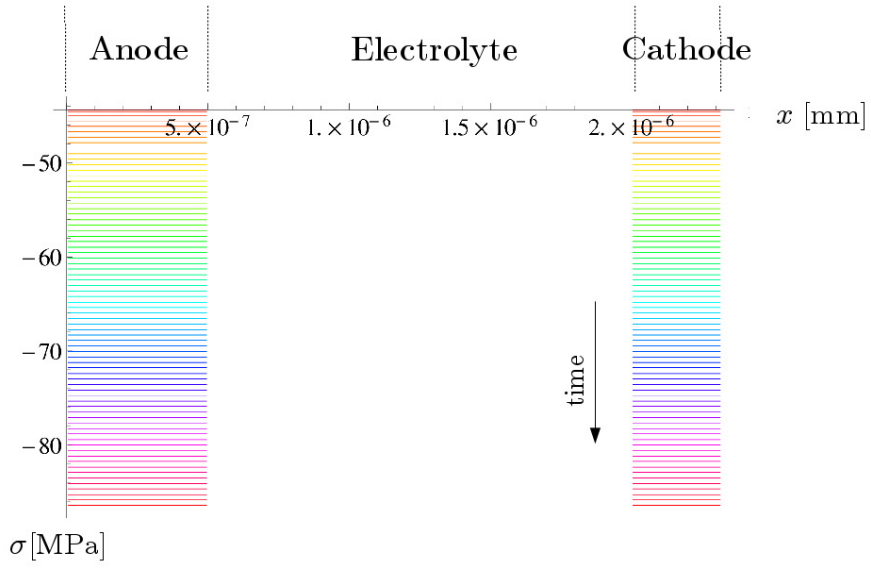

Figure 6.8: *Plot of the stresses σ parametrized in time along the solid-state battery.*

6.5.5 Remarks

In this chapter the microscale formulation proposed within the framework of a multiscale computational homogenization approach has been validated. Capacitive effects have been explicitly taken in to account via the electro-quasi-static formulation. The electroneutrality

assumption and Maxwell's laws have been used to describe the electric field. Electroneutrality has been taken into account to neglect Lorentz forces, whereas the influence of the charge effect in the solution has not been disregarded.
The set of balance equation of section 3.2.1, completed by proper constitutive theory (chapters 4 and 5) leaded to the numerical algorithm detailed in 6.5. The latter has been implemented in a Wolfram Mathematica package script and used to simulate the study case of an all-solid-state battery [21]. The outcomes of the numerical analyses, section 6.5.4, show that the multiphase model developed for porous electrodes, chapter 3, well reproduces the behavior of each component of the cell and their interactions. The processes affecting the all-solid-state battery during a single discharge process are cached by the simulations, denoting the robustness of the approach. Comparison with the results of [21] are satisfactory.

For future development, the possibility to extend the numerical analyses to more general problems (2D or 3D geometries, more complex material behavior, SEI formation) is envisaged.
The possibility to extend the approach to multiscale numerical analyses is guaranteed by the energetic meaning of the weak form. Some preliminary results of multiscale computational homogenization applied to Li-ion battery will be showed in chapter 7.

Part III

Ongoing research

Chapter 7
Toward multiscale numerical analyses

Processes in Li-ion batteries electrodes are modeled with the partial differential equations setting of diffusion-migration-intercalation problems and their mechanical coupling. This appears a new challenge for the computational homogenization technique, whose application to multi-physics problems does not represent a novelty [98–102].

Due to the lack of time, coupled two-scales computational homogenization analyses have not been carried out within this work. The (numerical) relations between the macroscopic input and output variables, particularly the tangent "stiffnesses" to be inserted in each incremental step of the Newton-Raphson scheme (7.7), have not been provided here. In principle they can be determined following the usual approach of the computational homogenization scheme: the reader may for instance refer to the one proposed in [98, 99] for thermo-mechanical analysis of heterogeneous solids.

A first step toward multiscale numerical analyses for batteries has been made and is described in this last chapter. The framework concerning liquid electrolyte, exposed in chapter 4, has been further applied to a two-dimensional problem to investigate the micro structural behavior of a multi-phase separator. Boundary conditions descend from the scale transition conditions (as detailed in section 3.4.1) peculiar of computational homogenization formulation for batteries [8, 9].
Concentrations and electric potential profiles, resulting from the numerical analyses, are reported in section 7.2. A strong influence of the geometry is observed from the results, in particular at the interface between fluid electrolyte and the separator membrane, suggesting that microscopic investigations might be crucial for a deep understanding of the overall battery behavior and its failure mechanisms, in line with recent experimental investigations [154].

7.1 Computation procedures

7.1.1 Discretization

The macroscale weak form can be written in the following semi-discrete approximated form

$$\begin{aligned} &\text{Find } y_h^M \in \mathcal{V}_h^{[0,T]} \text{ such that} \\ &\quad \frac{\mathrm{d}}{\mathrm{d}t} b\left(\hat{y}_h^M, z_h^M(t)\right) + a(\hat{y}_h^M, y_h^M(t)) = f(\hat{y}_h^M, t) \quad \forall \hat{y}_h^M \in \mathcal{V}_h \ , \ t \in (0,T) \end{aligned} \tag{7.1}$$

with $z^M = \{c^M_{\mathrm{Li}},\, c^M_{\mathrm{e}^-},\, c^M_{\mathrm{Li}^+},\, c^M_{\mathrm{X}^-}\}$, $y^M = \{\mu^M_{\mathrm{Li}}, \mu^M_{\mathrm{e}^-}, \mu^M_{\mathrm{Li}^+}, \mu^M_{\mathrm{X}^-}, \phi^M_s, \phi^M_e, \vec{u}^M\}$ and $y_h^M(0) = y_h^0$ an approximation of the initial datum. As for the weak forms of chapters 4, 5 and 6 the Galerkin approximation is adopted using as $\mathcal{V}_h$ the classical finite element space.

As motivated in section 3.1.2, the problem at hand requires concurrent time evolution across scales. An ODE in time have to be addressed for the microscale as well. The semi-discrete weak form reads:

$$\begin{aligned}&\text{Find } y_h^m \in \mathcal{V}_h^{[0,T]} \text{ such that}\\ &\quad \frac{\mathrm{d}}{\mathrm{d}t} b^m\left(\hat{y}_h^m, z_h^m(t)\right) + a(\hat{y}_h^m, y_h^m(t)) = f(\hat{y}_h^m, t) \quad \forall \hat{y}^m \in \mathcal{V}_h \ , \ t \in (0,T)\end{aligned} \tag{7.2}$$

with $z^m = \{c^m_{\mathrm{Li}},\, c^m_{\mathrm{e}^-},\, c^m_{\mathrm{Li}^+},\, c^m_{\mathrm{X}^-}\}$, $y^m = \{\mu^m_{\mathrm{Li}}, \mu^m_{\mathrm{e}^-}, \mu^m_{\mathrm{Li}^+}, \mu^m_{\mathrm{X}^-}, \phi^m_s, \phi^m_e, \vec{u}^m, \lambda^m\}$ and $\mathcal{V}_h$ the classical finite element space.

7.1.2 Time advancing by finite differences

A family of time-advancing methods based on the so-called θ-scheme can be built for the macroscale discrete problem (7.1).

$$\begin{aligned}&\frac{1}{\Delta t}\, b\left(\hat{y}_h^M, z_h^M(t+\Delta t) - z_h^M(t)\right) \,+\, a(\hat{y}_h^M,\, \theta\, y_h^M(t+\Delta t) \,+\, (1-\theta) y_h^M(t)) =\\ &\quad =\, \theta\, f(\hat{y}_h^M, t+\Delta t) +\, (1-\theta)\, f(\hat{y}_h^M, t) \quad \forall \hat{y}_h^M \in \mathcal{V}_h\end{aligned} \tag{7.3}$$

where $0 \leq \theta \leq 1$, $\Delta t = T/N$ is the time step, N is a positive integer and $y_h^0 \in \mathcal{V}_h$ is a suitable approximation of the initial datum. This includes the forward Euler scheme ($\theta = 0$), backward Euler ($\theta = 1$), and Crank-Nicolson ($\theta = 1/2$).

7.1.3 Newton-Raphson scheme

Depending on the constitutive assumptions, equations (7.2) and (7.3) can be non linear in y_h^m, y_h^M respectively, which is the usual case (see chapters 4, 5 and 6). Equation (7.3) may be solved by means of the Newton Raphson iterative method. Define function $g(y_h^M(t+\Delta t))$ as

$$\begin{aligned}&g(y_h^M(t+\Delta t)) =\\ &\quad = \frac{1}{\Delta t}\, b\left(\varphi_j, z_h^M(t+\Delta t) - z_h^M(t)\right) \,+\, a(\varphi_j,\, \theta\, y_h^M(t+\Delta t) \,+\, (1-\theta) y_h^M(t)) =\\ &\quad =\, \theta\, f(\varphi_j, t+\Delta t) +\, (1-\theta)\, f(\varphi_j, t)\end{aligned} \tag{7.4}$$

$\{\varphi_j | j = 1, ..., N_h\}$ being a basis for $\mathcal{V}_h$. Equation (7.3) reads

$$g(y_h^M(t+\Delta t)) = 0 \tag{7.5}$$

$$l_i \,\cdot\, \delta y \,+\, \frac{\mathrm{d}}{\mathrm{d}\epsilon} n_i[\, {}^{\mathtt{q}}y(t+\Delta t) + \epsilon\, \delta y\,]\Big|_{\epsilon=0} = \xi_i - l_i \,\cdot\, {}^{\mathtt{q}}y(t+\Delta t) \,+ n_i[\, {}^{\mathtt{q}}y(t+\Delta t)\,] \tag{7.6}$$

and the Newton Raphson iterative scheme in an abstract formalism can be obtained by making recourse to the notion of Gateaux derivative. Taking $\epsilon \in \mathbb{R}$ it reads:

$$g\Big({}^{\mathtt{q+1}}y_h^M(t+\Delta t)\Big) = g\Big({}^{\mathtt{q}}y_h^M(t+\Delta t)\Big) + \frac{\mathrm{d}}{\mathrm{d}\epsilon}\, g\Big({}^{\mathtt{q}}y_h^M(t+\Delta t) + \epsilon\, \delta y_h^M\Big)\Big|_{\epsilon=0} = 0 \tag{7.7}$$

to be solved for increment $\delta y_h^M = {}^{\mathtt{q+1}}y_h^M(t+\Delta t) - {}^{\mathtt{q+1}}y_h^M(t)$ iteratively until its norm is sufficiently small (refer to section 4.6.3). Within the computational homogenization procedure, the macroscopic Cauchy stress, mass fluxes, and electric fields are recovered from the numerical solution of the micro-scale problem (7.2) by means of micro to micro scale transitions (3.58). The Newton-Raphson iteration (7.7) requires macroscopic tangents. Their consistent derivation can be achieved in analogy with the scheme proposed in [98, 99] for thermo-mechanical analysis of heterogeneous solids.

7.2 Two-dimensional modeling of ionic transport in a solid electrolyte

A one dimensional mathematical description is generally accepted for the separator consistent with the geometry of the battery, which intrinsically dictates such an overall behavior. Such a geometrical description represents reality only in an average sense under adequate circumstances. The porous separator of an electrolytic cell is in fact a multi-phase structure that includes a network of interconnected and irregular pores and channels [155]. One-dimensional models can neither capture the underlying microstructure nor detail the processes that take place at such a scale. They are not capable, for instance, to model failure in the separator, where micro-structural events initiate damage and eventually lead to macroscopic short circuit. As the integrity of the separator is vital to the performance and safety of batteries [53, 54] multiscale approaches may be helpful in performing stress anayses, in particular, computational homogenization can be a useful tool to describe the separator pore network [54].

7.2.1 Description

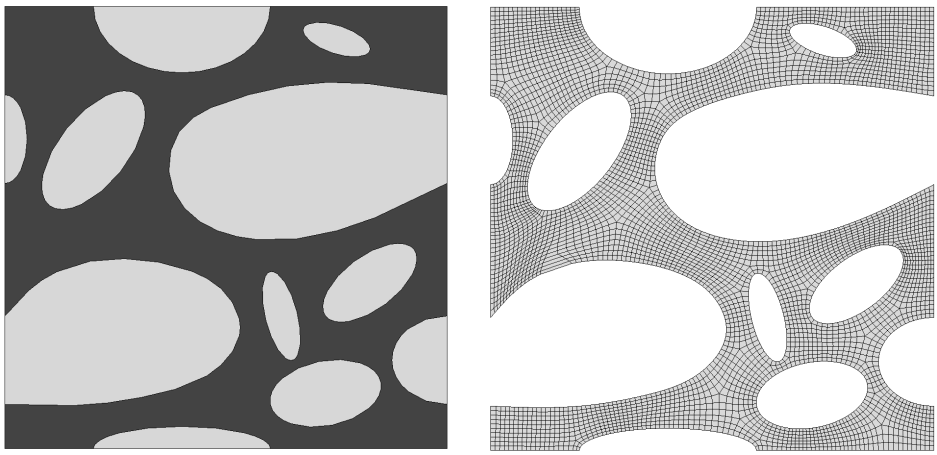

Figure 7.1: *Microscopic RVE (5μm edge) and its discretization with 4600 elements adopted in the numerical analysis. Two phases are considered, namely the electrolyte (dark gray) and the polymeric separator (light gray).*

Following the typical path of reasoning of computational homogenization (section 1.3.1), any point of the macroscale is related to its underlying microstructure through a properly defined RVE, see section 3.1.1. Numerical outcomes based on a two dimensional RVE, assumed to be the microscopic counterpart of the 1D separator of section 4.6.1, will be shown. The RVE, whose edges are 5μm long, is depicted in Figure 7.1. Two phases have been considered: a liquid electrolyte (dark gray) and a polymeric porous membrane (light gray). Temperature and material parameters of the electrolyte are taken from section 4.6.1. Since the polymeric membrane does not contribute to ionic transport, boundary conditions refer to the electrolyte only. Moreover, the following conditions apply along the *electrolyte/polymer interface*, denoted with Γ_{int}:

$$\vec{h}_{\mathrm{X}^-} \cdot \vec{n} \Big|_{\Gamma_{int}} (t) = \vec{h}_{\mathrm{Li}^+} \cdot \vec{n} \Big|_{\Gamma_{int}} (t) = 0 \tag{7.8}$$

Boundary conditions apply along the edges of the RVE occupied by the electrolyte $\partial V_{RVE} \cap \partial V_e$ and read:

$$c_{\mathrm{Li^+}}(\vec{x},t) = \nabla\left[\, c^M_{\mathrm{Li^+}} \,\right](t)\cdot(\vec{x}-\vec{x}_G) + c^M_{\mathrm{Li^+}}(t) \qquad \vec{x}\in\partial V_{RVE}\cap\partial V_e \tag{7.9a}$$

$$c_{\mathrm{X^-}}(\vec{x},t) = \nabla\left[\, c^M_{\mathrm{X^-}} \,\right](t)\cdot(\vec{x}-\vec{x}_G) + c^M_{\mathrm{X^-}}(t) \qquad \vec{x}\in\partial V_{RVE}\cap\partial V_e \tag{7.9b}$$

$$\phi_e(\vec{x},t) = \nabla\left[\, \phi^M_e \,\right](t)\cdot(\vec{x}-\vec{x}_G) + \phi^M_e(t) \qquad \vec{x}\in\partial V_{RVE}\cap\partial V_e \tag{7.9c}$$

They arise from scale transitions conditions (3.48), with concentrations c_α used in place of electrochemical potentials $\bar{\mu}_\alpha$. ∂V_{RVE} and ∂V_e represents the edges of the whole RVE (identified with V_{RVE}) and the boundary of the electrolyte domain (identified with V_e) respectively; vector $\vec{x}$ identifies the position of a generic point inside the RVE, while the centroid of the RVE is denoted with $\vec{x}_G$. Apex ^{M} defines quantities descending from the macroscale, namely the outcomes of section 4.6. Since macro and micro scale evolutions are concurrent in time (see section 3.1.2), any generic instant t coincides at both scales.

Figure 7.2 reports the evolution of concentrations and electric potential ϕ_e in time, evaluated macroscopically at point $x = 0.05$ mm - see Figure 4.1. In the same way, time evolution of $\nabla[\,c\,]$ and $\nabla[\,\phi_e\,]$ are depicted in Figure 7.2.

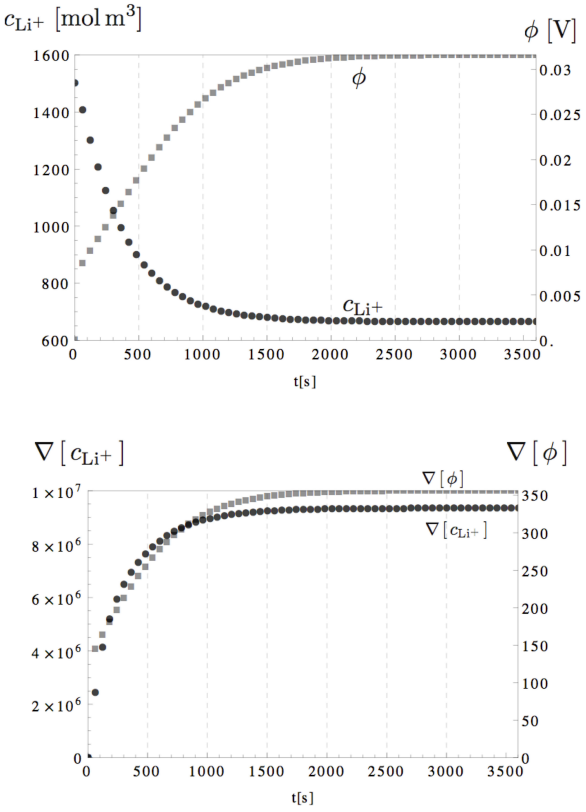

Figure 7.2: *Development of concentration c_{Li^+} (circles) and electric potential ϕ (squares in the left plot), as well as of concentration gradient $\nabla[\,c_{Li^+}\,]$ (circles) and electric potential gradient $\nabla[\,\phi\,]$ (squares in the right plot) experienced by the macroscopic point at the coordinate $x = 0.05$ mm. The values are the outcome of the numerical analysis discussed in section 4.6.*

Discretization and time advancing can be achieved as in section 4.6.2. The numerical algorithm implemented for 2D domain is detailed in appendix 4.16.

7.2.2 Simulations

The *Newton-Raphson* iterative scheme (4.53) has been implemented in an Abaqus User Element script.

Results refer to the mesh shown in Figure 7.1. To be consistent with the boundary conditions (7.9) and time history, Figure 7.2 refers to simulations with $\Delta t = 60$s. A homogeneous electric potential, and a constant concentration equal to c_{bulk} have been imposed at $t = 0$. According to Figure 7.2 the boundary conditions become steady after a few time steps, and similarly the values of the field inside the RVE evolve until their own steady state condition is approached. Figure 7.3 show concentrations and electric potential distributions at time $t = 3600$ s, once the steady state is reached.

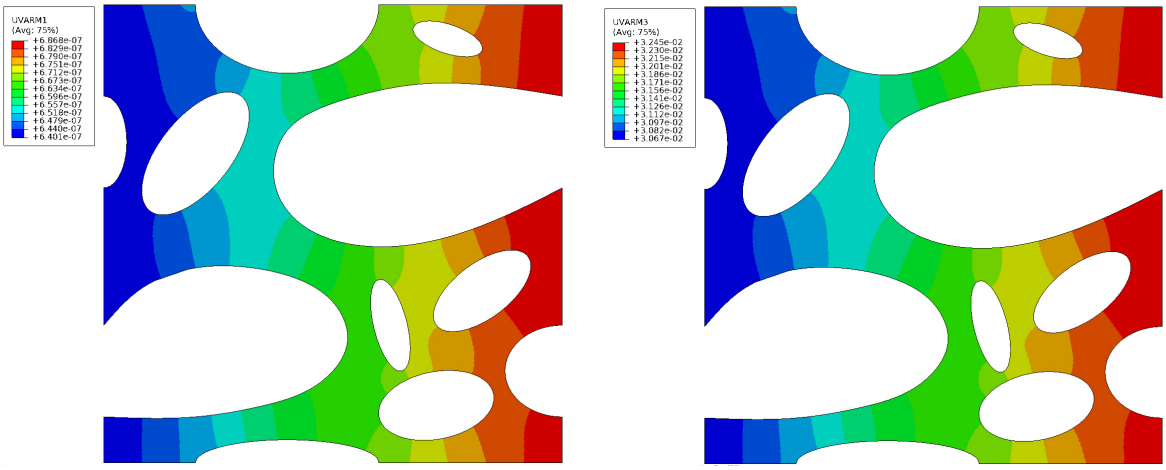

Figure 7.3: *Microscale ionic concentration c_{Li^+} and electric potential ϕ distribution at steady state ($t =$ 3600s) in the electrolyte.*

7.2.3 Remarks

To avoid the complexity of the non-uniform intercalation within each active particle of electrodes, it is customary in literature to restrict the analysis to one-dimensional problems, eventually focusing to nanowires [65], thin films [67], or to a single active particle without modeling the surrounding material and phenomena; neither the electrolyte nor the interface reaction are directly considered, but the electrochemical interactions are replaced by "a priori" given incoming flux, often claiming for axialsymmetry.

The numerical simulations here carried out evidence that the presence of holes in the geometry strongly influences the results. The profile of concentrations at the interface between electrolyte and separator is dictated by the macro scale and by the local microstructure, and it is hardly possible either to envisage any special symmetry or to predict the interface conditions "a priori". Similar results are expected for particles in the electrodes. These outcomes strengthen the conceptual framework of the multi scale approach that permeates this thesis, namely that performance of Li batteries strongly depends on the interaction between micro and nano-scale phenomena.

Chapter 8
Conclusions

A two-scale modeling of several electrochemical and mechanical processes that take place during charging/discharging cycles in Li-ion battery electrodes has been dealt with in the part I of the present thesis. The performance of batteries relies on the interaction between micro and nano-scale phenomena, in particular within the electrodes. Mechanical effects induced by cyclic lithiation/delithiation, as swelling and the consequent eventual mechanical failure, arise at the level of the nano-sized active particles. Unfortunately, modeling a single battery cell at such a scale is at present unfeasible, because of the huge computational cost. Therefore, nano-scale effects have to be incorporated into a multi-scale strategy, through averaging techniques and constitutive models that are derived from homogenization methods.

In this work a computational homogenization formulation has been proposed adopting a continuum approach at both scales. Capacitive effects have been explicitly taken into account via the *electro-quasi-static* formulation. Electroneutrality has been considered as an approximation towards the solution. The error introduced on the balance laws by ignoring the charge separation has been investigated, concluding that Lorentz forces can reasonably be neglected, whereas the influence of the charge effect on the solution should not be disregarded.

At the macro-scale, electrodes have been modeled as porous continua, whereas at the micro level they have been described as heterogeneous and multiphase media. Length and time scales have been investigated in section 3.1.

As established by Suquet [32], the basic concepts of computational homogenization consist in determining the microscopic boundary conditions from the macroscopic input variables (macro-to-micro transition) as well as in recovering the macroscopic output variables from the microstructural RVE solution (micro-to-macro transition). The latter scale transition, in mechanics named after Hill-Mandel, has been extensively reformulated for the multi-physics processes taking place in batteries. In order to keep the usual physical interpretation of power expenditure, which is a key concept in the multi scale approach, the variational framework here outlined selects potentials rather than concentrations as independent fields in the modelization. The procedure itself is independent on the constitutive laws at the micro-scale, provided that thermodynamic restrictions discussed in chapters 4 and 5 are satisfied and that the microscopic boundary value problem admits a unique solution.
Differently from [8], the steady-state mass and charge transport assumption that was taken at the microscale has been removed and the scale transitions are elaborated for a time dependent formulation. As a result, the internal expenditure of virtual power of mechanical forces, of charge and mass fluxes is completely preserved in the scale transition.

The second part of the thesis has been devoted to the validation of the microscale formulation. Electrolyte and active material modeling have been detailed separately in chapters 4 and 5 respectively. A whole cell has been considered in chapters 6.

Conductivity for binary ionic salts dissolved in non convective solutions has been investigated. Whereas two coupled parabolic equations are largely used in the literature to model the diffusion process, it is common to use electroneutrality condition (2.21) to model migration phenomena. The resulting electric field can be described by analytical expressions [10] but it is not constrained in any way to satisfy Maxwell's equations. This is a fundamental inherent paradox which is *not often acknowledged* according to [7].

In solving the Nernst-Planck equations, one determines the effect of the electric field, which only arises in the presence of a net charge separation. Yet, to determine the electric field by means of the electroneutrality condition, the approximation of zero charge separation is made, thus removing the cause of the electric field itself.

Besides this fundamental inconsistency, it has to be pointed out that methods based on electroneutrality formulate the problem in terms of the electric field. The overpotential, namely an integral estimation from the electric field, is usually the most valuable information one seeks. Reconstructing the potential from the electric field, especially in 2D or 3D, may be not straightforward and accurate.

In this contribution the electric potential is a primary variable and is evaluated directly in the numerical simulations.

Diffusion and migration have been described constitutively by means of Fick's law, established rigorously from general principles of non-equilibrium thermodynamics. The resulting governing equations have been expressed in a weak form that is physically equivalent to a power expenditure, in terms of the thermodynamic variables (concentrations, displacements, and the electric potential). The discrete counterpart of the weak form can be numerically solved via finite differences in time and finite elements in space, provided that suitable algorithms are used to handle the resulting non-linear system.

The weak form (4.3) is three-dimensional in nature, i.e. no 1D character influences the modeling at all as the 2D simulation provided in section 7.2 testifies. Nevertheless, one dimensional models can be formulated as a restriction of the general framework, as for the example shown in section 4.6.

Computations, based on Backward Euler and Newton Raphson schemes, show that the proposed methodology is efficient and reliable. Outcomes match the ones derived in [10].

The *assumption of ideal solutions far from saturation* has also been investigated. In the further hypothesis that concentrations are too high to neglect the role of saturation but still sufficiently low to exclude incomplete dissociation of the Li-salt. This conjecture is confirmed indeed by the data and the numerical simulations on real batteries.

Constitutive specification detailed in section 4.8 accounts for the saturation contribution. By comparing it with the mass flux constitutive equation adopted in [128], here formula (4.34), one notices that saturation has no effect on the diffusivity. Under the assumption of electroneutrality, it can be assessed that saturation does not impact the concentration profiles either. Indeed, the electroneutrality condition (2.21) is well approximated during the simulations and the influence of saturation on the concentration profiles is actually negligible.

Saturation does affect the electric potential in view of the mass flux equation (4.62) because it acts as to modify the ionic mobility, in turn inducing a higher potential gradient in the carried out simulations. Figures 4.13-4.14 confirm that the saturation may increase the electric potential by about 40% near the cathode for all C-rates. Saturation impacts by a similar magnitude in the internal entropy production, as conveyed in Figure 4.16.
In conclusion, saturation appears to be an unavoidable feature in a multi scale and multi

physics approach to battery modeling [8, 9]. Furthermore, the fully three-dimensional formulation that was proposed in [128] and the numerical algorithms that emanate from the weak form established therein have shown to be robust and capable to include the new constitutive specifications required to take into account of the saturation.

The ionic transport model has finally been reshaped on solid-electrolytes. Conservation laws (4.2) have been modified in section 4.11.1 to account for the Li^+ ions generated or consumed by ionization reaction acting as a rate controller. This results in a mass supply within the mass balance equation for ionic species.
Constitutive specification that include the saturation contribution are still suitable and have been used to complete the set of governing equations in section 4.8.
Numerical simulations show good agreement between the approach chosen by [21] and the one at hand.

Active particles have been treated as a binary Larche-Cahn system composed by the hosting material filled with Lithium and the free interstitial lattice material. The swelling effect induced by the presence of the Li concentration is accounted for by a constitutive coupling between Lithium chemical potential and stress tensor through the first invariant.
Active particles have been regarded as conductive material, Ohm's law has been used in place of differential Ampère law (2.14) accordingly.
The constitutive theories considered may appear simplistic with respect to the most up to date literature. The choice was consciously taken to perform a validation within a complex multiscale/multiphysics framework. More realistic theories will be adopted in future works inspired by [81, 148], strengthened by analogies with Hydrogen diffusion modeling.
The numerical algorithm descending form weak form (5.36) leads to satisfactory results when compared to the available analytical solutions, see 5.9.3.

The set of balance equations describing the microscale of a porous electrode, section 3.2.1, has been completed with constitutive theories detailed in chapters 4 and 5. The governing equations led to the numerical algorithm detailed in section 6.5. It has been used to simulate the study case of an all-solid-state battery [21]. The outcomes of the numerical analyses in terms of Lithium concentration profiles are compatible with the results of [21] despite the use of a liquid electrolyte model.

The computational homogenization technique presented here may provide a significant contribute to the multi physics simulation in the fundamental area of the mechanics of energy storage materials. If it will reach a sufficient maturity and robustness, the scheme can be attractive even for battery makers companies, interested in capturing a significant part of the expected strong increase in demand of Li-ion batteries.
The 2D numerical simulations carried out in section 7.2 constitute a significant step towards the 3D multi scale modeling of Li-ion batteries. Even if a fully coupled two-dimensional implementation has not been attained during this work, the potentiality of the method is envisaged and dependence of Li batteries performance on the interaction between micro and nano-scale phenomena highlighted.

Bibliography

[1] B. Scrosati and J. Garche. Lithium batteries: status, prospects and future. *Journal of Power Sources*, 195:2419–2430, 2010.

[2] A. Mukhopadhyay and B.V. Sheldon. Deformation and stress in electrode materials for Li-ion batteries. *Progress in material science*, 63:58–116, 2014.

[3] D. Datta, Junwen L., K. Nikhil, and B. S. Vivek. Enhanced lithiation in defective graphene. *Carbon*, 80:305–310, 2014.

[4] L. Luo, J. Wu, J. Luo, J.and Huang, and V.P. Dravid. Dynamics of electrochemical lithiation/delithiation of graphene-encapsulated silicon nanoparticles studied by in-situ tem. *Scientific Reports*, 4:1–4, 2014.

[5] A. Salvadori and D. Grazioli. Computer simulation for battery design and lifetime prediction. In B. Scrosati, J. Garche, and W. Tillmetz, editors, *Advances in battery technologies for electric road and off-road vehicles*, chapter 19. Woodhead Publishing, 2015.

[6] J. Newman and K.E. Thomas-Alyea. *Electrochemical systems*. John Wiley and Sons B.V., 2004.

[7] Dickinson E.J.F., Limon-Petersen J.G., and Compton R.G. The electroneutrality approximation in electrochemistry. *J Solid State Electrochem*, 15:1335–1345, 2011.

[8] A. Salvadori, E. Bosco, and D. Grazioli. A computational homogenization approach for Li-ion battery cells. Part 1 - Formulation. *Journal of the Mechanics and Physics of Solids*, 65:114–137, 2014.

[9] A. Salvadori, D. Grazioli, and M.G.D. Geers. Governing equations for a two-scale analysis of li-ion battery cells. submitted for publication in International Journal of Solids and Structures.

[10] D. Danilov and P.H.L. Notten. Mathematical modeling of ionic transport in the electrolyte of li-ion batteries. *Electrochimica Acta*, 53:5569–5578, 2008.

[11] A.J Bard and L.R. Faulkner. *Electrochemical Methods: Fundamentals and Applications*. Wiley, 2 edition, 2000.

[12] Huggins R.A. *Advanced Batteries: Materials Science Aspects*. Springer, 2010.

[13] Landau L.D., Pitaevskii L.P., and Lifshitz E.M. *Electrodynamics of Continuous Media*, volume 8 of *Course of Theoretical Physics*. Elsevier, 2nd edition, 1984.

[14] Larsson J. Electromagnetics from a quasistatic perspective. *Am. J. Phys.*, 75(3):230–239, 2007.

[15] F. Larche and J.W. Cahn. A linear theory of thermochemical equilibrium under stress. *Acta Metallurgica*, 21:1051–1063, 1973.

[16] M.E. Gurtin, E. Fried, and L. Anand. *The Mechanics and Thermodynamics of Continua*. Cambridge University Press, 2010.

[17] A. Kovetz. *The principles of electromagnetic theory*. Cambridge University Press, 1989.

[18] De Groot S.R. and Mazur P. *Non-Equilibrium Thermodynamics*. Dover, 1984.

[19] DeHoff R. *Thermodynamic in material science*. CRC Press - Taylor and Francis, 2006.

[20] L. Anand. A cahn-hilliard-type theory for species diffusion coupled with large elastic-plastic deformations. *Journal of the Mechanics and Physics of Solids*, 60(12):1983–2002, 2012.

[21] D. Danilov, R.A.H. Niessen, and P.H.L. Notten. Modeling all-solid-state li-ion batteries. *Journal of The Electrochemical Society*, 158(3):A215–A222, 2011.

[22] M. Armand and J.M. Tarascon. Building better batteries. *Nature*, 451:652–657, 2008.

[23] V.A. Sethuraman, M.J. Chon, M. Shimshak, V. Srinivasan, and P.R. Guduru. In situ measurements of stress evolution in silicon thin films during electrochemical lithiation and delithiation. *Journal of Power Sources*, 195:5062–5066, 2010.

[24] V.A. Sethuraman, N. Van Winkle, D.P. Abraham, A.F. Bower, and P.R. Guduru. Real-time stress measurements in lithium-ion battery negative electrodes. *Journal of Power Sources*, 206:334–342, 2012.

[25] J. W. Wang, Y. He, F. Fan, X.H. Liu, S. Xia, Y. Liu, C.T. Harris, H. Li, J.Y. Huang, S.X. Mao, and T. Zhu. Two-phase electrochemical lithiation in amorphous silicon. *Nano Letters*, 13(2):709–715, 2013.

[26] Matthew T. McDowell, Seok Woo Lee, Justin T. Harris, Brian A. Korgel, Chongmin Wang, William D. Nix, and Yi Cui. In situ tem of two-phase lithiation of amorphous silicon nanospheres. *Nano Letters*, 13(2):758–764, 2013.

[27] S. Kalnaus, K. Rhodes, and C. Daniel. A study of li-ion intercalation induced fracture of silicon particles used as anode material in li-ion battery. *Journal of Power sources*, 196:8116–8124, 2011.

[28] M. Doyle, T.F. Fuller, and J. Newman. Modeling of galvanostatic charge and discharge of the lithium/polymer/insertion cell. *J. Electrochem. Soc.*, 140:1526–1533, 1993.

[29] J. Marcicki, A.T. Conlisk, and G. Rizzoni. A lithium-ion battery model including electrical double layer effects. *Journal of Power Sources*, 125:157–169, 2014.

[30] M.G.D. Geers, V.G. Kouznetsova, and Brekelmans W.A.M. Multi-scale computational homogenization: trends and challenges. *Journal of Computational and Applied Mathematics*, 234:2175–2182, 2010.

[31] V.G. Kouznetsova, W.A.M. Brekelmans, and F.P.T. Baaijens. An approach to micro-macro modeling of heterogeneous materials. *Computational Mechanics*, 27:37–48, 2001.

[32] P.M. Suquet. Local and global aspects in the mathematical theory of plasticity. In A. Sawczuk and G. Bianchi, editors, *Plasticity today: modeling, methods and applications*, pages 279–310. Elsevier Applied Science Publishers, London, 1985.

[33] C. Miehe, J. Schroder, and J. Schotte. Computational homogenization analysis in finite plasticity. simulation of texture development in polycrystalline materials. *Computer Methods in Applied Mechanics and Engineering*, 171:387–418, 1999.

[34] F. Feyel and J.L. Chaboche. FE^2 multiscale approach for modelling the elastovis-coplastic behaviour of long fibre SiC/Ti composite materials. *Computer Methods in Applied Mechanics Engineering*, 183:309–330, 2000.

[35] K. Terada, M. Hori, T. Kyoya, and N. Kikuchi. Simulation of the multi-scale convergence in computational homogenization approaches. *International Journal of Solids and Structures*, 37(16):2285–2311, 2000.

[36] M. Mosby and K. Matous. Hierarchically parallel coupled finite strain multiscale solver for modeling heterogeneous layers. *International Journal for Numerical Methods in Engineering*, 2014.

[37] S. Ghosh, K. Lee, and S. Moorthy. Multiple scale analysis of heterogeneous elastic structures using homogenisation theory and voronoi cell finite element method. *International Journal of Solids and Structures*, 32(1):27–62, 1995.

[38] J.C. Michel, Moulinec H., and P. Suquet. Effective properties of composite materials with periodic microstructure: a computational approach. *Computer Methods in Applied Mechanics and Engineering*, 172:109–143, 1999.

[39] T.R. Ferguson and M.Z. Bazant. Nonequilibrium thermodynamics of porous electrodes. *Journal of The Electrochemical Society*, 159(12):A1967–A1985, 2012.

[40] J.M. Tarascon and M. Armand. Issues and challenges facing rechargeable lithium batteries. *Nature*, 414:359–367, 2001.

[41] R. Van Noorden. The rechargeable revolution: A better battery. *Nature*, 507:26–28, 2014.

[42] T. Georgi-Maschlera, B. Friedricha, R. Weyheb, H. Heegnc, and M. Rutzc. Development of a recycling process for Li-ion batteries. *Journal of Power Sources*, 207:173–182, 2012.

[43] A. Barré, B. Deguilhem, S. Grolleau, M. Gérard, F. Suard, and D. Riu. A review on lithium-ion battery ageing mechanisms and estimations. *Journal of Power sources*, 241:680–689, 2013.

[44] S. Allu, S. Kalnaus, W. Elwasif, S. Simunovic, J.A. Turner, and S. Pannala. A new open computational framework for highly-resolved coupled three-dimensional multiphysics simulations of Li-ion cells. *Journal of Power Sources*, 246:876–886, 2014.

[45] G. Bauer, V. Gravemeier, and W.A Wall. A 3D finite element approach for the coupled numerical simulation of electrochemical systems and fluid flow. *International Journal for Numerical Method in Engineering*, 86:1339–1359, 2011.

[46] G. Bauer, V. Gravemeier, and W.A Wall. A stabilized finite element method for the numerical simulation of multi-ion transport in electrochemical systems. *Computer Methods in Applied Mechanics and Engineering*, 223-224:199–210, 2012.

[47] S. Golmon, K. Maute, and M.L. Dunn. A design optimization methodology for Li^+ batteries. *Journal of Power Sources*, 253:239–250, 2014.

[48] R.T. Purkayastha and R.M. McMeeking. An integrated 2-d model of a lithium ion battery: the effect of material parameters and morphology on storage particle stress. *Computational Mechanics*, 50:209–227, 2012.

[49] R.E. Garcia, Y.M. Chiang, W.C. Carter, P. Limthongkul, and C.M. Bishop. Microstructural modeling and design of rechargeable lithium-ion batteries. *Journal of The Electrochemical Society*, 152:255–263, 2005.

[50] S. Golmon, K. Maute, and M.L. Dunn. Numerical modeling of electrochemical-mechanical interactions in lithium polymer batteries. *Computer and Structures*, 87:1567–1579, 2009.

[51] S. Golmon, K. Maute, and M.L. Dunn. Multiscale design optimization of lithium ion batteries using adjoint sensitivity analysis. *Int. J. Numer. Methods Eng.*, 92:475–494, 2012.

[52] M.Z. Bazant, K.T. Chu, and B.J. Bayly. Current-voltage relations for elecrochemical thin films. *SIAM Journal of Applied Mathematics*, 65:1463–1484, 2005.

[53] W. Wu, X. Xiao, X. Huang, and S. Yan. A multiphysics model for the in situ stress analysis of the separator in a lihium-ion battery cell. *Computational Materials Science*, 83:127–136, 2014.

[54] X. Xiao, W. Wu, and X. Huang. A multi-scale approach for the stress analysis of polymeric separators in a li-ion battery. *Journal of Power Sources*, 195:7649–7660, 2010.

[55] J. Christensen and J. Newman. Stress generation and fracture in lithium insertion materials. *Journal of Solid State Electrochemistry*, 10:293–319, 2006.

[56] V.A. Sethuraman, V. Srinivasan, A. F. Bower, and P.R. Guduru. In situ measurements of stress-potential coupling in lithiated silicon. *Journal of The Electrochemical Society*, 157:1253–1261, 2010.

[57] X.H. Liu, L. Zhong, S. Huang, S.X. Mao, T. Zhu, and J.Y. Huang. Size-dependent fracture of silicon nanoparticles during lithiation. *ACS Nano*, 6:1522–1531, 2012.

[58] K. Zhao, M. Pharr, S. Cai, J.J. Vlassak, and Z. Suo. Large plastic deformation in high-capacity lithium-ion batteries caused by charge and discharge. *J. Am. Ceram. Soc.*, 94(S1):S226–S235, 2011.

[59] Y.T. Cheng and M.W. Verbrugge. Evolution of stress within a spherical insertion electrode particle under potentiostatic and galvanostatic operation. *Journal of Power Sources*, 190:453–460, 2009.

[60] Y.T. Cheng and M.W. Verbrugge. Diffusion-induced stress, interfacial charge transfer, and criteria for avoiding crack initiation of electrode particles. *Journal of the Electrochemical Society*, 4:508–516, 2010.

[61] S. Huang, F. Fan, J. Li, S. Zhang, and T. Zhu. Stress generation during lithiation of high-capacity electrode particles in lithium ion batteries. *Acta Materiala*, 61:4354–4364, 2013.

[62] X.H. Liu, H. Zheng, L. Zhong, S. Huang, K. Karki, L.Q. Zhang, Y. Liu, A. Kushima, W.T. Liang, J.W. Wang, J.H. Cho, E. Epstein, S.A. Dayeh, S.T. Picraux, T. Zhu, J. Li, J.P. Sullivan, J. Cumings, C. Wang, S.X. Mao, Z.Z. Ye, S. Zhang, and J.Y. Huang. Anisotropic swelling and fracture of silicon nanowires during lithiation. *Nano Letters*, 11:3312–3318, 2011.

[63] X.H. Liu, J.W. Wang, S. Huang, F. Fan, X. Huang, Y. Liu, S. Krylyuk, J. Yoo, S.A. Dayeh, A.V. Davydov, S.X. Mao, S.T. Picraux, S. Zhang, J. Li, T. Zhu, and J.Y. Huang. In situ atomic-scale imaging of electrochemical lithiation in silicon. *Nature Nanotechnology*, 7:749–756, 2012.

[64] R. Deshpande, Y.T. Cheng, and M.W. Verbrugge. Modeling diffusion-induced stress in nanowire electrode structures. *Journal of Power Sources*, 195:5081–5088, 2010.

[65] I. Ryu, J. W. Choi, Y. Cui, and W.D. Nix. Size-dependent fracture of si nanowire battery anodes. *Journal of the Mechanics and Physics of Solids*, 59:1717–1730, 2011.

[66] T.K. Bhandakkar and H. Gao. Cohesive modeling of crack nucleation under diffusion induced stresses in a thin strip: Implications on the critical size for flaw tolerant battery electrodes. *International Journal of Solids and Structures*, 47:1424–1434, 2010.

[67] G. Bucci, S.P.V. Nadimpalli, V.A. Sethuraman, A.F. Bower, and P.R. Guduru. Measurement and modeling of the mechanical and electrochemical response of amorphous Si thin film electrodes during cyclic lithiation. *Journal of the Mechanics and Physics of Solids*, 62:276–294, 2014.

[68] S.P.V. Nadimpalli, V.A. Sethuraman, G. Bucci, V. Srinivasan, A.F. Bower, and P.R. Guduru. On plastic deformation and fracture in si films during electrochemical lithiation/delithiation cycling. *Journal of The Electrochemical Society*, 160:A1885–A1893, 2014.

[69] V.A. Sethuraman, M.J. Chon, M. Shimshak, M. Van Winkle, and P.R. Guduru. In situ measurement of biaxial modulus of Si anode for Li-ion batteries. *Electrochemistry Communications*, 12:1614–1617, 2010.

[70] X. Zhang, W. Shyy, and A.M. Sastry. Numerical simulation of intercalation-induced stress in Li-ion battery electrode particles. *Journal of the Electrochemical Society*, 154:A910–A916, 2007.

[71] Yang F. Interaction between diffusion and chemical stresses. *Materials Science and Engineering A*, 409:153–159, 2005.

[72] Li J.C.M. Physical chemistry of some microstructural phenomena. *Metallurgical Transaction*, 9A:1353–1380, 1978.

[73] K.E. Aifantis and J.P. Dempsey. Stable crack growth in nanostructured Li-batteries. *Journal of Power Sources*, 143:203–211, 2005.

[74] J.Y. Huang, L. Zhong, C.M. Wang, J.P. Sullivan, W. Xu, L.Q. Zhang, S.X. Mao, N.S. Hudak, X.H. Liu, A. Subramanian, L. Fan, H.and Qi, A. Kushima, and J. Li. In situ observation of the electrochemical lithiation of a single SnO_2 nanowire electrode. *Science*, 330:1515–1520, 2010.

[75] A.F. Bower and P.M. Guduru. A simple finite element model of diffusion, finite deformation, plasticity and fracture in lithium ion insertion electrode materials. *Modelling Simul. Mater. Sci. Eng.*, 20, 2012.

[76] Z. Cui, F. Gao, and J. Qu. Interface-reaction controlled diffusion in binary solids with applications to lithiation of silicon in lithium ion batteries. *Journal of the Mechanics and Physics of Solids*, 61:293–310, 2013.

[77] Suo Z. Brassart L., Zhao K. Cyclic plasticity and shakedown in high-capacity electrodes of lithium-ion batteries. *International Journal of Solids and Structures*, 50:1120–1129, 2013.

[78] M.J. Chon, V.A. Sethuraman, A. McCormick, V. Srinivasan, and P.R. Guduru. Real-time measurement of stress and damage evolution during initial lithiation of crystalline silicon. *Physical Review Letters*, 107:045503, 2011.

[79] K. Zhao, M. Pharr, Q. Wan, W.L. Wang, E. Kaxiras, J.J. Vlassak, and Z. Suoa. Concurrent reaction and plasticity during initial lithiation of crystalline silicon in Lithium-ion batteries. *Journal of The Electrochemical Society*, 159:A238–A243, 2012.

[80] Drozdov A. Viscoplastic response of electrode particles in li-ion batteries driven by insertion of lithium. *Int. Journal of Solids and Structures*, 51:690–705, 2014.

[81] Drozdov A.D. A model for the mechanical response of electrode particles induced by lithium diffusion in li-ion batteries. *Acta Mech.*, 225:2987–3005, 2014.

[82] A.H.M. Krom, R.W.J Koers, and A. Bakker. Hydrogen transport near a blunting crack tip. *Journal of the Mechanics and Physics of Solids*, 47:971–992, 1999.

[83] C. Di Leo and L. Anand. Hydrogen in metals: a coupled theory for species diffusion and large elastic-plastic deformations. *International Journal of Plasticity*, 2013.

[84] J. Zhang, B. Lu, Y. Song, and X. Ji. Diffusion induced stress in layered Li-ion battery electrode plates. *Journal of Power Sources*, 209:220–227, 2012.

[85] E. Sahraei, R. Hill, and T. Wierzbicki. Calibration and finite element simulation of pouch lithium-ion batteries for mechanical integrity. *Journal of Power Sources*, 201:307–321, 2012.

[86] T. Wierzbicki and E. Sahraei. Homogenized mechanical properties for the jellyroll of cylindrical lithium-ion cells. *Journal of Power Sources*, 241:467–476, 2013.

[87] E. Sahraei, J. Meier, and T. Wierzbicki. Characterizing and modeling mechanical properties and onset of short circuit for three types of lithium-ion pouch cells. *Journal of Power Sources*, 247:503–516, 2014.

[88] C.H. Hamann, A. Hamnett, and W. Vielstich. *Electrochemistry*. Wiley, 2007.

[89] P.M. Biesheuvel, M. van Soestbergenb, and M.Z. Bazant. Imposed currents in galvanic cells. *Electrochimica Acta*, 54:4857–4871, 2009.

[90] S. Renganathan, G. Sikha, S. Santhanagopalan, and R. E. White. Theoretical analysis of stresses in a lithium ion cell. *Journal of The Electrochemical Society*, 157:155–163, 2010.

[91] T.S. Dao, C.P. Vyasarayani, and J. McPhee. Simplification and order reduction of lithium-ion battery model based on porous-electrode theory. *Journal of Power Sources*, 198:329–337, 2012.

[92] I. Streeter and R.G. Compton. Numerical simulation of potential step chronoamperometry at low concentrations of supporting electrolyte. *The Journal of Physical Chemistry*, 112:13716–13728, 2008.

[93] M. Nie, D. Chalasani, D.P. Abraham, Y. Chen, A. Bose, and B.L. Lucht. Lithium ion battery graphite solid electrolyte interphase revealed by microscopy and spectroscopy. *The Journal of Physical Chemistry*, 117:1257–1267, 2013.

[94] Y. Xie, J. Li, and C. Yuan. Multiphysics modeling of lithium ion battery capacity fading process with solid-electrolyte interphase growth by elementary reaction kinetics. *Journal of Power Sources*, 248:172–179, 2014.

[95] Pinson M.B. and Bazant M.Z. Theory of SEI formation in rechargeable batteries: capacity fade, accelerated aging and lifetime prediction. *Journal of The Electrochemical Society*, 160:A243–A250, 2013.

[96] Suquet P. Elements of homogenization for inelastic solid mechanics. In E. Sanchez-Palencia and A. Zaoui, editors, *Homogenization Techniques for Composite Media. Lecture Notes in Physics*, volume 272, pages 193–198. Springer, Berlin/Heidelberg, 1987.

[97] R. Hill. Elastic properties of reinforced solids: Some theoretical principles. *Journal of the Mechanics and Physics of Solids*, pages 357–372, 11 1963.

[98] I. Ozdemir, W.A.M. Brekelmans, and M.G.D. Geers. Fe2 computational homogenization for the thermo-mechanical analysis of heterogeneous solids. *Comput. Methods Appl. Mech. Engrg.*, 198:602–613, 2008.

[99] I. Ozdemir, W.A.M. Brekelmans, and M.G.D. Geers. Computational homogenization for heat conduction in heterogeneous solids. *Int. J. Numer. Meth. Engng*, 73:185–204, 2008.

[100] T. Wu, I. Temizer, and P. Wriggers. Computational thermal homogenization of concrete. *Cement and Concrete Composites*, 35:59–70, 2013.

[101] T. Wu, I. Temizer, and P. Wriggers. Multiscale hydro-thermo-chemo-mechanical coupling: Application to alkali-silica reaction. *Computational Material Science*, 84:381–395, 2014.

[102] D. Zäh and C. Miehe. Computational homogenization in dissipative electro-mechanics of functional materials. *Computer Methods in Applied Mechanics and Engineering*, 267:487–510, 2013.

[103] F. Larsson, K. Runesson, and F. Su. Variationally consistent computational homogenization of transient heat flow. *International Journal for Numerical Methods in Engineering*, 81:1659–1686, 2010.

[104] K. Pham, V.G. Kouznetsova, and M.G.D. Geers. Transient computational homogenization for heterogeneous materials under dynamic excitation. *Journal of the Mechanics and Physics of Solids*, 61:2125–2146, 2013.

[105] Griffith D.J. *Introduction to Electrodynamics*. Prentice-Hall, Upper Saddle River, New Jersey, 3rd edition, 1999.

[106] H.A. Haus and J.R. Melcher. *Electromagnetic fields and energy*. Prentice-Hall, 1989.

[107] R. McMeeking and C.M. Landis. Electrostatic forces and stored energy for deformable dielectric materials. *ASME J. of Applied Mechanics*, 72:581–590, 2005.

[108] R.A. Toupin. The elastic dielectric. *J. Rational Mech. Anal.*, 5:849–914, 1956.

[109] C. Tang, K. Hackenberg, Q. Fu, P. Ajayan, and H. Ardebili. High ion conducting polymer nanocomposite electrolytes using hybrid nanofillers. *Nano Lett.*, 12:1152–1156, 2012.

[110] W.J. Drugan and J.R. Willis. A micromechanics-based nonlocal constitutive equation and estimates of representative volume element size for elastic composites. *Journal of the Mechanics and Physics of Solids*, 44(4):497 – 524, 1996.

[111] J.R. Willis. *Elasticity Theory of Composites*. Defense Technical Information Center, 1980.

[112] Z. Shan and A. M. Gokhale. Representative volume element for non-uniform microstructure. *Computational Materials Science*, 24(3):361 – 379, 2002.

[113] S. Swaminathan, S. Ghosh, and N. J. Pagano. Statistically equivalent representative volume elements for unidirectional composite microstructures: Part i - without damage. *Journal of Composite Materials*, 40(7):583–604, 2006.

[114] P.R. Shearing, L.E. Howard, J. Peter Stanley, N.P. Brandon, and S.J. Harris. Characterization of the 3-dimensional microstructure of a graphite negative electrode from a Li-ion battery. *Electrochemistry Communications*, 12(3):374 – 377, 2010.

[115] M. Ender, J. Joos, T. Carraro, and E. Ivers-Tiffèe. Three-dimensional reconstruction of a composite cathode for Lithium-ion cells. *Electrochemistry Communications*, 13(2):166 – 168, 2011.

[116] D. E. Stephenson, B. C. Walker, C. B. Skelton, E. P. Gorzkowski, D J. Rowenhorst, and D. R. Wheeler. Modeling 3D microstructure and ion transport in porous Li-ion battery electrodes. *J. Electrochem. Soc.*, 158:A781–A789, 2011.

[117] M.F. Ashby, P.J. Ferreira, and D.L. Schodek. *Nanomaterials, Nanotechnologies and Design*. Butterworth-Heinemann, 2009.

[118] Rubi J.M. and Kjelstrup S. Mesoscopic nonequilibrium thermodynamics gives the same thermodynamic basis to butler-volmer and nernst equations. *J. Phys. Chem. B*, 107:13471–13477, 2003.

[119] Oriani R.A. The diffusion and trapping of hydrogen in steel. *Acta Metallurgica*, 18(1):147–157, 1970.

[120] M.Z. Bazant, M.S. Kilic, B. Storey, and A. Ajdari. Towards an understanding of induced-charge electrokinetics at large applied voltages in concentrated solutions. *Advances in colloid and interface science*, 152:48–88, 2009.

[121] A.F. Bower, P.M. Guduru, and V.A. Sethuraman. A finite strain model of stress, diffusion, plastic flow and electrochemical reactions in a lithium-ion half-cell. *Journal of the Mechanics and Physics of Solids*, 59:804–828, 2011.

[122] E. Detournay and A.H.D. Cheng. Fundamental of poroelasticity. In C. Fairhurst, editor, *Comprehensive Rock Engineering: Principles, Practice and Projects*, volume 2: Analysis and Design Methods, chapter 5, pages 113–171. Pergamon Press, 1993.

[123] A. Quarteroni and A. Valli. *Numerical approximation of partial differential equations*. Springer Verlag, Berlin, 1997.

[124] Miehe C. Strain-driven homogenization of inelastic microstructures and composites based on an incremental variational formulation. *International Journal for Numerical Methods in Engineering*, 55:1285–1322, 2002.

[125] Miehe C. Computational micro-to-macro transitions for discretized micro-structures of heterogeneous materials at finite strains based on the minimization of averaged incremental energy. *Computer Methods in Applied Mechanics and Engineering*, 192:559–591, 2003.

[126] O. van der Sluis, P. J. G. Schreurs, W. A. M. Brekelmans, and Meijer H. E. H. Overall behaviour of heterogeneous elastoviscoplastic materials: effect of microstructural modelling. *Mechanics of Materials*, 32:449–462, 2000.

[127] R. Hill. Continuum micromechanics of elastoplastic polycrystals. *Journal of the Mechanics and Physics of Solids*, pages 89–101, 13 1965.

[128] A. Salvadori, D. Grazioli, M.G.D. Geers, D. Danilov, and P.H.L Notten. A novel approach in modeling ionic transport in the electrolyte of (li-ion) batteries. submitted for publication in Journal of Power Sources, 2014.

[129] A. Salvadori, D. Grazioli, M. Magri, M.G.D. Geers, D. Danilov, and P.H.L. Notten. A novel approach in modeling ionic transport in the electrolyte of (li-ion) batteries: the role of saturation. submitted for publication in Journal of Power Sources.

[130] A. Salvadori, D. Grazioli, M.G.D. Geers, D. Danilov, and P.H.L. Notten. A novel multi physics approach in modeling all solid state (li-ion) batteries. submitted for publication in Journal of Electrochemical Society.

[131] T.J. Rademaker, G.R.A. Akkermans, D. Danilov, and P.H.L. Notten. On the deviation of electro-neutrality in li-ion battery electrolytes. *Journal of The Electrochemical Society*, 161(8):E3365–E3372, 2014.

[132] C.W. Wang and A.M. Sastry. Mesoscale modeling of a li-ion polymer cell. *Journal of the Electrochemical Society*, 154:A1035–A1047, 2007.

[133] J. Christensen. Modeling diffusion-induced stress in li-ion cells with porous electrodes. *Journal of The Electrochemical Society*, 157:366–380, 2010.

[134] V. Zadin, D. Danilov, D. Brandell, P.H.L. Notten, and A. Aabloo. Finite element simulations of 3d ionic transportation properties in li-ion electrodes. *Electrochimica Acta*, 65:165–173, 2012.

[135] E.B. Tadmor, R.E. Miller, and R.S. Elliott. *Continuum Mechanics and Thermodynamics: From Fundamental Concepts to Governing Equations*. Cambridge University Press, 2011.

[136] Valoen L.R. and Reimers J.N. Transport properties of lipf6-based li-ion battery electrolytes. *Journal of The Electrochemical Society*, 152(5):A882–A891, 2005.

[137] S.H. Lam. Multicomponent diffusion revisited. *PHYSICS OF FLUIDS*, 18:073101, 2006.

[138] D. Bothe. On the maxwell-stefan approach to multicomponent diffusion. *Progress in Nonlinear Differential Equations and Their Applications*, 80:81–93, 2011.

[139] C. Miehe, S. Mauthe, and H. Ulmer. Formulation and numerical exploitation of mixed variational principles for coupled problems of cahn-hilliard-type and standard diffusion in elastic solids. *Int. J. for Num. Meth. in Engrg.*, 99:737–762, 2014.

[140] H. Yang, F. Fan, W. Liang, X. Guo, T. Zhu, and S. Zhang. A chemo-mechanical model of lithiation in silicon. *Journal of the Mechanics and Physics of Solids*, 70:349–361, 2014.

[141] C. Di Leo, E. Rejovitzky, and L. Anand. A cahn-hilliard-type phase-field theory for species diffusion coupled with large elastic deformations: Application to phase-separating li-ion electrode materials. *Journal of the Mechanics and Physics of Solids*, 70:1–29, 2014.

[142] P. Sofronis and R.M. McMeeking. Numerical analysis of hydrogen transport near a blunting crack tip. *Journal of the Mechanics and Physics of Solids*, 37(317-350), 1989.

[143] V. Malave, J. Berger, H. Zhu, and R.J. Kee. A computational model of the mechanical behavior within reconstructed lixcoo2li-ion battery cathode particles. *Electrochimica Acta*, 130:707–717, 2014.

[144] J. Lemaitre and J.L. Chaboche. *Mechanics of solid materials*. Cambridge University Press, 2000.

[145] W. Han and B.D. Reddy. *Plasticity*. Springer-Verlag, New York, 1999.

[146] L. Anand. A thermo-mechanically-coupled theory accounting for hydrogen diffusion and large elastic-viscoplastic deformations of metals. *International Journal of Solids and Structures*, (48):962–971, 2011.

[147] M. Gu, Z. Wang, J.G. Connel, D.E. Perea, L.J. Lauhon, F. Gao, and C. Wang. Electronic origin for the phase transition from amorphous lixsi to crystalline li_{15} si_4. *ACS Nano*, (7):6303–6309, 2013.

[148] A.D. Drozdov. Viscoplastic response of electrode particles in Li-ion batteries driven by insertion of lithium. *International Journal of Solids and Structures*, 51:690–705, 2014.

[149] F. Larche and J.W. Cahn. Non linear theory of thermochemical equilibrium under stress. *Acta Metallurgica*, 26:53–60, 1978.

[150] A.J. Kumnick and H.H Johnson. Deep trapping states for hydrogen in deformed iron. *Acta Metallurgica*, 28:33–39, 1980.

[151] Bower A. F. *Applied Mechanics of Solids*. CRC Press - Taylor and Francis, 2009.

[152] R.T. Purkayastha and R.M. McMeeking. A parameter study of intercalation of lithium into storage particles in a lithium-ion battery. *Computational Materials Science*, 80:2–14, 2013.

[153] D. de Souza Neto, Perić and Owen D.R.J. *Computational Methods for Plasticity*. John Wiley and sons, 2008.

[154] J. Wang, Y. Chen-Wiegart, and J. Wang. In operando tracking phase transformation evolution of lithium iron phosphate with hard x-ray microscopy. *Nature Communications*, 5, 2014.

[155] I.V. Thorat, D.E. Stephenson, N.A. Zacharias, K. Zaghib, J.N. Harb, and D.R. Wheeler. Quantifying tortuosity in porous li-ion battery materials. *Journal of Power Sources*, 188:592–600, 2009.